The role of cation chloride co-transporters (CCCs) as potential neuroprotective targets in ischaemic stroke

Miguel Ángel Stanislas Martín-Aragón Baudel

(Bsc, MSc)

Supervisory team:

Dr Amy Poole (DoS)

Professor Mark Darlison

Dr Jenny Fraser

Dr Mick Rae

A thesis submitted in partial fulfilment of the requirements of Edinburgh Napier University, for the award of Doctor of Philosophy.

October 2017

Declaration

‘I, Miguel Ángel Stanislas Martín-Aragón Baudel confirm that the work presented in this thesis is my own. Where information has been derived from other sources, I confirm that this has been indicated in the thesis.'

Signed:

Dedication

This thesis is dedicated to the memory of Professor Mark Darlison. For his passion, encouragement and example at overcoming difficult situations. He gave me the opportunity to start my career in science and for that, I will always be grateful to him.

Acknowledgments

First, I would like thank the best family ever for their unbelievable support and encouragement during my doctoral research, with special thanks to Monique Lavaure without whom the whole adventure in Edinburgh would not have been possible. To my nephews. Also to Emma Watson for her patience, love and support throughout this long journey.

I would like to thank my directors of studies: Dr Amy Poole and Professor Mark Darlison for giving me the opportunity to undertake this PhD, but also to Dr Jenny Fraser and Dr Mick Rae for all their guidance, patience and support during this project. They have all made me the scientist I am today and I will always be grateful to them and deeply miss them.

Edinburgh Napier friends for making these years an amazing time of my life: Hannah, Kirsty, Filipa, Lee, Alex, Joe, Sophie, Victor, Lewis, Charlotte, Mark…and all the PGR community, thanks!

Professor Arsenio Fernandez and the Neurosciences group in the University of León, especially to Berta, María and Diego for their help and without whom this project would not have been possible.

La GETA ubetense, todos unos fenómenos.

Granaínos antiguos: Amapolos de mi vida, Jesús, Javi, Pepe, Auri, Elena, Ana, Danielica, Amu, Poyatos, Lourdes, Lina, Vinci, Zenzations…os quiero!

Edinburgh friends: Joan, Jean Matthieu, Giulia, Amanda, John, Basia and Galacticos F.C.

Abstract

Stroke is one of the major causes of death and disability worldwide. The area that surrounds the infarcted core is the location of the continuing damage that takes place hours and days following an insult, and is referred to as the penumbra. By creating an oxygen deprived environment in the neuronal-like PC12 and NT2 cells and an *in vivo* photothrombotic model of stroke (PTS) in mice, two different strategies were created to replicate the conditions of an ischaemic brain.

In differentiated PC12 and NT2 cells, following hypoxia, preferential activation of HIF-2α transcription and protein expression was detected. Increased expression of the neural progenitor stem cell-like markers, thought to be transcriptionally regulated by HIF-2α, were also observed. Furthermore, hypoxia caused loss of neuronal characteristics in differentiated cells. This is highly significant as it shows neuronal cells possess molecular mechanisms which could trigger recovery following ischaemic insult.

The expression of the chloride co-transporters, NKCC1 and KCC2, mediators of the GABAergic response, was assessed following hypoxia in differentiated PC12 and NT2 cells and PTS. In PC12 and NT2 cells exposed to hypoxia, the expression of KCC2 was significantly decreased at both the transcript and protein level whereas NKCC1 expression remained unmodified. In the *in vivo* model, the development of the penumbra in the days following injury was assessed with specific markers allowing the identification of the penumbra up to 200 μm from the ischaemic core and a progressive neuronal loss was observed within. Our results show an increase in the number of neurons expressing NKCC1 in the penumbra up to 5 days following the insult when compared to the contralateral hemisphere. On the contrary, KCC2 positive cells were dramatically decreased in this area. In mice treated with bumetanide, an NKCC1 antagonist, a significant reduction in neuronal loss was observed. Our results show a reversal on the chloride co-transporters expression *in vitro* and *in vivo* and how treatments targeting these channels might represent a novel strategy to reduce the damage associated with stroke.

Abbreviations

AMPA: DL-γ-amino-3-hydroxy-5-methyl-4-isoxazole propionic acid

ATP: adenosine triphosphate

BBB: blood-brain barrier

BDNF: brain derived neurotrophic factor

CCC: cation-chloride co-transporters

CA1: *cornu Ammonis* 1

Ca9: carbonic anhydrase IX

Caspr1: contactin-associated protein 1

CHOP: C/EBP homologous protein

$[Cl^-]_i$: intracellular chloride concentration

CNS: central nervous system

CT: computer tomography

EPO: erythropoietin

ER: endoplasmic reticulum

GABA: γ-Aminobutyric acid

$GABA_AR$: γ-Aminobutyric acid type A receptor

GFAP: glial fibrillary acidic protein

Grp94-76: glucose-related proteins 94-76

HIF: hypoxia inducible factor

HRE: hypoxia responsive element

HSP70: heat shock protein 70

IGE: increased glial enrichment

KCC1-4: K^+-Cl^- co-transporters 1-4

LTP: Long-term potentiation

MCAO: middle cerebral artery occlusion

MRI: magnetic resonance imaging

NEFH: Neurofilament heavy polypeptide

NGF: nerve growth factor

NKCC1: Na^+-K^+-$2Cl^-$ co-transporter 1

NF-κβ: nuclear factor kappa-light-chain-enhancer of activated B cells

NMDA: *N*-methyl-D-aspartate

Nrn1: neuritin

NO: nitric oxide

NSE: neuron specific enolase

Oct4: octamer-binding transcription factor 4

PHD: prolyl-hydroxylase domain

PID: peri-infarct depolarisation

Ptbp2: polypyrimidine tract-binding protein 2

PTS: photothrombotic stroke

pVHL: von Hippel-Lindau protein

qPCR: real-time quantitative polymerase-chain-reaction

RA: retinoic acid

ROS: reactive oxygen species

t-PA: tissue type-plasminogen activator

Tmod1: tropomodulin 1

TNFα: tumour necrosis factor α

UPR: unfolded protein response

VEGF: vascular endothelial growth factor

WNK3: with no lysine kinase 3

Table of Contents

List of Figures

List of Tables

1. Introduction

1.1 Stroke

Stroke is the second leading cause of death, and the leading cause of disability, worldwide (World Health Organisation, 2014). The consequences have devastating effects, due to irreversible neuronal death, ranging from impaired speech and loss of vision, to movement deficits. For approximately one third of patients, a stroke will be fatal, for another third it will cause severe to very severe motor impairments, while the remainder will recover but have an increased risk of having another event (Go *et al*., 2014). In the United Kingdom, more than 100,000 individuals will suffer a stroke each year (SSNAP, 2016), which carries a huge personal and economic burden to society. The estimated annual cost of stroke in the UK, which includes health care services, treatment, and loss of productivity, is around £9 billion (Saka *et al*., 2009). Despite this, while approximately £241 is spent each year on medical research for each cancer sufferer, less than £48 is spent per stroke patient (Stroke Association, 2017).

There are currently few pharmacological strategies employed to reduce the damage and social burden triggered by this pathology. The harm caused by the interruption of blood flow to the brain evolves over the following hours and days (Go *et al*., 2014), so it is critical to identify new therapeutic targets that could reduce the neuronal death associated with the spread of the damage.

1.1.1 Different types of stroke

The most prevalent type of stroke in the UK is ischaemic, which accounts for 85% of all cases (Intercollegiate Stroke Working Party, 2016). This results from either atherosclerosis in large arteries, a blood clot forming in the heart and travelling to the brain, or lacunar strokes, which affect small arteries that provide blood to deeper areas of the brain. In contrast, haemorrhagic strokes are a consequence of either a primary intracerebral haemorrhage or a subarachnoid haemorrhage caused by bleeding in the area between the arachnoid membrane and the pia matter, normally produced by trauma, and result in a mortality of 30% (Gonzalez-Perez *et al*., 2013). The majority of haemorrhagic strokes occur due to weakening of arteries and concurrent high blood pressure. Since the two types of stroke have very different causes and prognoses, it is important to distinguish between them in order to provide the most appropriate treatment.

Distinguishing between the different types of stroke can only be performed once the patient is admitted to hospital, by either magnetic resonance imaging (MRI) or computer tomography (CT). Due to the need for highly-specialised equipment, and cost, a diagnosis is not usually made directly after admission. In the UK, almost nine out of ten stroke patients receive brain scan within 12 hours, taking an average of seven hours from the onset of symptoms to be admitted to a stroke unit (SSNAP, 2016). However, since neuronal cell death begins soon after the onset of ischaemia, rapid diagnosis and treatment are essential to limit long-term damage (Goyal *et al*., 2015). Furthermore, the type of treatment administered is dependent upon the

nature of the stroke. For example, prescribing anti-coagulants to help reduce their risk of developing further blood clots in the future in a haemorrhagic event, would have the opposite of the desired effect.

1.1.2 Current treatments for ischaemic stroke

Despite years of intensive research, the only current effective and approved treatments for ischaemic stroke rely on the pharmacological and/or mechanical revascularisation of the affected artery. Mechanical revascularisation can only be performed when a large artery is affected. In such cases, when large thrombi are resistant to pharmacological dissolution, a mechanical thrombectomy can produce a favourable clinical outcome (Jeromel *et al*., 2013; Akbik *et al*., 2016). Tissue type-plasminogen activator (t-PA), commercially known as Alteplase, remains the only Federal Drug Administration-approved drug in use for this purpose. Its mode of action is to dissolve the clot causing the infarct; however, many patients do not benefit from this treatment because of various exclusion criteria, the most important being its short therapeutic window of 3 to 4.5 hours (Fugate and Rabinstein 2015; Holmes *et al*., 2015). In addition, according to European guidelines (The European Agency for the Evaluation of Medicinal Products, 2002), alteplase cannot be used on patients more than 80 years of age, as this demographic have an increased risk of haemorrhage and mortality (Longstreth *et al*., 2010; Wardlaw *et al*., 2012). Major side effects of t-PA include an increased risk of haemorrhage in ischemic tissue, activation of matrix metalloproteinases that can disrupt the blood-brain barrier (BBB), and induction of excitotoxicity due to excessive glutamate release. t-PA induces

an increase in the influx of calcium via a plasmin-independent cleavage of the NR1 subunit of the *N*-methyl-D-aspartate (NMDA) receptor, potentiating receptor signalling (reviewed in Yepes *et al*., 2009 and discussed in more detail in section 1.7). Thus, current research is aimed at developing a more fibrin-specific agent with a shorter half-life and less neurotoxic side effects than t-PA (Frendl and Csiba 2011). Interestingly, a recent study in an animal model of stroke has shown an increase in the therapeutic window of t-PA by combining it with 2-(4-methoxyphenyl)ethyl-2-acetamido-2-deoxy-β-d-pyranoside (SalA-4g; Yu *et al*., 2016). This effect is due to an increase in glucose uptake via elevated glucose transporter 3 expression (Yu *et al*., 2014), improving brain energy metabolism.

1.1.3 Risk factors for ischaemic stroke

Risk factors for stroke include hypertension, obesity, diabetes, smoking, and high cholesterol (Hankey 2006), many of which are on the increase. Interestingly, mortality from stroke has decreased over time due to better management of risk factors, education and the general improvements to health systems. Interestingly, there is a sex-specific difference in the occurrence of stroke, being more common in males than in females. However, women are more severely affected (a one-month case fatality of 24.7% compared with 19.7% for men; Appelros *et al*., 2009). Together with the aging population, it seems reasonable to conclude that the occurrence of stroke will not significantly decrease in the near future, and that the number of patients suffering from stroke-associated disabilities will likely grow. It is, therefore, essential to find and develop novel and effective approaches to

either prevent neuronal death that occurs in both ischaemic and haemorrhagic strokes and/or promote functional recovery. After a stroke, neurons within the core of the infarct are unlikely to be salvageable (Muir *et al*., 2006). However, it may be possible to rescue those within the surrounding area, the penumbra, which would limit motor and other deficits (Figure 1.1). Salvaging the penumbra requires understanding of the early molecular events occurring after an ischaemic insult; including changes in gene expression, biochemical pathways and neuronal ion regulation.

1.2 The ischaemic core versus the penumbra

The ischaemic core, which is the brain area immediately impacted by a dramatic reduction in blood supply after a stroke, becomes rapidly and irreversibly damaged affecting neuronal, glial and vascular cells (Figure 1.1). The infarcted tissue suffers from oxygen and glucose deprivation, leading to neuronal death as a consequence of bioenergetic failure, reduced adenosine triphosphate (ATP) and impairment of ionic homeostasis across the cell membrane (Astrup *et al*., 1981). Lack of oxygen inhibits mitochondrial activity and inefficient anaerobic glucose metabolism generates lactate as an end product (Kalogeris *et al*., 2012). Calcium overload, accumulation of oxygen free radicals and the stimulation of intracellular lysosomal enzymes results in the loss of cell membrane function (Sims and Muyderman 2010). Neurons also begin to undergo apoptosis, but due to the lack of ATP they shift from an apoptotic route to a necrotic one, leading to unprogrammed cell death (Figure 1.1; Yuan 2009; Chelluboina *et al*., 2014). This appears to be

mediated by the caspase cleavage of calcium pumps, altering intracellular calcium homeostasis, which ultimately triggers necrosis (Schwab *et al*., 2002). These cellular cascades are triggered within minutes of the onset of stroke, making protection of the ischemic core essentially impossible (Go *et al*., 2014). This region is therefore considered as non-salvageable tissue. In contrast, the penumbra that surrounds the ischaemic core is only partially metabolically compromised due to collateral blood supply and therefore may be salvaged. This area is of great therapeutic relevance because it is the location of the ensuing damage that takes place in the hours and days following an insult (Hartings *et al*., 2003).

The penumbra has been classically defined as the area that surrounds the core, yet has sufficient collateral blood flow to be salvaged (Figure 1.1). Regions within the brain with a cerebral blood flow below 20 ml/100 g/min define this area; this is compared with a normal blood flow of ~50 ml/100g/min. When blood flow is less than 10 ml/100 g/min, the tissue loses ionic homeostasis and forms the infarct core (Hakim 1998). Neuroimaging techniques have provided a method to anatomically distinguish between the core and penumbra (Wey *et al*., 2013). The method of choice to discriminate between these two regions is positron emission tomography/single photon emission CT, which measures cerebral blood flow and glucose metabolism.

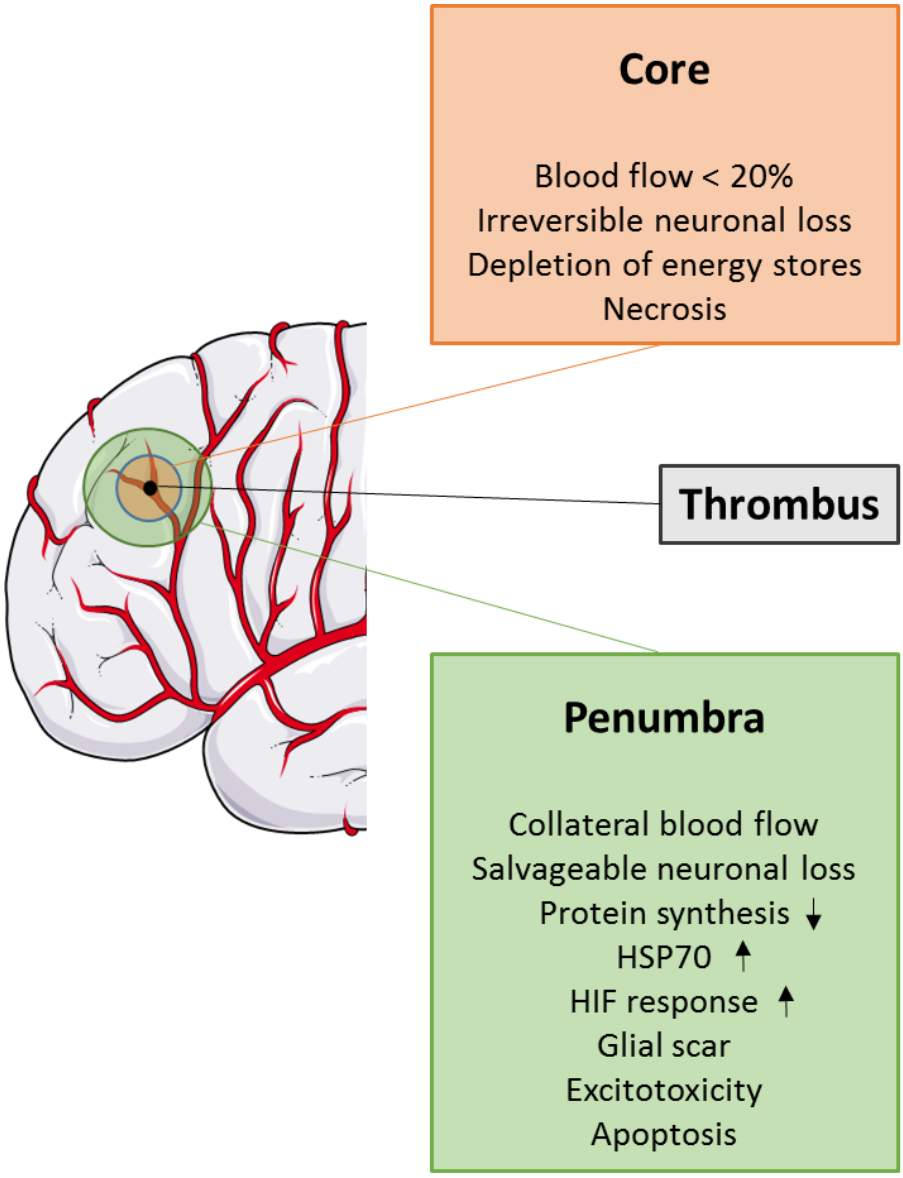

Figure 1.1. The ischaemic core and penumbra. Two physiologically and molecularly defined areas develop following a thrombus formation in the brain, the ischaemic core and the penumbra. The precise extent of the penumbra within the peri-infarct tissue is currently unclear; however, different physiological and molecular characteristics define each area (shown in boxes).

1.2.1 Development of the penumbra

There are also a number of molecular events that help to understand the development of the penumbra, and its progression towards a damaged core-like state.

1.2.1.1 Protein stress

Protein synthesis is a highly energy dependent process which is therefore compromised following an ischaemic event. A decrease in protein synthesis is observed, which is mediated by the unfolded protein response (UPR) in the endoplasmic reticulum, and translational arrest mainly through the phosphorylation of eukaryotic initiation factor 2 (Figure 1.1; eIF2; Hata *et al*., 2000; DeGracia and Hu 2007). Activation of the UPR increases the ability of the endoplasmic reticulum to deal with the accumulation of misfolded proteins, which arises due to stress, and this is beneficial in the short-term. However, prolonged induction leads to apoptosis due to global translational arrest (Han *et al*., 2009). Expression of the UPR response genes appears to be decreased in aged animals (Llorente *et al*., 2013), which could be a factor contributing to the higher mortality observed in the aged population.

Heat shock protein 70 (HSP70) is an inducible molecular chaperone, the expression of which is induced under different stress conditions. This molecule binds to nascent polypeptides preventing their aggregation, supporting protein folding and trafficking across intracellular compartments. It is particularly relevant in ischaemia as it is considered to have neuroprotective potential (Rajdev *et al*., 2000), and it is not expressed in the

adult brain under normal physiological conditions. HSP70 is strongly induced in neurons of the penumbra, at both the mRNA and protein level, but not in the core where little or no mRNA is found, apart from in blood vessels where significant HSP70 protein levels have been detected (Zhan *et al*., 2008; De La Rosa *et al*., 2013). Modified versions of HSP70 with increased BBB permeability (Doeppner *et al*., 2009; Doeppner *et al*., 2013) or recombinant HSP70 formulated in alginate granules with retarded release of protein (Shevtsov *et al*., 2014) have provided neuroprotection in different animal models of stroke, making this protein a very interesting target to promote neuroprotection following ischaemic stroke.

1.2.1.2 Peri-infarct depolarisations

The penumbra is thought to develop due to anoxic depolarisation-like events known as peri-infarct depolarisations (PIDs) that propagate from the ischaemic core (Nedergaard and Hansen 1993). PIDs are triggered by an increase in extracellular concentration of potassium, and the vast release of excitatory neurotransmitters. The resultant spontaneous and continuous neuronal depolarisations deplete the glucose pool in the penumbra (Feuerstein *et al*., 2010) and, consequently, depolarised neurons lack the energy to repolarize. This progressive process causes the observed spreading effect, resulting in increased infarct volume (Back *et al*., 1996; Hartings *et al*., 2003). However, they also provide the opportunity for neuroprotective intervention (Ramos-Cabrer *et al*., 2011). Constant depolarisations have also been shown to induce BBB disruption (Gursoy-Ozdemir *et al*., 2004), providing a drug delivery route to limit the growth of

infarct tissue. The wave of depolarisation can also be beneficial, in the long term, by triggering axonal sprouting and, thus, the formation of new connections in the brain (Hinman *et al*., 2013).

The energy demand of the brain is achieved by an increase in blood flow to satisfy the requirements for glucose and oxygen. However, during the spread of PIDs, a loss of vasoreactivity due to diminished vasodilation and, occasionally, even vasoconstriction is observed (Chang *et al*., 2010). This leads to a glucose and oxygen supply that is insufficient for the high demands of the ischemic tissue necessary to restore the ionic balance and membrane repolarisation. The observed vasoconstrictor response is due to an increase in the extracellular potassium concentration, as a result of reduced sodium-potassium ATPase activity, and a decrease in nitric oxide production by the inhibition of nitric oxide synthase (Shin *et al*., 2006). This overrides the vasodilatory effect of low pH, caused by anaerobic metabolism (Dreier 2011). The inhibition of PIDs with either channel blockers or antagonists, and targeting the vasoconstrictor response, are obvious candidates for neuroprotective strategies in stroke. However, a large number of clinical trials with channel blockers, specifically NMDA receptor antagonists, have failed to translate bench findings into successful patient therapies (O'Collins *et al*., 2006; Tymianski 2010; Grupke *et al*., 2015 and covered in detail in section 1.7).

1.3 Glial scar

Following stroke there is an increase in the number of glial cells (i.e. microglia, oligodendrocytes and astrocytes) in the area immediately bordering the infarct within the penumbra, which is called the glial scar. The glial scar consists predominately of reactive astrocytes and proteoglycans (Silver and Miller 2004). Reactive astroglyosis is a finely regulated process of alterations in gene expression and cellular changes in astrocytes that occur in response to various central nervous system (CNS) insults, such as stroke (Sofroniew 2009). In its extreme form, reactive astroglyosis can lead to astrocyte proliferation and glial scar formation (Carlén *et al*., 2009).

The glial scar surrounds the ischaemic core, and confers both beneficial and detrimental effects. During the acute phase of ischaemia, the glial scar prevents spreading of the core through different mechanisms such as, uptake of excitotoxic glutamate (Swanson *et al*., 2004), protection from oxidative stress via glutathione production (Chen *et al*., 2001), limiting the responses to vasogenic oedema (Zador *et al*., 2009), protection from growth factors and free radicals release (Rolls *et al*., 2009), and promoting axonal regeneration (Anderson *et al*., 2016). Furthermore, genetic ablation or attenuation of reactive astroglyosis has been shown to increase infarct size and neuronal loss following ischaemia (Li *et al*., 2008).

Conversely, glial scar formation has also been shown to interfere with the innate process of axonal sprouting, by producing growth-inhibitory molecules

such as chondroitin sulphate proteoglycans, and creating a physical barrier to regenerating axons (Carmichael *et al*., 2016). Thus, the beneficial or detrimental role of the glial scar may be dependent on timing, as it appears to be beneficial in the acute phase, but detrimental to the promotion of neuronal recovery. Old age is associated with increase in mortality, susceptibility and poor recovery after stroke (Go *et al*., 2014). Aged animals, that are also more likely to suffer from a stroke, present an increased astrocytic and microglial reactivity and premature glial scar formation (Popa-Wagner *et al*., 2007). This rapid glial scar formation may impede the recovery of neuronal function compared to younger animals (Badan *et al*., 2003; Anuncibay-Soto *et al*., 2014).

1.4 Reperfusion injury and inflammation

The primary goal in the early treatment of ischaemic stroke is achieving the rapid revascularisation of the affected blood vessel(s) in order to restore the blood supply. However, paradoxically, reperfusion can lead to further injury. The BBB is composed of endothelial cells together with pericytes, astrocytes, neurons, and extracellular-matrix (comprising the neurovascular unit). It maintains cerebral homeostasis by preventing hydrophilic and large molecules from entering the brain. After a stroke, the release of reactive oxygen species and massive ionic dysregulation leads to the breakdown of the BBB, and activation of inflammatory processes. Furthermore, blood vessels that have been weakened by an ischaemic episode can rupture upon re-establishment of blood flow and, thus, cause secondary haemorrhagic

strokes (Sandoval and Witt 2008), exacerbating the morbidity and mortality following an ischaemic event.

Two types of inflammation take place in the brain after a stroke: cytotoxic and vasogenic. Cytotoxic oedema is caused by the ionic dysregulation that follows energy depletion, as the entrance of ions into cells (sodium entrance exceeds potassium loss) is accompanied by water and, thus, cell swelling (Young *et al*., 1987). Vasogenic oedema is due to the breakdown of the BBB, which allows the cellular entrance of large macromolecules, as well as intravascular to extravascular fluid movement, and produces an increase in brain volume (Schoknecht *et al*., 2015). The formation of cerebral oedema can result, if untreated, in elevated intracranial pressure, reduced cerebral blood flow, and ultimately contribute to stroke mortality (Khanna *et al*., 2014).

Recombinant human erythropoietin is a promising candidate for the prevention of oedema formation in acute ischaemic stroke (Ehrenreich *et al*., 2009). The expression of human erythropoietin is regulated by hypoxia inducible factor (HIF)-1/2α, and is proposed to reduce brain oedema and infarction through maintenance of matrix metalloproteinase-mediated BBB integrity (Wang *et al*., 2014; Zhao *et al*., 2015).

1.5 Neuronal adaptation to hypoxia: the HIF response

Neurons suffer from a dramatic decrease in oxygen availability following an ischaemic insult, a condition known as hypoxia. Neurons have evolved adaptive mechanisms which enable them to survive this decrease in oxygen availability. Therefore, hypoxia triggers a large number of physiological and pathophysiological molecular responses. Hypoxia inducible factors (HIFs) are the best-described regulators of oxygen homeostasis and critical for adaptation to hypoxic insults (Semenza 2012). In normoxic conditions, HIF-α is hydroxylated by the prolyl-hydroxylase domain (PHD) family of dioxygenases. This hydroxylation promotes the binding of von Hippel-Lindau protein (pVHL) which forms the substrate for the recognition and ubiquitination of the complex, facilitating proteosomal degradation (Figure 1.2; Schofield and Ratcliffe 2004). Following a hypoxic insult, HIF-α is stabilised, binds to HIF-β and translocates into the nucleus, where it binds to genes possessing a hypoxia responsive element (HRE) in their regulatory region, promoting their expression (Ke and Costa 2006). There are three HIF-α subunits, HIF-1α, -2α and -3α; HIF-1α and 2α are structurally similar whilst HIF-3α is thought to be an alternative splice form, which may negatively regulate HIF-1α function (Maynard *et al*., 2005; Yamashita *et al*., 2008).

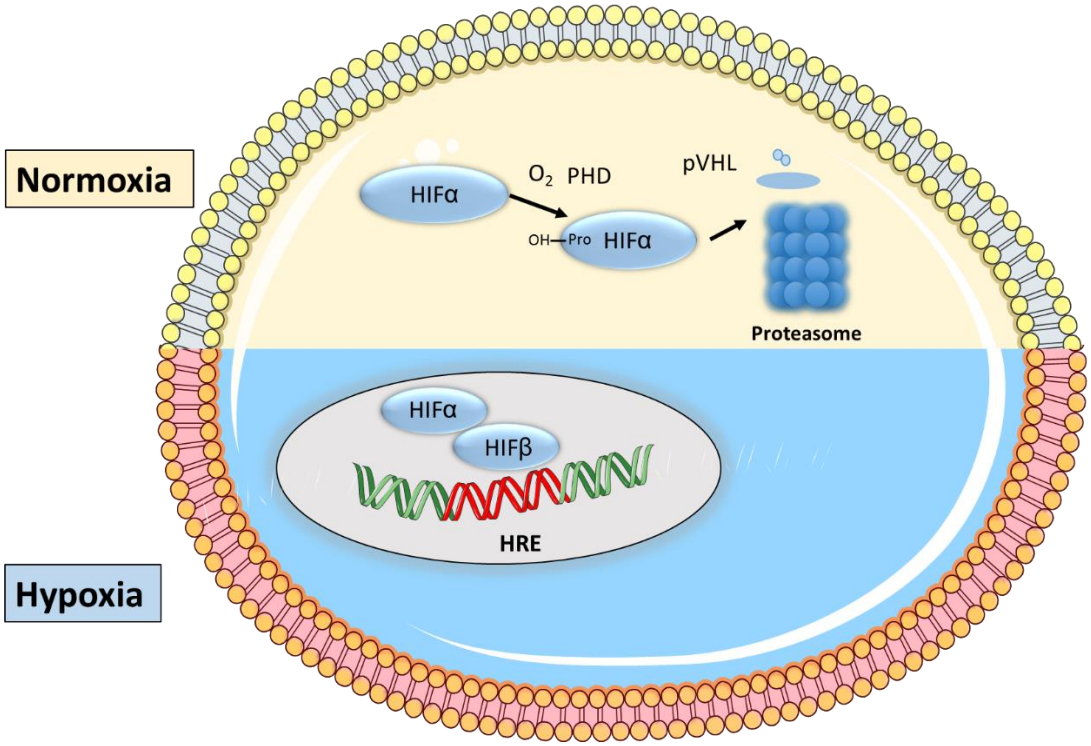

Figure 1.2 The HIF response in normoxia and hypoxia. Under normal physiological levels of oxygen HIF-1/2α are rapidly degraded through the ubiquitin protease pathway. Under hypoxia, HIF-1α/2α can bind to the HIFβ subunit and translocate into the nucleus promoting the transcription of different hypoxia-responsive genes bearing the hypoxia responsive element (HRE) in their regulatory sequence. pVHL: von Hippel-Lindau protein; PHD: prolyl-hydroxylase domain dyoxygenases.

Whilst HIF-1α and 2α share common transcriptional gene targets (Koh and Powis 2012), they also regulate distinct subsets of genes and elicit differerent cellular responses. HIF-1α regulates glycolytic genes such as pyruvate dehydrogenase kinase (Pdk) to activate anaerobic glycolysis in order to maintain ATP production under low O_2 tension (Kim *et al*., 2006). It has also been shown to regulate the expression of carbonic anhydrase IX (Ca9) which has role in intracellular pH maintenance (Kaluz *et al*., 2009), and can activate

BCL2/adenovirus E1B 19 kDa protein-interacting protein 3 (Bnip3) to trigger apoptosis (Guo *et al*., 2001). HIF-1α is also involved in the activation of genes that participate in the UPR in order to decrease protein stress such as glucose-related proteins 94-76 (*Grp94-76*), C/EBP homologous protein (*CHOP*) or the protein disulphide isomerase (*PDI*) *(*Keith *et al*., 2012). HIF-1 is predominantly induced in the penumbra (Bergeron *et al*., 1999) and is therefore considered a good marker of this therapeutically relevant area (Figure 1.1; Shi 2009). Conversely, HIF-2α promotes other adaptations to reduce neuronal death following hypoxic stress such as angiogenesis, cell division and tissue regeneration by regulating expression of erythropoietin (EPO), Cyclin D1 and the stem cell marker, octamer-binding transcription factor 4 (Oct4), amongst other targets (Raval *et al*., 2005; Covello *et al*., 2006; Haase 2013).

Despite the limited regenerative capacity of the nervous system, a degree of spontaneous recovery can occur following ischaemic stroke (Carmichael 2016). Studies suggest HIF mediated angiogenesis and neurogenesis are central to this process (Ralph *et al*., 2004; Shi 2009; Barteczek *et al*., 2016). Neuron-specific knockout of HIF-1α dramatically increases ischaemic damage caused by transient middle cerebral artery occlusion (MCAO) and HIF-1α loss increases infarct volume and mortality (Baranova *et al*., 2007). Indirect induction of HIF signalling via genetic ablation of *Phd2* also reduces infarct size and dramatically improves sensorimotor function following transient ischaemic insult (Reischl *et al*., 2014). Conversely, Helton et al. (2005) found that neuron-specific loss of HIF-1α in mice led to neuroprotection following acute ischaemia. Therefore, the exact function and

precise timing of the HIF response following ischaemic insults still needs to be ascertained, as both detrimental and beneficial effects of HIF have been observed in different experimental models of stroke (Shi 2009).

HIF-α's role in the pathophysiology of ischaemic insult is complicated as HIF-1α and -2α signalling display temporal differences (Koh and Powis 2012); HIF-1α appears to be involved in the acute response whilst HIF-2α mediates the response to chronic hypoxic stress (Holmquist-Mengelbier *et al*., 2006). The timescale of HIF signalling is critical for effective recovery from ischaemic insult, as whilst genetic targeting of neuronal HIF-1α and HIF-2α was beneficial in acute stages, loss of HIF-1α and -2α correlated with increased apoptosis and reduced sensorimotor function at later stages (Barteczek *et al*., 2017). This may be due to HIF-2α regulating VEGF signalling and the importance of angiogenesis in post-stroke neurogenesis (Li *et al*., 2016). Together, these studies indicate the intricacies of HIF signalling, their neuroprotective role and importance in recovery from ischaemic damage.

1.6 Ion dysregulation

Although the weight of the human brain is only about 2% of total body weight, it has a high metabolic activity and uses 20% of the oxygen and 25% of the glucose consumed by the entire body (Zauner *et al*., 2002). This is required to generate sufficient ATP to maintain the high demand for energy needed for action and synaptic potentials (Magistretti and Allaman, 2015). Following

global ischaemia, the available ATP is consumed within 2 minutes due to the inhibition of mitochondrial ATP synthesis (Caplan 2000). The membrane-bound sodium-potassium ATPase consumes 70% of the brain-derived ATP, and this pump plays a key role in ion homeostasis by extruding sodium from the cell. This results in a relatively low intracellular sodium concentration, and a comparatively low external potassium concentration (Figure 1.3). Due to the ATP depletion that follows an ischaemic episode, the tightly regulated sodium-potassium ATPase-dependent homeostasis is lost. However, there are additional ionic transporters, both ATP-dependent and independent ones, involved in the maintenance of ionic gradients. Many of these transporters are dysregulated during ischaemic brain injury, contributing to cytotoxic cell swelling, neuronal depolarisation and ultimately cell death (Kahle *et al*., 2009; Sun and Kahle 2014).

Glial cells are also very important players in the maintenance of the tightly-controlled ion regulation in the brain as they interact with neurons and regulate their function (Fields *et al*., 2015). Ischaemic injury affects neuronal and glial ionic homeostasis and this significantly alters glial responses in the brain. This is due to their contribution to the regulation of extracellular ion concentrations necessary for neuronal excitability (Pannasch *et al*., 2011); Therefore, the modification of intra-glial ionic homeostasis in response to ischaemic injury, has a crucial role in inducing and maintaining glial responses in the ischemic brain (Annunziato *et al*., 2013).

1.7 Excitotoxicity and NMDA receptors

NMDA receptors are found throughout the brain, playing an important role in synaptic development and learning and memory (Monyer *et al*., 1994; Sanz-Clemente *et al*., 2013). During an ischaemic event, energetic failure and the loss of ionic gradients leads to an increase in presynaptic glutamate release, and failure of glutamate re-uptake mechanisms (Rossi *et al*., 2000). This causes an increase in extracellular glutamate levels. Astrocytes are the principal mediators of glutamate recycling from the extracellular space (Uwechue *et al*., 2012). The expression of the transcription factors, tumour necrosis factor α (TNFα) and nuclear factor kappa-light-chain-enhancer of activated B cells (NF-κβ) are increased during hypoxia and these downregulate the activity of excitatory amino acid transporters 1 and 2, EAAT1 and EAAT2, in astrocytes (Boycott *et al*., 2008). This contributes to the over-activation of DL-γ-amino-3-hydroxy-5-methyl-4-isoxazole propionic acid (AMPA) and NMDA receptors, and an increased intracellular calcium concentration that triggers caspase activation, free radical formation and, eventually, cell death (Figure 1.3; Szydlowska and Tymianski 2010). This phenomenon is known as excitotoxicity (Olney and Sharpe 1969) and it is elicited by the onset of stroke being a major driver of neuronal death in the penumbra. Most studied neuroprotectants for the treatment of stroke have targeted the AMPA and the NMDA receptor, which are glutamate-activated ion channels (Besancon *et al*., 2008; Krzyżanowska *et al*., 2014). However, despite promising results of NMDA receptor antagonists *in vitro* and in *in vivo* animal models, all compounds have failed in clinical trials (Xu and Pan 2013).

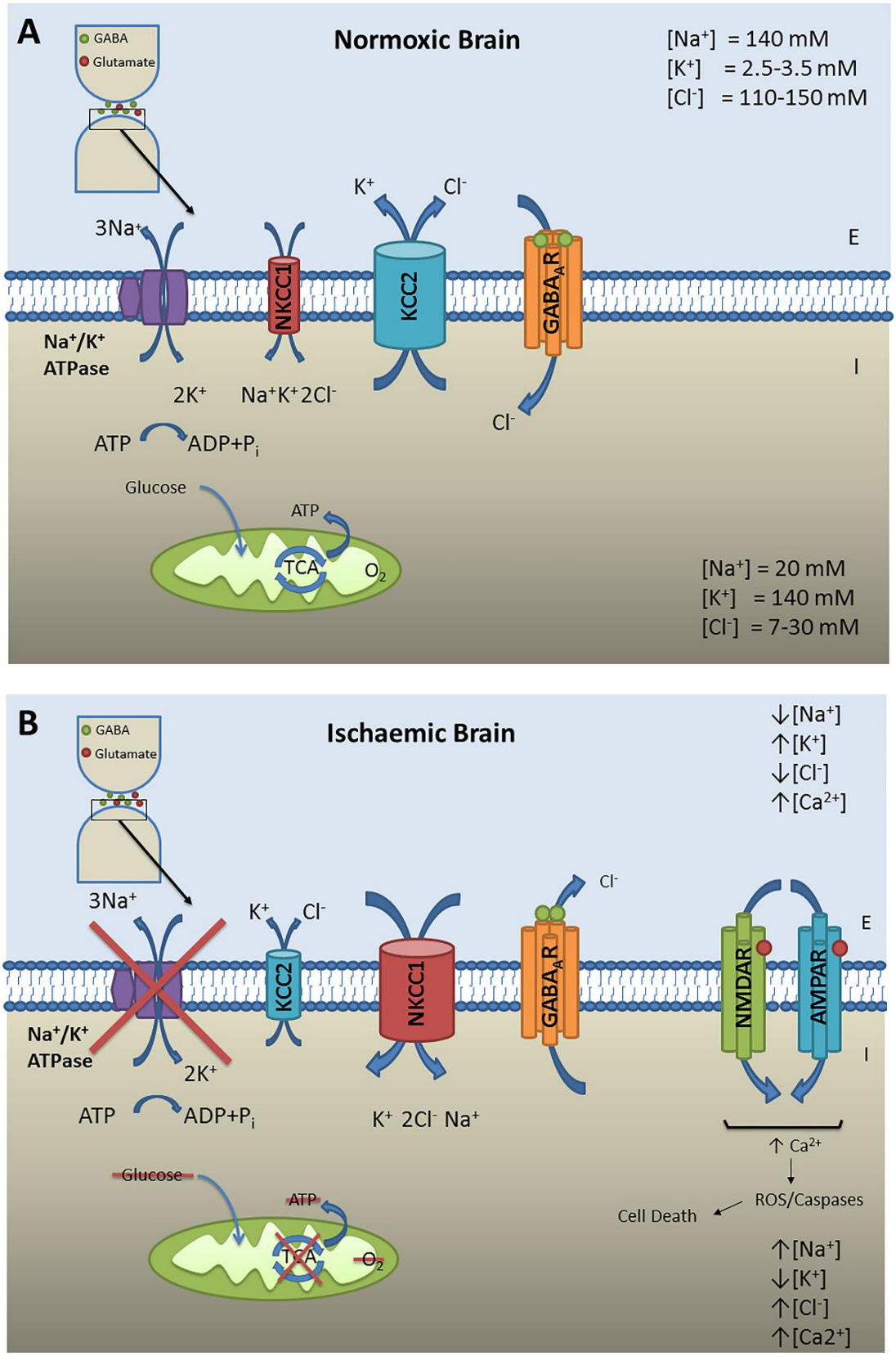

Figure 1.3. Ionic balance in normoxic vs. ischaemic brain, and the development of excitotoxicity.

Figure 1.3. A. Under normal physiological conditions, the energy produced in the form of ATP by the tricarboxylic acid cycle is utilised by the Na^+/K^+ ATPase pump to maintain ionic homeostasis between the extracellular (E) and intracellular (I) spaces. Under normoxic conditions, KCC2 is highly expressed when compared to NKCC1, thereby maintaining a chloride gradient across the neuronal membrane with a high extracellular concentration and a low intracellular concentration. Upon GABA release from a presynaptic neuron, $GABA_A$ receptors are activated leading to chloride influx and subsequent hyperpolarisation of the post-synaptic neuron. **B.** An ischaemic brain suffers from a rapid energy and oxygen depletion that leads to an intense ion dysregulation. The Na^+/K^+ ATPase is unable to maintain sodium and potassium homeostasis and NKCC1 is up-regulated, modifying the chloride gradient. When $GABA_A$ receptors are activated, chloride effluxes from the neuron resulting in depolarisation. In addition, glutamate release is greatly increased in the minutes immediately following stroke onset, contributing to the wave of depolarisation and an intracellular calcium overload mediated by NMDA and AMPA receptors. This increased calcium concentration generates reactive oxygen species (ROS) and causes caspase activation, that ultimately leads to cell death.

1.7.1 The failure of glutamate receptor modulators for ischaemic stroke

Partial success was originally achieved in rat and mouse animal models of ischaemic stroke with two non-competitive NMDA receptor antagonists, MK-801 (Margaill *et al*., 1996) and Dextrorphan (Steinberg *et al*., 1995), both of which exhibit a neuroprotective effect within therapeutic windows of 30 minutes and 2 hours, respectively. These data indicate that the therapeutic window is too short, after the ischaemic injury, for these compounds to be of benefit. Other NMDA receptor antagonists have subsequently been tested, such as Memantine, Cerestat (CNS 1102) and Selfotel (CGS19755). Although all of these drugs were effective in animal models in both histological and behavioural studies (reviewed in Lau and Tymianski 2010), all of the corresponding human clinical trials were abandoned due to a lack of therapeutic effect, increased rates of mortality and/or unacceptable side effects such as hallucinations and psychotropic episodes (Morris *et al*., 1999; Davis *et al*., 2000; Albers *et al*., 2001).

1.7.2 Novel glutamate receptor modulators for ischaemic stroke

While activity of NMDA receptors is required for balanced cognitive, behavioral and physiological functioning, complete blockade of the receptor would intuitively lead to broad and unpredictable effects. A more downstream-specific approach has been developed in animals in which the compound NA-1 blocks the interaction between NMDA receptors and the scaffold protein postsynaptic density-95 (PSD-95) to inhibit nitric oxide (NO) signalling (Instrum and Sun 2013). NA-1 disrupts the link between NMDA receptors and the neurotoxic NO cell death signalling pathway, without

disturbing normal NMDA receptor function. Treatment with NA-1 has produced both neuroprotection, and preservation of neurological function in a primate model of stroke (Cook *et al*., 2012), and in a promising phase 2 clinical trial in humans (Hill *et al*., 2012). NA-1 is currently undergoing a phase 3 clinical trial (FRONTIER trial, 2014).

A dual role for NMDA receptors in the development of stroke has been suggested in recent studies. Whereas the more abundant, extrasynaptic NMDA receptors promote cell death, synaptic NMDA receptors might be neuroprotective through the calcium-dependent activation of survival genes, suppression of death genes, and protection against oxidative stress (Hardingham and Bading 2010; Baxter *et al*., 2015; Brassai *et al*., 2015). Activation of extrasynaptic NMDA receptors has opposing actions: i.) shutting down the cyclic AMP response element binding protein (CREB) pathway and inactivation of the protein kinases ERK (extracellular signal-regulated kinase) 1/2; and ii.) activation of the forkhead box O (FOXO) and calpain cell death pathways (Wahl *et al*., 2009). Thus, more effort could be expended to elucidate the differentially-located NMDA receptors, and their down-stream signalling pathways, as a prelude to seeking neuroprotective strategies for ischaemic stroke.

AMPA receptors are also candidates for neurorehabilitation in stroke. Like NMDA receptor agonists, early administration of positive allosteric modulators of AMPA receptors are detrimental to stroke recovery, because they contribute to excitotoxicity (Mehta *et al*., 2013). Ampakines potentiate the excitatory signalling of AMPA receptors, whereas a new generation of

drugs known as type II ampakines, increase the intracellular concentration of brain derived neurotrophic factor (BDNF), which is essential, together with NMDA receptors, for long-term potentiation (LTP) and rehabilitation post-stroke (Ploughman *et al*., 2009). LTP is a form of plasticity that involves a long-lasting strengthening of synaptic transmission, and which is triggered by brief periods of high-frequency stimulation (Bliss and Lomo 1973). An elegant study by Clarkson *et al*. (2011) showed improved motor recovery in a focal stroke model in young mice, where type II ampakines were administered five days after ischaemia, through potentiation of the AMPA-BDNF signalling system. However, early administration of the drug, given at the time of induction of cerebral ischaemia, increased stroke damage. By combining the ampakine CX1837, with BDNF, the level of which is reduced in aged populations, a significantly improved recovery two weeks after insult was observed in aged mice (Clarkson *et al*., 2015). From the above, it may be concluded that blockade of NMDA/AMPA receptor channels could be either beneficial or harmful to neurons depending on their spatial location and the time of administration of a pharmacological agent.

1.8 Cation chloride co-transporters (CCCs)

1.8.1 $GABA_AR$ activity is dependent on Cl^- gradient

γ-Aminobutyric acid (GABA) type A receptors ($GABA_AR$) are ligand-gated ion channels that are the principal mediators of synaptic inhibition in the mature human brain. The chloride ion gradient across the neuronal membrane is crucial for the nature of GABAergic signalling. The direction of chloride movement is dependent upon the chloride gradient; chloride entry through $GABA_AR$ leads to hyperpolarisation while chloride extrusion results in cellular depolarisation (Figure 1.3; Rivera *et al*., 1999; Delpire 2000; Kaila *et al*., 2014). Cation-chloride co-transporters (CCCs) mediate coupled transport of sodium, potassium and chloride ions across neuronal membranes, thereby regulating the chloride electrochemical gradient (Kaila *et al*., 2014).

1.8.2 The CCC family

The CCC proteins are classified in terms of their physiological function into three categories: two members are Na^+-K^+-$2Cl^-$ co-transporters (NKCC1 and NKCC2), one is a Na^+-Cl^- co-transporter (NCC), and four are K^+-Cl^- co-transporters (KCC1 to KCC4). All CCCs are expressed in the mammalian nervous system at different developmental stages with the exception of NCC and NKCC2, which are found predominantly in the kidney where they play a key role in the salt transport pathway (Haas 1994; Liu *et al*., 2011). However, a novel study has shown that the expression of NKCC2 in brain plays a role in osmoregulation following hydration insult (Konopacka *et al*., 2015). The remaining two members of the CCC family, CCC interacting protein (CIP1)

and CCC9, have no known physiological role. However, CIP1 is thought to possibly be involved in the activation of KCC2 (Wenz *et al*., 2009). Homo- and hetero-oligomers have been described for almost all CCCs. Associations of KCC1 and KCC3, KCC2 and KCC4, and NKCC1 and KCC4, have been found however, to date there is no conclusive data detailing how the different oligomerisation patterns affect protein function (Simard *et al*., 2007; Hartmann and Nothwang 2014).

The genes *SLC12A1-9* encode nine members of the CCC family, all of which are glycoproteins, having molecular weights of between 120 and 200 kDa. The predicted secondary structure of CCCs (only confirmed for NKCC1, by Gerelsaikhan and Turner 2000) comprises 12 transmembrane (TM) segments with a relatively small amino-terminus and a large carboxy-terminus, both of which are intracellular (Figure 1.4). All KCC isoforms exhibit a long extracellular loop between the fifth and sixth TM domains, whereas the two NKCC isoforms present a large extracellular sequence between the seventh and eighth TM segments; these regions contain extracellular sites for *N*-linked glycosylation (Hebert *et al*., 2004).

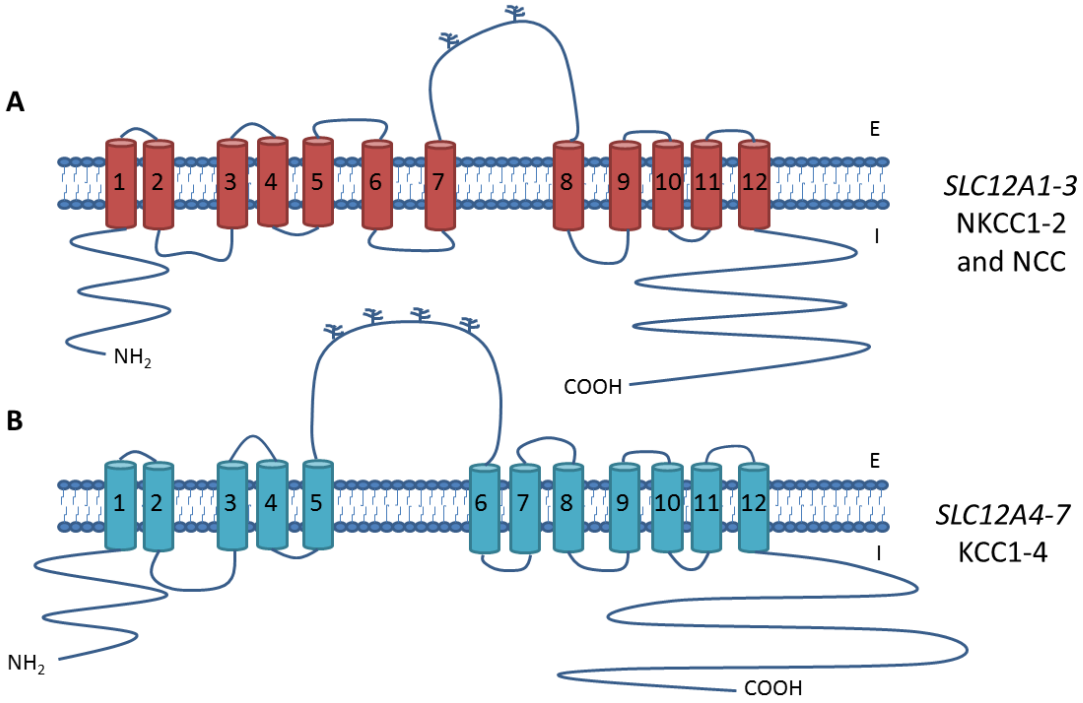

Figure 1.4. Schematic diagram of the secondary structure of the cation chloride co-transporter (CCC) family. (**A**) Chloride importers (NKCC1-2 and NCC) and (**B**) extruders (KCC1-4) of the SLC12A family of proteins all share a similar topology. Each CCC comprises 12 transmembrane (TM) domains, intracellular amino (-NH2) and carboxyl (COOH) terminals and a larger extracellular loop containing sites for N-glycosylation. This larger extracellular loop appears between TM 7 and 8 in NKCC1-2 peptides and NCC with two N-linked glycosylated extracellular (E) domains. However, in KCC1-4 the larger extracellular loop is located between TM domains 5 and 6 with four N-linked glycosylation sites.

1.8.3 Reversal of the Cl^- gradient in neuropathologies

In early neuronal development (Rivera *et al*., 1999), and in certain pathological states, such as, cerebral oedema, traumatic and ischemic brain injury, temporal lobe epilepsy, schizophrenia, Andermann syndrome, Bartter syndrome and cancer, the normal gene expression patterns of CCCs appear altered (Uyanik *et al*., 2006; Benarroch 2013; Kaila *et al*., 2014; Kahle *et al*., 2015). In many cases, the changes in the expression of the CCCs lead to a reversal of the chloride gradient in neurons, resulting in subsequent $GABA_AR$-mediated excitation (Figure 1.3; Huberfeld *et al.*, 2007).

1.8.4 NKCC1

1.8.4.1 NKCC1 in early development

Under physiological conditions, the activity of NKCC1 modulates the intracellular chloride concentration in neurons, glia, BBB endothelial cells, and choroid plexus epithelial cells (Gerelsaikhan and Turner 2000). Thereby maintaining cellular volume against changes in extracellular osmolality and intracellular solute content to prevent either excessive cell swelling or shrinkage (Kahle *et al*., 2009). In rodents, during embryonic and early postnatal life, NKCC1 shows robust expression, promoting an influx of chloride ions into the neuron that ultimately triggers GABA-mediated excitation and, hence, depolarisation (Figure 1.3 ; Pfeffer *et al*., 2009). This chloride influx is achieved through an electroneutral Na^+-K^+-$2Cl^-$ co-transport mechanism, coupled with the activity of the sodium-potassium ATPase, that leads to a $GABA_A$ receptor-mediated chloride efflux. The depolarising

GABA-mediated effect is necessary for normal mammalian brain development (Ben-Ari 2002; Wang and Kriegstein 2008).

1.8.4.2 NKCC1 splice variants

There are two different splice variants of NKCC1 termed NKCC1a and NKCC1b. Both are functional and ubiquitously expressed, but a considerably higher expression of the NKCC1b mRNA is detected in the adult brain (Vibat *et al*., 2001). Furthermore, NKCC1b appears to undergo a more robust up-regulation during development compared to NKCC1a (Morita *et al*., 2014). The difference between these two NKCC1 isoforms is a 16 amino-acid insertion encoded by exon 21 in the carboxy-terminus of NKCC1a, which contains a protein kinase A phosphorylation site (Blaesse *et al*., 2009). Four novel splice variants of NKCC1, and changes in their expression, have recently been identified in brain, associated with schizophrenia and early brain development (Morita *et al*., 2014).

1.8.4.3 NKCC1 regulation in stroke

In a rat model of focal cerebral ischemia/reperfusion injury, created via 2-hour middle cerebral artery occlusion (MCAO) and 24-hour reperfusion, NKCC1 transcript and protein expression were found to be significantly up-regulated in cortical neurons, as well as in lysates from rat cerebral cortex and striatum (Yan *et al*., 2003; Wang *et al*., 2014). Elevated extracellular concentration of potassium, glutamate and interleukin-6, which occur in cerebral ischaemia, are known to stimulate NKCC1 activity in both neurons

and astrocytes (Chen and Sun 2005). The stimulation of NKCC1 via extracellular potassium seems to be calcium-dependent, as the activity of NKCC1 in astrocytes is completely abolished by either blocking L-type voltage-dependent calcium channels with nifedipine or by the removal of extracellular calcium (Su *et al*., 2002).

Activation of NKCC1 is dependent on its phosphorylation state. Increased NKCC1 phosphorylation, on threonine184 and threonine189 (located in the intracellular amino-terminal domain; Figure 1.4) by either STE20 (sterile20)/SPS-1 related proline-alanine-rich kinase (SPAK) or oxidative stress response kinase (OSR1), which are both serine-threonine kinases, has been demonstrated to induce the activation of NKCC1 in mouse brain (Piechotta *et al*., 2002). Oestradiol increases SPAK and OSR1 expression in a transcription-dependent manner, which subsequently leads to increased phosphorylation of NKCC1 *in vivo* (Nugent *et al*., 2012). Oestradiol is, thus, believed to up-regulate the activity of NKCC1 and promote $GABA_AR$-mediated depolarisation (Mccarthy 2009). In a rat focal ischaemia model, oestradiol treatment has been shown to promote neurogenesis in the subventricular zone of the brain, improving neurological outcome (Zheng *et al*., 2013). This suggests that oestradiol has the potential to promote neurorehabilitation following stroke and that this effect might be due to the up-regulation of NKCC1 activity via oestradiol, promoting $GABA_AR$-mediated depolarisation.

Co-expression of WNK3 (with-no-lysine kinase 3) and NKCC1, in neurons, results in robust phosphorylation of threonine212 and threonine217, two

other known regulatory sites in NKCC1, and a consequent increase in NKCC1 activity (Kahle *et al*., 2005; Begum *et al*., 2015). The amino-terminus of NKCC1 contains a highly conserved RVNFVD sequence, which is the target of protein phosphatase 1, which recognises the consensus motif: RVXFXD; when this sequence is mutated, NKCC1 activity is increased (Gagnon and Delpire 2010). Also, calyculin A, a protein phosphatase 1 inhibitor, restores the activity of NKCC1 (Dowd and Forbush 2003).

1.8.4.4 Pharmacological modulation of NKCC1 in stroke

Several studies have implicated NKCC1 in the development of oedema and cell death after the onset of stroke, suggesting that blocking NKCC1 might be a potential neuroprotective target (Kahle *et al*., 2009; Szydlowska and Tymianski 2010; Begum *et al*., 2015). The NKCC1 antagonist bumetanide, significantly attenuated neuronal sodium overload and decreased cell death in a pharmacological study, with a concurrent decrease in infarct volume and brain oedema (Chen *et al*., 2005). Bumetanide administration, after focal cerebral ischaemia in rats given 1 week after ischemia, and continued for 3 weeks, increased behavioral recovery and promoted neurogenesis 28 days post-insult (Xu *et al*., 2016). Low concentrations(2-10 μM) of bumetanide can be used to inhibit NKCCs *in vitro* without significantly affecting KCCs function; however, higher concentrations have been shown to antagonise both NKCC1 and KCC2 function (Payne *et al*., 2003; Hamidi and Avoli 2015). Similar effects were seen in mice deficient for the NKCC1 gene compared to wild-type controls (Chen *et al*., 2005). NKCC1 is expressed at the luminal side of endothelial cells of the BBB, where it can come into contact with

intravenously-administered bumetanide, which decreases brain oedema (O'Donnell *et al*., 2004).

Bumetanide has poor pharmacokinetic properties that limit its access to BBB-protected brain areas (Cleary *et al*., 2013). Therefore, bumetanide pro-drugs that mask the hydrophilic carboxyl group with esters are currently being tested as anti-stroke therapies and in other neurological disorders, such as epilepsy (Töllner *et al*., 2014; Erker *et al*., 2016). This masking facilitates transport into the brain, where the active molecule is released (Löscher *et al*., 2013). Bumetanide due to its role in diuresis, has been widely prescribed for chronic conditions, such as hypertension, broncho-pulmonary dysplasia, nephritic syndromes and heart congestion with few side effects. In the treatment of neurological conditions such as autism, the only side-effect observed in 30% of children in a randomised trial, was hypokalaemia, which could be easily overcome with a potassium-containing syrup (Lemonnier *et al*., 2012). This study showed a significant reduction in the severity of autism and Asperger syndrome in children. However, severe problems such as diuresis, hypokalemic alkalosis, and hearing loss have been related to the use of bumetanide *in vivo* (Puskarjov *et al*., 2014; Pressler *et al*., 2015); these effects should be critically taken into account when evaluating clinical work that utilises bumetanide for the treatment of neurological conditions in children.

In low oxygen conditions, such as in brain ischaemia after stroke, a series of molecular cascades are activated. The most important is driven by HIF-1α, which triggers the transcription of a number of genes involved in cell

proliferation and survival, glucose and iron metabolism, and angiogenesis (Ke and Costa 2006, see section 1.5). A recent study has highlighted the involvement of NKCC1 in mediating neurogenesis after traumatic brain injury through the activation of CREB and the HIF-1α pathway and proposed the HIF-1α-mediated up-regulation of NKCC1 (Lu *et al*., 2015). All of the above information indicates that either specifically blocking the activity of NKCC1 or down-regulating its expression may offer a useful neuroprotective strategy in ischaemic stroke. However, in the long term following an ischaemic event, increasing NKCC1 expression/activity might be beneficial to promote neurorehabilitation.

1.8.5 KCC2

KCC2 opposes the activity of NKCC1 by extruding chloride (Figure 1.3). There are two splice variants of KCC2, KCC2a and KCC2b, both functional; the KCC2b isoform is up-regulated after birth in rodents and is considered to be the isoform responsible for the developmental shift in the GABAergic response (Rivera *et al*., 1999). This developmental shift in humans takes place at the beginning of the last trimester of gestation (Sedmak *et al*., 2015). KCC2b differs in its 5'-untranslated region and 5'-coding region compared to KCC2a. Thus, the resulting protein isoform has a distinct amino-terminus and is 23 residues shorter than KCC2a (Uvarov *et al*., 2007). The two isoforms are generated by the use of alternate promoters, and alternate first exons that provide the complexity needed for the observed temporal-specific gene expression patterns (Uvarov *et al*., 2007).

1.8.5.1 KCC2 function and regulation

KCC2 exhibits a unique feature in that it is expressed only in central nervous system neurons, where, alongside NKCC1, plays a crucial role in the regulation of neuronal excitability and development of the postnatal brain (Figure 1.3 ;Payne *et al*., 1996; Rivera *et al*., 1999). Furthermore, independent of its ion transport role, it has been linked to glutamatergic dendritic spine formation (Li *et al*., 2007; Fiumelli *et al*., 2013; Llano *et al*., 2015). KCC2 is responsible for maintaining a low $[Cl^-]_i$ in neurons by extruding chloride ions and, thus, producing a hyperpolarising effect when GABA and glycine bind to their cognate receptors, resulting in inhibition of synaptic transmission (Figure 1.3; Rivera *et al*., 1999; Blaesse *et al*., 2009). The restricted expression pattern of KCC2 is guaranteed by the presence in its gene sequence of a neuronal transcription factor Egr4 binding site, which enhances KCC2 expression, and neuron restrictive silencing elements (Uvarov *et al*., 2005; Uvarov *et al*., 2006). The neuropeptide oxytocin has recently been shown to participate in the developmental up-regulation of KCC2, that ultimately induces the switch in GABA-mediated function, by promoting KCC2 phosphorylation and insertion of the co-transporter into the neuronal membrane (Leonzino *et al*., 2016). However, projections from oxytocinergic nuclei have only a relatively small number of targets (Boccia *et al*., 2013), yet developmental up-regulation of KCC2 is seen in the vast majority of central nervous system neurons (Sedmak *et al*., 2015), implying other regulatory mechanisms.

Studies with mice deficient for KCC2 reveal the importance of this co-transporter in neuronal function, because its absence leads to death after birth due to respiratory failure (Hübner *et al*., 2001). Specific deletion of the KCC2b isoform ($KCC2b^{-/-}$) in mice produced low body weight and generalised seizures were observed (Woo *et al*., 2002). Finally, in an interesting investigation by Tornberg et al., (2005), a reduction in the expression of both isoforms to 17% of their normal values, led to increased anxiety, difficulty in spatial learning, and impaired sensitivity to thermal and mechanical stimuli. RNA interference, using short-hairpin RNAs, has also been used to knock down KCC2 expression in the rat (Pellegrino *et al*., 2011). Suppression of KCC2 function reduced neuronal resistance to toxic insults such as lipofectamine-mediated oxidative stress and NMDA receptor activation. On the contrary, over-expression of KCC2, in the mouse, increased neuronal resistance to these insults (Pellegrino *et al*., 2011). Although the other members of the KCC family are not predominant in the brain, following NMDA treatment, over-expression of KCC3 also increased neuronal survival, indicating the importance of potential compensatory mechanisms exerted by other KCC members (Pellegrino *et al*., 2011). KCC3 has also been shown to participate in cell volume homeostasis (Adragna *et al*., 2015), and its deletion leads to locomotor deficits (Ding and Delpire 2014). KCC4-deficient mice are deaf due to a rapid degeneration of hair cells within the ear (Boettger *et al*., 2002). These data suggest the importance of KCCs as potential neuroprotective targets; this is underscored by the neurological phenotypes of transgenic, particularly for KCC2, KCC3 and KCC4 (Gagnon and Delpire 2013).

BDNF and its receptor tropomyosin-related kinase B/tyrosine receptor kinase B (TrkB) are thought to be involved in the regulation of the mRNA that encodes KCC2b (Ludwig *et al*., 2011). For the down-regulation of KCC2, two different intracellular TrkB signalling cascades are required: src homology 2 domain-containing transforming protein (Shc) and phospholipase Cγ (Puskarjov *et al*., 2012). Interestingly, when only the Shc pathway is activated, up-regulation of KCC2 occurs. However, mice deficient for BDNF showed that this molecule is not necessary for the developmental up-regulation of KCC2 expression, but is essential for the triggering of neonatal seizures (Puskarjov *et al*., 2015). Calcium and BDNF are responsible for the activation of calpain, which mediates the cleavage of a fragment from KCC2 that is essential for its' function (Puskarjov *et al*., 2012). Its regulation is important for the changes in neuronal plasticity, mediated by KCC2, in different pathological states and during development.

1.8.5.2 KCC2 role in different neuropathologies

Changes in the expression of KCC2 have been observed in different neuropathologies, such as schizophrenia (Hyde *et al*., 2011), epilepsy (Huberfeld *et al*., 2007), and traumatic and ischaemic brain injury (Kahle *et al*., 2008). In post-mortem samples from schizophrenic patients, down-regulation of KCC2 mRNA was observed by Hyde *et al*. (2011); in contrast, others have not found any difference, but did observe up-regulation of the transcripts for the kinases, WNK3 and OXSR1 (Arion and Lewis 2011). For temporal lobe epilepsy, the data derive from biopsies and relate to mRNA levels of KCC2 as detected by *in situ* hybridisation (Huberfeld *et al*., 2007).

In animal models of traumatic and ischaemic brain injury, KCC2 mRNA and protein have been reported to be down-regulated (Bonislawski *et al*., 2007; Jaenisch *et al*., 2010; Wu *et al*., 2016).

Stimulation of the AMPA/BDNF signalling pathway promotes motor recovery after stroke (Clarkson *et al*., 2011). It is conceivable that this recovery is aided by down-regulation of KCC2 expression via BDNF. The effect of this might be to produce a switch in $GABA_AR$-mediated signalling, and promote neuronal depolarisation. This possibility is supported by another investigation (Clarkson *et al*., 2010) that found that reducing extrasynaptic GABAergic tonic inhibition promoted post-stroke functional recovery (Figure 1.4). Type II ampakines bind to AMPA receptors producing slow deactivation and desensitisation, increasing the expression of BDNF and inducing its release (Simmons *et al*., 2009). Prolonged AMPA receptor activation via glutamate, and the action of BDNF, both promote neuronal remodelling and LTP (Clarkson *et al*., 2011). BDNF binds to the TrkB receptor and, via the CREB pathway, down-regulates KCC2 gene expression (Figure 1.5). This modifies the chloride balance across the membrane, decreasing extracellular levels of chloride and causing a decrease in GABA-mediated inhibition that further contributes to LTP and neuronal remodelling. Finally, L655,708 specifically targets α5-subunit-containing $GABA_A$ receptors and might, therefore, decrease the elevated tonic inhibition in extra-synaptic circuits of cortical neurons in the peri-infarct zone (Clarkson *et al*., 2010).

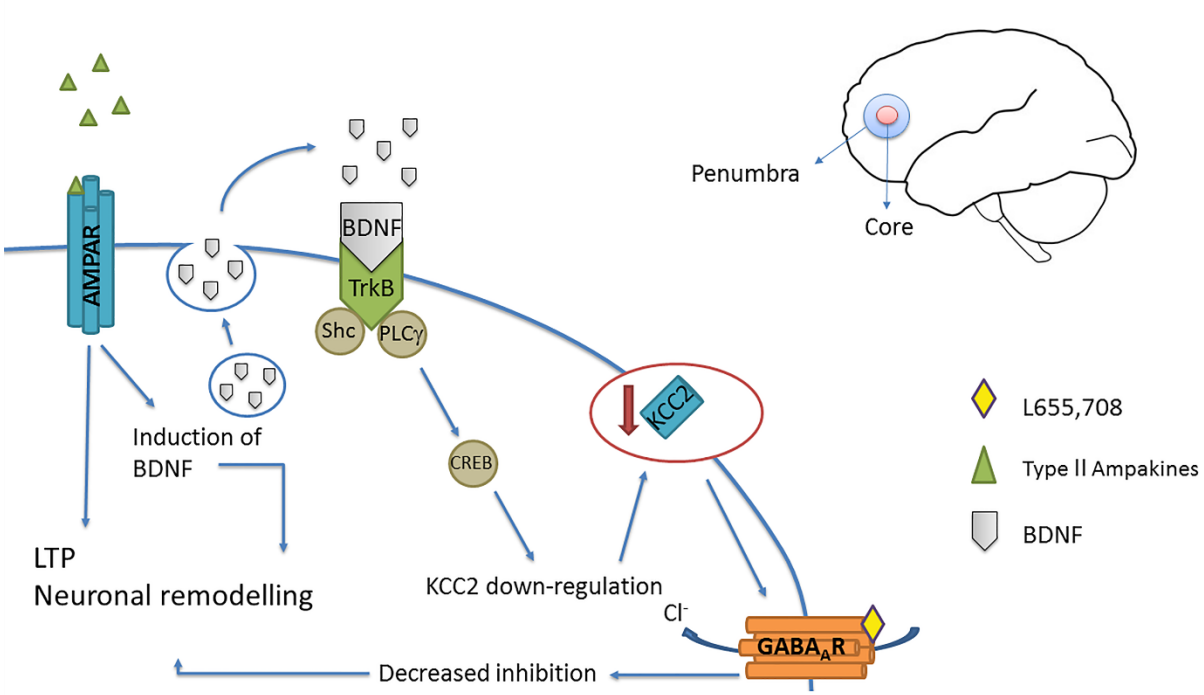

Figure 1.5. Post-stroke neurorehabilitation model in the penumbra. Two potential molecular pathways could promote long term potentiation (LTP), and neuronal remodeling, in the peri-infarct zone (penumbra) through treatment with type II ampakines and the α5-specific $GABA_AR$ inverse agonist, L655,708. BDNF: brain-derived neurotrophic factor; TrkB: tropomyosin-related kinase B/tyrosine receptor kinase B; Shc: src homology 2 domain-containing transforming protein; PLCγ: phospholipase Cγ; $GABA_AR$: γ-Aminobutyric acid type A receptor.

1.8.5.3 KCC2 in stroke

Following six hours of the 4-vessel occlusion model of ischaemic stroke in mice, KCC2 protein was shown to be increased in the dendritic regions of pyramidal cells in the *cornu Ammonis* 1 (CA1) region of the hippocampus, showing no morphological signs of damage (Lin *et al*., 2015). In the same

tissue, 48 hours after stroke induction, the CA1 pyramidal cells begin to degenerate, and a progressive down-regulation of both KCC2 and HSP72 (heat shock protein 72) expression is observed. An increase or decrease of HSP72 expression has been found to exacerbate or attenuate hypothalamic neuronal death respectively (Lin *et al*., 2015), and is considered a biomarker of the penumbra (Agulla *et al*., 2014). Interestingly, parvalbumin-containing interneurons, which possess strong KCC2 gene expression, and glutamatergic input, readily survive even in regions of complete pyramidal cell loss (Papp *et al*., 2008). The high expression of KCC2, together with extremely low expression of NMDA receptors (Nyíri *et al*., 2003), and the high number of extrasynaptic $GABA_A$ receptors, may explain the extraordinary resistance of parvalbumin-containing interneurons to ischemia in CA1 pyramidal cells (Papp *et al*., 2008). Furthermore, there is an up-regulation of KCC2 in the hippocampus of patients with temporal lobe epilepsy (Karlócai *et al*., 2016). These data suggest that up-regulation of KCC2 might participate in the protection against cell death, at least in the hippocampus.

A study by Jaenisch and colleagues (2010), showed a decrease in KCC2 expression following transient focal cerebral ischemia in rats. The investigation showed that the long-term survival of neurons in the ischaemic core required a maintained expression of KCC2; these cells were identified as GABAergic parvalbumin-expressing interneurons. The identification of either KCC2 specific activators or allosteric modulators, that reduce $[Cl^-]_i$, could have a critical impact on neurorehabilitation strategies. Optimisation of the first-in-class arylmethylidine family of compounds resulted in the identification of a KCC2-selective analogue (CLP257) that lowers $[Cl^-]_i$.

Furthermore, CLP257 restored impaired chloride transport in neurons with diminished KCC2 activity, and alleviated hypersensitivity in a rat model of neuropathic pain (Gagnon and Delpire 2013). CLP257 has recently been used in an *in vitro* model of ictogenesis, together with the non-specific KCC2 inhibitor VU0240551, to demonstrate the role of KCC2 in modulating the epileptic response (Hamidi and Avoli 2015). However, VU024055 has serious off target effects, which limit its usefulness for studies on KCC2 (Delpire *et al*., 2012). A specific KCC2 antagonist, VU0463271, has been developed (Delpire *et al*., 2012), and used to induce epileptiform discharges (Sivakumaran *et al*., 2015). It has also been used to demonstrate the critical role of KCC2 in regulating seizure event duration (Kelley *et al*., 2016).

1.9 Spatial and temporal vulnerability to ischaemia

Ischaemia affects the brain in a differential manner. The most susceptible areas are the neocortex, the dorsolateral striatum, and the CA1 region of the hippocampus (Baron *et al*., 2013). The hippocampus has long been known to present a selective vulnerability to ischaemia, and there the CA1 layer seems to be the most sensitive region, while the dentate gyrus appears to be the most resistant (Schmidt-Kastner 2015). However, in contrast to cortical cell death, which is rapid in onset, neuronal loss in CA1 is delayed (occurring three to five days after insult). This delayed neuronal death, and its molecular basis, are not yet fully understood. Interestingly, this vulnerability appears to be age-dependent, because older animals suffer a greater neuronal loss after ischaemia than younger animals (Llorente *et al*., 2013; Lalonde and Mielke

2014). Finally, it is important to acknowledge that the use of KCC2 as a therapeutic target in stroke could be challenging due to the differential expression timing between the chronic and recovery phase, as increasing KCC2 expression could protect against injury, but decreasing KCC2 levels could promote recovery in the days following injury.

1.10 Summary and general aims

The penumbra is recruited in the hours to days following stroke into the ischaemic core. Therefore, reducing the penumbral tissue at risk of infarction increases recovery of stroke patients. However, to understand how the penumbra can be salvaged, we need to understand how it evolves after stroke. Recent studies have highlighted the potential of cation chloride co-transporters as targets for the development of neuroprotective strategies in stroke both in the short term, to reduce the excitotoxic effect observed in the development of the penumbra, and in the long term, to promote functional recovery. KCC2 is thought to be down-regulated following an ischaemic insult, whereas NKCC1 is suggested to be up-regulated. The reversal of the chloride gradient decreases $GABA_AR$-mediated inhibition contributing to the excitotoxic effect described above. Increasing KCC2 and decreasing NKCC1 expression/activity seems to be an obvious neuroprotective strategy. However, KCC2 inhibition also seems to provide a novel strategy to promote axonal growth and neuronal remodeling in the long term. Therefore, understanding the timing of these changes, in detail, using well characterised models, could play a pivotal role in future therapeutic strategies.

In order to study the impact of CCC expression on neuronal loss following ischaemic stroke, two different models were developed:

1. An *in vitro* model of hypoxia with the neuron-like PC12 and NT2 cells. This model was created to mimic the effect of a stroke in neurons in order to study the mechanisms that lead to neuronal adaptation after hypoxic insult.

2. An *in vivo* model of photothrombotic stroke (PTS). This model was created to characterise the evolution of tissue damage in the mouse PTS model of ischaemic stroke and for the first time quantify the spread of the glial scar and the penumbra in the days following PTS in order to physically and molecularly establish the parameters of the peri-infarct zone.

Aim 1: To investigate molecular mechanisms of neuronal adaptation to acute hypoxic stress in neuronal-like cells *in vitro*.

Aim 2: To characterise the penumbra following photothrombotic stroke in mice by establishing appropriate markers to study the extent and evolution of the penumbra.

Aim 3: To investigate the impact of ischaemic stroke on the expression profile of the CCCs and assess their role as potential neuroprotective targets.

2. Materials and Methods

***Reagents and chemicals*:** All reagents and chemicals were obtained from Sigma Aldrich (Gillingham, UK) or Thermo Fischer Scientific (Paisley, UK) unless otherwise specified.

2.1 Cell lines

Cells were obtained from the American Type Culture Collection (ATCC). The PC12 cell line is derived from a transplantable rat pheochromocytoma of the adrenal medulla (Greene *et al*., 1976). The NTERA-2 cl.D1 (NT2) cell line is derived from a pluripotent human testicular embryonal carcinoma. MCF-7 cells were a generous gift from Dr Jenny Fraser at passage number 5. MCF-7 is a human breast adenocarcinoma cell line that was used as a positive control for hypoxia experiments as previous studies have shown they display a strong response to hypoxic insult (Bando *et al*., 2003).

2.2 Cell culture media and conditions

Dulbecco's modified Eagle's media (DMEM) was supplemented with 10% (v/v) heat-inactivated foetal bovine serum (FBS), penicillin (10 units/mL) and streptomycin (10 µg/mL) (P/S) (complete culture media). Cells were grown at 37 °C in 5% (v/v) CO_2 atmosphere under high humid conditions. Medium was changed twice per week and cultures were passaged at a ratio of 1:6 once per week or when they reached confluence. Cells were maintained

under these conditions unless otherwise specified. PC12 cells were cultured in complete culture media plus 5% (v/v) horse serum. All experiments were performed with cells at passage number 2 to 20.

2.2.1 Passaging cells

When cells reached approximately 90% confluency, they were washed with phosphate buffered saline (PBS) and incubated for 5 minutes with 3 mL trypsin/ethylenediaminetetraacetic acid (EDTA) 0.05% (v/v,) at 37ºC. Following detachment, the enzymatic activity of trypsin was neutralised by adding 6 mL of complete culture media. Cell pellets were collected by centrifugation at 170g for 3 minutes at room temperature (Hettich Zentrifuggen, Tuttlingen, Germany; Universal 230R). The cell pellet was resuspended in 10 mL of complete cell culture media. A ratio of 1:10 cells were then reseeded into a new T75 flask (Corning, Wiesbaden, Germany).

2.2.2 Cryopreservation of cells

In order to freeze cells, confluent flasks were harvested by trypsinisation and collected by centrifugation as previously described (section 2.2.1). The cell pellet was resuspended in freezing media (10% (v/v) dimethyl-sulfoxide (DMSO) in 90% (v/v) FBS) and $3x10^6$ cells were aliquoted in 1.5 mL cryovials (Simport, Beloeil, Canada, PK/100). Vials were transferred to -80ºC wrapped in standard blue tissue roll in order to decrease the freezing rate. Vials were then transferred into liquid nitrogen for long-term storage.

2.2.3 Cell counting

A Neubauer improved bright line haemocytometer (Marienfeld, Lauda-Königshofen, Germany) was used to determine cell number and concentration. Following trypsinisation, cell pellets were resuspended in complete media and 100 µL of the cell suspension was transferred into a 1.5 mL microfuge tube, diluted 1:1 (v/v) with Trypan blue and 10 µL was pipetted onto the haemocytometer. Trypan blue is a dye exclusion method as it stains non-viable cells by traversing their damaged membrane while living cells, with an intact membrane, are not stained (Strober 2001). Four 4x4 grids on the haemocytometer were counted and a viable:non-viable ratio recorded and averaged. This was multiplied by the dilution factor and by 10^4 (volume of a grid is 1 mm^2 surface area x 0.1 mm depth = 10^{-4} cm^3 or 10^{-4} mL), giving the total viable cells/mL.

2.2.4 Poly-L-lysine coating

Cell vessels for the PC12 cell line were coated with poly-L-lysine. A 0.1 mg/mL solution was prepared in dH_2O and surfaces were coated with 1 mL of the solution per 25 cm^2. Flasks or plates were incubated for 5 minutes at 37ºC before the solution was removed and surfaces thoroughly rinsed with dH_2O and allowed to dry for at least 2 hours at room temperature.

2.3 Differentiation of cell lines

2.3.1 PC12 cells

PC12 cells differentiate into a neuronal like phenotype following treatment with nerve growth factor (NGF) with a reversible loss of mitotic activity *(*Greene *et al*., 1976).

Cells were seeded in 6-well plates at a density of $2x10^6$ cells/well in a final volume of 2 mL and cultured under standard conditions for 24 hours prior to treatment. The media was removed and differentiation media (200 nM NGF, 1% (v/v) horse serum and 1% (v/v) penicillin-streptomycin on DMEM) was added to the cultures. Differentiation media was changed every 2-3 days over 7-8 days. Cell morphology was analysed at different time points during differentiation via bright field microscopy and images were captured using an inverted microscope and camera (Zeiss, Primovert and Axiocam) at 20X magnification.

2.3.2 NT2 cells

Human NT2 cells can be induced to differentiate into neuron-like cells following retinoic acid (RA) treatment (Andrews, 1984). NT2 cells were differentiated into a neuronal population following the method described by Pleasure *et al*. (1992). Cells were seeded at a density of 1 $x10^6$ into a T75 flask. Complete culture media supplemented with all-trans-retinoic acid (ATRA, 10^{-5} M) was added to the culture after 24 hours. Cells were grown for 4 weeks and ATRA-enriched media was changed twice per week. After 4

weeks of ATRA treatment, cells were passaged at a ratio 1:6 into new culture flasks. This was done by incubating in trypsin for 30 seconds to dislodge the cells. Cells were then washed, centrifuged and replated into a new flask. When the cells were replated, the culture media was supplemented with the mitotic inhibitor cytosine arabinoside (1 μM) and 10 μM fluorodeoxyuridine and cells were incubated for 2 weeks with media changes every 3-4 days.

2.4 Harvesting cells

In order to harvest cells, flasks were incubated on ice and washed twice with cold PBS. Cells were then detached with a cell scraper into 10 mL of PBS and cell pellets collected by centrifugation at 170g for 3 minutes at 4°C. Cell pellets were stored at -80 °C or immediately used.

2.5 Induction of hypoxia *in vitro*

A modular hypoxia chamber (Billups-Rothenberg, Inc. Del Mar, CA, USA) provides an excellent platform to simulate hypoxic conditions. Following differentiation (section 2.3), culture media was replaced with fresh differentiation media and flasks were placed into the modular chamber. The lid was attached and a gas mixture of 1% O_2 and 99% N_2 at (BOC, 230 bar, 121852-V, Cambuslang, Glasgow, UK) was used to flush the chamber at a flow rate of 20 L/minute for 10 minutes. The chamber containing the cells was placed into the incubator at 37°C. After 1 hour, the chamber was removed and purged with 1% O_2 and 99% N_2 for a further 10 minutes in order

to remove any oxygen released by the media. Finally, the chamber was returned to the incubator for the desired experimental exposure.

2.6 Cell viability assays

2.6.1 3-(4,5-dimethylthiazol-2-yl)-2,5-diphenyltetrazolium bromide (MTT)

Mitochondrial metabolic activity was assessed through the MTT colorimetric assay (Mosmann 1983). This method is based on the reduction of tetrazolium into the purple product formazan by active dehydrogenases present in mitochondria. The increase in formazan product is therefore proportional to the amount of metabolically active cells. Briefly, cells were seeded at a concentration of 10^5 cells/well in 100 µL of complete culture media in a 96-well plate 24 hours prior to the experiment. MTT was prepared as a 5 mg/mL stock solution in PBS. Media was removed and fresh complete culture media was added to each well with 10 µL/well of the stock MTT (0.5 mg/mL). Negative controls contained media only without any cells. As a positive control, 10 µL of 0.5% (v/v) triton X-100 solution was added to kill the cells. Triton X-100 is a strong detergent that can be used to lyse cells and obtain a controlled value of 100% cell death. The 96-well plate was then incubated for 4 hours at 37°C. The converted MTT product was solubilised by adding 100 µL of 0.01M HCl in isopropanol into the media. Absorbance was measured at 570 nm and 680 nm using a plate reader (Elisa Reader LT-5000MS, LabTech International Ltd., Uckfield, UK) and data analysed using Labtech Manta Lite software (LabTech International). Absorbance was normalised by subtracting the 680 nm reference readings and the blank

readings to the 570 nm values of the samples. Normoxic cells were considered to represent 100% in viability and results were expressed as a percentage in viability compared to normoxic conditions.

2.6.2 Alamar blue®

Alamar blue® can also be used to determine cell viability. It is based on the same principle as the MTT as it relies on the conversion of resazurin to the fluorescent molecule, resorufin by mitochondrial dehydrogenases (Fields and Lancaster 1993). It presents the advantage of being non-toxic to cells and thus, it can be readily added during the experimental exposure. Cells were seeded at 10^5 cells/well in a 96-well plate in 100 µL of complete culture media and incubated under standard conditions. After 24 hours media was removed and 100 µL of fresh complete culture media was added to each well. Alamar blue® was added at a final concentration of 10% (v/v) to each well. Negative controls were included containing media only without any cells. As a positive control, 10 µL of 0.5% (v/v) triton X-100 solution was added to lyse the cells. AlamarBlue® can be detected by absorbance. Absorbance was monitored at 550 nm, using 600 nm as a reference wavelength to normalise using a plate reader (Elisa Reader LT-5000MS, LabTech International), and data analysed using Labtech Manta Lite software (LabTech International).

2.7 Isolation of RNA

2.7.1 Diethylpyrocarbonate (DEPC) treatment of distilled water

DEPC is a nonspecific inhibitor of RNases. It is typically used to treat water and solutions before working with easily degraded RNA. In order to prepare a 0.1% (v/v) DEPC solution in distilled water the desired volume, solution was incubated overnight at room temperature and subsequently autoclaved (2150 mBar, 121°C) in order to inactivate any trace of DEPC. DEPC-treated water was used for all subsequent RNA/DNA analyses.

2.7.2 Isolation of total RNA

Cells were harvested as previously described (section 2.4) and cell pellets homogenised by resuspending in Tri® reagent (Ambion®, Paisley, UK) at a ratio of 1 mL per 1 $x10^6$ cells. To ensure complete dissociation of nucleoprotein complexes, samples were incubated 5 minutes at room temperature. Following this, 100 µL of 1 bromo-3-chloropropane per mL of Tri® used was added to the sample. Samples were vortexed and incubated at room temperature for 5 minutes prior to centrifugation at 12,000g (Centrifuge 5415R, Eppendorf®, Stevenage, UK) for 15 minutes at 4°C. The aqueous phase, containing RNA, was transferred to a fresh tube and 500 µL of 2-propanol per mL of Tri® was added and samples incubated 5 minutes at RT. After centrifugation at 12,000g for 10 minutes at 4°C, the supernatant was removed and the pellet was washed by adding 1 mL of 75% (v/v) ethanol per mL of Tri® reagent. A final centrifugation at 7,500g for 5 minutes at 4°C was performed before the RNA pellet was air dried for 10 minutes and

resuspended in an appropriate volume of 0.001% (v/v) DEPC (diethylpyrocarbonate) treated H_2O (DNase- and RNase-free H_2O).

2.7.3 Determining the integrity and purity of extracted RNA

The purity and integrity of extracted RNA was assessed by fluorescence using the Agilent 2100 Bioanalyzer (Agilent Technologies Ltd., Stockport, UK). This gives the concentration of the RNA, absorbance ratios at A260/280, indicates any protein contamination, and provides an RNA integrity number (RIN). All samples were prepared according to the manufacturer's protocol with the Agilent RNA600 Nano Kit (Agilent Technologies Ltd, 5067-1511). Briefly, each sample was analysed on an RNA chip which contains an interconnected set of microchannels that is used for separation of nucleic acid fragments based on their size as they are driven through it electrophoretically. Values were calculated by the 2100 Expert Software (Agilent Technologies Ltd). All samples used in further experiments had an A260/280 ratio above 1.8 and a RIN above 7.5 to ensure the quality of the extracted RNA.

2.8 DNase treatment of RNA samples prior to real-time quantitative polymerase-chain-reaction (qPCR)

To eliminate genomic DNA from the extracted RNA sample, DNase digestion was performed containing 1 µg of RNA in DEPC-H_2O, 1 µL of RQ1 RNase-free DNase 10 X reaction buffer, 1 U/µg of RNA RQ1 RNase-free DNase (Promega, Huntingdon, UK) and DEPC-treated water in a final volume of 10

µL. Samples were incubated at 37°C for 30 minutes and 1 µL of RQ1 DNase Stop Solution was added to terminate the reaction. Samples were incubated at 65 °C for 10 minutes in order to inactivate the DNase.

2.9 Reverse transcription (RT) of RNA to generate complementary cDNA

RNA samples were reverse transcribed in order to synthesise cDNA for subsequent use in quantification of gene expression via qPCR. The nanoScript 2 Reverse Transcription (RT) premix kit (Primer Design, Southampton, UK) was used in all experiments. This kit contains an optimised blend of random nonamer and oligo dTs. Following the manufacturer's protocol, 20 µL of RT premix was dispensed into thin-wall tubes together with 1 µg of RNA in a final volume of 25 µL per reaction. Reactions were incubated at 42°C for 20 minutes and then at 72°C for 10 minutes in order to heat inactivate the enzyme. Negative controls included reactions containing cDNA from a reaction without reverse transcriptase. Reactions were performed using a thermal cycler (2720 Thermal Cycler, Applied Biosystems ®, UK) and cDNA was either used immediately in qPCR or stored at -20°C.

2.10 Quantification of gene expression

2.10.1 Oligonucleotides design and preparation

All oligonucleotides were designed according to the general criteria for qPCR (Thornton and Basu, 2011): 40-60 G+C % (guanine and cytosine), T_m (melting temperature) between 58-64°C, 18 to 24 nucleotides in length, and produce a 80-250 base pair (bp) product (Table 2.1). Oligonucleotide pairs were designed to include exon boundaries either in the oligonucleotide itself or the sequence amplified and thus, avoid genomic amplification. Oligonucleotides were designed using rat and human sequences from the National Centre for Biotechnology Information (NCBI) gene database (www.ncbi.nlm.nih.gov/). To verify that the amplicon was present in the different isoforms of each transcript, some of the oligonucleotides were aligned with human sequences of the different human isoforms if they have not yet been described in rat. When genes were highly conserved between species, it was assumed that rat present the same isoforms as human. All alignments were performed with an online DNA alignment tool from JustBio software and mRNA sequences were obtained from NCBI. Oligonucleotides were synthesised by Eurofins MWG Operon (Ebersberg, Germany).

Each lyophilised oligonucleotide was pulse-centrifuged to collect the material at the bottom of the tube and resuspended in H_2O to a stock concentration of 100 µM and stored at -20°C. All oligonucleotide were diluted to 6 µM in DEPC water prior to qPCR analyses.

Table 2.1. **PCR oligonucleotides designed for specific amplification of specific gene transcripts**. Forward (F) and reverse (R) oligonucleotides used for mRNA expression.

Target gene	Sequence 5'-3'	Species specificity
CA9	F: AGGGTGTCATCTGGACTGTG R: TGTGTGGCTCGGAAGTTCAG	Human/Rat
Caspr1	F: TGACTCTGAACTTGGAGGGTCGTG R: TATAGCGCATCCATGTGCCAGTCT	Human/Rat
CD44	F: GGATCAGGCATTGATGATGATGA R: TTGGGTTCCACTGGGTCC	Human/Rat
CHOP	F: AGCTGGAAGCCTGGTATGAGG R: GTGCTTGTGACCTCTGCTGG	Human/Rat
Grp78	F: TATGGTGCTGCTGTCCAGG R: CTGAGACTTCTTGGTAGGCAC	Human/Rat
HIF-1α	F: GTACCCTAACTAGCCGAGGAAGAA R: GTGAATGTGGCCTGTGCAGT F: GCATCTCCACCTTCTACCC R: CTCTTTCCTGCTCTGTCTG	Human[1] Rat[2]
HIF-2α	F: ACCTGGAAGGTCTTGCACTGC R: TCACACATGATGATGAGGCAGG	Human/Rat
HIF-3α	F: AGGATTGCAGAAGTGGCTGG R: ATACTGCCCTGTTACTGCCTG	Human/Rat
NEFH	F: AGGAGTGGTTCCGAGTGAG R: GGAGATAACTGAGTACCGGC	Human/Rat
Nrn1	F: GCATCTGGTGAATAATCGCTCACG R: ACTGAAGGAGGCGACGACAATAGC	Human/Rat
PDI	F: TGCCCAAGAGTGTGTCTGAC R: CTGGTTGTCGGTGTGGTC	Human/Rat
Ptbp2	F: TTTGTCCGGTTCGGCAATGG R: GGACTACTGAGAACACTGCCTG	Human/Rat
SLC2A1	F: GCTGTGCTTATGGGCTTCTC R: CACATACATGGGCACAAAGC F: CCTTGCCTGAGACCAGTTGAA R: ACAGCAGGGCAGGAGTGTC	Human Rat[3]

Table 2.1 continued.

Target gene	Sequence 5'-3'	Species specificity
SLC2A3	F: CAATGCTCCTGAGAAGATCATAAAGG R: GAATTGCGCCTGCCAAAG	Human
	F: CGCCTGATTATTGGCATCTT R: TCCAAACCAAAGACCTGAGC	Rat[4]
SLC12A2	F: TTTAGTGAGAACTTTGGACCG R: AAGAGCGTTCCTTTGGGTATG	Human/Rat
Tmod1	F: GCTCTTGCTGAAATGCTGAA R: AAGGCTGGCTCTGGTTGTC	Human/Rat
Vimentin	F: AGATTCAGGAACAGCATGTCC R: AGCCTCAGAGAGGTCAGC	Human/Rat

References: [1]Dales *et al*., 2010, [2]Zhao *et al*., 2014, [3]Campen *et al*., 2016, [4]Weisova *et al*., 2009

2.10.2 qPCR

qPCR was carried out in 20 μL reactions containing 300 nM oligonucleotides, 1X PrimerDesign Precision qPCR Mastermix containing SYBR green, and 25 ng of cDNA in RNAse/DNAse free DEPC-H_2O. Negative controls included reactions containing cDNA from a reaction without reverse transcriptase (negative control) and cDNA replaced with nuclease-free water (template negative). Reactions were performed in triplicate in 96-well bright white plates (Primer Design) sealed with adhesive optical seals (Applied Biosystems). The reaction was performed in a thermal cycler, StepOne™ Real Time PCR system (Applied Biosystems). Instrument settings were as follows: 10 minutes at 95°C for enzyme activation plus 40 cycles of 15 sec at 95°C for denaturation and 1 minute at 60°C for the data collection. An additional step was performed in order to produce a melt curve of the amplicon by reading fluorescence as the temperature increased by 0.3 °C from 60 to 95 °C. This allowed the identification of single and specific amplified products. Data was analysed using StepOne™ Software V2.2 (Applied Biosystems, USA)

2.10.3 Relative quantification of mRNA levels

The mean cycle threshold (Ct) determined for the reference gene was used to normalise relative mRNA expression levels of the genes of interest following the $2^{-[delta][delta]Ct}$ method (Livak and Schmittgen, 2001), where:

[delta][delta]Ct = [delta]Ct,sample - [delta]Ct,reference

This value represents the fold change in gene expression of a particular gene of interest in the experimental conditions that the cells were exposed to. Three repetitions per primer set and mRNA sample utilised and at least three independent experiments (n=3) were carried out. Ct values above 35 were excluded for data analysis, as they imply low efficiency (Bustin *et al*., 2011). Primer specificity was assessed by melting curves, and primer sets that produced more than one product were excluded and redesigned as previously explained.

2.10.4 Identification of reference genes

GeNorm (Primer Design) experiments were carried out in order to select stable reference genes; a gene where expression remain stable across different samples over time and that shows a robust and similar expression between sample tests. This information was necessary in order to normalise the results obtained in the qPCRs.

In total, 12 genes from each species (human and rat) were tested against cDNA from the 3 cell lines. All oligomers and reagents were provided by GeNorm primer kit (Primer Design, ge-SY-12) (Table 2.2).

The qPCR mix and amplification conditions for each reaction was prepared as previously stated in section 2.10.2. Analysis of reference gene stability was performed with qbase+ software (Biogazelle, Zwijnaarde, Belgium).

Table 2.2. Candidate reference genes tested in this study. Reference genes from GeNorm (Primer Design) kits specific to either rat (*Rattus norvegicus*) or human (*Homo sapiens*) were used.

Gene symbol	***Gene target***	***Species***
18S	*18S Ribosomal RNA, mRNA.*	Human/Rat
ACTB	*actin, beta, mRNA.*	Human/Rat
ATP5B	*ATP synthase, mRNA.*	Human/Rat
B2M	*beta-2 microglobulin, mRNA.*	Human/Rat
CANX	*calnexin, mRNA.*	Rat
CYC1	*cytochrome c-1, mRNA.*	Human/Rat
EIF4A2	*eukaryotic translation initiation factor 4A2, mRNA*.	Human
GAPDH	*glyceraldehyde-3-phosphate dehydrogenase, mRNA.*	Human/Rat
MDH1	*malate dehydrogenase 1, mRNA*.	Rat
RPL13	*ribosomal protein L13, mRNA*.	Human/Rat
SDHA	*succinate dehydrogenase, mRNA.*	Human
TOP1	*topoisomerase I, mRNA*.	Human/Rat
UBC	*ubiquitin C, mRNA.*	Human/Rat
YWHAZ	*tyrosine 3-monooxygenase, mRNA.*	Human/Rat

2.11 Immune detection of proteins

2.11.1 Protein Extraction

A lysis buffer containing 50 mM Tris, pH 8, 150 nM NaCl, 5 mM EDTA, 1% NP40 and 1% protease inhibitor cocktail (4-(2-Aminoethyl) benzenesulfonyl fluoride hydrochloride 1 mM, aprotinin 800 nM, bestatin 50 µM, E64 15 µM, leupeptin 20 µM, pepstatin A 10 µM, Thermo Scientific) was prepared and chilled on ice before use. Cell pellets were harvested according to section 2.4 and resuspended in approximately 3X the volume of the pellet (60-100 µL) and incubated on ice for 30 minutes. The samples were centrifuged at 16000g for 5 minutes at 4°C. The supernatant containing the soluble proteins was transferred to sterile 1.5 mL microcentrifuge tubes and immediately quantified or stored at -80° C until further use.

2.11.2 Bicinchoninic acid (BCA) assay

Proteins were quantified using the bicinchoninic acid assay (BCA) according to the manufacturer's protocol. Briefly, the BCA working reagent was prepared by mixing BCA and 4% (w/v) copper (II) sulphate pentahydrate in a 50:1 ratio. Twenty five µL of diluted protein sample (1:20 in protein lysis buffer) were mixed with 200 µL of BCA working reagent and added into a 96-well plate. All the samples were tested in triplicate. Bovine serum albumin was used to construct a standard curve of known concentrations with a range of 200-1000 µg/mL. The absorbance was measured at 562 nm in a plate reader (ELISA Reader LT-5000MS, LabTech International) and data analysed using Labtech Manta Lite software (LabTech International)

2.11.3 Sodium dodecyl sulphate - polyacrylamide gel electrophoresis (SDS-PAGE)

Protein samples were prepared in 2x Laemmli buffer (4% SDS, 20% glycerol, 10% 2-mercaptoethanol, 0.004% bromophenol blue and 0.125 M Tris HCl, pH 6.8). Samples were diluted to a final concentration of 1 µg/µL in 2 x Lammli buffer and boiled at 100 °C in a heating block for 5 minutes prior to use.

Acrylamide resolving gels ranging from 8-15% (w/v) were used depending on the size of the protein of interest. The composition of the gel was as follows: 8-15% (w/v) acrylamide (30% (w/v) stock acrylamide); resolving Tris solution (0.375 mM Tris-HCl, 0.1% (w/v) SDS adjusted to pH 8.8 with 1N HCl) and 10% (w/v) ammonium persulphate. Finally, 0.1% (v/v) of the polymerising agent N,N,N',N'-tetramethylethyenediamine was added to the mixture in order to promote polymerisation. The mixture was carefully mixed to avoid creating bubbles and poured between two glass plates of the casting module, leaving a 3 cm gap of the top. A 1mL overlay of isopropanol was layered on the top of the resolving gel to create an even surface and minimise contact with air. After 30 minutes polymerisation, the isopropanol was carefully decanted, the top of the gel was rinsed with dH_2O and blotted dry with filter paper.

The composition of the stacking gel was as follows: 5% (v/v) polyacrylamide, stacking Tris solution (37.5 mM Tris HCl, 0.1% (v/v) SDS adjusted to pH 6.8 with 1 N HCl) and 10% (w/v) ammonium persulphate. TEMED 0.1% (v/v) was added to the mixture to promote polymerisation.

The stacking gel solution was added directly on top of the resolving gel, a comb was inserted and the gel left to polymerise for a further 30 minutes at room temperature. When the gel was completely set, the comb was removed and any un-polymerised material was removed from the wells by rinsing with Tris-glycine electrophoresis buffer (5 mM Tris-base; 50 mM glycine, pH 8.3; 0.02 % (w/v) SDS).

2.11.4 Resolving SDS-PAGE gels

The gel was removed from the casting chamber, placed into the electrophoresis tank and submerged in Tris-glycine electrophoresis buffer. Samples were loaded into the wells together with a pre-stained broad range protein marker (PageRuler™ Prestained Protein Ladder, 10 to 180 kDa, Thermo Fischer). The gel was resolved at 50 V for 15 minutes then the voltage was increased to 100 V and the gel was resolved until the dye front had reached the bottom of the gel.

2.11.5 Staining and visualization of the protein gel

Gels were rinsed in dH_2O for 15 minutes and submerged in IRDye blue stain (LI-COR Biosciences, Cambridge, UK) for 1 hour. Destaining was carried out by removing the stain and adding dH_2O for 30 minutes under agitation. Gels were scanned at 700 nm using the LiCOR imaging system (Odissey-3074, LI-COR, Cambridge, UK) and Image Studio v2.0 software.

2.12 Immunoblotting

Proteins resolved on SDS-PAGE were transferred onto nitrocellulose membranes using the method of Towbin (1979). Nitrocellulose membrane (0.2 µm, Optiran BA-S 83) and 2 mm thick filter paper (Whatman International Ltd., UK) along with two fibre pads, were pre-soaked for 15 minutes in 1 X continuous transfer buffer (25 mM Tris; 192 mM glycine; 20 % (v/v) methanol; pH 8.3). Using forceps throughout, the blot sandwich was assembled under transfer buffer to minimise air bubbles. Sandwiches were prepared by arranging them in the following order: two layers of filter paper, the gel, the pre-soaked nitrocellulose membrane and another 2 layers of filter paper with the gel facing the negative pole. The electrophoresis tank was filled with pre-chilled transfer buffer and the gel was transferred by electrophoresis at 100 V for 60 minutes.

In order to assess for equal loading between different protein samples, nitrocellulose membranes were ink-stained with 0.1% (v/v) India Ink (Pelikan, Fount India Black) in 1X Tris-buffered saline (TBS; 50 mM Tris-HCl pH 7.4; 0.9 % (w/v) NaCl) /0.1 % (v/v) Tween®20 (TBS-T) for 5 minutes. Unbound sites in the nitrocellulose membrane filter were saturated by incubating the blot in 50 mL 3% (w/v) non-fat dry milk (Marvel) in 1 X TBS-T for 1 hour with gentle rotation at room temperature.

Primary antibodies (see table 2.3) were diluted 1:1000 unless otherwise specified, in 3% (w/v) non-fat dry milk containing TBS-T and poured into the membrane. This was incubated at room temperature for 30 minutes to 1 hour

at 50 rpm to allow the antibody to bind, and then overnight at 4ºC. Any unbound primary antibody was removed the following day by washing the membrane in TBS-T 3 times for 5 minutes.

Fluorescence-conjugated secondary antibodies (LI-COR® see table 2.3) were diluted 1:10000-20000 in 3 % (w/v) non-fat dry milk in 1 X TBS, 0.01 % (w/v) SDS and incubated on the membrane with gentle agitation (50 rpm) for 1 hour at room temperature in the dark. Any unbound secondary antibody was removed and the membrane was washed with TBS-T for 3 x 5 minutes with gentle agitation. Membranes were scanned at 700 or 800 nm wavelength using the LI-COR imaging system (Odissey-3074, LI-COR, Cambridge, UK) and Image Studio v2.0 software.

Table 2.3. Primary antibodies used in this study. Western blotting (WB) and immunohistochemistry (IHC).

Target species	Host species	Application /dilution	Supplier and catalogue number
Actin	Goat	WB	Santa Cruz, #SC-1615
Capase-3	Rabbit	WB, IHC	CST, #9661
CD44	Mouse	WB	CST, #5640
GFAP	Mouse	IHC	abcam, #10062
GLUT-3	Rabbit	WB 1:400	abcam, #ab15311
GLUT-1	Rabbit	WB	EMD Millipore, #07-1401
GRP78-BIP	Rabbit	WB	abcam, #ab21685
HIF-1	Mouse	WB	abcam, #ab1
HIF-2	Goat	WB 1:500	R&D Systems, #AF2886
HIF-3	Rabbit	WB 1:750	Acris antibodies, #AP20606PU-N
HSP70	Rabbit	IHC, WB	abcam, #ab181606
HSP70	Goat	IHC	Santa Cruz, #sc1060
KCC1	Goat	WB	Aviva Systems, #OAEB01912
KCC2	Rabbit	WB, IHC 1:200	Merck Millipore, #07-432
KCC3	Rabbit	WB 1:200	Abgent, #AP12382a

Table 2.3 continued

Target species	Host species	Application /Dilution	Supplier and catalogue number
NeuN	Rabbit	IHC	abcam, #ab177487
KCC4	Rabbit	WB 1:200	Abgent, #AP12392a
NKCC1	Mouse	IHC	DSHB, T4-s
NKCC1	Goat	WB	Santa Cruz, #sc-21547
NKCC1	Rabbit	WB 1:400	Aviva Systems, #ARP43805
NSE	Mouse	WB	abcam, #AB16808
PDI	Mouse	WB	abcam, #ab2792
Vimentin	Mouse	WB	BD Sciences, #550513

Table 2.4. Secondary antibodies used in this study. Western blotting (WB) and immunohistochemistry (IHC).

Target species	Host species	Fluorochrome	Application/ Dilution	Supplier and catalogue number
Goat IgG	Donkey	680LT IRDye	WB 1:10000-1:20000	LI-COR, #925-68024
Rabbit IgG	Goat	680LT IRDye	WB 1:10000-1:20000	LI-COR, #925-68021
Mouse IgM	Goat	800CW IRDye	WB 1:10000-1:20000	LI-COR, #925-32280
Rabbit IgG	Goat	Alexa fluor 488	IHC 1:500	Thermo Fischer, #A-11008
Rabbit IgG	Mouse	Alexa fluor 564	IHC 1:500	Thermo Fischer, #A11011

2.13 *In vivo* experiments

2.13.1 Animal and tissue samples

Thirty six Swiss mice weighting 35-40 g (*Mus musculus* 3 months-old), were obtained from León University (Spain). Animals were kept under a controlled temperature environment (22 ± 2 ºC), relative humidity (55 ± 10%), ventilation (12 to 15 air changes per hour), photoperiod (12 h light/12 h darkness) and fed ad libitum (Pellet, Panlab, Spain). All experimental procedures were carried out following the Guidelines of the European Union Council (86/609/EU) and Spanish regulations (RD 53/2013, BOE 8/2/2013) for the use of laboratory animals, and were approved by the Ethics Committee of the University of Leon. All efforts were made to minimize animal number and suffering.

2.13.2 Photothrombotic model of stroke

Mice were placed in a transparent induction chamber and anaesthetised with a 3.5% (v/v) isofluorane in a 100% (v/v) oxygen gas mixture. When deep anaesthesia was reached, the mice were removed from the chamber and placed on a heating pad in order to maintain the body temperature at 37°C. A face mask was immediately placed on the mouse and isofluorane levels reduced to 1.5% (v/v). The animals were placed in the prone position and the scalp was shaved with a razor. The skin was disinfected with 70% (v/v) ethanol. An incision was made along the midline from the eye level to the neck using a scalpel and skin retractors were used to expose the skull. An opaque mask was fixed with cyanoacrylate onto the skull over the bregma

point of the left parietal bone. This mask delimits the area of the lesion and presents an aperture which allows the laser to irradiate exclusively a 1.5 mm diameter area. The diaphragm was located 2 mm caudal to the bregma point and 2 mm lateral to the sagittal suture, which includes a large part of the sensorimotor cortex (Franklin 1997).

Mice were injected with 50 mg/kg Rose Bengal solution intraperitoneally with a 1 mL syringe. After 5 minutes, photothrombosis was induced by illuminating the left hemisphere of the mouse with a green light laser (532 nm and 5 mW) for 15 minutes. At this point a second dose of Rose Bengal was injected and the region illuminated for another 15 minutes. Following illumination and photothrombosis, the mask and skin retractors were removed and the incision closed with 2 chirurgical staples (Fine Science Tools, Canada). The mouse was returned to its cage and kept in the dark for 24 hours in order to allow complete elimination of any circulating Rose Bengal and avoid unwanted photothrombosis and secondary damage. Animals were kept under the standard conditions previously mentioned until euthanised.

2.13.3 Drug Administration

The effect of modulating chloride transport after stroke was analysed by treating mice with specific cation-chloride cotransporter (CCC) modulators. The NKCC1 antagonist, Bumetanide (10 mg/kg), and KCC2 agonist CLP257 (100 mg/kg; both Tocris Bioscience, UK) were dissolved in 0.1% DMSO in NaCl and administered intraperitoneally 1 and 24 h after PT. Dosage was

based on previous literature (Gagnon et al., 2013; Loscher *et al*., 2013). Vehicle and naïve mice were included as controls.

2.13.4 Perfusion and sampling

Following the different exposure times after photothrombosis, mice were anaesthetised with an intraperitoneal injection of pentobarbital (200 mg/kg) (Euta-Lender, Normon Laboratories, Spain). Mice were perfused through the left ventricle with 100 mL saline solution (NaCl 0.9%) at room temperature followed by 100 mL 4% paraformaldehyde in PBS (50 mM, pH 7.4) at 4 ºC. The brain was extracted and transferred to a 4% paraformaldehyde in PBS solution and postfixed for 24 hours. The brain was transferred to a cryoprotective solution containing 30% sacarose in PBS (50 mM, pH 7.4) at 4 ºC for 48 hours. Brains were imbibed in an optimum cutting temperature solution (Tissue-teck, Sakura Finetek, EEUU) in PBS 50 mM, pH 7.4, 30% sacarose (1:1) for 30 minutes to maintain tissue integrity during the slicing process.

2.13.5 Tissue slicing

The brain was divided into two hemispheres, the ipsilateral hemisphere where the injury occurred and the contralateral hemisphere, which was not directly affected by phothrombotic stroke. Forty micron-thick brain sagittal sections were cut with a microtome for free floating processing (Microm HM450, Microm Laborgerate GmbH, Alemania). Sections were washed in PBS and endogenous peroxidases were inhibited with 3% H_2O_2 and 3% methanol in PBS, pH 7.4, for 20 minutes. Endogenous biotin was inhibited

with Blocking Kit (Vector Laboratories, Burlingame, CA, USA). Samples were stored on PBS with 0.025% (v/v) sodium azide in order to prevent fungal growth.

2.13.6 Cresyl Violet staining

From each animal, 3 sections were stained with Cresyl Violet in order to confirm the existence of the injury. This method uses a basic aniline dye to stain RNA blue, and is used to highlight important structural features of neurons (Kluver and Barrera 1953). The Nissl substance, which is located in the rough endoplasmic reticulum, appears dark blue due to staining of ribosomal RNA, giving the cytoplasm a mottled appearance. Individual granules of extra-nuclear RNA are named Nissl granules (ribosomes). DNA present in the nucleus stains a similar colour.

Sections were washed in water in order to eliminate the presence of salts. Slides were immersed through 2x 3 minutes changes of 100% ethanol and the tissue was defatted by 3 immersions in 10% xylene for 15 minutes. Following this, sections were immersed for 10 minutes in 100% ethanol and finally washed with water. Sections were stained with 0.5% (v/v) Cresyl Violet in water for 10 minutes and quickly rinsed with water to remove the excess. Next, the sections were immersed in 70% ethanol and dehydrated with 2x 3 minutes changes of 100% ethanol. Finally, sections were cleared in xylene and mounted on positively charged slides and air dried. A drop of 1,4-diazabicyclo[2.2.2]octane (DABCO) 3% in glycerol:PBS (1:1) was added on top of each section and finally a cover slip was added. The slides were

imaged using a Zeiss Primovert inverted microscope at a 20X magnification and images captured with a Zeiss Axiocam camera.

2.14 Immunohistochemistry

Tissue sections were washed 3 times for 10 minutes in 50 mM PBS pH 7.4 at room temperature to eliminate the sodium azide from the tissue. Antigen retrieval was performed by incubating the samples in preheated sodium citrate buffer (10mM sodium citrate, 0.05% (v/v) Tween-20, pH 6.0) for 30 minutes at 80°C. Non-specific binding was blocked by incubating the sections in 0.2% Triton X-100, 20% serum in PBS for 1 hour and 15 minutes. The species-specific serum used varied according to the secondary antibody host. Immunolabelling was performed using a variety of primary antibodies at specific concentrations (see Table 2.3). The sections were incubated overnight at 4°C with the primary antibody diluted in 0.2% Triton X-100, 2% serum in PBS. Labelling was detected by incubating sections for 1 h with a fluorescence-conjugated secondary antibody (see Table 2.3) followed by incubation for 20 minutes with 4',6-Diamidino-2-Phenylindole, Dihydrochloride (DAPI) diluted 1:1000. Sections were washed 3 times for 10 minutes after each incubation. Sections were mounted on positively charged slides and air dried before 3% (v/v) DABCO in glycerol:PBS (1:1) was added to improve the lifetime of the dye. Finally a cover slip was added. The specificity of the immune reactions was controlled by omitting either the primary and/or secondary antibodies. Imaging of the slides was performed using a Zeiss LSM 800 (Carl Zeiss Microscopy) confocal microscope.

2.15 Data Analysis

Analysis of the .czi image files obtained with confocal microscopy was carried out with ZEN 2 (blue edition) software (Carl Zeiss Microscopy GmbH, 2011) and/or ImageJ Fiji 1.51g.

2.15.1 Calculating the Mean fluorescence intensity of antibody staining in brain slices

The mean fluorescence intensity was measured within a given area surrounding the photothrombosised brain. The mean intensity value was measured up to 600 μm from the border of the necrosised area with ZEN 2 blue using the measure tool on the ZEN blue software. Stained sections from three different mice from each time point post photothrombotic stroke (days 1, 3 and 5 days) were analysed for each mouse, three different slices were analysed.

2.15.2 Assessing the decay in fluorescence intensity across the infarcted zone

The decay in fluorescence in the area surrounding the photothrombotic stroke was also analysed. This allowed the extent of the damage and its evolution 1, 3 and 5 days following photothrombotic stroke induction to be defined. In order to do this, fluorescence was measured up to 500 μm from the infarcted zone at regular intervals as shown in figure 2.1. The profile function of ZEN 2 blue was used in order to plot intensity of the fluorescence signal against the distance from the border of the injury. A table with the intensity of each channel at each distance was exported into Microsoft Excel

to construct the graphs. The fluorescent signal across the brain section from the infarcted zone was normalised against DAPI intensity. This was repeated twice per section, in 3 different mice per time point studied and represented as normalised fluorescence intensity over time.

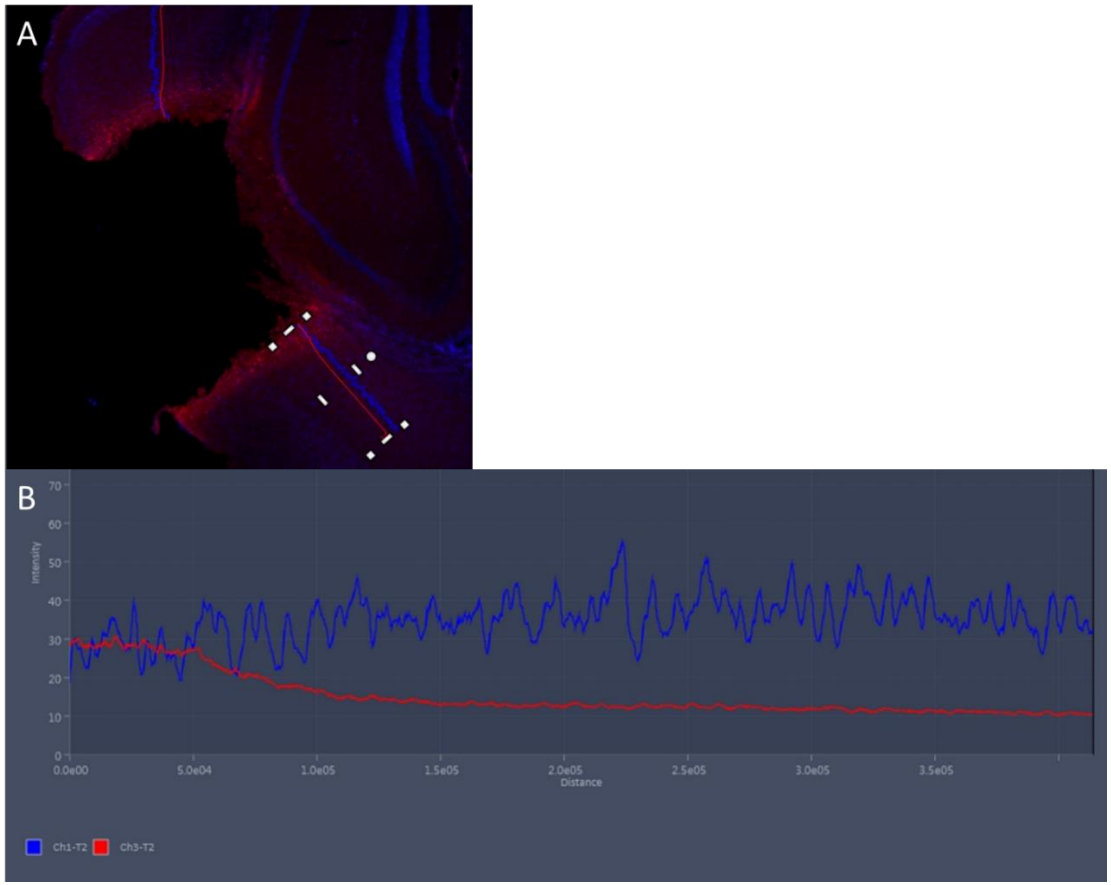

Figure 2.1 Schematic representation of the method used to analyse the decay in fluorescence intensity across the infarcted zone. An area of 500 µm length and 200 µm wide from the infarcted zone (white box, A) was drawn at each side of the injury. The intensity of the fluorescence signal against the distance was also analysed. A representative trace showing the fluorescence intensity is shown (B).

2.15.3 Counting the number of positively stained cells within the infarcted zone.

In order to calculate the number of cells staining positive with a specific antibody, sections were analysed. Three different fields of view of the cortex, 200 and 400 μm from each side of the ischaemic core were taken under x 63 magnification (Figure 2.2). The total number of cells within each field of view was calculated by measuring nuclear staining using DAPI. The images were exported to ImageJ Fiji 1.51g, where the different channels were split and then transformed into black and white images. Using the counter tool, the number of antibody-positive cells were counted and the data was exported into a Microsoft Excel spreadsheet. Finally, the number of positively stained cells were represented as ratios of expression or normalised to the total number of DAPI stained cells within the field of view.

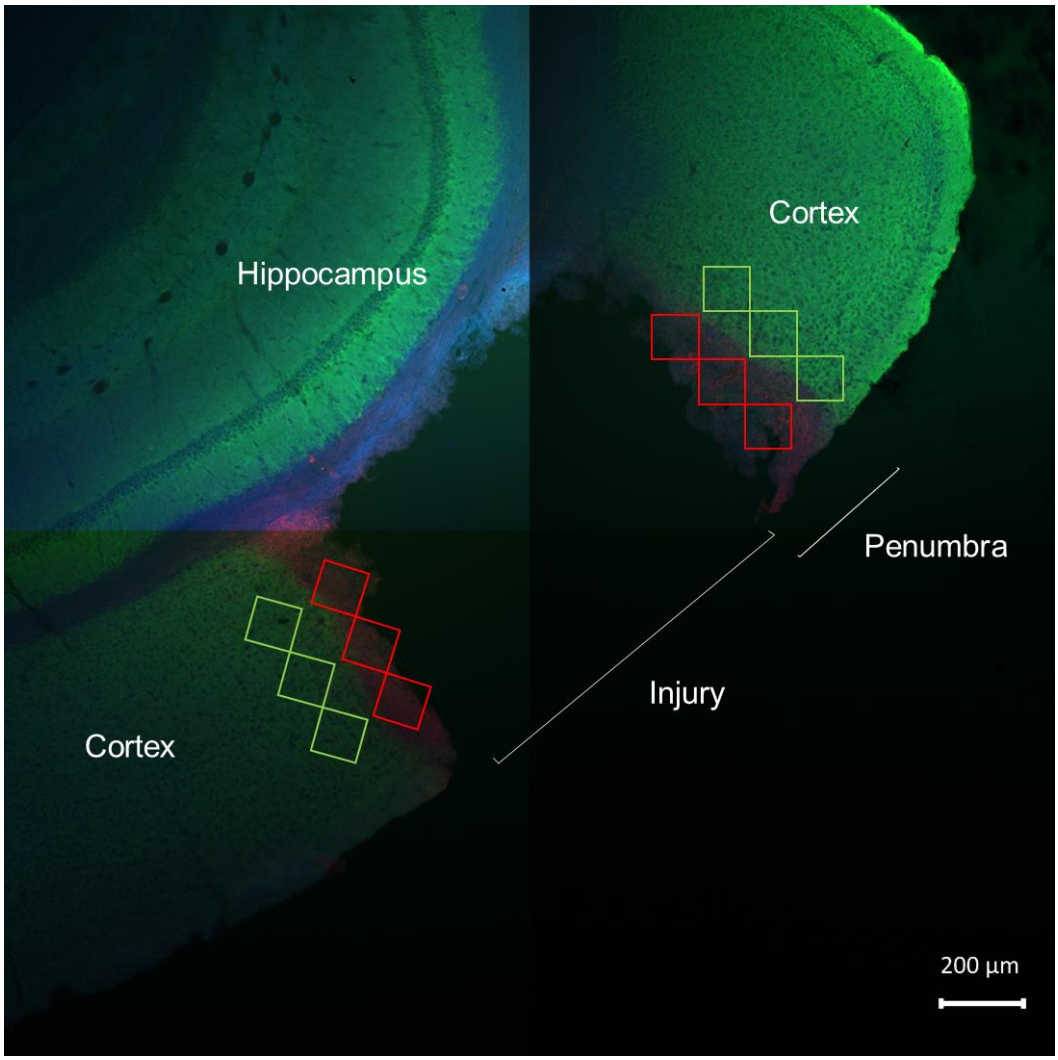

Figure 2.2 Schematic representation of the method used to analyse the number of positively stained cells. A representative image of a section stained with KCC2 (green) and NKCC1 (red) and various regions highlighted. The different fields of view that were analysed 100 and 200 µM from the edge of the photothrombotic injury are indicated by red and green boxes respectively.

2.16 Statistical analysis

All analyses were conducted using GraphPad Prism v7.0 (GraphPad Software Inc). Results are shown as the mean of three independent experiments ± SEM. Significance was determined using unpaired Student's *t*-test where only single comparisons were made or one/two-ways ANOVA with different correction for multiple comparisons that were specificied for each particular case. Data was deemed significant if *:$p<0.05$; **: $p \leq 0.01$, ***: $p \leq 0.001$.

3. Establishing an *in vitro* neuronal-like model of brain hypoxia to investigate the importance of the HIF-mediated adaptation to hypoxic stress.

3.1 Introduction

Occlusion of cerebral arteries causes irreversible neuronal damage as disrupted blood flow starves neurons of oxygen and glucose. The resultant failure in energy synthesis perturbs the ability to maintain ionic gradients, triggering a cascade of events leading to apoptotic cell death and irreversible neuronal loss (Lipton 2006). The penumbra is the moderately perfused region surrounding the blockage. Here, blood flow and oxygen availability are restricted, yet sufficient to maintain ATP synthesis to sustain ionic gradients (Liu *et al*., 2010). Cells in the penumbra are highly stressed and extremely vulnerable and must adapt in order to survive such harsh conditions. Adaptation is central to neuronal recovery.

Oxygen homeostasis is essential to maintain the energy demands of cells, as it is ultimately responsible for the production of ATP. Brain injury after an ischaemic stroke is a result of a disruption in the blood flow and subsequent energetic homeostasis failure. Reduced levels of oxygen activate a variety of protective and adaptive cellular responses that if sustained can lead to

neuronal apoptosis (Bossenmeyer *et al*., 1998). Hypoxia inducible transcription factors (HIFs) respond to a decrease in oxygen by promoting the transcription of genes involved in cell survival, proliferation and apoptosis (Baranova *et al*., 2007, Barteczek *et al*., 2016, Shi 2009).

3.1.1 HIFs as key regulators of hypoxic adaptation

HIFs are responsible for the transcription of a large number of genes, most of them involved in promoting and increasing oxygen delivery, cell survival and proliferation, as an adaptive response to low levels of oxygen (Figure 3.1) (Giaccia *et al*., 2003, Semenza *et al*., 2003, Koh and Powis, 2012). HIFs are heterodimers comprising an oxygen-dependant α subunit (HIF-1α, HIF-2α, and HIF-3α) and a constitutively expressed HIF-1β subunit which when associated conform the HIF-1, HIF-2 and HIF-3 transcriptional factors. HIF-1α and HIF-2α are the best-characterised subunits, whereas HIF-3α function remains unclear. HIF-1α is rapidly (< five minutes) degraded in the presence of oxygen (Berra *et al*., 2001). Under normoxia, HIF-α subunits are hydroxylated at conserved proline residues. The hydroxylation of two proline residues in HIF-1α and HIF-2α by prolyl hydroxylase domain proteins (PHD) is regulated by O_2 availability (Kaelin and Ratcliffe, 2008) and it is required for the binding of the von Hippel–Lindau protein (pVHL), which leads to HIF-α ubiquitination and proteasomal degradation (Ohh *et al*., 2000). Under hypoxia, PHD activity is diminished, as O_2 and α-ketoglutarate are cofactors required for its activity, and stabilized HIF proteins translocate into the nucleus where they can recognise hypoxia responsive elements (HRE) in the

genome promoting the transcription of hypoxia-responsive genes (Majmundar *et al*., 2010).

Although HIF-1 and HIF-2 share some common gene targets such as the vascular endothelial growth factor (VEGF) to promote angiogenesis (Koh and Powis, 2012; Figure 3.1), they also promote specific adaptations to hypoxia. HIF-1 preferentially promotes glycolytic enzymes such as glucose transporter 1 (*GLUT1*) and lactate dehydrogenase A (*LDHA*), genes involved in pH regulation such as carbonic anhydrase 9 (*CA-IX*) and genes that promote apoptosis or the unfolded protein response (UPR) such as glucose-related proteins 94-76 (*Grp94-76*), C/EBP homologous protein (*CHOP*) or the protein disulfide isomerase (*PDI*) *(*Keith *et al*., 2012).

HIF-1α mRNA has a very short half-life as it is rapidly degraded or translated into its protein form (Ke and Costa, 2006). HIF-1α mRNA stability is regulated by RNA-binding proteins (RBPs) such as the polypyrimidine tract-binding protein 2 (Ptbp2), micro RNAs (miRNAs) and antisense RNAs (Galbán and Gorospe, 2009). Antisense levels of HIF-1α (aHIF) are increased after prolonged hypoxia and triggers the downregulation of HIF-1α mRNA (Uchida *et al*., 2004). This rapid and tightly regulated HIF-1α mRNA kinetics makes it difficult to detect changes in HIF-1α mRNA under hypoxic conditions compared to normoxia by qPCR. Thus, the protein stability of HIF-1α is a better approach to detect HIF-1α induction.

HIF-2 is now considered the main regulator of erythropoietin (EPO) production (Rankin *et al*., 2007, Barteczek *et al*., 2016), which is an important adaptation to hypoxia as EPO promotes red blood cells production and thus, increases tissue oxygenation. HIF-2 has also been associated with the maintenance of stem cell characteristics (Koh and Powis, 2012). The maintenance of neuroblastoma cells in an undifferentiated state requires the expression of HIF-2 (Pietras *et al*., 2009). CD44 is a transmembrane glycoprotein implicated in cell–matrix adhesion and matrix-mediated cell signalling. It is considered a cancer stem cell marker (Keysar and Jimeno, 2010) and it has recently been shown to be widely expressed in several precursor cells during cerebellum development (Naruse *et al*., 2013). Vimentin, an intermediate filament protein, is another neuronal precursor marker as its expression essential for neuritogenesis and it is substituted by neurofilaments in the adult brain (Yabe *et al*., 2003).

Finally, the function of HIF-3α in the hypoxic response remains unclear. It has been generally recognised to inhibit HIF-1α translocation to the nucleus (Heikkil *et al*., 2011).However recent studies have shown the ability of some HIF-3 variants to act as an oxygen regulator transcription factor (Duan, 2016).

3.1.2 Modelling hypoxia in neuronal-like cell lines *in vitro*

Several methods have been developed in order to simulate the physiological conditions of low oxygen levels that occur during an ischaemic event. Some metals are known to act as chemical hypoxia-mimicking agents including

cobalt chloride, nickel chloride and desferrioxamine (Goldberg *et al*., 1988). Cobalt chloride ($CoCl_2$) induces hypoxia-inducible factor 1 alpha (HIF-1α) and HIF-3α stabilisation (Wang *et al*., 2006), but in addition, it has recently been shown to inhibit HIF-2α-dependent gene expression (Befani *et al*., 2013). It is therefore a good method to induce HIF-1α and the molecular mechanisms it triggers, but it does not induce an overall physiological response to hypoxia. Hypoxic modular chambers allow the control of atmospheric oxygen in order to mimic the low oxygen concentration that neurons suffer after a stroke. This model has been extensively used in a large number of studies (Papers *et al*., 2001, Gao *et al*., 2004, Wu and Yotnda, 2011) and offers a more realistic approach to the hypoxic conditions of an ischaemic stroke. Pluripotent cell lines such as PC12 and NT2, can be differentiated into neurons and have previously been used as a model to study hypoxia and other neurodegenerative diseases (Dalen *et al*., 2009, Darbinian, 2013, Grau and Greene, 2012, Lahiani e*t al*., 2015, Leiser *et al*., 2011, Lan *et al*., 2011, Hill *et al*., 2012). Their availability to grow in large numbers and their homogeneity makes them ideal candidates to study signalling pathways.

The establishment of an *in vitro* model of stroke complements *in vivo* and *ex vivo* models in order to study the effects of cerebral ischaemia in neurons. Such models permit further manipulation of the experimental conditions, which can lead to a better understanding of the molecular processes involved in triggering neuronal death.

Culturing primary neuronal cells is challenging as mature neurons do not undergo cell division and there is a high economic cost in maintaining an animal availability. To overcome this difficulty, several secondary sources derived from tumours have been made available and recognised as valid models to study neuronal differentiation and neurodegenerative diseases (Datta *et al*., 2013). Different neuronal cell lines have been used as an inexpensive and easy to maintain source of cultured neuronal-like cells. The most widely used cell lines are PC12 and NT2 cells, although other cell lines such as SH-SY5Y, or the murine embryonic stem cells F9 and P19, are also employed in different research fields (Resende *et al*., 2007, Lopes *et al*., 2010, Kovalevich and Langford, 2013).

PC12 cells treated with nerve growth factor (NGF) differentiate into dopaminergic-like neurons, developing neurites, synapse-like junctions (Jeon *et al*., 2010) and release the neurotransmitters acetylcholine (Hirsch *et al.,* 1993), dopamine and glutamate (Kumar *et al*., 1998). NGF is a neuropeptide that plays a role in the differentiation and maintenance of neurons and it has long been considered a method for developing neuron-like cells (Greene *et al*., 1976). In PC12 cells exposed to NGF, cell proliferation stops, neurite outgrowth is induced and the acquisition of biochemical and morphological characteristics of sympathetic neurons is stimulated.

NT2 cells stop dividing and differentiate into post-mitotic neuron-like cells upon treatment with retinoic acid (RA) (Andrews, 1984). Retinoic acid-differentiated NT2 cells display elaborate processes that differentiate into

axons and dendrites (Pleasure *et al*., 1992). In addition, these differentiated cells elaborate classic synaptic contacts and express GABAergic (Neelands *et al*., 1998), glutamatergic (Haile *et al*., 2014), dopaminergic (Zigova *et al*., 2000) cholinergic, catecholaminergic (Guillemain *et al*., 2000) and serotoninergic markers (Podrygajlo *et al*., 2009).

3.1.3 HIFs as modulators of the hypoxic response following stroke.

Despite the limited regenerative capacity of the nervous system, a degree of spontaneous recovery occurs following ischaemic stroke (Carmichael, 2016). Studies suggest *HIF* mediated angiogenesis and neurogenesis are central to this process. Neuron-specific knockout of *HIF-1α* dramatically increases ischaemic damage caused by transient cerebral artery occlusion and *HIF-1α* loss significantly increases infarct volume and mortality (Baranova *et al*., 2007). Indirect induction of *HIF* signalling via genetic ablation of *Phd*2 also reduces infarct size and dramatically improves sensorimotor function following transient ischaemic insult (Reischl *et al*., 2014).

HIF-α's *role* in the pathophysiology of ischaemic insult is however complicated as HIF-1α and -2α signalling display temporal differences (Koh and Powis, 2012); HIF-1α appears to be involved in the acute response whilst HIF-2α mediates the response to chronic hypoxic stress (Holmquist-Mengelbier *et al*., 2006). The timescale of HIF signalling is critical for effective recovery from ischaemic insult as whilst genetic targeting of neuronal *HIF-1α* and *HIF-2α* was beneficial in acute stages, loss of *HIF-1α* and *-2α* correlated with increased apoptosis and reduced sensorimotor function at later stages

(Barteczek *et al*., 2016). This may be due to *HIF-2α* tuning *VEGF* signalling and the importance of angiogenesis in post-stroke neurogenesis (Li *et al*., 2016). Together, these studies indicate the intricacies of HIF signalling, their neuroprotective role and importance in recovery from ischaemic damage.

In this chapter, the responses and adaptations following hypoxia of the neuronal-like cell lines PC12 and NT2 were analysed. A reliable system to induce PC12 and NT2 cells differentiation into neuron-like cell was achieved. The effect the cell viability, gene and protein expression of chemically-induced and atmospheric hypoxia was assessed. Specifically, the importance of HIF-2α signalling in neuronal adaptation and survival following hypoxic stress was further studied as a novel strategy to reduce the damage associated with stroke and promote neurorehabilitation in a more effective manner than currently available therapies.

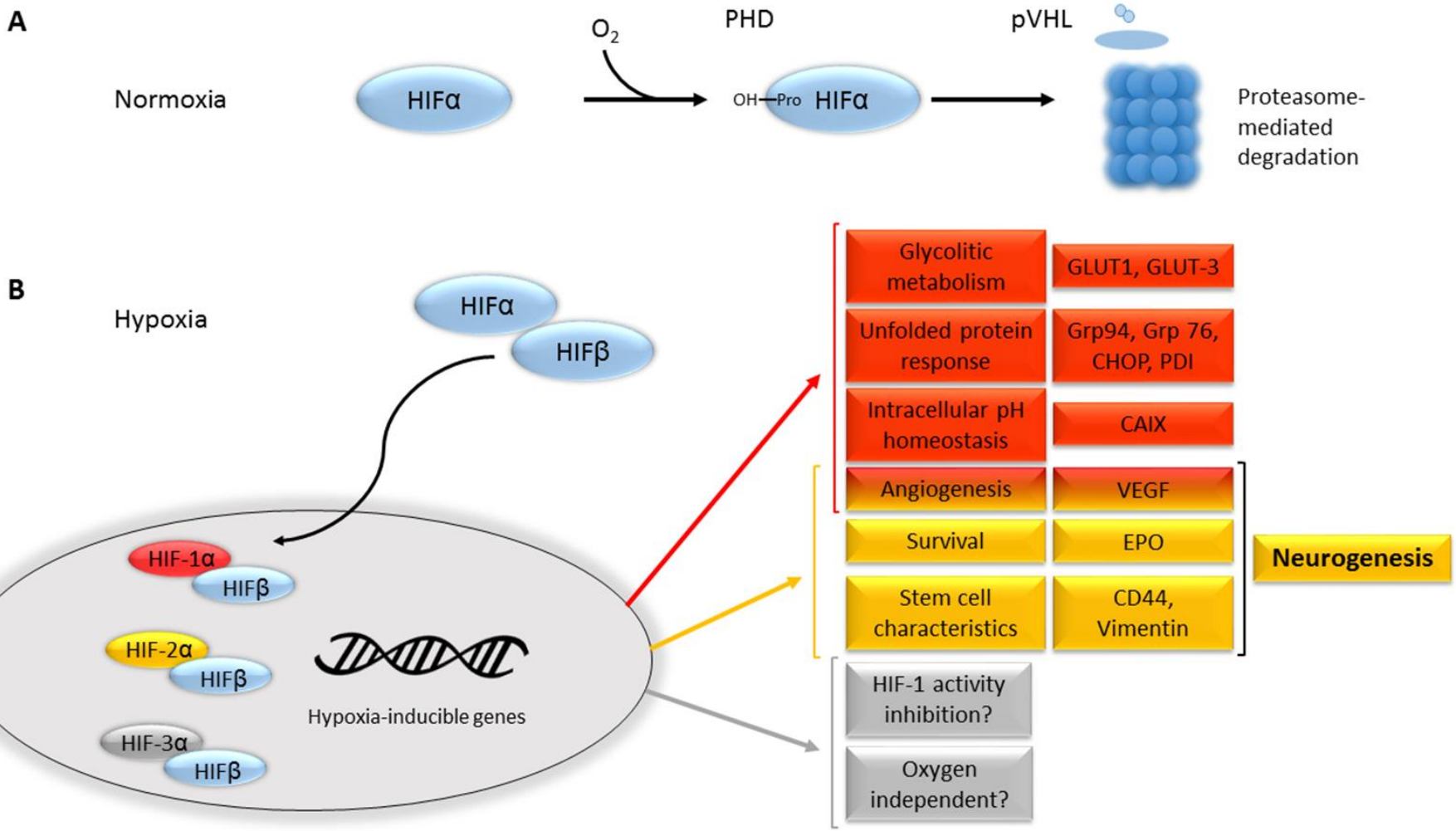
A
Normoxia
HIFα
O2
PHD
OH—Pro HIFα
pVHL
Proteasome-mediated degradation
B
Hypoxia
HIFα
HIFβ
HIF-1α
HIFβ
HIF-2α
HIFβ
HIF-3α
HIFβ
Hypoxia-inducible genes
Glycolitic metabolism
GLUT1, GLUT-3
Unfolded protein response
Grp94, Grp 76, CHOP, PDI
Intracellular pH homeostasis
CAIX
Angiogenesis
VEGF
Survival
EPO
Stem cell characteristics
CD44, Vimentin
Neurogenesis
HIF-1 activity inhibition?
Oxygen independent?

Figure 3.1 The HIF family of proteins promote different adaptations to hypoxia. Under normal physiological levels of oxygen HIF-1α/2α are hydroxylated by specific prolil hydroxylases (PHD) on conserved proline residues. This hydroxylation promotes the binding of von Hippel-Lindau protein (pVHL) which forms the substrate for the recognition and ubiquitination of the complex facilitating proteosomal degradation. Under hypoxia, PHD activity is inhibited and HIF-1α/2α can bind to the HIFβ subunit and translocate into the nucleus promoting the transcription of different hypoxia-responsive genes. HIF-1α promotes different adaptations like glycolytic metabolism, the glucose transporter 1 (GLUT1) and glucose transporter 3 (GLUT3) being major regulators; activates the unfoldedprotein response through glucose-related proteins 94-76 (Grp94 and Grp76), C/EBP homologous protein (CHOP) or the protein disulfide isomerase (PDI); regulates intracellular pH homeostasis through carbonic anhydrase 9 (Ca9); and promotes angiogenesis via the vascular endothelial growth factor (VEGF). HIF-2α shares some of these adaptations with HIF-1α like angiogenesis but it also promotes specific ones like survival through the regulation of erythropoietin (EPO) and stem cell characterisitics like CD44 and vimentin. HIF-3α is considered a negative regulator of HIF-1α and has oxygen independent functions although its role is not yet fully comprehended.

3.2 Aims

Aim 1. To create an *in vitro* model of hypoxia in neuronal-like cell lines in order to mimic the effect of a stroke in neurons.

Aim 2. To study the mechanisms that lead to neuronal adaptation after a hypoxic insult produced by a shortage of oxygen following a stroke-like event in this model.

3.3 Research Questions

RQ1. Are PC12 and NT2 cell lines valid to study neuronal ischaemia?

RQ2. How does hypoxia affect the viability of neuronal-like cells?

RQ3. Which adaptive response does hypoxia trigger in neuronal-like cells?

3.4 Results

3.4.1 Neuronal differentiation in pluripotent cell lines

3.4.1.1 Morphological assessment of the directed differentiation of PC12 and NT2 cells via microscopy

PC12 cells were treated with NGF (500 nM) and differentiation into neurons was assessed using visual, immune-based and gene-based techniques. As expected, NGF treatment rapidly initiated signs of PC12 differentiation (Figure 3.2). Untreated cells presented round cell bodies, however, after 24 hours of treatment, PC12 cells started producing projections, which became thicker and longer on days two and three reaching more than two-fold the length of the cell body at five days post-treatment (Figure 3.2). After eight days, the cells displayed a typical neuronal morphology with long projections and interlaced axons and dendrites. This was assessed by bright field microscopy (Figure 3.2).

The Molecular Probes® Neurite Outgrowth Staining Kit was used in order to assess neurite outgrowth and thus confirm the visual observations previously made in Figure 3.2. Neurite outgrowth was monitored via bright orange-red staining of outer cell membrane surfaces during the 8 days of NGF treatment (Figure 3.3). This immunostaining reported the same pattern of neurite elongation: projections started to appear one day following NGF treatment,

becoming longer and with more ramifications after three days of treatment and displaying a neuronal-like morphology after eight days.

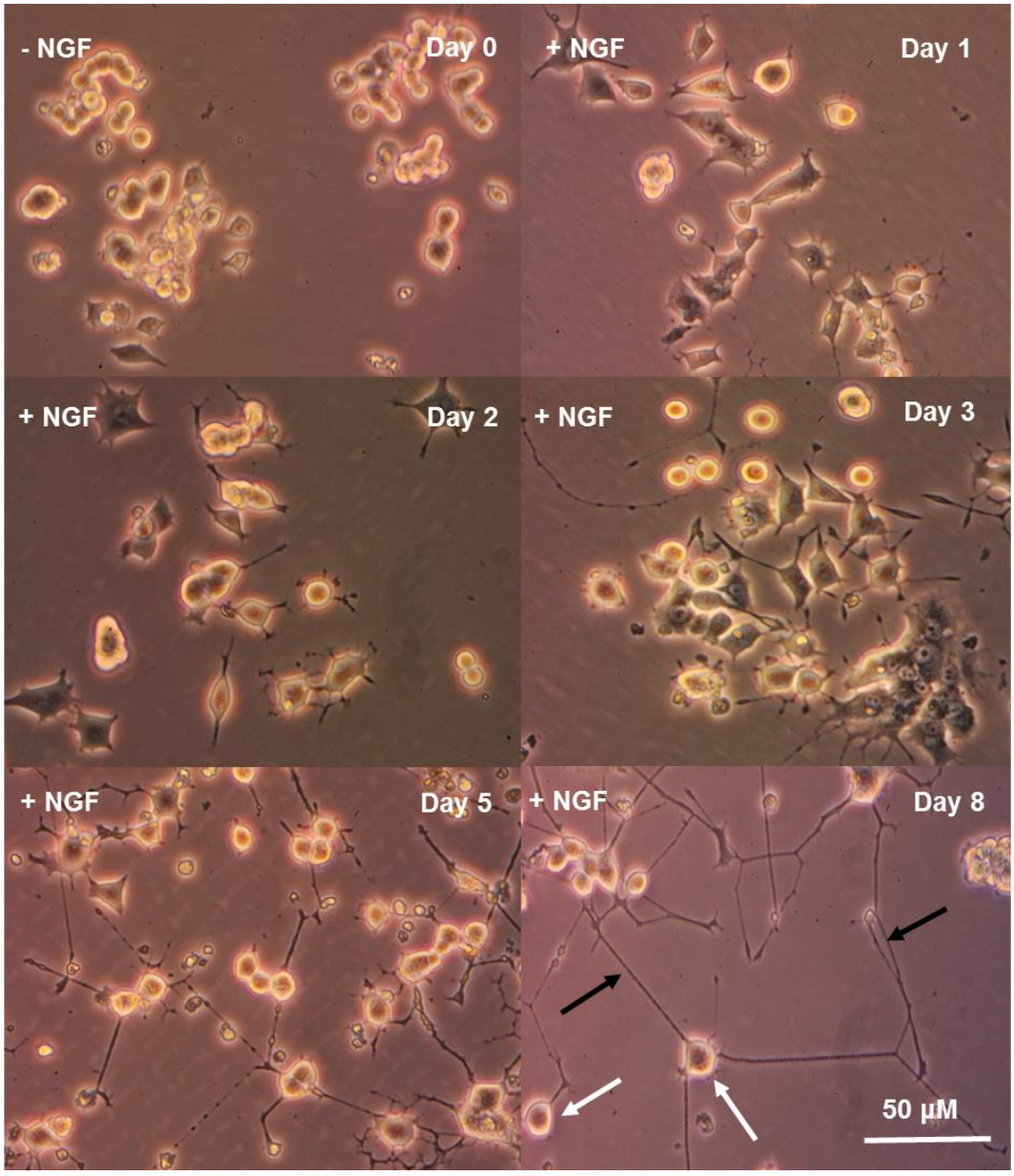

Figure 3.2 Neurite growth factor (NGF) promotes differentiation of PC12 into neuron-like cells. Representative bright-field microscopy images of PC12 cell morphology after one, two, three, five and eight days in the presence of NGF (20 x magnification). Typical differentiated neurons displayed bright cell bodies (white arrows) and neurites (black arrows).

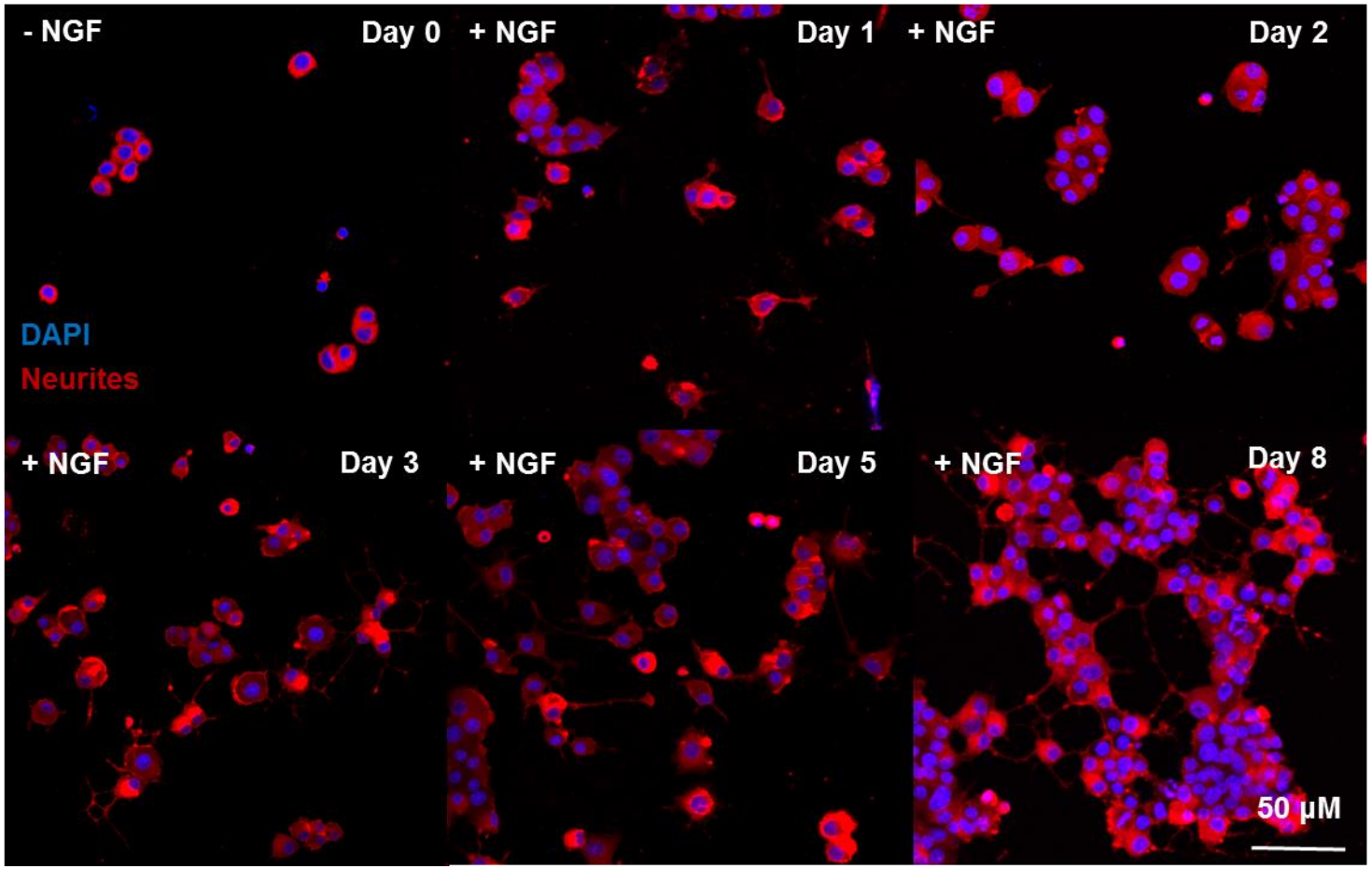

Figure 3.3. NGF promotes PC12 differentiation into neuron-like cells. Representative fluorescence microscopy images of PC12 cell morphology after one, two, three, five and eight days in the presence of NGF (20 x magnification). Cells were stained for the membranes of neurite extensions (red) and DNA (DAPI, blue).

Neurite length is considered to be indicative of neural differentiation and it has been reported in many studies that a neurite length of twice the length of the cell body is an indicator of a fully differentiated neuron (Blackman *et al*., 1993; Das *et al*., 2004). In order to determine the extent of differentiation the number of neurites and their length was quantified. After two days of NGF treatment, most cells presented at least one neurite (Figure 3.4A). Two neurites were observed following three days of the start of the treatment, with many cells presenting up to three neurites at the end of the eight days of treatment (Figure 3.4A). The length of these neurites was measured along the differentiation process. The average length of the cell bodies was 12 μm (Figure 3.4B, dotted line). NGF-treated PC12 cells contained neuronal processes longer than two times the length of the cell body (24 μm) after three days of NGF treatment (Figure 3.4 B). The length of the neurites was significantly different from two times the diameter of the cell body after eight days, reaching 60 μm. Finally, cells bearing at least two neurites with a length equal to, or greater than, two times the diameter of the cell body were considered differentiated and expressed as a percentage of the total number of cells in a field of view (Figure 3.4 C.). Considering the two parameters, 18% of the cells were differentiated after two days, 23% after three days, 57% after five days and 91% after eight days of NGF treatment. Therefore, eight days of NGF treatment induced PC12 differentiation according to the parameters previously mentioned.

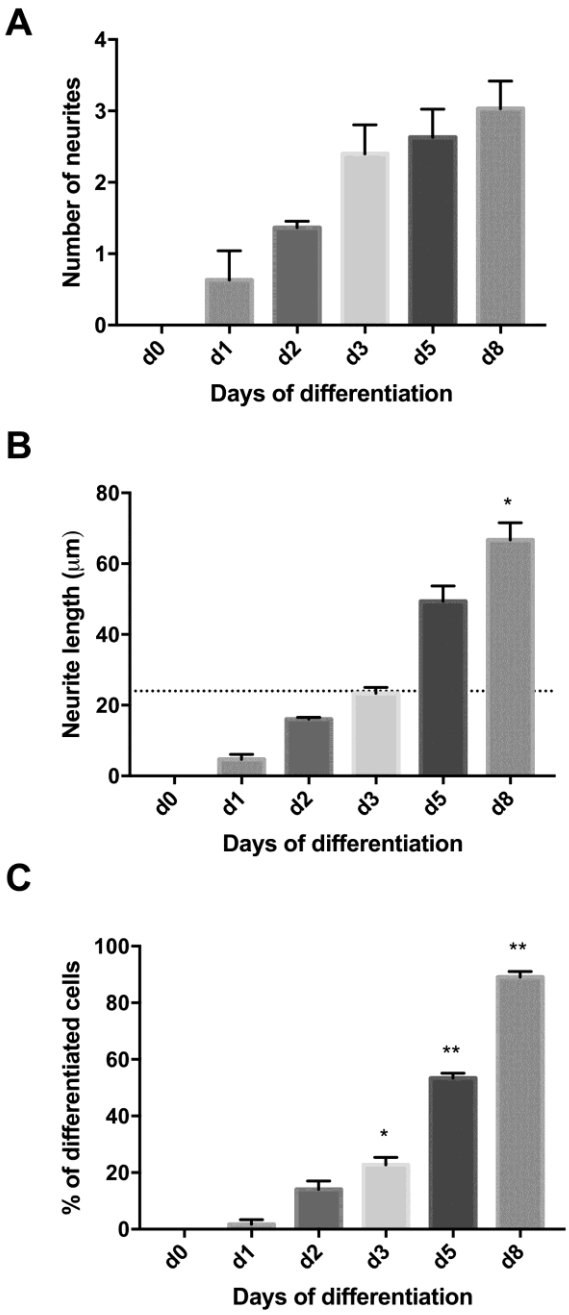

Figure 3.4 The number and length of neurites define the percentage of differentiated cells. PC12 cells were cultured in the absence or presence of 500 nM NGF for up to eight days. The number of neurites (**A**) and neurite length (**B**) were used as a measure to identify differentiated cells (**C**). The dotted line represents the mean of the cell diameter. Results are represented as mean ± SEM (n=3). One-way ANOVA with Dunnett's multiple comparisons test.

3.4.1.2 Morphological assessment of the directed differentiation of PC12 and NT2 cells via microscopy

Human NT2 cells can be induced to differentiate into neuron-like cells following RA treatment. After one week of RA treatment (10 μM), NT2 cells started producing axons and dendrites, becoming thicker and longer, > two-fold the length of the cell body after one week (Figure 3.5). Four weeks after RA treatment cells displayed longer projections and a typical neuronal morphology, interlaced axons and dendrites (white arrow) and ganglion like clusters (black arrow), as observed with primary neuronal cultures. In order to produce homogenous population of neuron-like cells, they were treated with the mitotic inhibitor cytosine β-D-arabinofuranoside (C-Ara), for a further two weeks to remove any non-differentiated cells from the culture.

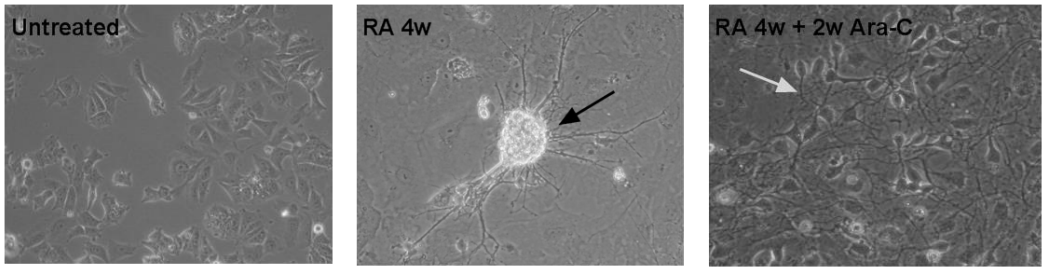

Figure 3.5. Retinoic acid (RA) promotes differentiation of NT2 into neuron-like cells. Representative bright-field microscopy images following NT2 differentiation. NT2 cells were treated with 10 μM RA for four weeks (RA 4w) and the mitotic inhibitor cytosine arabinoside (1 μM) for two weeks (RA 4w + 2w Ara-C). Typical differentiated neuron-like cells displayed ganglion-like clusters (black arrow) and interlaced axons (white arrow).

3.4.1.2 Gene expression assessment of the directed differentiation of PC12 and NT2 cells via qPCR

During differentiation, the PC12 and NT2 cells gene expression profile is modified (Lee *et al*., 2005). Specific genes are up-regulated or down-regulated in order to confer cells with a neuron-like phenotype. Neuritin mRNA is involved in promoting neurite outgrowth in the differentiating fields of the developing CNS and in regions associated with neural plasticity (Naeve *et al*., 1997, Cappelletti *et al*., 2007). Tropomodulin binds at the pointed end of actin filaments and regulates their length, being implicated in neuronal organisation and plasticity (Rao *et al*., 2014). Contactin associated protein 1 (Caspr1) is an axonal transmembrane molecule primarily localised at the paranodal junctions that flank the node of Ranvier and its expression is greatly reduced during myelination (Einheber *et al*., 1997). The neuron specific enolase (NSE) is a well-characterised and widely used marker of neuroendocrine and neuronal cells (Marangos and Schmechel, 1987). KCC2 is another neuron-specific marker with a restricted expression pattern guaranteed by the presence, in its gene sequence, of a neuronal transcription factor Egr4 binding site, which enhances KCC2 expression, and neuron restrictive silencing elements (Uvarov *et al*., 2005, 2006).

Quantitative RT-PCR (qPCR) was subsequently used to analyse relative changes in the gene expression of neuronal markers during PC12 and NT2 cells differentiation. mRNA quantification showed a modified gene expression profile of neuritin 1 (*Nrn1*), tropomodulin 1 (*Tmod1*) and contactin-associated

protein 1(*Caspr1*) during differentiation that further indicated the phenotypic and genotypic characteristics of neurons (Figure 3.6 and Figure 3.7). In PC12 cells, a 2.6-fold increase in *Nrn1* expression was observed after one day of treatment with NGF, maintained over following days and reached a seven-fold change eight days after starting the treatment (Figure 3.6 A). The gene expression of *Tmod1* increased 10-fold after one day of NGF treatment and remained relatively stable during the rest of the differentiation process (Figure 3.6 B). Unlike *Nrn1* and *Tmod1*, *Caspr-1* displayed a 2.9-fold decrease in expression after one day of NGF treatment (Figure 3.6 C). This decrease was less pronounced three and five days after treatment reaching the maximum down-regulation after eight days of differentiation with a 3.3-fold decrease in gene expression (Figure 3.6 C).

NT2 cells displayed a similar pattern of variation in gene expression following RA treatment. *Nrn1* expression was significantly modified by a 2.1-fold increase after four weeks and a 3.2-fold change after six weeks (Figure 3.7 A). *Tmod1* expression was significantly increased by a 9.1-fold after four weeks and a 12.2-fold after six weeks (Figure 3.7 B). Finally, *Caspr1* displayed a 1.2–fold decrease four weeks following RA treatment and a significant 1.8-fold decrease after six weeks (Figure 3.7 C).

These findings show that expression of *neuritin* and *tropomodulin* is up-regulated in NGF-treated PC12 cells and RA-treated NT2 cells compared to untreated cells and that the up-regulation reaches a significant change after eight days and six weeks of treatment in PC12 and NT2 cells respectively.

Up-regulation of these genes is as characteristic of neuronal differentiation (Cappelletti *et al*., 2007; Rao *et al*., 2014). Furthermore, down-regulation of Caspr-1 gene expression is in agreement with previous studies (Lee *et al*., 2005). NGF-treated PC12 cells display an increase in myelinisation and Caspr-1 expression is reduced during this process (Einheber *et al.,* 1997).

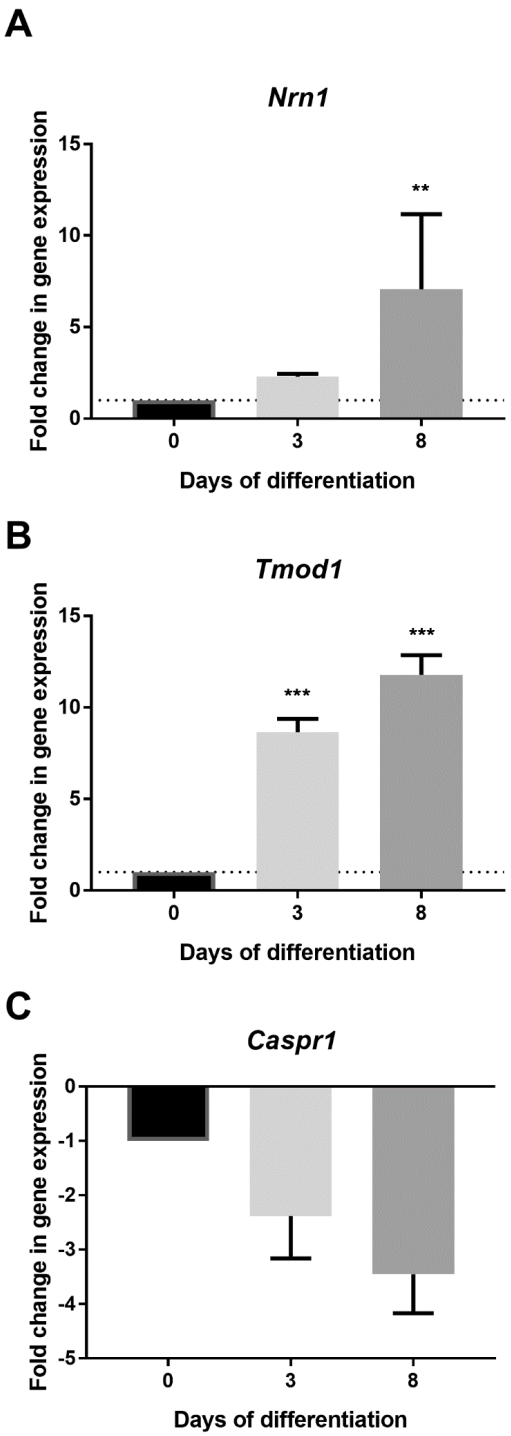

Figure 3.6. NGF triggers neuron-like gene expression in PC12 cells. PC12 cells were treated with 500 nM NGF for 8 days. Relative *Ntn1*, *Tmod1* and *Caspr1* mRNA expression in differentiated PC12 cells was analysed by qPCR. Results are expressed as the mean ±SEM (n=3). One-way ANOVA with Dunnett's multiple comparisons test.

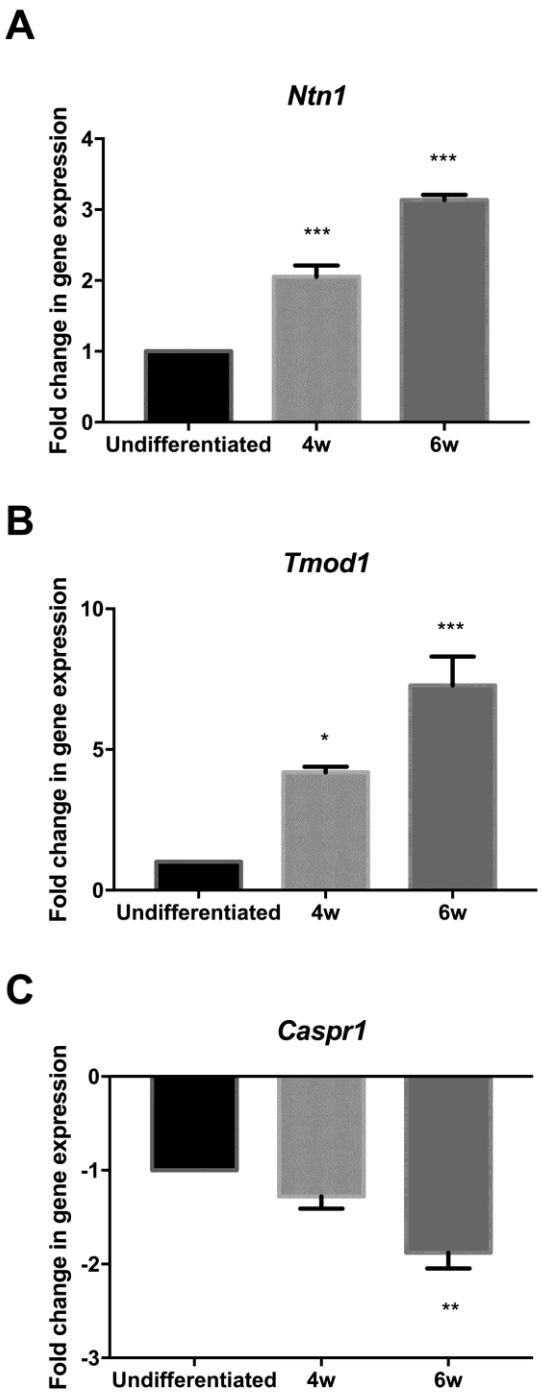

Figure 3.7 RA triggers neuron-like gene expression in NT2 cells. NT2 cells were treated with 10 μM RA for 4 weeks (4w) and a further 2 weeks with 1 μM Ara-C (6w). Relative *Ntn1*, *Tmod1* and *Caspr1* mRNA expression in differentiated NT2 cells was analysed by qPCR. Results are expressed as the mean ±SEM (n=3). One-way ANOVA with Dunnett's multiple comparisons test.

3.1.4.3 Protein expression assessment of the directed differentiation of PC12 and NT2 cells via immunoblotting

The expression of the different neuronal specific markers NSE and KCC2 was assessed by immunoblotting in differentiated PC12 and NT2 cells (Figure 3.8). An increase in the intensity for the neuron-specific enolase (NSE) band was observed in differentiated PC12 and NT2 cells compared to undifferentiated lysates, where a low basal level was detected. This change was even more evident when protein lysates were analysed for the neuron specific chloride co-transporter KCC2. The changes observed in protein expression following differentiation show that treatment with NGF and RA induces the expression of neuron-specific protein markers in PC12 and NT2 cells.

Overall, the morphological, genetic and protein data of this study indicates that the treatment of PC12 cells with NGF for eight days and of NT2 cells with RA for four weeks and a further two weeks with 1 µM Ara-C induces a differentiation consistent with a neuronal-like phenotype.

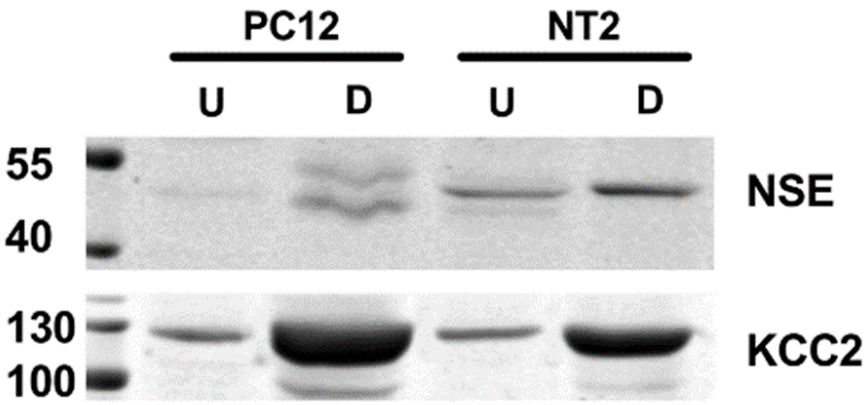

Figure 3.8 Analysis of the neuronal markers NSE and KCC2 following differentiation of PC12 and NT2 cells. Representative immunoblot analysis showing NSE and KCC2 protein expression. PC12 and NT2 cells were left untreated (U) or differentiated (D) with either 500 μM NGF for eight days or 10 μM RA for four weeks and a further two weeks with 1 μM Ara-C.

3.4.2 Cell viability following the induction of hypoxia in differentiated PC12 and NT2 cells

A hypoxic chamber provides an excellent platform to investigate neuronal responses to hypoxia. Neuronal-like cells were incubated inside a modular chamber containing a 1% O_2, 99% N_2 gas mixture in all hypoxic experiments. MCF7, a breast cancer cell line, was also used as a control as it is known to produce robust induction of HIF-1α upon chemically-induced hypoxia (An *et al*., 1998)

3.4.2.1 Assessing the impact of hypoxia on mitochondrial activity

The viability of PC12 and NT2 cells were analysed in order to determine a suitable exposure time to hypoxia. The mitochondrial activity of differentiated PC12, NT2 and MCF7 cells was analysed using the Alamar blue assay after subjecting them to two, four, eight and 24 hours of hypoxia (Figure 3.9). Alamar blue was used to measure cell viability as it can be incorporated during the hypoxic exposure while the MTT assay needs post-hypoxia time for development and that would involve reoxygenation of the cultured cells.

As can be seen in Figure 3.9, a hypoxic insult of two hours did not produce a decrease in cell viability of MCF7, PC12 and NT2 cells. MCF7 cells showed a strong decrease in cell viability after four hours of hypoxia, with only 35% of the cells being viable, 18% after eight hours and only 13% after 24 hours. PC12 cells also showed an intense decrease in mitochondrial respiration: 44% after four hours, 24% after eight hours and 7% after 24 hours. Finally,

NT2 cells displayed a strong resistance to moderate hypoxia; at four hours 68% of the cells were viable, 34% after eight hours and 14% after 24 hours.

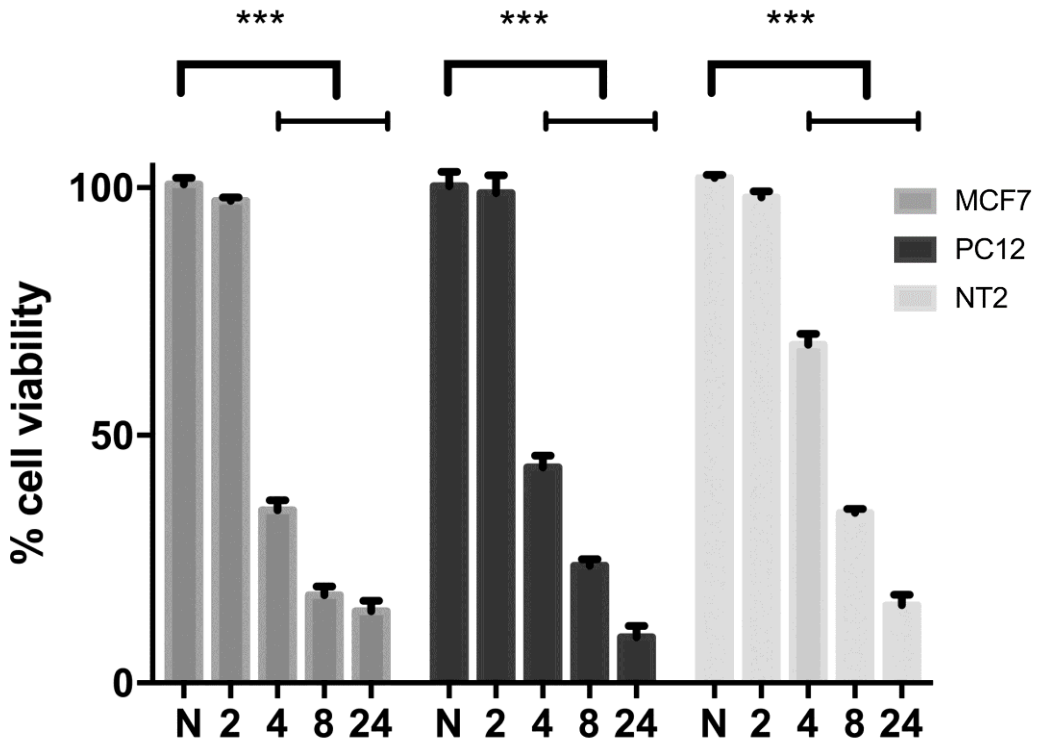

Figure 3.9. Mitochondrial activity is significantly compromised by hypoxia. MCF7, PC12 and NT2 cells viability was analysed using Alamar blue two, four, eight and 24 hours after exposure to hypoxia (1% O_2). Viability is expressed as a percentage of normoxic cell viability. Results are expressed as the mean ±SEM (n=3). One-way ANOVA with Tukey's multiple comparisons test.

3.4.2.2 Assessing the impact of hypoxia on cell viability

HIF-1α stabilisation during hypoxia leads to the inhibition of mitochondrial activity by affecting the production of NAD(P)H (Papandreou *et al*., 2006) which is needed for reducing agent-based assays like MTT and Alamar blue. Thus, it is possible that the reduction observed in cell viability is actually reflecting a decrease in mitochondrial respiration. Therefore, an alternative assay was used in order to analyse the effect of hypoxia on cellular viability. Trypan blue is a dye exclusion test that allows the assessment of cell viability as it is able to enter the damaged membranes of dead cells whereas it does not interact with viable cells possessing intact cell membranes. Cells were treated for eight hours under hypoxic conditions and then the cell viability was analysed by the Trypan blue exclusion dye (Figure 3.10). Eight hours of hypoxic insult significantly decreased cell viability in MCF7 cells by 30%, 26% in PC12 cells and 55% in NT2 cells. At longer exposure times (24 hours) a large number of floating cells was observed. Eight hours of hypoxia produced a change in the colour of the media and this increase in the pH acidity of the media is thought to reflect a change in the metabolism in the cells. Therefore, eight hours of hypoxia was subsequently used in further experiments (unless otherwise stated) as it provided with a sufficient hypoxic insult yet it produced sufficient viable cells to analyse.

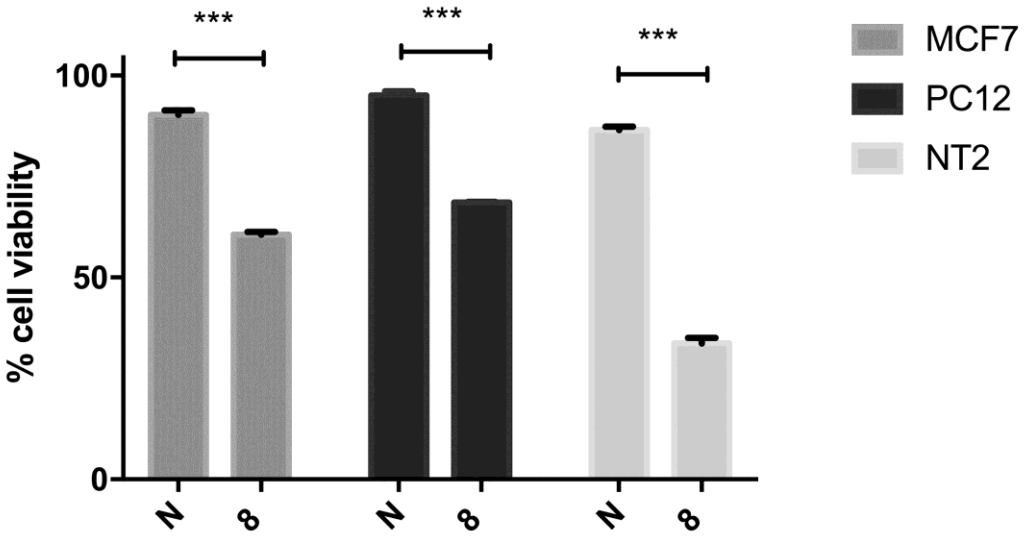

Figure 3.10. Cell viability was significantly reduced after 8 hours of hypoxia. MCF7, PC12 and NT2 cells were exposed to hypoxia (1% O_2) for eight hours. Trypan blue was employed to record a viable:non-viable ratio. Results are represented as mean percentage of viable cells ± SEM of three independent experiments. Two-tailed unpaired Student's *t* test.

3.4.3. *HIF-1-3α* changes in gene and protein expression following hypoxia

In order to study the impact of hypoxia upon the neuronal-like PC12 and NT2 cell lines, the expression of the HIF family of genes and proteins was assessed.

3.4.3.1 Identifying suitable housekeeping genes

In order to find a candidate reference gene that showed a stable expression after hypoxia, the stability of a panel of reference genes (*GAPDH, CYC1, MDH1, B2M, ACTB, YWHAZ, 18S, CANX, UBC, RPL13A, TOP1* and *ATP5B*) was investigated. The Ct values were analysed with the geNorm algorithm, which selects an optimal reference gene out of a larger set of candidates. The so called M-value describes the variation of a gene compared to all other candidate genes, selecting the pair of genes with the lowest M-value as the optimum pair of reference genes (Vandesompele *et al*., 2002). Values lower than 1.5 are arbitrarily suggested as stable genes, with increased gene stability as the M-value gets smaller. The reference genes selected under our experimental conditions were *TOP1* for PC12 and *ACTB* for MCF7 and NT2.

3.4.3.2 *HIF-1-3α* changes in gene expression following hypoxia

Neuronal-like PC12 and NT2 cell adaptation to hypoxic stress was investigated by assessing *HIF-1, 2 and-3α* gene expression The fold change in *HIF-1-3*α gene expression was assessed in each cell line 8 hours after

exposure to hypoxia (Figure 3.11). Unexpectedly, *HIF-1α* was not induced following the insult in PC12 cells and just a 1.8-fold increase was observed in NT2 cells. These results are in contrast with the strong 12-fold increase of *HIF-1α* transcript observed in MCF-7 cells. Surprisingly, hypoxia triggered a significant increase in *HIF-2α* mRNA expression in differentiated PC12 and NT2 cells (2.4- and 2.6- fold respectively, Figure 3.14) whilst *HIF-2α* expression in hypoxic MCF7 cells was significantly decreased. *HIF-3α* mRNA showed relatively stable levels of expression in PC12 and NT2 cells and was relatively unchanged in response to hypoxia (Figure 3.11). By contrast, *HIF-3α* mRNA was dramatically up-regulated in MCF7 cells by hypoxic insult. These results were particularly striking, as a strong *HIF-1α* response was expected for the three cell lines. However, the robust response observed in MCF7 cells and the fact that all exposures were conducted in parallel for the different cell lines, validate the use of a modular chamber as a platform to induce hypoxic adaptation.

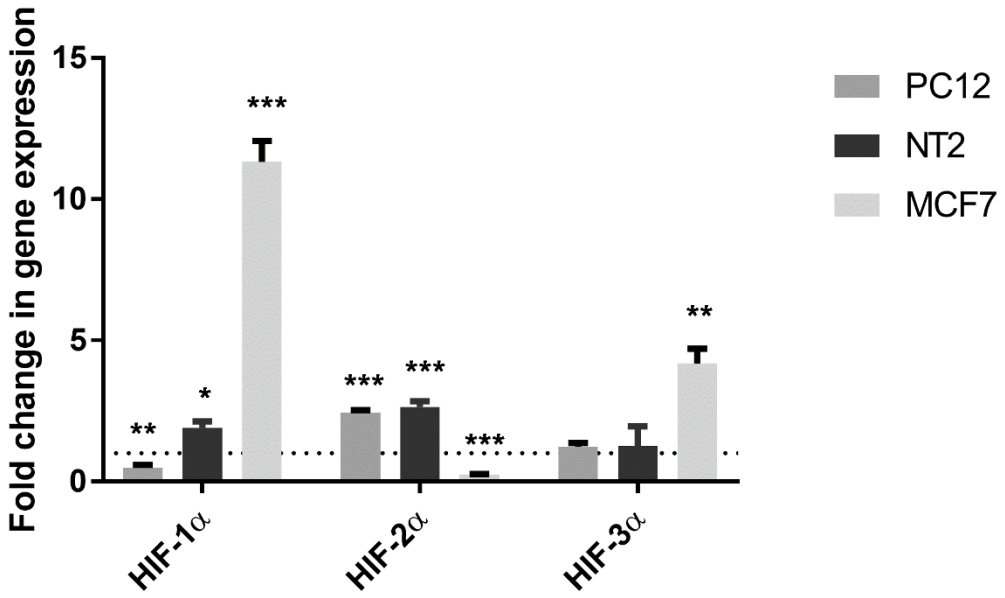

Figure 3.11. Hypoxia triggers up-regulation of the mediators of the hypoxic response, HIF-2α and HIF-3α, in neuronal-like cell lines. Relative HIF1-3α mRNA expression was analysed in MCF7 and differentiated PC12 and NT2 cells exposed to eight hours of hypoxia by qPCR. The dotted line represents basal gene expression. Data is expressed as mean ± SEM (n=3). Two-tailed unpaired Student's *t* test.

Previous studies in endothelial cells have shown that sustained hypoxia progressively decreases *HIF-1α* mRNA expression with its level peaking after three hours of hypoxia and decreasing by 50% after six hours (Chamboredon *et al*., 2011). Endothelial cells are, however, the primary sensors of oxygen levels in the blood so a different behaviour in neuronal-like cells was expected. This means that eight hours of hypoxia might be a late stage to detect *HIF-1 α* expression. However, the up-regulation of *HIF-2α* and *HIF-3α* and absence of *HIF-1 α* might also suggest that neuronal cell response to hypoxia differs to that of endothelial cells.

3.4.3.3 *HIF-1-3α* changes in protein expression following hypoxia

HIF-1α mRNA was not induced in PC12 cells and only a small activation could be detected in NT2 cells; however, hypoxia causes HIF-1α stabilisation and it was expected that a clear induction of HIF-1α would be seen at the protein level. Protein expression was therefore analysed to determine whether transcriptional changes corresponded to translational expression of HIF-1α.

MCF7, PC12 and NT2 cells were exposed to hypoxia for one, two, four, eight and 24 hours before HIF-1α expression was analysed by immunoblotting. Antibodies corresponding two different epitopes of HIF-1α were used at 400-550 and 610-727 aa (Table 2.3, Figure 3.12). Surprisingly, HIF-1α protein induction was not detected in either neuronal-like cell line at any time point (Figure 3.13). A variety of conditions and antibody dilutions were tested in

order to determine whether the lack of induction was due to a technical error, but HIF-1α remained undetectable. By including MCF7 cells as a positive control for HIF-1α induction the experimental conditions of the chamber and validity of the antibodies was confirmed. In MCF-7 cells HIF-1α induction was detected two hours following the hypoxic insult as evident by two bands at ~120 and ~115 KDa. This reached a maximum intensity at four-eight hours and HIF-1α protein was still detected at 24 hours. MCF7 cells at eight and 24 hours after hypoxia were then used as positive controls for the rest of the experiments.

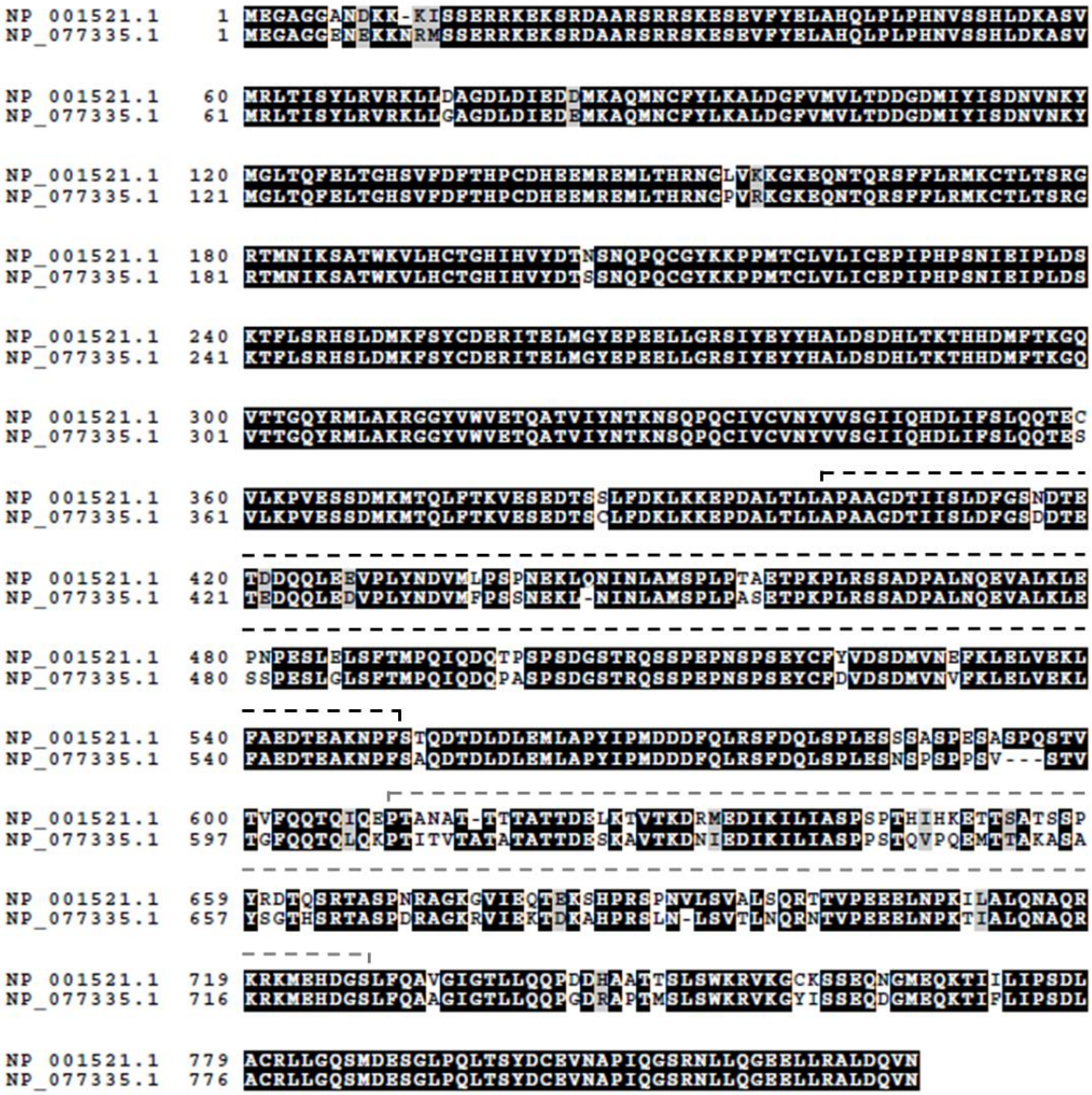

Figure 3.12 alignment of the human and rat HIF-1α protein sequences.

The sequences were aligned using ClustalW version 2 (Larkin *et al*., 2007) and BoxShade for the output format .The location of epitopes bound by HIF-1α antibodies #H1alpha67 (Abcam) corresponding to amino acids 400 to 550 (black dotted line) and #610958 (BD Biosciences) corresponding to amino-acids 610 to 727 (grey dotted line) are highlighted.

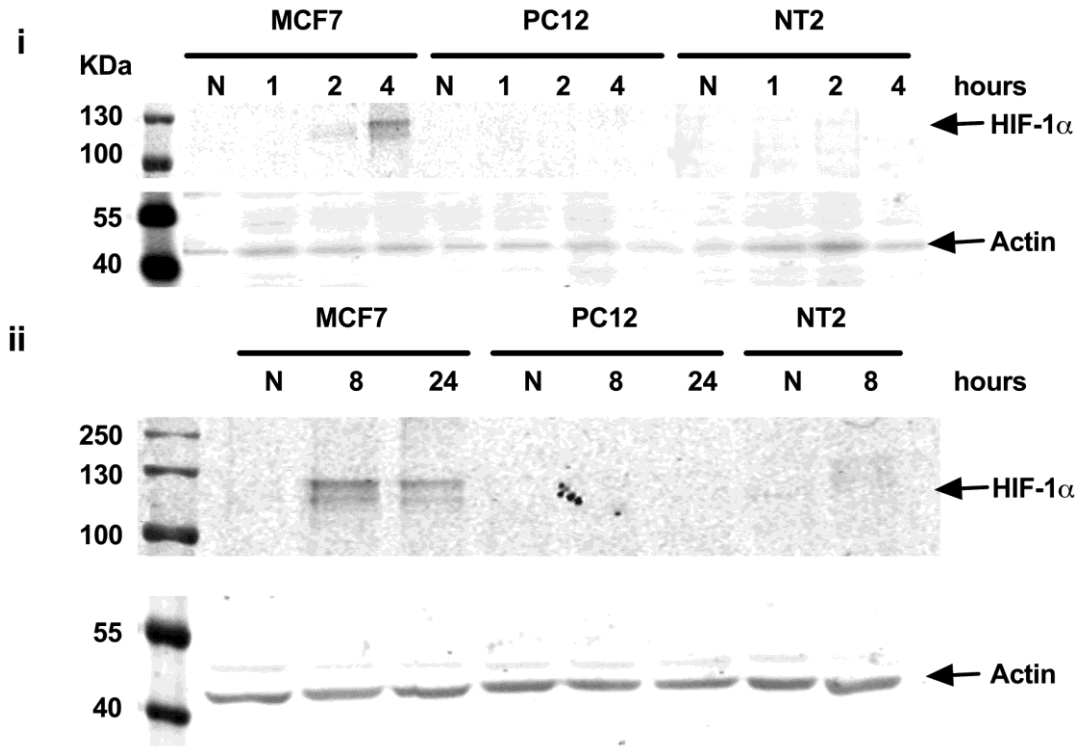

Figure 3.13. Analysis of HIF-1α protein expression in PC12 and NT2 neuronal-like cell lines following hypoxia. Representative immunoblots of HIF-1α protein expression in MCF7 and differentiated PC12 and NT2 cells in normoxic conditions (**N**) 1, 2, 4 (**i**), 8 or 24 (**ii**) hours after exposure to hypoxia. Immunoblotting with actin was used to check equal protein loading.

Bands corresponding to HIF-2α were readily detected in PC12, NT2 and MCF7 cells and their intensity increased after four hours of hypoxia (Figure3.14 A). HIF-3α expression was evident in both neuronal-like cell lines under normoxic conditions (Figure 3.14 B), however, a differential response to hypoxia was observed between PC12 and NT2 cells. HIF-3α expression was initially induced by hypoxia in PC12 cells yet reduced below basal expression at 8 hours (Figure3.14 B). By contrast, the intensity of HIF-3α expression progressively decreased in NT2 cells after four hours of hypoxia. HIF-3α expression was not detected in MCF7 cells under either normoxic or hypoxic conditions.

These results remarkably suggest that HIF-1α is not stabilised under the experimental conditions tested here. The up-regulation observed in the gene and protein expression of HIF-2α and HIF-3α suggested an alternative adaptation to hypoxia mediated by different regulators. Apoptosis and HIF downstream targets were analysed in order to determine a potential minimal activation of HIF-1α that immunoblotting could not detect but sufficient to induce a transcriptional response.

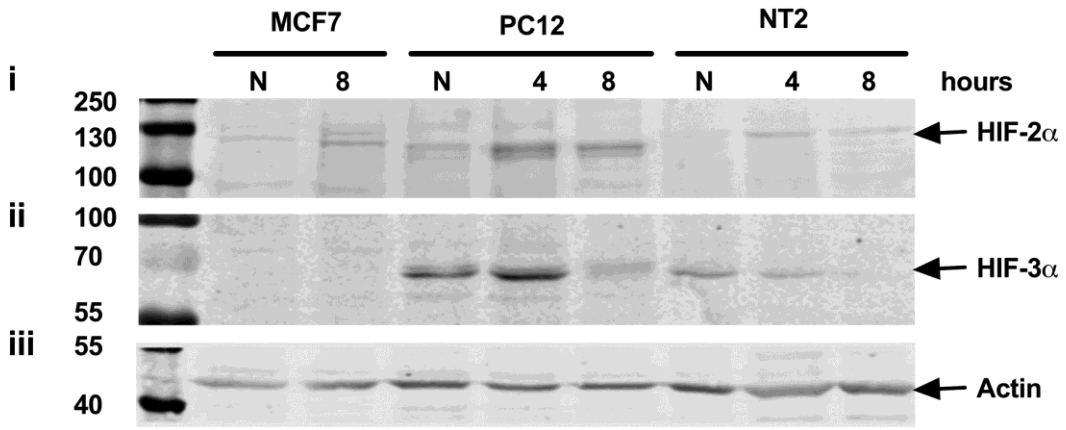

Figure 3.14. Analysis of HIF-2α and HIF-3α protein expression in PC12 and NT2 neuronal-like cell lines following hypoxia. Representative immunoblots of HIF-2α (**i**), HIF-3α (**ii**) protein expression in MCF7 and differentiated PC12 and NT2 cells in normoxic conditions (**N**) and four, eight or 24 hours after exposure to hypoxia. Immunoblotting with actin was used to check equal protein loading (**iii**).

3.4.4 Analysis of caspase-3 –mediated apoptosis following hypoxia

Differential cellular responses to hypoxia can range from adaptation of gene expression to apoptotic cell death under severe/prolonged hypoxia (Figure 3.1). Caspase-3 is cleaved as a result of mitochondrial signalling and other pro-apoptotic factors (Porter and Jänicke, 1999); it is therefore active when cells are undergoing severe stress, orchestrating apoptotic signalling. Thus, the activation of caspase-3 in neuronal-like cell lines PC12 and NT2 was experimentally tested by immunoblotting after hypoxia in order to assess whether apoptotic death was occurring rather than adaptation.

Uncleaved caspase-3 (35 kDa) is present in cell lysates after eight and 24 hours of hypoxia and under controlled conditions of normoxia (C), however the active and cleaved form (17-19 kDa) was not detected under our conditions (Figure 3.15). The lack of cleaved caspase-3 indicates that caspase-3 mediated apoptosis is not occurring. The results from the gene and protein expression profile of HIF-1-3α (Figures 3.11, 3.13 and 3.14) suggest that adaptation to hypoxia is occurring in PC12 and NT2 cells, yet that cellular death is not taking place or at least not via caspase-3-mediated apoptosis.

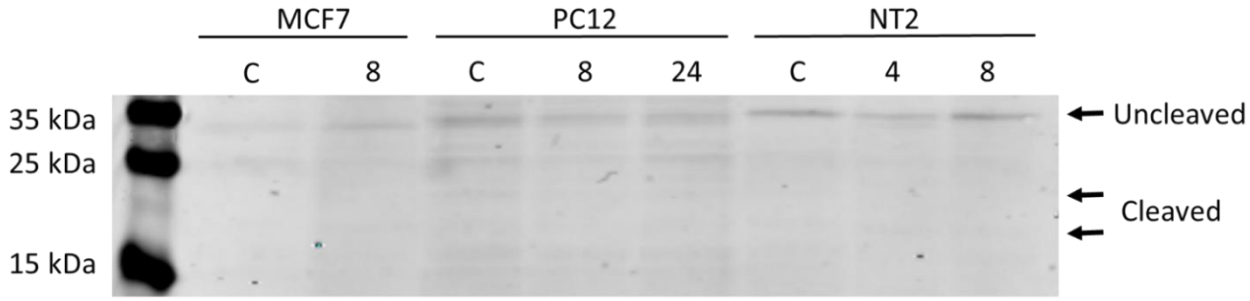

Figure 3.15. Hypoxic insult does not trigger apoptosis in neuronal-like cells. Representative immunoblot of caspase-3 protein expression in PC12, NT2 and MCF7 cells following exposure to hypoxia (1% O_2) for 8 and 24 hours or left untreated under normoxic conditions (C).

3.4.5 Analysis of HIF-1α and HIF-2α activation via downstream target expression

To further analyse potential differences in hypoxic adaptation in neuronal-like cells, regulators of *HIF-1α* and *HIF-2α* signalling were investigated. Ptbp2, stabilises *HIF-1α* mRNA promoting its translation, thus playing an essential role in HIF-1α protein up-regulation during hypoxia (Schepens *et al*., 2005). Ptbp2 interacts with the internal ribosome entry site (IRES) in the 5′-untranslated region (5′-UTR) of the *HIF-1α* mRNA allowing its efficient translation during hypoxic conditions and serum starvation (Schepens *et al*., 2005). Carbonic anhydrase isoform 9 (Ca9) is a transmembrane isozyme of the CA family that catalyses the reversible hydration of CO_2. *Ca9* is one of the most hypoxic-sensitive genes with a hypoxia-responsive element in its promoter region, while HIF-1α but not HIF-2α activates *Ca9* transcription (Kaluz *et al*., 2009). *Slc2A1 and Slc2A3*, encode the glucose transporters, GLUT1 and 3, and their expression is regulated by HIF-1α and HIF-2α (Zhang *et al*., 2009).

The fold change in *Ptbp2, Ca9, Slc2A1* and *Slc2A3* gene expression was analysed after eight hours of hypoxia in PC12, NT2 and MCF7 cells (Figure 3.16). Ptbp2 showed a 4 and 7.6-fold change in gene expression in the neuronal-like cell lines PC12 and NT2 respectively, while little change was observed in MCF7 cells expression. Surprisingly, *Ca9* expression remained unchanged after hypoxia in PC12 cells with a slight 1.2-fold upregulation in NT2 cells, whereas a 4.3-fold change in gene expression was observed in MCF7 cells. *Slc2A1* expression was significantly increased in neuronal-like

PC12 and NT2 cells, and MCF7 cells in response to hypoxia (Figure 3.16). A small but significant increase in *Slc2A3* expression was also detected in neuronal-like PC12 and NT2 cells following hypoxia (Figure 3.16) however *Slc2A3* expression was not detected in MCF7 cells or induced by hypoxic insult (Figure 3.16). This is in keeping with the fact GLUT3 is a neuronal glucose transporter (Vannucci *et al*., 1997).

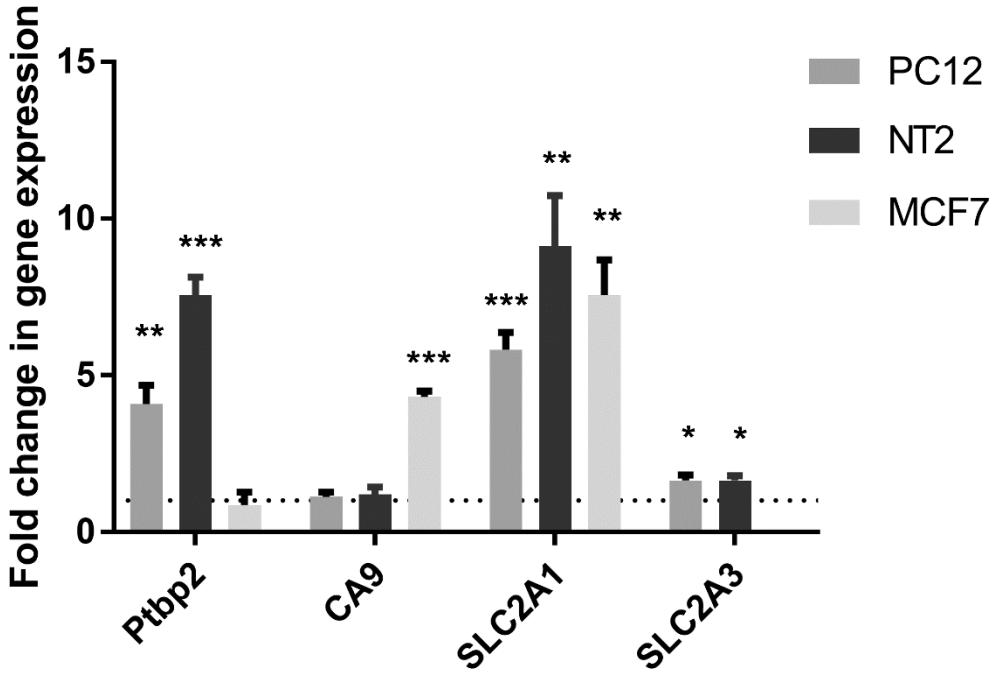

Figure 3.16. Hypoxia triggers the up-regulation of HIF-1α dependant genes in neuronal-like cell lines. Relative expression of HIF-1α related target genes (*Ptbp2*, *CA9*, *SLC2A1* and *SLC2A3*) were analysed in MCF7 and differentiated PC12 and NT2 cells, eight hours after hypoxia, using qPCR. The dotted line represents basal gene expression. Data is expressed as mean ± SEM (n=3). Two-tailed, unpaired Student's *t* test.

Cerebral hypoxia alters glucose metabolism and the expression of glucose transporters such as GLUT1 and GLUT3 (Vannucci *et al*., 1998, Maurer *et al*., 2006). Levels of GLUT1 and GLUT3 are known to be increased through both HIF-1α and HIF-2α -dependent mechanism under these conditions in the brain (Zhang *et al*., 2009). Here, the effect of hypoxia on GLUT1 and 3 was assessed as a marker of hypoxia. Heat shock protein 70 (HSP70) is an inducible molecular chaperone, which is activated under different stress conditions. HSP70 is up-regulated during ischaemia in the brain (De La Rosa *et al*., 2013). The induction of HSP70 was studied in neuron-like cells after different treatments of hypoxia.

The results displayed in Figure 3.17 show a small increase in the intensity of staining of the band corresponding to GLUT1 after eight hours of hypoxia in MCF-7 cells. However, induction of GLUT1 was not observed in PC12 or NT2 cells following the insult. Higher molecular weight bands were detected by the human anti-GLUT1 antibody. These are thought to represent post-translationally modified forms (Kitagawa *et al*., 1995). GLUT3 expression was detected in the neuronal-like cell lines PC12 and NT2 as opposed to MCF-7 cells, where no expression was observed. This is in agreement with previous studies indicating that GLUT3 is an almost exclusively neuronal glucose transporter (Simpson *et al*., 2008). Increased GLUT3 expression was not observed in either cell line after the hypoxic insults. HSP70 is constitutively expressed but up-regulated in response to different stress situations such as hypoxia (Giffard *et al*., 2008). The immunoblot for HSP70 suggests an activation and a minor up-regulation of HSP70 protein under our hypoxic

conditions in NT2 cells after four hours of hypoxia (Figure 3.17). However, induction was not observed in PC12 cells after four, eight or 24 hours of hypoxia or in MCF7 cells.

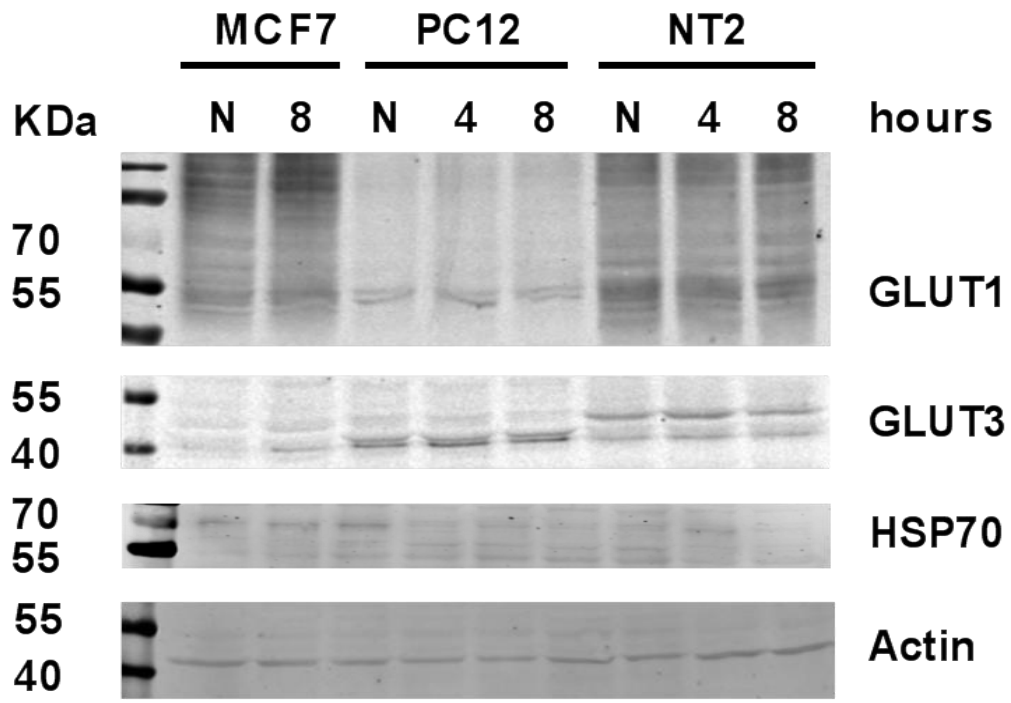

Figure 3.17. Activation of HIF-1α related targets after hypoxia in the MCF7, PC12 and NT2 cell lines. Representative immunoblot of GLUT1, GLUT3 and HSP70 protein expression in PC12, NT2 and MCF7 cells following exposure to hypoxia (1% O_2) for four and eight hours or left untreated under normoxic conditions (N). Immunoblotting with actin was used to check equal protein loading.

Despite the lack of a strong HIF-1α induction in PC12 and NT2 cells, acute hypoxia was achieved. MCF7 cells were used as a positive control throughout and hypoxia was induced simultaneously with NT2 and PC12 cells. HIF-1α stabilisation was rapidly detected in MCF7 cells and intense activation of *HIF-1α* signalling was observed (Figure 3.16). Marked induction of *Ptbp2 and Slc2A1* was observed in hypoxic PC12 and NT2 cells; genes thought to be specifically regulated by HIF-1α (Chen *et al*., 2001). However, many HIF-1α specific genes have more recently been shown to be regulated by HIF-2α, including *Slc2A1* (GLUT-1)(Harvey *et al*., 2007), underscoring the importance of HIF-2α signalling in hypoxic adaptation of neuronal-like cells.

3.4.6 Analysis of the unfolded protein response (UPR) after hypoxia

Hypoxic stress triggers accumulation of misfolded proteins in the endoplasmic reticulum (ER) (Roussel *et al.,* 2013)**.** The unfolded protein response (UPR) serves to redress ER homeostasis by fine-tuning protein translation and enhancing folding capacity (Ron, 2002). Growing evidence suggests HIF and UPR dependent pathways interact to coordinate gene expression, metabolism and cell survival (Pereira *et al*., 2014). The unfolded protein response (UPR) serves primarily to restore ER function by decreasing the quantity of misfolded proteins that must be correctly processed in the ER and enhances ER protein processing capacity. There are several key proteins induced to protect from this damage. Amongst them, the chaperones glucose related protein (GRP78) (also known as BIP) and protein di-sulfide isomerase (PDI) are induced in order to restore the correct folding of proteins.

GRP78 is strongly induced by perturbations in ER protein homeostasis following hypoxia via HIF-1α (Paris *et al*., 2005).

The UPR can also induce transcription of the pro-apoptotic transcription factor CCAAT-enhancer-binding protein homologous protein (CHOP) and following GRP78 release from ER stress receptors, caspase 7 and caspase 12 are activated, thereby triggering apoptosis (Oyadomari and Mori 2004; Nishitoh, 2012). Thus, the UPR regulates the balance between survival and cell death in stressed cells, and the up-regulation of the GRPs represents a major adaptive protective action.

Expression of UPR markers, *Grp78, PDI* and *CHOP*, was measured via qPCR in neuronal-like PC12 and NT2 cells, eight hours after hypoxic insult (Figure 3.18). *Grp78* expression was unchanged by hypoxia in PC12 and NT2 cells yet was significantly increased in MCF7 cells (Figure 3.18). *CHOP* expression was also unchanged by hypoxia in NT2 cells yet was significantly reduced in hypoxic PC12 cells and increased in hypoxic MCF7 cells (Figure 3.18). *PDI* expression was relatively unchanged in hypoxic PC12 cells but showed a small but significant reduction in hypoxic NT2 cells (Figure 3.18).

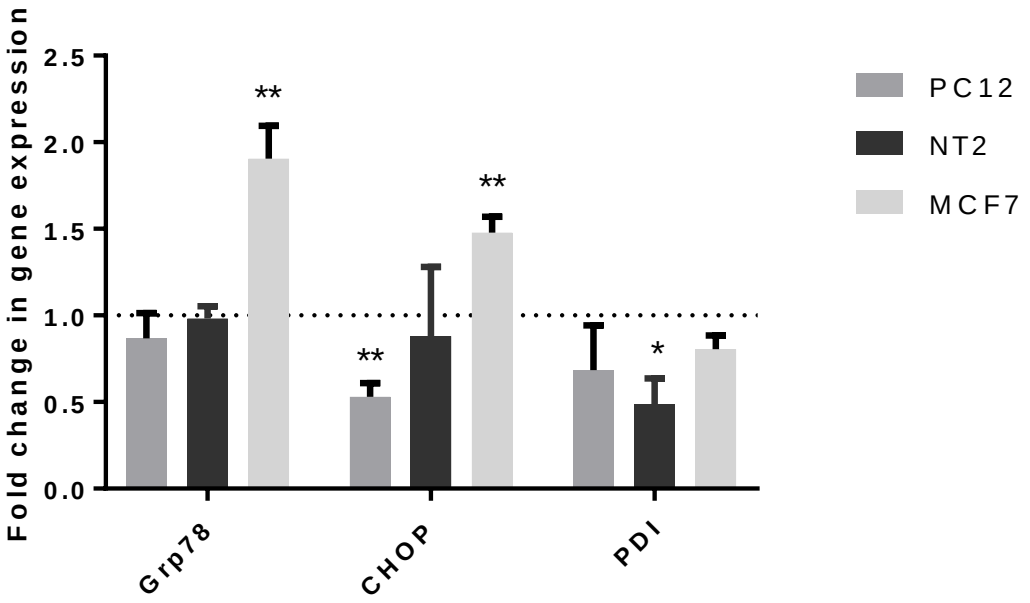

Figure 3.18 UPR response after hypoxia. Relative expression of UPR related genes Grp78, CHOP and PDI were analysed in MCF7 and differentiated PC12 and NT2 cells, eight hours after hypoxia, using qPCR. The dotted line represents basal gene expression. Data is expressed as mean ± SEM (n=3). Two-tailed, unpaired Student's *t* test.

In addition, the protein expression of the UPR markers GRP78, PDI and CHOP was analysed following 8 hours of hypoxia (Figure 3.19). The band corresponding to GRP78 was detected in PC12, NT2 and MCF7 cells although no changes in the intensity of the staining were detected following hypoxia. Strong immunostaining for CHOP was found in MCF7 and PC12 cells and a faint band corresponding to the molecular weight of CHOP in NT2 cells, although changes in expression were not observable in either cell line. Finally, and in agreement with our previous results, PDI expression was detected in PC12, NT2 and MCF7 cells with no induction following hypoxia. Overall, this data suggests neuronal-like cells present a higher

resistance to ER stress following hypoxia under our experimental conditions.

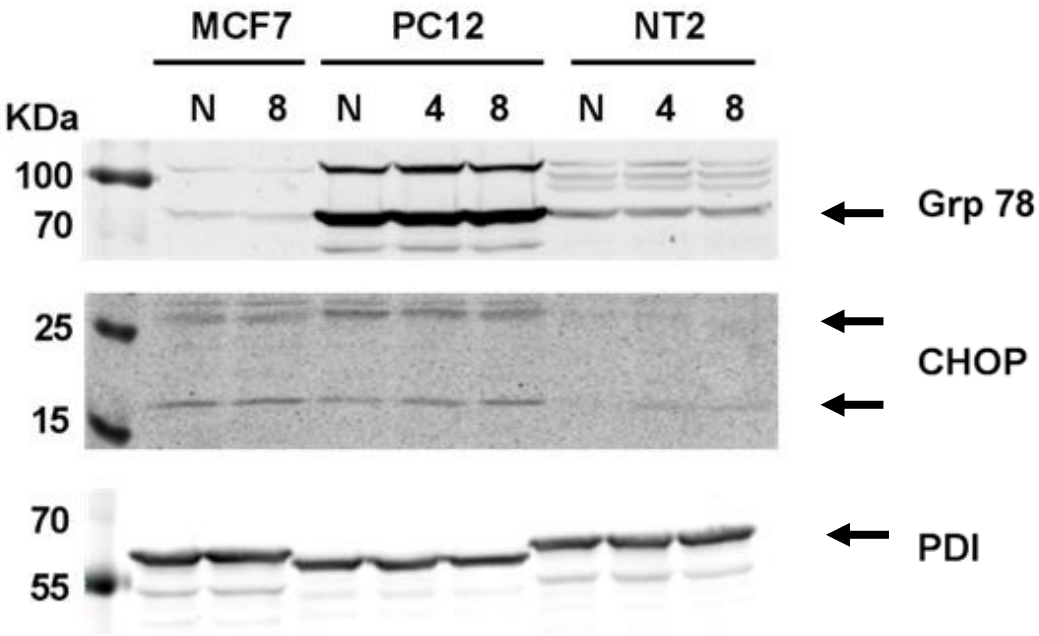

Figure 3.19. Analysis of the UPR response elements CHP, PDI and GRP78 protein expression in PC12 and NT2 neuronal-like cell lines following hypoxia. Representative immunoblot of Grp 78, CHOP and PDI protein expression in PC12, NT2 and MCF7 cells following exposure to hypoxia (1% O_2) for four and eight hours or left untreated under normoxic conditions (N).

3.4.7 Characterisation HIF-2α signalling in neuron-like cells after hypoxia

Whilst HIF-2α shares some target genes with HIF-1α, it also promotes different adaptations to hypoxic stress (Figure 3.1, (Koh and Powis, 2012; Jochmanova *et al*., 2013). HIF-2α is responsible for the activation of EPO (Chavez et al 2006) which in turn regulates hematopoiesis in order to increase the oxygen supply. EPO has also been reported to play an important role during neurogenesis (Tsai *et al*., 2006), promoting cell proliferation, survival and differentiation. HIF-2α regulates expression of stem cell markers (Li *et al*., 2009) and maintains the undifferentiated state via expression of neural crest and stem cell-associated genes (Pietras *et al*., 2009). Vimentin and CD44 are highly expressed in neuronal precursor cells (Sanin *et al*., 2013; Naruse *et al*., 2015), however expression declines during development as neurons become post-mitotic. In post-mitotic neurons, vimentin is replaced by neurofilaments (Arvidsson *et al*., 2002).

Neurofilament heavy polypeptide (*NEFH*), *vimentin*, and *CD44* expression in hypoxic neuronal-like PC12 and NT2 cells by qPCR. Neuronal marker*, NEFH* (Usoskin *et al*., 2014) expression was evident in differentiated PC12 and NT2 cells yet undetected in MCF7 cells (Figure 3.20); basal expression was also unaffected by hypoxic insult in PC12 and NT2 cells. *Vimentin* expression was significantly up-regulated in PC12 and NT2 cells following hypoxia (Figure 3.20). *CD44* expression was also dramatically increased in hypoxic PC12 cells, whilst expression was only modestly effected in hypoxic NT2 cells (1.6-

fold increase, Figure 3.20). *Vimentin* and *CD44* expression were not significantly altered in hypoxic MCF7 cells (Figure 3.20).

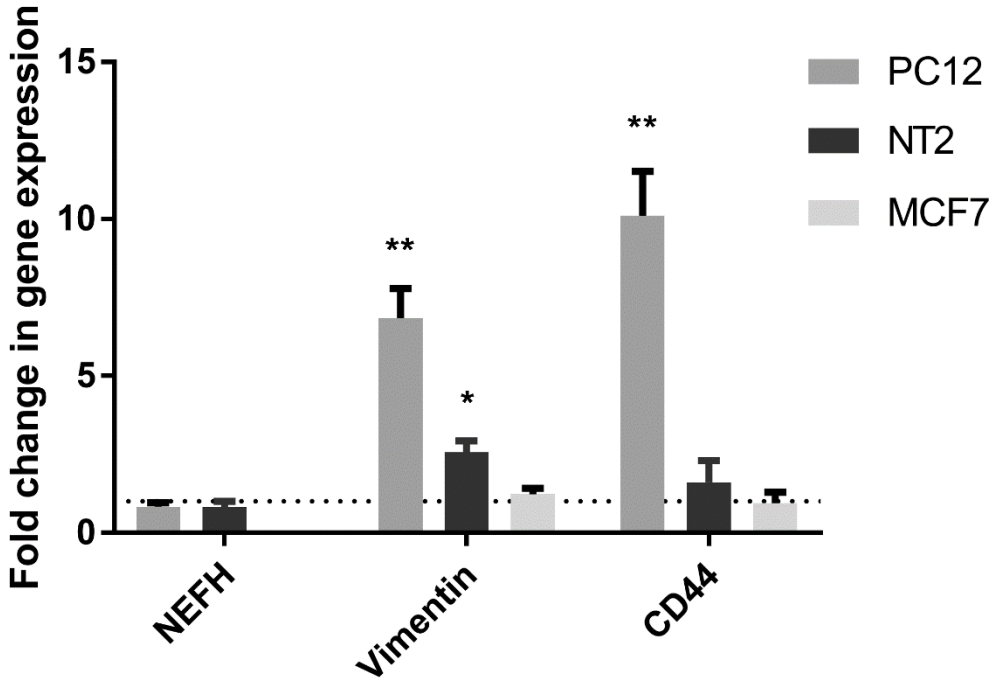

Figure 3.20. Hypoxia triggers the up-regulation of HIF-2α dependant genes in neuronal-like cell lines. Relative expression of HIF-2α related target genes *NEFH, Vimentin and CD44* were analysed in MCF7 and differentiated PC12 and NT2 cells, eight hours after hypoxia, using qPCR. The dotted line represents basal gene expression. Data is expressed as mean ± SEM (n=3). Two-tailed, unpaired Student's *t* test.

The induction of HIF-2α, vimentin and CD44 was also investigated by immunoblot (Figure 3.21). HIF-2 α was induced in both PC12 and NT2 cells after eight and 24 hours and four and eight hours of hypoxia respectively. However, MCF7 cells showed a different pattern as HIF-2α was not induced after hypoxia. This result is in agreement with the down-regulation in the HIF-2α gene expression following hypoxia in MCF7 cells (Figure 3.11). CD44 was markedly activated in NT2 cells after four hours and a strong expression was still present after eight hours. MCF7 showed again a different behaviour to PC12 and NT2 cells, as a faint activity was detected in normoxia, which was further down-regulated after 24 hours of hypoxia. Finally, a strong band at 50 kDa corresponding to the molecular weight of vimentin was detected in NT2 cells and an up-regulation was observed after four and eight hours of hypoxic insult. Vimentin was not detected in either MCF7 cells, suggesting no expression of this protein, or PC12 cells. CD44 and vimentin were not detected in PC12 cells due to a lack of epitope availability for the human-specific CD44 and vimentin antibodies in rat PC12 cells.

Together these findings show strong induction of HIF-2α regulated genes in hypoxic neuronal-like cells and suggest the HIF-2α dependant cellular regeneration arm of the adaptive hypoxic response predominates over the HIF-1α arm in neuronal-like cell lines following acute hypoxia.

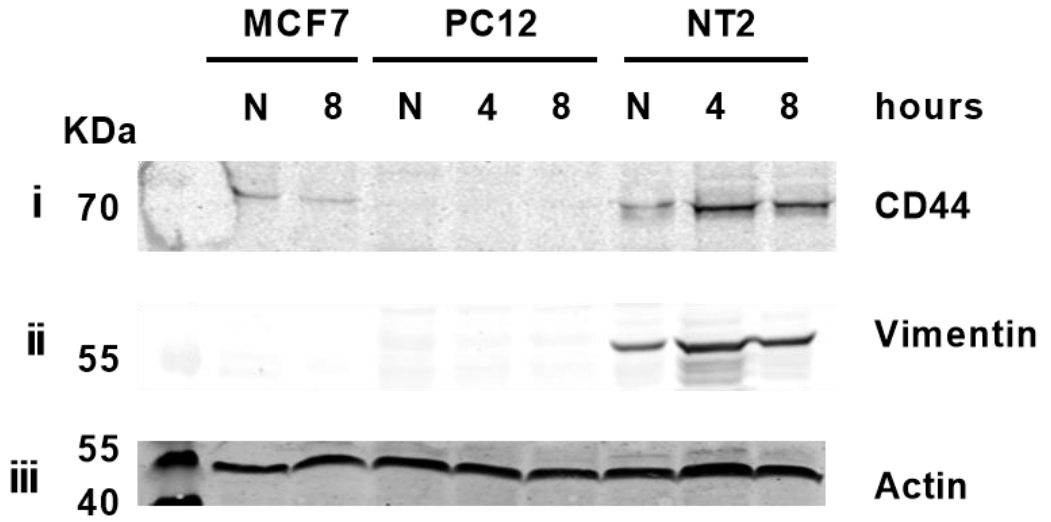

Figure 3.21. Activation of the HIF-2α response after hypoxia in MCF7, PC12 and NT2 cells. Representative immunoblot of Cd44 and vimentin protein expression in PC12, NT2 and MCF7 cells following exposure to hypoxia (1% O_2) for four and eight hours or left untreated under normoxic conditions (N). Immunoblotting with actin was used to check equal protein loading.

3.4.8 Hypoxia promotes a regression to undifferentiated states in neuronal-like cells

NSE and KCC2 are dramatically induced following neuronal differentiation of PC12 and NT2 cells (Figure 3.8). NSE and KCC2 expression was assessed by immunoblotting to determine whether hypoxia could reverse neuronal-like differentiation. The dramatic increase in NSE expression was attenuated following hypoxia in differentiated PC12 cells, whereas NSE expression remained unchanged by hypoxia in differentiated NT2 cells (Figure 3.22). The striking induction of KCC2 expression observed following differentiation was also dramatically reversed in hypoxic PC12 cells after as little as 8 hours of hypoxic insult and severely reduced in hypoxic NT2 cells (Figure 3.22).

Differentiated PC12 and NT2 display neurite-like processes and gangliar structures (Figures 3.2, 3.3 and 3.5). The neuronal-like morphology was dramatically modified in as little as 8 hours of hypoxic insult (Figure 3.23); the number of PC12 and NT2 cells presenting with neurites was dramatically reduced and the length of neurites was evidently shortened.

These results combined with the observed HIF-2α dependant induction of neural progenitor cell markers (Figures 3.20 and 3.21) suggest adaptations promoted by HIF-2α following hypoxic insult could drive neuronal-like cells into a more undifferentiated and potentially stem-like phenotype.

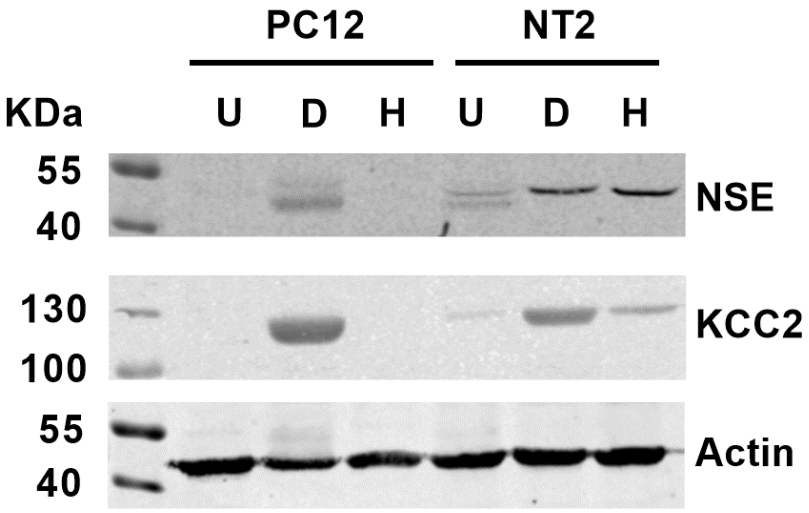

Figure 3.22 Hypoxia induces the loss of neuronal markers in PC12 and NT2 cells. Representative immunoblot of NSE and KCC2 protein expression in PC12 and NT2 cells undifferentiated (U), differentiated (D) or differentiated cells following exposure to hypoxia (1% O_2) for eight hours (H). Immunoblotting with actin was used to check equal protein loading.

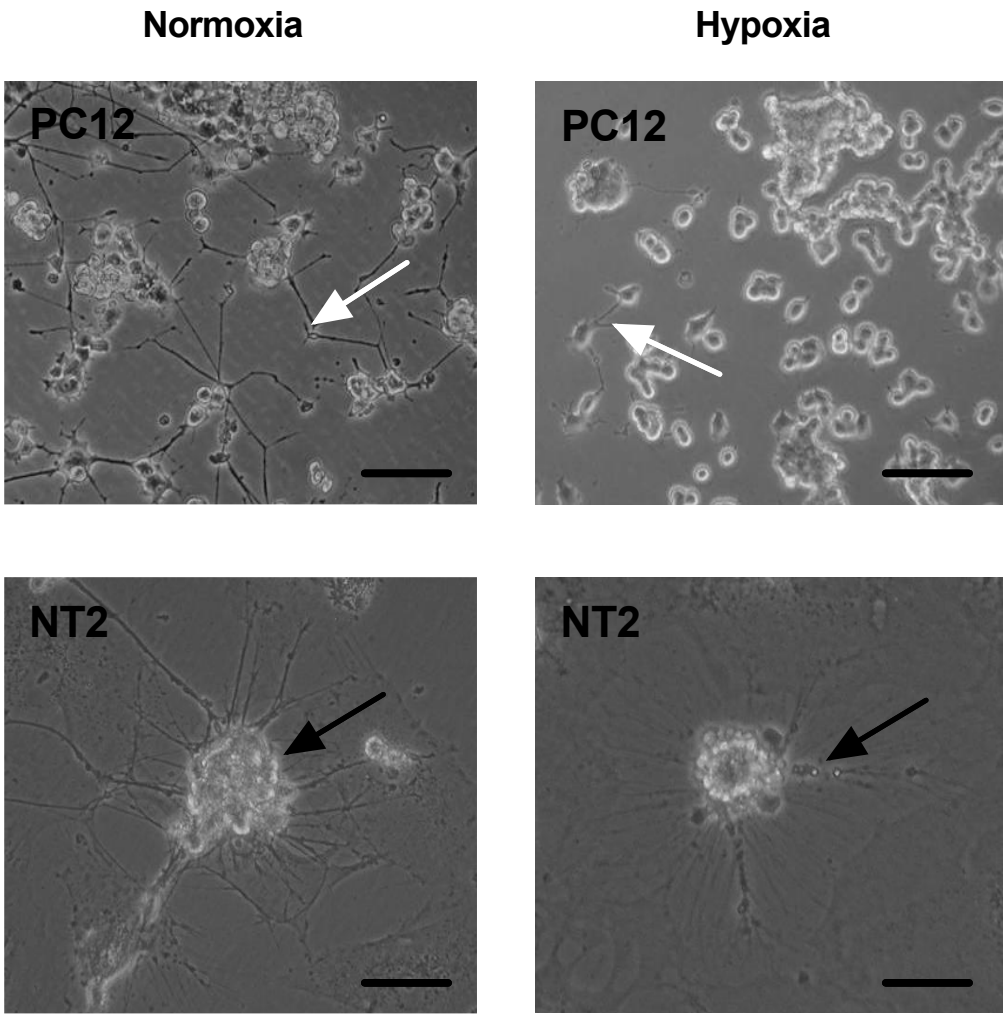

Figure 3.23. Hypoxia induces the change in the morphology of neuron-like cells into undifferentiated-like states. Representative bright-field microscopy images of differentiated PC12 and NT2 morphology after exposure to 8 hours of normoxia or hypoxia (20 x magnification). Scale bar represents 50 μm. White arrows indicate interlaced axon-like structures and black arrows indicate ganglion-like clusters.

3.5 Discussion

3.5.1 PC12 and NT2 cells as a model of neuronal-like cells

Morphological analysis, membrane staining and the analysis of the changes in gene and protein expression of PC12 and NT2 cells during differentiation, showed the methodology used offered a confident source of post-mitotic and fully differentiated neuron-like cells. The neuronal characteristics of these differentiated cell lines have been extensively covered in the literature (Haile *et al*., 2014, Jeon *et al*., 2010, Kumar *et al*., 1998, Neelands *et al*., 1998, Podrygajlo *et al*., 2009). In this study, the morphological changes observed and the neurite extension over time, indicated a neuron-like phenotype (Figures 3.2 to 3.5). Furthermore, the changes in the gene expression of *neuritin*, *tropomodulin* and *Caspr-1* and protein expression of NSE and KCC2 further indicated the differentiation into a neuron-like genotype (Figures 3.6 to 3.8).

PC12 and NT2 cells have been extensively used as a model for studying neuronal differentiation and neurological pathologies such as stroke (Tabakman *et al*., 2002, Pedersen *et al*., 2007, Angelica and Fong, 2008, Lan *et al*., 2011, Chiu *et al*., 2014). NT2 cells have undergone phase one and two clinical trials as cell grafts for stroke patients (Kondziolka *et al*., 2005, Manley *et al*., 2015). Therefore, it can be concluded that differentiated PC12 and NT2 cells are a valid source of neuronal-like cells in order to study molecular responses to hypoxia very similar to those encountered *in vivo* after a stroke. Furthermore, the advantage of *in vitro* models of cerebral ischemia is that

they can provide information at a cellular and molecular level on the mechanisms behind the insult that are not possible *in vivo*. However, our model represents a neuronal-like cell culture, whereas the brain is composed of a great number of different cellular types, with astrocytes playing a major role in regulating neuronal behaviour and the response to ischaemic insults (Takano *et al*., 2009) and this should be considered when extrapolating results.

3.5.2 HIF-1α – mediated response to hypoxia in neuronal-like cell lines

Many studies have addressed the involvement of HIF-1α in neuronal adaptation to hypoxia (Sharp and Bernaudin 2004; Ratan *et al*., 2007) and point to HIF-1α as the major regulator of the hypoxic response (Figure 3.1). HIF-2α, HIF-3α and their downstream pathways have received far less attention, however more recent work shows HIF-2α signalling is an essential component of hypoxic adaptation. HIF-1α is preferentially activated under severe (≤ 1% O_2) or acute (≤ 24 hours) hypoxia whilst HIF-2α activation occurs under more physiological hypoxia (≤ 5% O_2) and persists under chronic (≥ 24 hours) insult (Koh and Powis, 2012, Koumenis, 2006). In reality, these pathways are complimentary and co-ordinated signalling, and both HIF-1α and HIF-2α are required to promote survival and adaption following hypoxic insult (Figure 3.1). To our knowledge, this is the first study to dissect the importance of HIF dependant adaptation and downstream signalling in neuronal-like cells following hypoxia.

HIF-1α expression and induction following hypoxia has previously been reported in PC12 and NT2 cells (Frøyland *et al*., 2008; Zhdanov *et al*., 2013) therefore our observed lack of HIF-1α induction and signalling was surprising. However, closer scrutiny reveals fundamental methodological differences which account for this; employing undifferentiated cells (Hui *et al*., 2006; Koumenis, 2006), cells cultured on uncoated plates (Naranjo-Suárez et al 2003), using different exposure times (Li *et al*., 2015) or oxygen concentrations conferring mild hypoxia (Zhdanov *et al*., 2013). Our model utilises fully differentiated post-mitotic neuronal-like cells, therefore is more representative of neuronal cell function than undifferentiated cells.

Despite the lack of HIF-1α induction in PC12 and NT2 cells, it was clear that the methodology and hypoxic conditions were appropriate. The drop in the pH of the media (seen through the change of colour in the media) and MCF7 cells hypoxic induction, performed in the same chamber at the same time, indicated that hypoxia was taking place (Figure 3.16, A and C), so there was no methodological problem. However, the induction of *Ptbp2* (Figure 3.16), which is specifically controlled at a transcriptional level by HIF-1α (Chen *et al*., 2001), indicates that the activation of this transcription factor takes place but might not be detected with our experimental approach.

HIF-1α regulation is complex and factors other than oxygen might contribute to the activity of this transcription factor (Koh *et al*., 2008). It is important to know that both neuroprotective and detrimental effects of HIF-1α have been observed in different models of ischemia (Helton, 2005; Baranova *et al*.,

2007). A more recent study with knockout mice, has revealed that the combined loss of HIF-1α and HIF-2α is detrimental for functional recovery after stroke but surprisingly beneficial in the early acute phase of stroke (Barteczek *et al*., 2016). Thus, the spatial, temporal and severity-dependent role of HIF-1α and the molecular mechanisms involved in its actions are in need of further research.

PC12 and NT2 cell lines subjected to hypoxic insults appear to be resistant to the activation of HIF-1α. Data shown here indicates that neuronal-like cells might use an alternative method of adaptation to hypoxia mediated by an interplay of the different members of the HIF family of transcription factors rather than the general conception of HIF-1α as the major regulator of the hypoxic response. Interestingly, we show how HIF-2α and HIF-3α transcripts are up-regulated following hypoxia and how this response seems to be dominant over the HIF-1α mediated response.

3.5.3 HIF-2α as a novel mediator of the hypoxic response in neuronal-like cell lines

Many studies have addressed the involvement of HIF-1α in neuronal adaptation to hypoxia. The involvement of HIF-2α and specially HIF-3α and their downstream pathways has on the other hand been generally disregarded by the scientific community. To our knowledge, this is the first study that combines the different HIF-mediated responses and their downstream metabolic counterparts on neuronal-like cells following hypoxia.

The major finding of this study was that hypoxia activates the pro-proliferative HIF-2α pathway in PC12 and NT2 cells (Figure 3.20) and that this response seems to be dominant over the HIF-1α pathway. Furthermore, up-regulation of the stem cell marker, CD44, and the early progenitor neuronal marker, vimentin, indicates a regression of this cells to pro-proliferative states after hypoxia. NGF mediates the down-regulation of HIF-2α at a protein level in PC12 cells (Naranjo-Suárez *et al*., 2003). However, under our experimental conditions, both hypoxic and normoxic PC12 cells had been treated with NGF and HIF-2α protein expression was detected.

Surprisingly, neuronal-like PC12 and NT2 cells are resistant to HIF-1α stabilisation in response to acute hypoxia (Figures 3.11 and 3.13) and activation of HIF-1α dependant downstream signalling was absent (Figures 3.16 to 3.20). Instead, significant induction of *HIF-2α* mRNA and stabilisation of HIF-2α and HIF-3α protein was evident in hypoxic PC12 and NT2 cells suggesting the HIF-2α arm of the hypoxic adaptive response may predominate over HIF-1α dependant mechanisms in neuronal-like cells.

HIF-2α regulates several target genes involved in cell proliferation and regeneration, including *OCT4*; a transcription factor which maintains stem-cell-like characteristics (Nichols *et al*., 1998) and human embryonic and adult neural stem cell pluripotency (Forristal *et al*., 2010; Kim *et al*., 2009). HIF-2α signalling also maintains cells in an undifferentiated state**.** Increased expression of the stem cell marker, CD44 and early neuronal progenitor

marker, vimentin was readily observed in hypoxic neuronal like cells (Figure 3.23 and 3.24) and was accompanied by loss of neuronal markers, NSE and KCC2 and neuronal morphology (Figure 3.25 and 3.26). HIF-2α dependant hypoxic adaptation therefore promotes regression of neuronal-like cells to a more undifferentiated, and potentially proliferative, state. By reverting neuron-like cells to a more stem cell-like state, HIF-2α dependant mechanism may to trigger regeneration and neuronal recovery following hypoxic insult (Figure 3.1). Preferentially activating the HIF-2α dependant arm of the hypoxic adaptive response could therefore represent a novel strategy to minimise damage associated with ischaemic stroke and promote neurorehabilitation.

In the brain, adult neurogenesis takes place in the subgranular zone of the hippocampus and the subventricular zone (Ming and Song, 2011). It is well accepted that neurogenesis can also be driven by astrocytes acting as neural stem cells (Doetsch 2003). Neurogenesis in other adult CNS regions is generally believed to be very limited under normal physiological conditions, but could be induced after injury (Gould, 2007). Stroke induces cell proliferation and migration of new neurons to infarct sites, the vast majority of which fail to survive over long-term, presumably due to a lack of functional connections and trophic support (Arvidsson *et al*., 2002). However recent evidence suggest that neurogenesis can take place in areas that are normally non-neurogenic like striatum and cerebral cortex (Lindvall and Kokaia, 2015). Mild hypoxia (3 hours) has been shown to induce neuronal proliferation (Bossenmeyer-Pourié *et al*., 1999), although this study used cultured

embryonic rat brain cells which may have an increased resistance to hypoxia. Exogenous administration of EPO, a HIF-2α target, has also been shown to induce angiogenesis and neurogenesis after neonatal ischaemia in rats (Iwai *et al*., 2007). A recent work by Barteczeck et al. (2016) with knockout mice for HIF-1α and HIF-2α suggests partial compensatory mechanism between the two transcription factors but also reveal how specific target genes, such as EPO, are differentially regulated.

It is crucial to understand the mechanisms that promote self-repair and how non-neurogenic areas in the brain can revert to neural stem/progenitor cells. Our results show the HIF-2α pathway predominates over the HIF-1α pathway and that this adaption could promote regression to proliferative states. By completely understanding this mechanism and translating these results to *in vivo* models, it could represent a novel therapeutic approach to stimulate recovery after stroke.

Ischaemic neuronal injury is a multifunctional process (Martín-Aragón Baudel *et al*., 2017). Spatial and temporal factors combined with the intensity of ischaemic challenge will all impact upon HIF dependant adaptation and whether downstream signalling promotes neuroprotection, ischaemia induced cell death or neuroproliferation. These areas require significantly greater research. Specific therapeutic agents targeting HIF-1α and HIF-2α are needed to delineate the intricacies of HIF signalling and understand their therapeutic potential. Desferoximine pretreatment can reduce the neuronal lesion in global ischaemia in mice (Baranova *et al*., 2007), whilst exogenous

administration of HIF-2α's target, EPO can promote angiogenesis and neurogenesis following neonatal ischaemia in rats (Iwai *et al*., 2007).

Understanding the mechanisms involved in promoting self-repair and how non-neurogenic areas in the brain can revert to neural stem/progenitor cells is crucial. Our results show the HIF-2α arm of the hypoxic adaptive response may predominate over the HIF-1α arm and indicate this could promote regression to proliferative states. Therapeutic manipulation of the endogenous pathways driving neuronal adaptation to hypoxic stress could represent exciting possibilities to promote neurogenesis in the penumbra and enhance neuronal recovery after ischaemic stroke.

4. Characterising the penumbra in a photothrombotic model of ischaemic stroke

4.1 Introduction

Human neuronal tissue is rapidly and irretrievably lost in the brain as stroke progresses. It is estimated that a typical patient will lose 1.9 million neurons each minute if untreated (Saver 2006). This loss adds to the morbidity and disability that takes place following an ischaemic injury. It is therefore critical to rapidly salvage and protect the affected neuronal tissue in order to reduce morbidity and increase the quality of life of stroke survivors.

4.1.1 The ischaemic core and penumbra in stroke

The evolution of damage in stroke is a dynamic and spatiotemporal process. The ischaemic core is the infarct area immediately affected by the reduction in blood supply to the brain and occurs when blood flows is less than 30% (Yu *et al*., 2016). It is characterised by suffering from rapid and irreversible neuronal loss and is therefore considered as non-salvageable tissue (Olsen *et al*., 1983). The penumbra surrounds the ischaemic core in the peri-infarct zone, where the blood supply is sufficient to be salvaged due to collateral blood supply *(*Astrup *et al*., 1981). However, collateral arteries are not sufficient in the long term to sustain the energetic demands of this area subsequently it is characterised by a serious reduction of normal

physiological function and hypoxic adaptation (Figure 4.1). If untreated, in the hours and days following an ischaemic event, the penumbra develops towards a core-like state due to repeated deleterious events that spread out from the core, including excitotoxicity, peri-infarct depolarisations, oxidative stress and inflammatory responses that ultimately increase the volume of the infarct (Hartings *et al*., 2003). If reperfusion of the tissue takes place in a timely fashion, the penumbra can be salvaged and increased penumbral volume correlates with improved neuronal recovery. Therefore, it is of critical urgency to develop neuroprotective strategies targeted towards reducing neuronal loss in the penumbra thus, improving patient outcome (Ramos-Cabrer *et al*., 2011; Martín-Aragón Baudel *et al*., 2017). Subsequently, this would alleviate the tremendous social and economic burden of stroke.

Numerous studies have revealed the importance of the molecular events that take place in the penumbra in order to identify potential neuroprotective targets in this area (Del Zoppo *et al*., 2011; Iadecola and Anrather 2011). However, many of these studies fail to precisely characterise the penumbra in the animal model used and simply refer to this as the peri-infarct region. This is the first study to investigate the spatial and temporal development of the penumbra in mouse cortex in the five days following photothrombotic stroke (PTS) utilising a molecular approach (Figure 4.1). Different markers of the penumbra were used in order to map the molecular processes occurring in this area, such as apoptosis, neuronal stress and the formation of a glial scar. For the first time in the mouse model of PTS, the molecular

characterisation elucidated the precise location of the penumbra around the infarct in order to identify potential neuroprotective targets.

4.1.2. Imaging the ischaemic core and penumbra

Various approaches have been employed to locate the penumbra and distinguish it from the ischaemic core and adjacent healthy tissue. Imaging regional cerebral blood flow provided the basis for defining core and penumbra (Astrup *et al*., 1981) and thus, positron emission tomography (PET) was long considered as the gold standard to identify this region in clinical diagnosis (Baron 1996). However, the limited availability and high cost of this technique has recently turned attention to magnetic resonance imaging (MRI) and whole brain computed tomography perfusion (CTP), which have allowed selection of eligible patients for reperfusion therapy outside the normal treatment window of 4.5 hours following the stroke onset (Kidwell 2013; Yu *et al*., 2016). Better brain imaging techniques are needed to select patients who can benefit most from identification of penumbral tissue, which would be at risk of further infarction if reperfusion of the infarcted zone is not achieved.

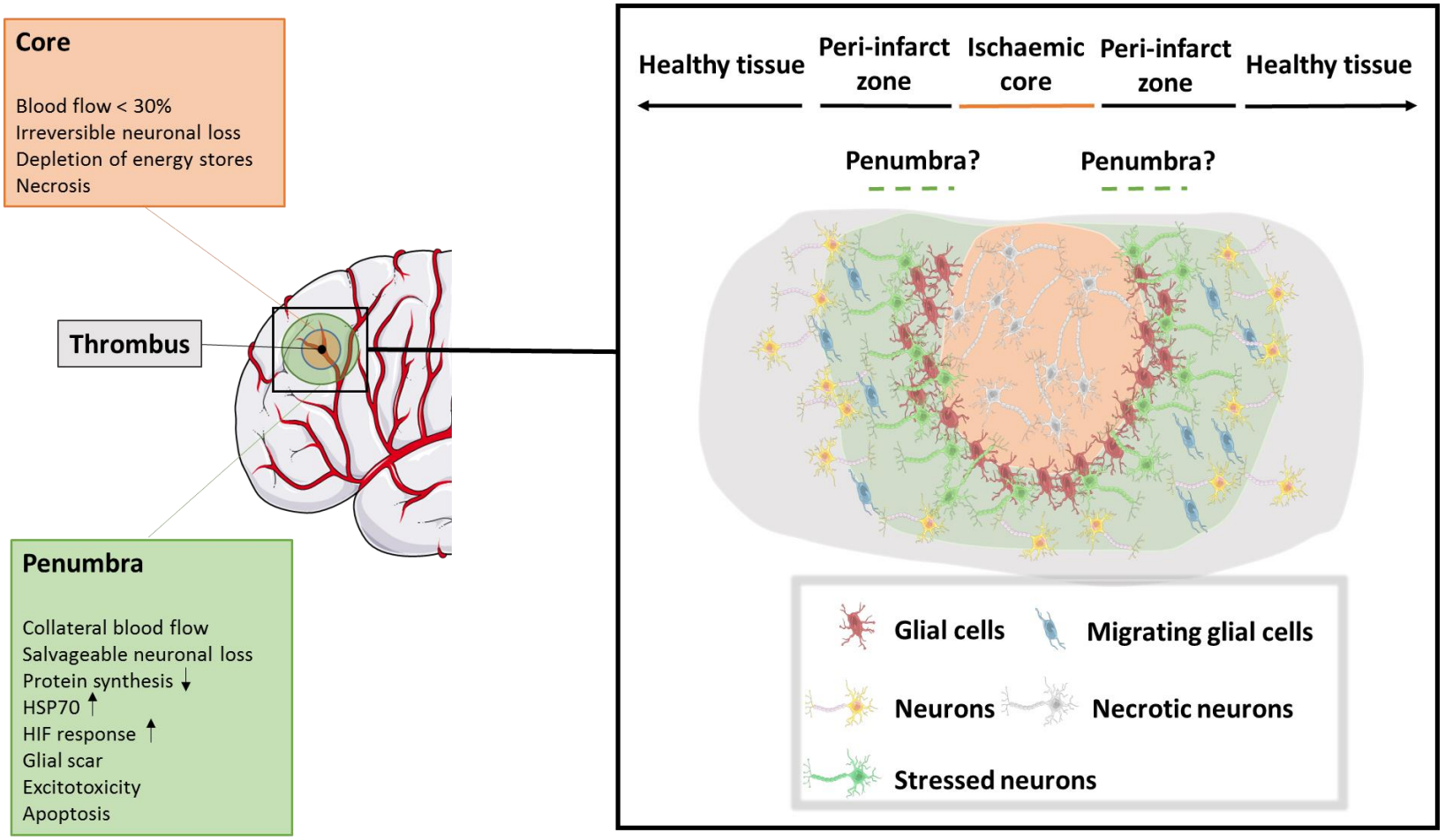

Figure 4.1. The ischaemic core and penumbra. Two physiologically and molecularly defined areas develop following a thrombus formation in the brain; the ischaemic core and the penumbra. Characteristics and adaptations are indicated. The ischaemic core, containing necrotic neurons, glial scar and stressed neurons in the peri-infarct zone are shown. Potential location of the penumbra within peri-infarct area is also indicated.

4.1.3 Models of Ischaemic stroke

In vitro models of ischaemic stroke do not fully replicate the conditions observed in human disease, therefore animal models are needed to study the mechanisms involved in development of ischaemic cell death and neural repair following stroke. Various animal models have been employed (Carmichael 2005; Casals *et al*., 2011), however, these models differ widely in their ability to simulate the conditions observed in humans following ischaemic stroke, and have limitations. Furthermore, poor characterisation of these have contributed to failure of numerous clinical trials due to low translational success rate from animal findings into patients (Dirnagl and Endres 2014).

Middle cerebral artery occlusion (MCAO) remains the most widely used rodent model as it closely replicates the conditions of an ischaemic stroke. However, this model produces a very large infarct that does not relate to the infarction size observed in humans (Figure 4.2). MCAO also presents problems of reproducibility as well as local issues with surgery-derived trauma (MacRae 2011). Some models are best suited to study mechanisms of cell damage whereas others are more appropriate to study neural repair (Fluri *et al*., 2015). Choosing the appropriate model is critical in order to increase the translational success of bench findings.

The photothrombotic stroke (PTS) model was refined in rats by Watson and colleagues in 1985. In this model, a light sensitive dye (Rose Bengal) is administered through intraperitoneal injection. When illuminated, through the

intact skull, with a cold light source, the dye releases singlets of oxygen, which in turn leads to damage of endothelial cells, platelet aggregation and clot formation in a defined region of the brain. The main advantages of this technique are that it is highly reproducible; it affects a highly delimited area of the brain (Figure 4.2) and is less invasive than other techniques to induce ischaemic damage (Carmichael 2005; Labat-gest and Tomasi 2013). Furthermore, in PTS, the contralateral hemisphere is not damaged, providing a useful control for the infarcted ipsilateral hemisphere. However, the PTS procedure also has limitations as it occludes a large number of vessels in the illuminated area; this, differs in most cases of thrombotic stroke in humans, where the interruption of blood flow takes place in a single terminal artery. Finally, the resulting penumbra in the PTS is thought to be reduced in size compared to MCAO (Figure 4.2; Witte *et al*., 2000), but it has proven sufficient to provide a useful platform to study the molecular mechanisms that induce neuronal damage and neuronal repair following ischaemic stroke.

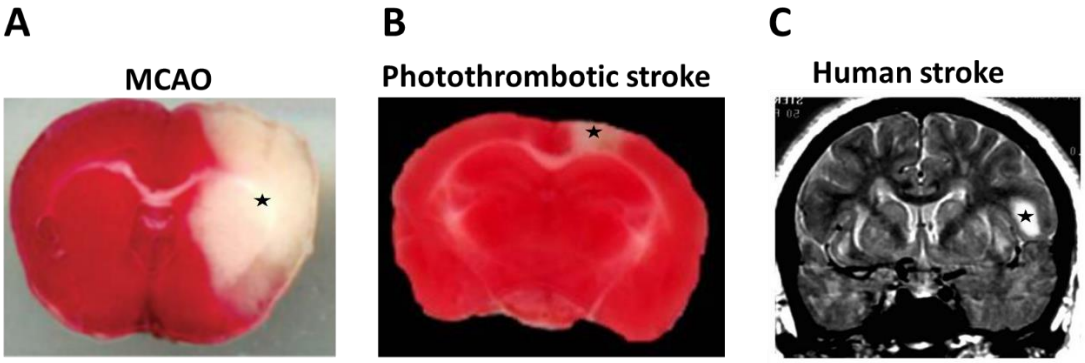

Figure 4.2. Comparison of the lesion volume induced by MCAO, photothrombotic stroke and a typical human stroke. A: Coronal section of a rat brain 24 hours post-MCAO stained with triphenyl tetrazolium chloride (TTC) showing the infarcted area (clear stain) and the healthy tissue (red stain) (Image taken from Connell *et al*., 2013). **B:** TTC-stained mouse brain five days post-PTS, (Image taken from Bierbower *et al*., 2015). **C:** T2-weighted MRI image from a stroke patient with an infarct more representative of average human stroke size (Image taken from Carmichael 2005). Stars indicate the location of the infarct.

4.1.4. Molecular markers of the penumbra

The assessment of potential neuroprotective markers within the penumbra requires characterisation of its extent and evolution in the days following ischaemic stroke, allowing identification of molecular events intrinsic to this region. Molecular events within the penumbra involve translational arrest through the unfolded protein response (UPR) (DeGracia and Hu 2007), high concentrations of intracellular calcium that lead to free radical release (Szydlowska and Tymianski 2010) and other cellular cascades that ultimately can ultimately activate apoptosis. These molecular events contribute to the

progression of the penumbra towards a non-salvageable core-like state. The increase in expression of several markers, such as glial fibrillary acidic protein (GFAP) (Hoehn *et al*., 2005; Huang *et al*., 2014), heat shock protein 70 (HSP70) (Zhan *et al*., 2009; De La Rosa *et al*., 2013), hypoxia-inducible factor 1 alpha (HIF-1α) (Bergeron *et al*., 1999), caspase 3 (Deng *et al*., 2016) or a diminished immunoreactivity of microtubule-associated protein 2 (MAP2) (Popp *et al*., 2009) have previously been used to identify the penumbra in both animal models and human patients.

4.1.4.1 Caspase-3

Neuronal apoptosis is a major factor driving the development of the penumbra towards a core-like state following ischaemic stroke. Neurons undergo apoptosis in the hours after stroke through the activation of caspase-3 (Kim *et al*., 2000). Once cleaved and activated, caspase-3 is the key executioner of the apoptotic cascade and is upregulated by increased intracellular concentration of calcium (Juin *et al*., 1998). Caspase-3 expression and activity are significantly increased in the brain following stroke (Manabat *et al*., 2003), and there is a correlation between increased caspase-3 expression, infarct expansion and poorer neurological outcome in human patients (Rosell *et al*., 2008). Cleaved caspase-3, as a marker of apoptosis, could therefore represent a useful marker of the penumbra.

Autophagy has revealed itself as another important process linked with cell death in the penumbra (Rami and Kögel 2008). LC-3 and Beclin-1 are both

well characterised markers of autophagy and are found to be increased in the penumbra following ischaemia (Rami and Kögel 2008; Pamenter *et al*., 2012). Whether the activation of autophagy presents advantageous or detrimental effects on neuronal survival remains to be ascertained. Finally, necrotic mechanisms of cellular death have also been demonstrated following an ischaemic insult in the penumbra, therefore the involvement of either apoptosis or necrosis depends on the severity of injury and the presence of reperfusion (Yuan 2009).

4.1.4.2 HSP70

When endoplasmic reticulum (ER) function is disrupted by stress, such as ischaemia, the UPR is activated (DeGracia and Hu 2007). Therefore, following stroke there is an increase in the number of misfolded proteins in the penumbra (Caldeira *et al*., 2014). The UPR-mediated response includes a global decrease in protein synthesis and a concurrent increase in the expression of proteins involved in the UPR stress response in order to clear misfolded proteins and decrease the demand on ER function (Yang and Paschen 2016).

HSP70 is a molecular chaperone. Its expression is induced under different cellular stress conditions (Brown 2007). HSP70 binds to nascent polypeptides preventing their aggregation and supporting their proper protein folding and trafficking across intracellular compartments (Mayer and Bukau 2005). HSP70 is particularly relevant in ischaemia as it is considered to have

neuroprotective potential (Rajdev *et al*., 2000). HSP70 mRNA and protein expression is strongly induced in neurons of the penumbra, while HSP70 expression is not found in neurons within the core (Zhan *et al*., 2009; De La Rosa *et al*., 2013). HSP70 has also been reported to play a role in reducing post-stroke brain damage through anti-inflammatory mechanisms (Doeppner *et al*., 2013).

The many protective roles of HSP70 in ischaemia are summarised in Figure 4.3. HSP70 is involved in downregulating the activity of the pro-apoptotic agents Fas, SMAC and the Tumour Necrosis Factor Receptor (TNFR), and inducing the anti-apoptotic protein Bcl-2 (Giffard *et al*., 2008). Overexpression of HSP72, a member of the HSP70 family of proteins, also provides neuroprotection (Xu *et al*., 2011). Therefore, HSP70 and its family members play a central role in adaptation to ischaemic stress and cell death and are considered to be excellent markers of stressed neurons within the penumbra of ischaemic stroke (Popp *et al*., 2009).

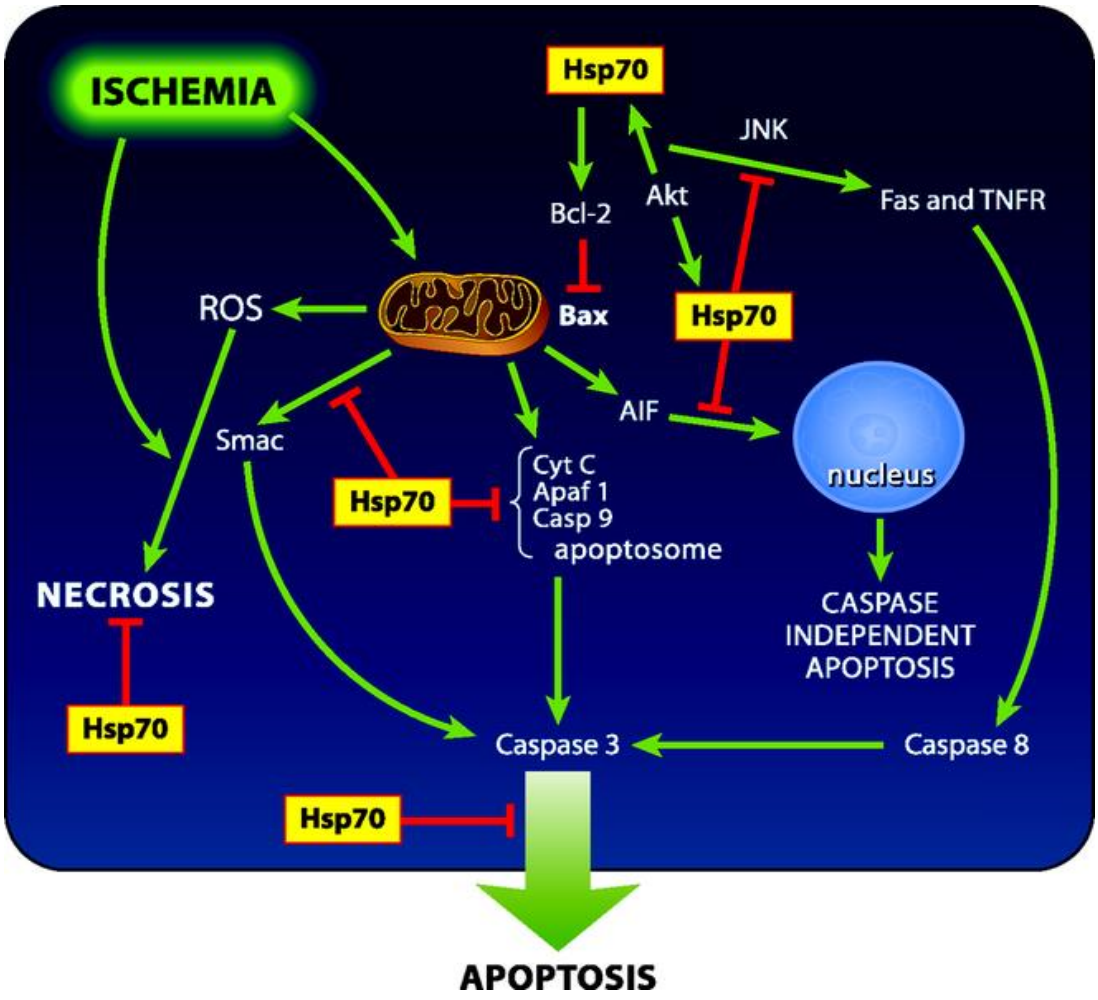

Figure 4.3. **HSP70 is involved in modulating distinct cell death pathways induced by ischaemia.** Green arrows indicate increased activity or expression and the red barred ends indicate steps that are blocked, or reduced when HSP70 is overexpressed. Cyt C = cytochrome c; Casp 9: caspase 9; JNK: c Jun N terminal Kinase; Apaf-1: apoptosis protease activating factor 1; ROS: reactive oxygen species; AIF: apoptosis inducing factor; Bcl-2 (B-cell lymphoma 2); Bax (Bcl-2 Associated X); Smac (Second Mitochondria-Derived Activator Of Caspase) (adapted from Giffard *et al*., 2008).

4.1.4.3 GFAP

Glial cells is the ‘umbrella’ term that refers to microglia, oligodendrocytes and astrocytes. Following a stroke there is an increase in the number of glial cells found in the area bordering the infarct core, which is known as the glial scar (Figure 4.1). This scar surrounds the area of damage, and confers both beneficial and detrimental effects on ischaemic tissue (Liddelow and Barres 2016). One of the hallmarks of molecular and cellular events after ischemia in the penumbra is astrogliosis, which is characterised by the increased presence of reactive astrocytes with enhanced expression of GFAP (Barreto *et al*., 2011). In addition to the activation of GFAP-positive astrocytes within the area, glial cells from the subventricular zone have been shown to proliferate and migrate to the border of the infarcted area (Figure 4.1, Shen *et al*., 2010; Abeysinghe *et al*., 2014).

During the acute phase of ischaemia, the glial scar prevents the spread of the core, stimulates revascularisation of blood capillaries, promotes axonal regeneration (Anderson *et al*., 2016) and limits the responses to inflammation, growth factors and free radicals (Rolls *et al*., 2009). However, the scar can interfere with the innate process of axonal sprouting, by secreting growth-inhibitory molecules such as chondroitin sulphate proteoglycans and creating a physical barrier to regenerating axons (Carmichael *et al*., 2016). Thus, the beneficial or detrimental role of the glial scar may be time-dependent; it appears to be beneficial in the acute phase, but detrimental to the promotion of recovery (Liddelow and Barres 2016).

Aged animals, which are more likely to suffer from a stroke, present an increased astrocytic and microglial reactivity in the peri-infarct zone, which may account for their reduced functional recovery compared to younger animals following ischaemic stroke (Badan *et al*., 2003; Anuncibay-Soto *et al*., 2014).

Most research in the field of molecular adaptation in the penumbra following ischaemic stroke investigates responses in the peri-infarct area (which includes penumbra and healthy tissue), often lacking an in-depth characterisation of the penumbra. Therefore, the results obtained in some studies could potentially over/underestimate findings due to an overlap between penumbra and healthy tissue.

The aim of this study was to fully characterise the evolving penumbra in the photothrombotic model of stroke, focusing on markers of adaptation to cell stress (HSP70), neuronal death (Caspase-3) and the glial response (GFAP). Careful analysis of relevant markers allows characterisation of the parameters of the penumbra and map the development in the days following PTS. It would also provide a platform to study different molecular mechanisms involved in the development of the injury.

4.2 Aims

Aim 1. To characterise the evolution of tissue damage in the mouse photothrombotic stroke (PTS) model of ischaemic stroke.

Aim 2. To assess the extent of the glial scar and the penumbra in the days following PTS in order to establish the parameters of the peri-infarct zone.

Aim 3. To assess neuronal loss in the penumbra.

4.3 Research Questions

RQ1. Are any of the hypothesised biomarkers currently suggested to identify neuronal death, stress and glial response valid for defining the penumbra?

RQ2. What is the extent of the penumbra in the days following photothrombotic insult?

RQ3. Is there neuronal loss in the penumbra in the days following the photothrombotic insult contributing to the expansion of the ischaemic core?

4.4 Results

4.4.1 Visual assessment of the region of neuronal injury surrounding the ischemic core

The photothrombotic stroke was performed in mice two mm caudal to the bregma point and two mm lateral to the sagittal suture, a region that includes a large part of the sensorimotor cortex of the brain (Paxinos and Franklin 2013) (Figure 4.4 A). Following PTS, the two hemispheres were separated and labelled as ipsilateral (damaged) and contralateral (non-damaged) and sectioned obtaining transversal rostrocaudal slices (following the head to tail axis) of 40 µm. Visual observations allowed the identification of the damage (Figure 4.4 B) and therefore brains that showed a similar infarcted area and location were used for further analysis to avoid differing extents of injury.

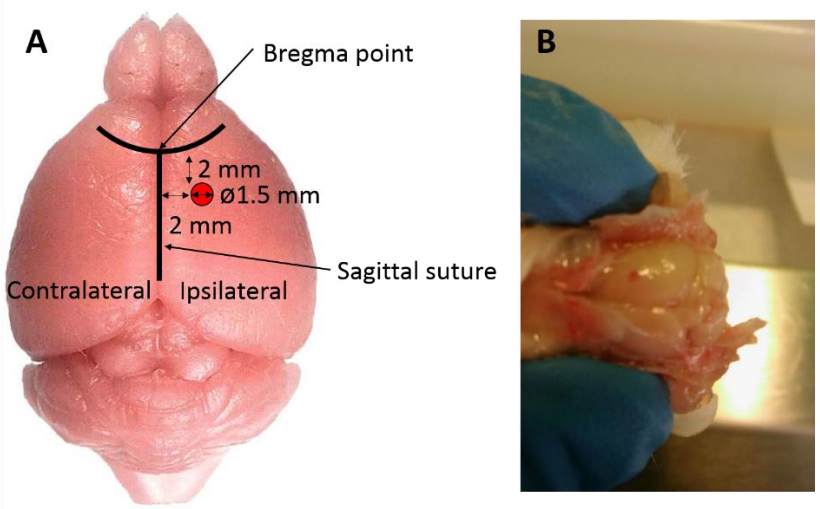

Figure 4.4. The photothrombotic injury location. (A) Schematic representation of the location of the injury in the mouse brain (red dot), which was located two mm caudal to the bregma point and two mm lateral to the sagittal suture and had a diameter of 1.5 mm. **(B)** Representative image of

a three month-old Swiss mouse brain following photothrombotic stroke showing the injured area (red dot).

Cresyl Violet is an organic compound that stains the Nissl substance in the cytoplasm of neurons (Krutsay 1970). It is used to assess the damage in infarcted areas, as it allows morphological characterisation of different brain regions, and regions of proliferation showing a darker stain. The ischaemic core was evident following PTS in all the brains analysed as this area was lost following the sectioning of the brains and immunostaining procedure. (Figure 4.5 black arrows). Cresyl violet staining demonstrated that the infarcted area was located in the frontal cortex and the extent of the infarct was reproducible (Fig. 4.5 A, B and C). Images of brains at days one, three and five following PTS showed some differences in staining between the various time points analysed. Neuronal proliferation (red arrows) appeared at the edges of the damaged area (darker stain) three and five days following PTS (Figure 4.5 B and C) but not one day post insult (Figure 4.5 A). Figure 4.5 A-C represent a comparison between three brains from different animals and further variances were attributed to differences between sections and during the Nissl staining procedure. The region affected by PTS consistently included areas of the motor and somatosensory cortex (Figure 4.5 D)

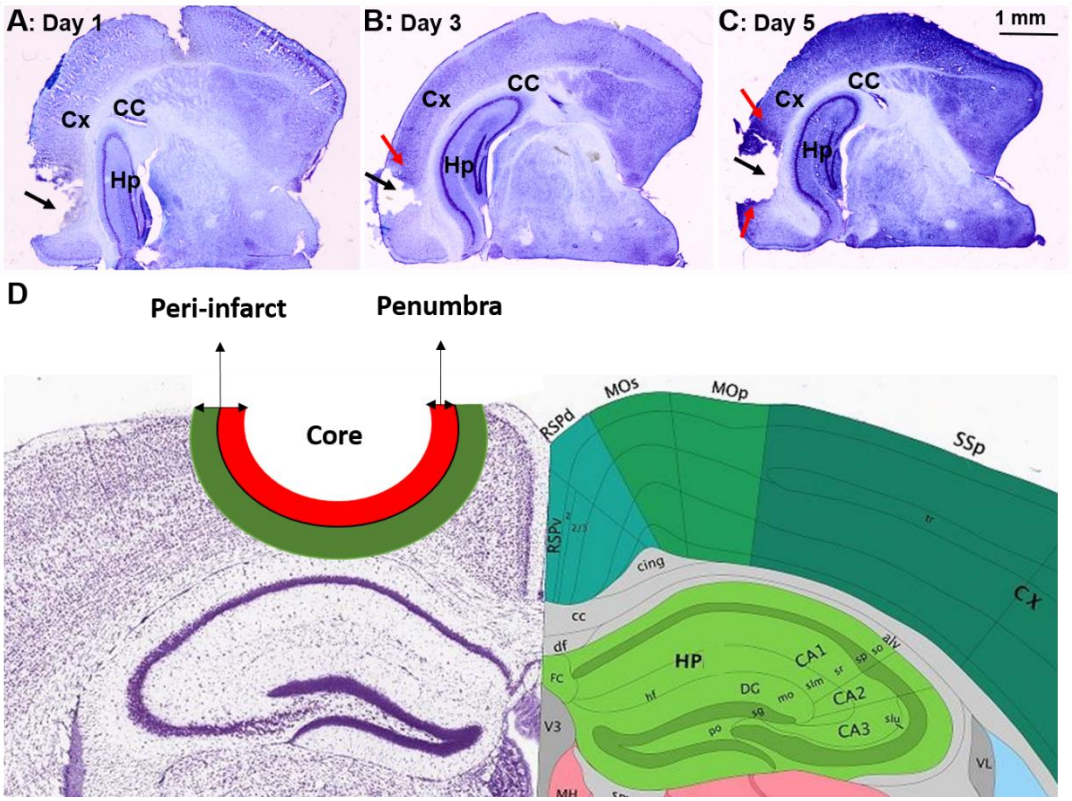

Figure 4.5. Damage inflicted by photothrombotic insult in mouse is reproducible in extent and location. Representative images of 40 µm transversal rostrocaudal sections of the ipsilateral brain stained with cresyl violet, one (**A**), three (**B**) and five (**C**) days after photothrombotic injury. Different brain regions are observed: Cx: Cortex; Hp: Hippocampus; CC: Corpus callosum. Black arrows indicate the area were the injury was performed, red arrows indicate areas of potential proliferation. **D** Schematic representation of the ischaemic core, peri-infarct and penumbra in the photothrombotic model of stroke. The peri-infarct zone is located between the primary somatosensory cortex (SSp Cx) and primary motor cortex (MO Cx). Image modified from Allen Mouse Brain Atlas (2015).

4.4.2 Identifying markers of penumbral tissue in a model of PTS

The penumbra is the partially perfused area surrounding the ischaemic core. It is a region where apoptotic cell death takes place, neurons undergo protein stress and there is an activation and migration of glial cells to form the glial scar. Therefore, caspase-3, HSP70 and GFAP were used as markers of these processes, respectively, to determine whether they would be suitable to analyse the evolution of the penumbra in the days following PTS.

4.4.2.1 Assessment of apoptosis in the penumbra

In order to determine whether apoptotic mechanisms were activated in response to ischaemic damage in the area surrounding the photothrombotic injury, cleaved caspase-3 expression was assessed via confocal microscopy. Immunolabelling of this protein was confined to the area immediately surrounding the injury (Figure 4.6 A). Specific expression of cleaved caspase-3 was detected in single cells in the area bordering the infarcted core one, three and five days after the injury (Figure 4.6 C, D and E). Expression of cleaved caspase 3 was not detected in the contralateral hemispheres (Figure 4.6 B). Apoptosis was therefore evident up to five days following PTS. However, expression of cleaved caspase-3 was low and concomitant high level background staining was observed in the contralateral and ipsilateral hemispheres (Figure 4.6). Furthermore, cleaved caspase-3 immunolabelling did not define a specific region with physiological relevance as expression was only evident in discrete cells, therefore it was deemed unsuitable as a marker to determine location and extension of the penumbra in this model.

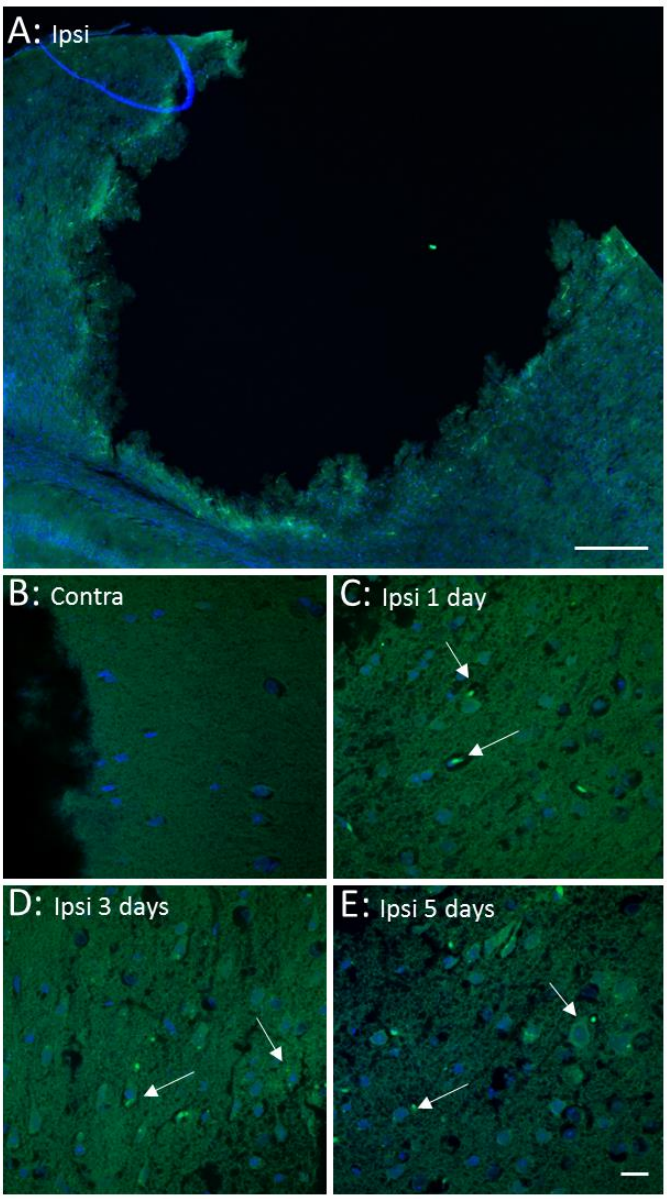

Figure 4.6. Caspase-3-mediated apoptosis is observed in the peri-infarct zone surrounding the ischaemic core. Representative images of mouse cortex following PTS immunostained for cleaved caspase 3 (green) and DAPI (blue). **A:** Tile scan representing the full extent of the damaged area (10 x magnification) one day following PTS in the ipsilateral hemisphere (ipsi). Scale bar represents 200 μm. Higher magnification (63x) representing single cells positive for cleaved caspase 3 (arrows) in contralateral hemisphere (contra) (**B**), one day (**C**), three days (**D**) and five days (**E**) following the insult. Scale bar represents 20 μm.

4.4.2.2 Assessing cell stress in the penumbra

Cleaved caspase-3 staining did not allow precise definition of the extent and location of the penumbra, therefore, an alternative marker was employed. Heat shock proteins (HSPs) have a function in the adaptive response to hypoxic insults by participating in protein-protein interactions, such as protein folding, assembly, secretion, and degradation. HSP70 is expressed in all cell types following an ischaemic event, particularly neurons within the penumbra (Sharp *et al*., 2013). Therefore, HSP70 represents not only a suitable marker of the penumbra but also a potentially interesting clinical target for neuroprotection.

The presence of HSP70 was assessed in the PTS model as a tool to measure the extent of the stressed region in the peri-infarct region and to assess whether activation of neuroprotection was taking place. Two different antibodies were tested in order to detect specific staining for HSP70 (Figure 4.7). Both antibodies revealed strong HSP70 immunolabelling in the area surrounding the injury three days following PTS (Figure 4.7 A-C and D-F). Immunolabeling with the Santa Cruz anti-HSP70 antibody was highly specific (Figure 4.7 A-B), although specific marking was not observed in the contralateral hemisphere (Figure 4.7 C). Immunolabelling with the Abcam antibody provided a more defined marking for HSP70-induced neurons within the peri-infarct region (Figure 4.7 D-F) and lighter immunolabelling, corresponding to constitutively expressed HSP70, could be detected in the contralateral hemisphere (Figure 4.7 F).

The Abcam antibody was employed in the following experiments as it detected both the induced form and to a certain degree, the constitutively-expressed HSP70. HSP70 immunolabelling showed an induction of HSP70 expression in the border surrounding the infarct core and could therefore be used in subsequent experiments to analyse the development and extent of the penumbra following PTS.

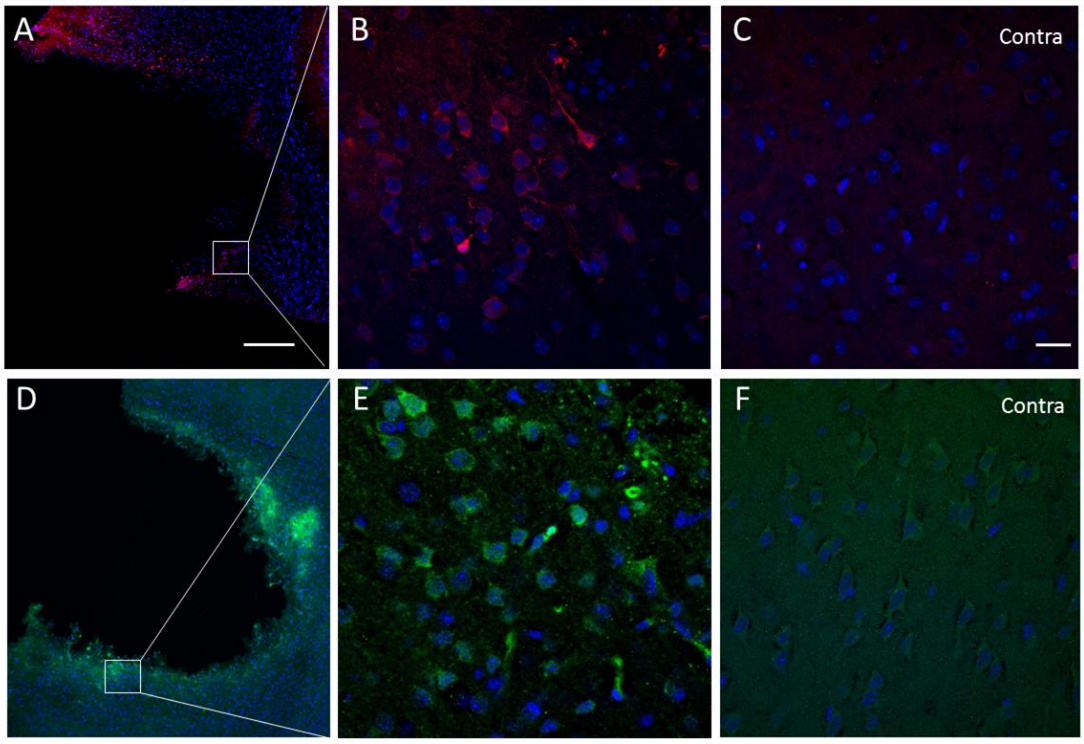

Figure 4.7. HSP70 localises in the peri-infarct area of the photothrombotic lesion. Representative images of HSP70 immunolabeling of mouse cortex three days following PTS, staining with HSP70 antibodies from Santa Cruz (A, B, C; red) or Abcam (D, E, F; green). Cell nuclei were stained with DAPI (blue). Tile scan of the injured area (A and D, 10 x magnification, scale bar represents 200 µm). Detailed image of the labelling in the ipsilateral (B and E) and contralateral (contra C and F) cortex (63x magnification, scale bar represents 20 µm).

4.2.2.3 Assessment of the glial response

The expression pattern of GFAP was determined to investigate the formation of the glial scar in the mouse brain following PTS (Figure 4.8). Glial cells migrate and seal the area surrounding the core and GFAP expression is enhanced in reactive astrocytes responding to injuries in the CNS (Sofroniew and Vinters 2010). GFAP expression is therefore considered a hallmark of the penumbra (Silver and Miller 2004, Cregg *et al*., 2014).

An intense immunolabelling for GFAP was observed in the border surrounding the injury at the different time points analysed following photothrombotic insult (Figure 4.8). Three days following PTS a distinct border of glial cells was evident with highly reactive GFAP-positive cells forming a physical glial scar surrounding the infarcted core (Figure 4.8 A). Increased immunoreactivity was evident in the cortex around the core. At higher magnification, some glial processes can be observed within the membrane of GFAP positive cells (Figure 4.8 B arrows), a further indication of the presence of reactive astrocytes (Sofroniew and Vinters 2010). These results indicated that a distinct and detectable glial scar forms in the region bordering the photothrombotic injury and is clearly evident in mouse brain following PTS.

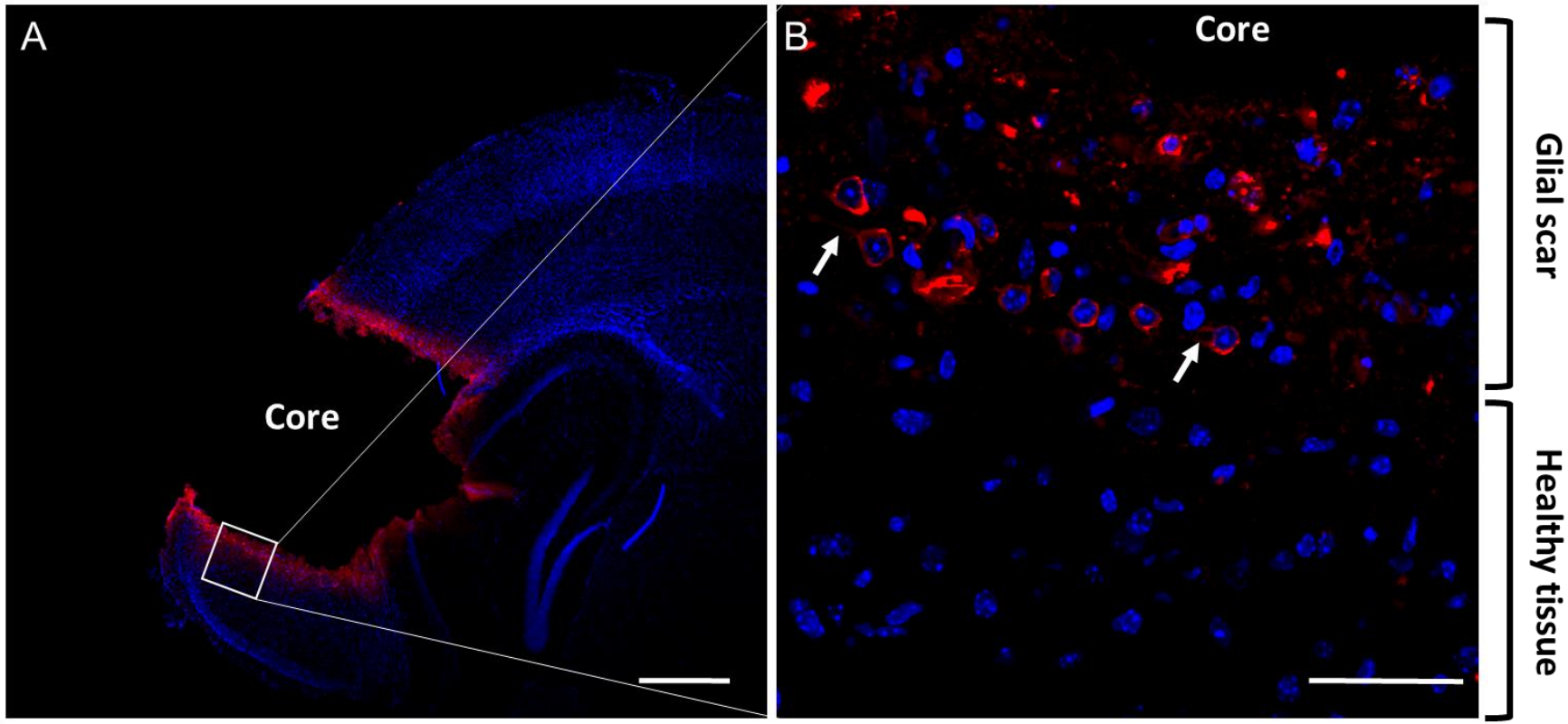

Figure 4.8. Glial cells are recruited to the area surrounding the photothrombotic stroke forming the glial scar. Representative mouse brain images displaying GFAP (red) and (DAPI) immunolabelling three days after photothrombotic insult. **A:** General overview of the marking for GFAP at x 10 magnification (A). **B:** detailed x 63 magnification. Arrows indicate extended processes. Scale bars represent 500 μm (A) and 50 μm (B).

4.4.3 Tracking the development of the glial scar and penumbra

The identification of distinct immunolabeling for GFAP and HSP70, indicative of the formation of a glial scar and stressed neurons respectively in the area immediately adjacent to the photothrombotic injury, make GFAP and HSP70 excellent markers to define and study the penumbra following PTS in mouse. The development of the penumbra was therefore assessed in the days following the photothrombotic insult in the motor and somatosensory cortex using these key markers. Serial confocal images were taken at the border of the ischemic penumbra for unbiased image analysis to assess the evoultion of the penumbra. In order to achieve this, two methodologies were utilised: 1) quantifying the mean fluorescence intensity for GFAP and HSP70 in the area surrounding the injury and 2) quantifying the decay in fluorescence intensity of GFAP and HSP70 from the core into the adjacent healthy tissue through the peri-infarct zone.

4.4.3.1. Assessing the mean fluorescence intensity of GFAP and HSP70 in the peri-infarct area

The mean fluorescence intensity of GFAP and HSP70 staining was measured up to 600 µm from the border of the infarcted area (Figure 4.9). This allowed a preliminary assessment of the increase in immunolabelling for markers of neuronal stress and the glial scar, in order to define the exact location of the penumbra within in the peri-infarct area.

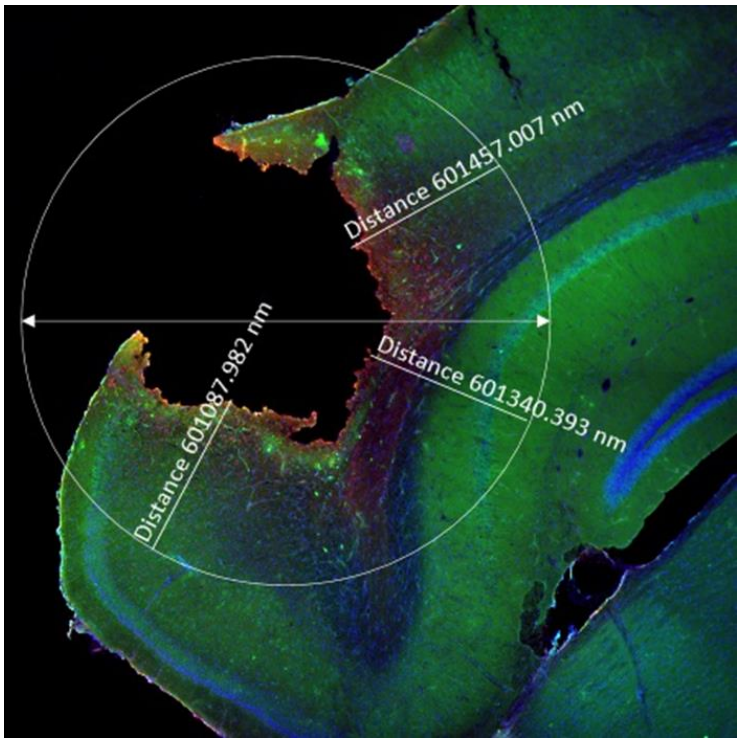

Figure 4.9. Assessing the mean fluorescence intensity in the area surrounding the photothrombotic injury. Representative image of the methodology followed in order to measure the mean fluorescence intensity of GFAP (red) and HSP70 (green) staining in the different mouse brain sections one, three and five days post PTS. The mean fluorescence intensity within an area of approximately 600 μm from the infarcted border was measured and fluorescence recorded. The image shown is a 40 μm ipsilateral brain section three days following PTS.

Brains of mice were analysed, one, three and five days following PTS and compared to untreated mice. Furthermore, three different mice per time point and nine different brain slices per mouse were analysed in order to obtain statistical significance. A significantly greater intensity of HSP70 fluorescence was observed in PTS brains compared to representative matching regions in untreated controls (Figure 4.10 panel A; $p = 0.006$ at one day, $p = 0.033$ at three days and $p = 0.054$ at five days). In contrast, no significant differences in the mean fluorescence intensity of HSP70 staining were observed between the different time points. The significant increase in HSP70 staining indicated that specific neuronal stress was evident in the peri infarct zone up to five days following PTS. The lack of significant difference in HSP70 staining indicates that neuronal stress is immediately induced and then sustained in the peri-infarct area up to five days following the photothrombotic insult.

Analysis of GFAP immunolabeling revealed a significantly higher immunostaining for GFAP in the penumbra up to five days following PTS compared to control mice (Figure 4.10 panel B; $p = 0.0015$ at one day, $p = 0.0162$ at three days and $p = 0.0189$ at five days). At one day following the insult, GFAP showed a more robust increase in the mean fluorescence intensity, whereas, at three and five days post-PTS this increase was less pronounced yet still significant. When comparing the different days analysed following PTS, the increase in mean fluorescence intensity of GFAP three and five days following PTS was lower than one day post insult ($p = 0.27$ and $p = 0.24$ respectively). The decrease in the intensity of GFAP-positive cells

in this area indicates that the glial scar is rapidly formed following PTS, declining over time.

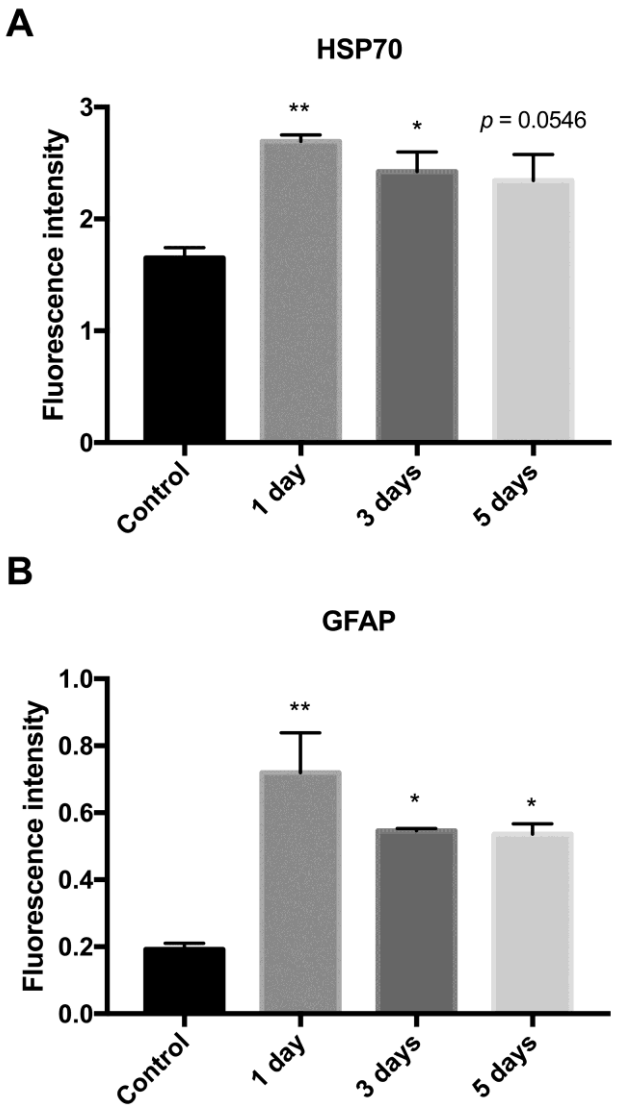

Figure 4.10. Assessment of the mean fluorescence intensity for HSP70 and GFAP staining in the peri-infarct zone of mouse brain following PTS. The mean fluorescence intensity was measured as stated in Figure 4.9. Fluorescence intensity is expressed as the mean ± SEM (n=3) normalised against the mean fluorescence intensity of DAPI staining in the same region. Statistical analysis was performed compared to control and between the different time points analysed. One-way ANOVA with Tukey's multiple comparisons test.

The data provided a general overview of the abundance of glial cells and stressed neurons, as represented by GFAP and HSP70 staining, in the area surrounding the photothrombotised tissue. In order to delimit the precise extent of the penumbra in the PTS model, the decay in intensity of fluorescence for GFAP and HSP70 staining from the ischaemic core into the healthy tissue was analysed.

4.4.3.2. Assessing the decay in fluorescence intensity of HSP70 and GFAP from the ischaemic core into the healthy tissue

In order to understand the precise location and extent of the penumbra, the decay in fluorescence for GFAP and HSP70 staining from the ischaemic core into the adjacent healthy tissue was analysed. Regions of 500 μm length and 200 μm width were marked on the brain cortex and aligned at the edge of the ischaemic core. The fluorescence across two sections at either side of the ipsilateral hemisphere and corresponding regions in the contralateral hemisphere were obtained at regular intervals (5 μm) for GFAP (Figure 4.11 A) and HSP70 (Figure 4.11 B). Data was normalised against DAPI fluorescence in order to represent data independent of cellular density. Nine brain sections per mouse (n=3 per time point) were analysed in order to obtain statistical significance and represent the injury across the z axis allowing the definition of the extent of the peri-infarct zone and the temporal changes within, one, three and five days post-injury.

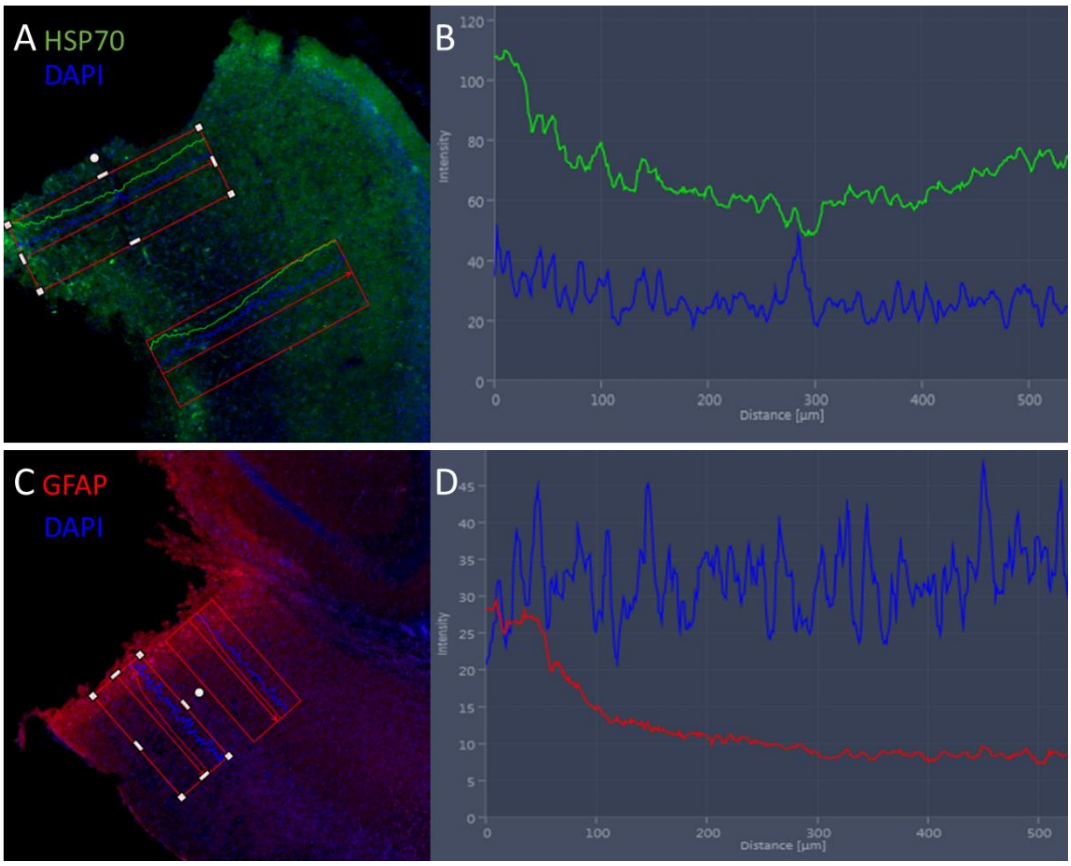

Figure 4.11. Assessing the decay in fluorescence of HSP70 and GFAP from the ischaemic core into the healthy tissue. Representative images of mouse brain sections stained with HSP70 (**A**) or GFAP (**C**) and analysed by confocal microscopy. Rectangles (500 x 200 µm) spanning the region in the cortex from the border of the infarcted core into the adjacent healthy tissue were applied to the image and the fluorescence within was measured. Fluorescence from DAPI staining (shown in blue) was also obtained to normalise for cellular density. Representative images of the fluorescent quantitation obtained from the zones are highlighted in micrographs showing HSP70 (green, **B**), GFAP (red, **D**) and DAPI (blue).

Data collected through this method was represented as the mean fluorescence intensity for GFAP and HSP70 staining at five μm regular intervals zero to 500 μm from the ischaemic core (Figure 4.12). This data was normalised to DAPI fluorescence intensity in order to accommodate differences in cellular density in the regions analysed. Statistical analysis was performed at 100 μm intervals compared to a matching cortex region in the contralateral hemisphere.

HSP70 expression was significantly higher compared to the contralateral hemisphere at each time point following the insult, up to 200 μm from the ischaemic core (Figure 4.12 A; $p < 0.001$ for one and five days, $p = 0.03$ for three days). These results indicate that HSP70 was concentrated into a region of 200 μm in the cortex region that surrounds the ischaemic core up to five days following PTS.

The fluorescence intensity for GFAP immunolabeling in the ipsilateral hemisphere was significantly higher compared to the contralateral hemisphere up to 400 μm from the ischaemic core, one day after PTS was induced (Figure 4.12, B; $p < 0.001$). Less robust, but still significantly higher fluorescence intensity of GFAP staining across this region, was observed three and five days following the insult compared to the contralateral hemisphere (Figure 4.12, B; 200 μm: $p < 0.001$ for three and five days; 300 μm: $p < 0.001$ for three days, $p = 0.008$ for five days; 400 μm: $p = 0.02$ for 3 days, $p = 0.03$ for five days).

This data and the visual observations made through immunostaining (Figure 4.8 and 4.11 B) clearly differentiate two distinct areas surrounding the photothrombotic insult, a glial scar up to 200 μm from the core and an area of increased glial immunoreactivity between 200 and 400 μm from the core.

By combining data sets obtained with GFAP and HSP70 staining, it was evident that an area of neuronal stress and the formation of a glial scar, both hallmarks of the penumbra, represent a good strategy to define the extent and expansion of the penumbra in this model. Furthermore, this data clearly identified two distinct areas within the peri-infarct zone a penumbra 200 μm from the ischaemic core and an area of increased glial enrichment (IGE) between 200 and 400 μm from the ischaemic core (Figure 4.12 C).

The immunofluorescence data displayed in Figure 4.12 was also represented as a continuous analysis of fluorescence from the ischaemic core into the healthy tissue in order to detect differences in the fluorescence decay at the different days studied following PTS (Figure 4.13).

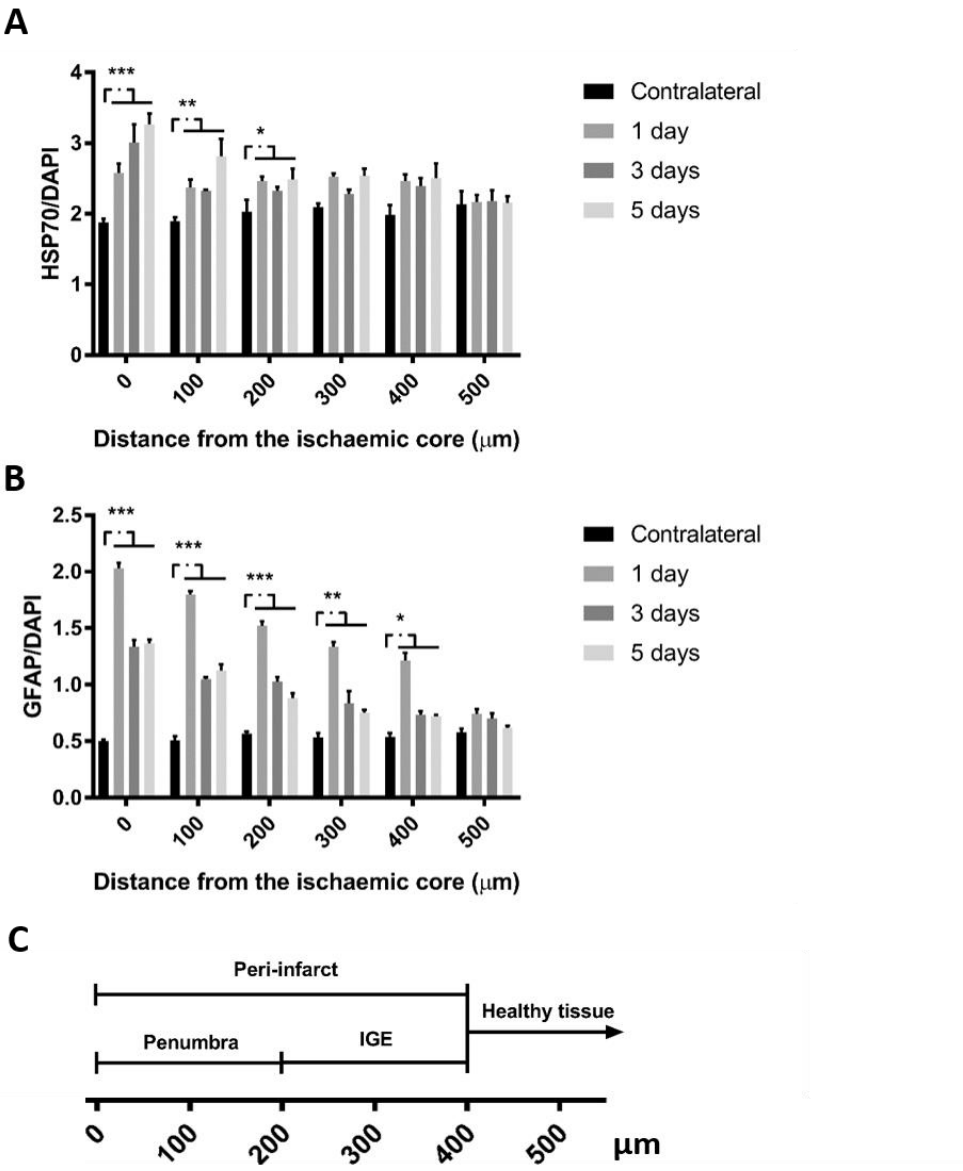

Figure 4.12 GFAP and HSP70 immunolabelling define a neuronal stress and IGE area that are hallmarks of the penumbra. The mean fluorescence intensity values for HSP70 (**A**) and GFAP (**B**) were analysed across the distance from the border of the ischaemic core into the adjacent healthy tissue. The results displayed are normalised against DAPI mean fluorescence intensity and given as mean ± SEM (n=3). Two-way ANOVA with Tukey's multiple comparisons test. **C**. Schematic summary of the findings dividing the peri-infarct zone into the penumbra (0-200 μm from the infarcted core) and increased glial enrichment (IGE) zone (200-400 μm).

Expression of HSP70 was marginally higher in ipsilateral sections five days following PTS compared to one and three days, although no significant differences were observed at the different time points analysed (Figure 4.13, A). These results were in agreement with previous results shown in Figure 4.10. The pattern of HSP70 fluorescence decay was very similar one, three and five days following PTS. This implies that neuronal stress is maintained up to five days following photothrombotic insult in the penumbra and therefore, whilst stressed, this tissue still has potential to be salvaged.

A significantly higher intensity of GFAP fluorescence was observed one day after the insult compared to three and five days post-injury at all distances up to 400 μm from the ischaemic core (Figure 4.13 B; $p < 0.001$). This is in agreement with previous data represented in Figure 4.10. The pattern of GFAP expression across the region surrounding the core three and five days following the insult was very similar (Figure 4.13 A). This indicates that the highest glial intensity was observed one day following PTS in a region radiating 400 μm from the ischaemic core, suggesting that the glial scar is rapidly formed following the insult.

Overall, these results indicate that in this PTS model the penumbra is located up to 200 μm from the ischaemic core. A transition area is also evident between 200 and 400 μm from the ischaemic core, which contains a significant increase in glial activity, representing an increase in glial enrichment (IGE) zone (Figure 4.13). The area affected by PTS included areas of the motor and somatosensory cortex (Figure 4.4).

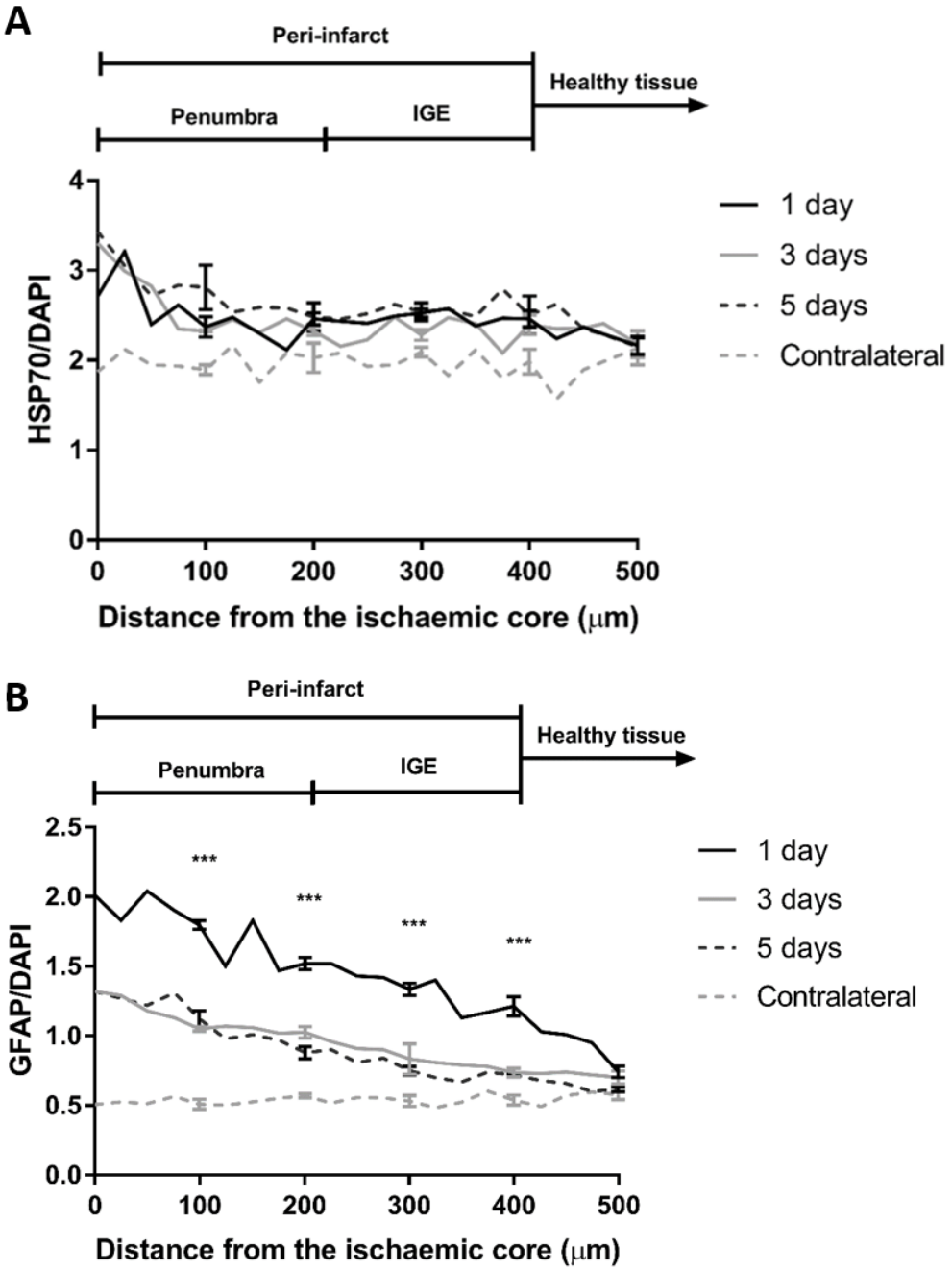

Figure 4.13. Tracking the neuronal stress and glial scar development in the days following PTS. The mean fluorescence intensity for HSP70 (**A**) and GFAP (**B**) staining were measured across the distance from the border of the ischaemic core into the adjacent healthy tissue as in Figure 4.11. The fluorescence intensity was normalised against the mean fluorescence intensity of DAPI staining and expressed as mean ± SEM, (n=3). Two-way ANOVA with Tukey's multiple comparisons test.

4.4.4. Assessing neuronal loss in the defined penumbra

Following the characterisation of the extent and development of the penumbra in mice in the days following PTS, neuronal loss was then assessed in this area. Serial confocal images of 200 µm x 200 µm were taken at the border of the ischaemic core for unbiased stereological analysis to quantitate the response of neurons to injury in the penumbra (as described in section 2.15.2). Mouse brain sections were labelled with the established neuronal marker NeuN (Mullen *et al*., 1992) to quantify the number of neurons in the penumbra in the days following ischaemic insult. DAPI was used to counterstain the total number of cell nuclei (Figure 4.14). NeuN is predominantly expressed in the nucleus, although some cytoplasmic staining was observed (Figure 4.14 B and D). Distinct areas containing neuronal cells (DAPI and NeuN-positive) were observed within the penumbra (Figure 4.14, white arrows). Other cell types were identified within the penumbra as revealed by DAPI-positive and NeuN-negative cells (Figure 4.14, red arrows). The location of these cells and the previous results shown in Figures 4.8, 4.9 and 4.11 suggest these were most likely glial cells.

NeuN positive cells in the penumbral cortex were normalised against DAPI positive cells one, three and five days following the insult and expressed as a ratio. Mice not photothrombosised presented a NeuN/DAPI ratio of 0.9, indicating a strong presence of neurons in the area (Figure 4.15). A significant decrease in NeuN-positive neurons was evident one, three and five days following the insult (Figure 4.15 $p = 0.04$ for one day and $p < 0.001$ for three and five days). The NeuN/DAPI ratio decreased to 0.66 one day following the

insult and further decreased to 0.59 three days after the insult. A significant decrease in NeuN-positive cells was observed five days post-insult when compared to three days (p = 0.03) reaching a NeuN/DAPI ratio of 0.42. This indicates significant neuronal loss occurs in the penumbra up to five days following PTS.

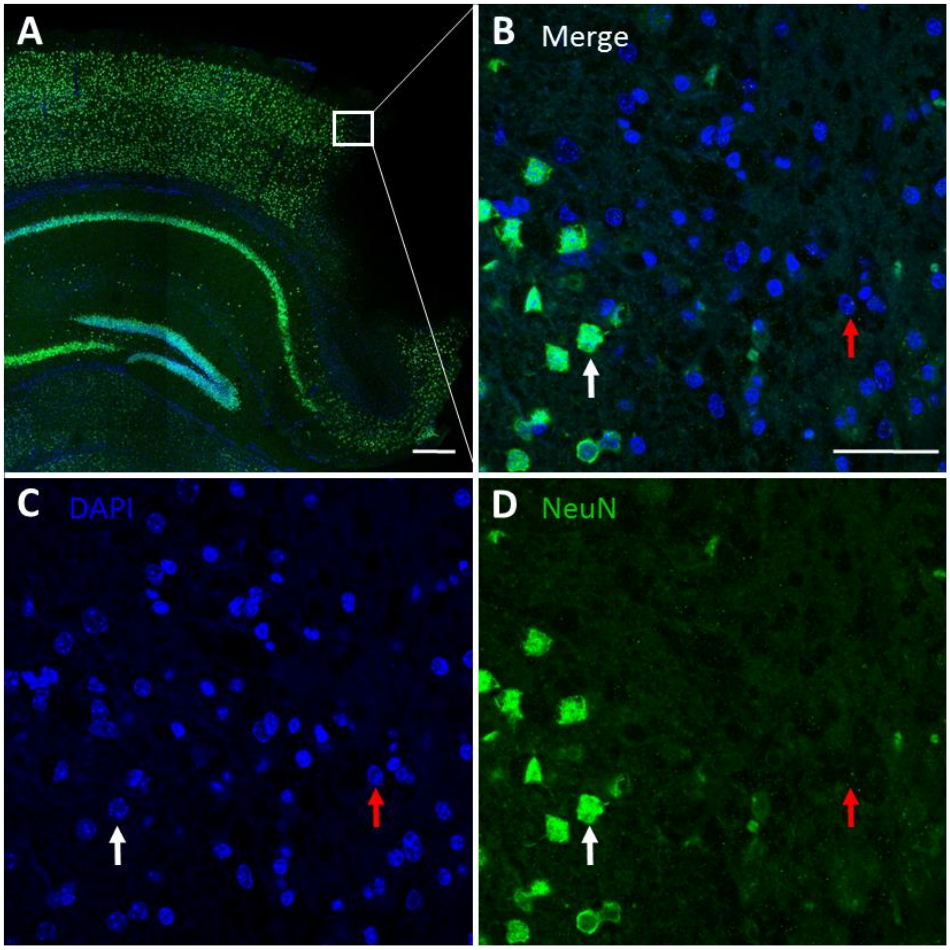

Figure 4.14. Neuronal loss in the penumbra following PTS. Representative confocal images of NeuN staining in the penumbra at low (10 x, **A**) and high magnification (63 x, **B**, **C** and **D**). NeuN (green) and DAPI (blue) positive neurons (white arrow) and non-neuronal cell types only positive for DAPI (red arrow) are represented in mouse brain, five days following PTS. Scale bar represents 200 µm (**A**) or 50 µm (**B**, **C** and **D**).

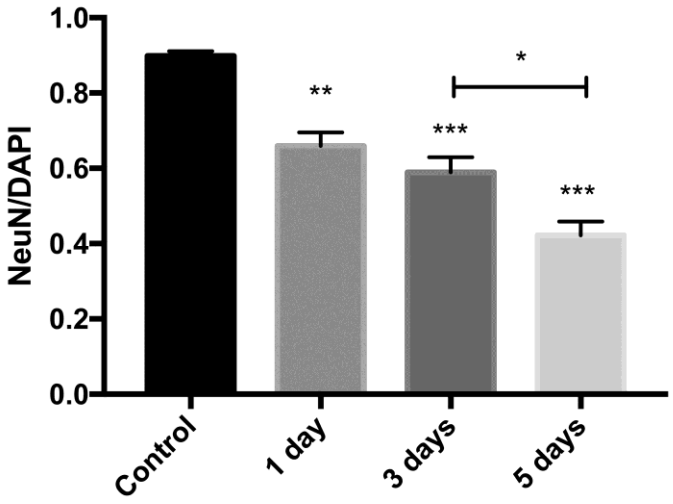

Figure 4.15. Quantifying neuronal loss in the penumbra five days after photothrombotic stroke. NeuN/DAPI ratio 200 μm from the ischaemic core represented in untreated control and one, three and five days following the ischaemic insult. Results are represented as the mean ± SEM (n=3). One-way ANOVA with Tukey's multiple comparisons test.

The aim of this study was to identify markers in order to characterise the penumbra in the PTS model in mice. The analysis was fundamental to highlight the penumbra as a therapeutically relevant region. Overall, the results indicate neuronal stress and glial scar formation, represented by HSP70 and GFAP immunolabelling, as suitable markers to study the penumbra in PTS. The penumbra was established as the area extending 200 μm from the ischaemic core. The results also identified an area of increased glial enrichment in the area between 200 and 400 μm from the core. Finally, a significant neuronal loss was identified in the penumbra through NeuN immunolabelling, which was sustained up to five days following the ischaemic insult.

4.5 Discussion

The mortality and morbidity associated with stroke is correlated with the ensuing expansion of cell death from the ischaemic core into the surrounding penumbra (Heiss 2010). The slow development of cell death in the penumbra, which takes place in the hours to days following the ischaemic onset, makes the study of this area an attractive target for the development of neuroprotective strategies. Cells within the penumbra have the potential for recovery and survival of the neurons within is associated with better prognosis (Del Zoppo *et al*., 2011), therefore, this region is an important therapeutic target to be considered for interventional therapy.

The aims of this study were to characterise the evolution of tissue damage in the mouse PTS model of ischaemic stroke, to assess the spread of neuronal stress and glial response in the days following PTS in order to establish the extent of the penumbra and to assess neuronal loss in the then characterised penumbra.

4.5.1 Photothrombosis in modelling stroke

Several models have tried to simulate the conditions observed following ischaemic stroke. These models can be broadly categorised into three groups: i) *in vitro* hypoxia, ii) *in vivo* global ischaemia and iii) *in vivo* focal ischaemia. Organotypic brain slice cultures, primary cultures and neuronal differentiated cell cultures diminish the experimental cost and number of animals used in stroke research and provide a good platform to perform wide-

spectrum analysis of the cellular responses to oxygen and glucose deprivation and understand basic cellular and biochemical mechanisms activated by ischaemic stroke (Holloway and Gavins 2016). However, *in vitro* models do not represent the complex intrinsic 3D structure and dynamics that exist between different cell types in the brain. *In vitro* models require longer oxygen deprivation insults, ATP depletion is less severe and glutamate release is delayed when compared to *in vivo* models (Woodruff *et al*., 2011). Global ischaemia models, which are produced by multiple vessel occlusion, are particularly relevant to study ischaemic events derived of cardiac arrest or asphyxia (McBean and Kelly 1998) but less representative of an ischaemic stroke in humans. MCAO, a standardised model of focal ischaemia, produces large infarction volumes and is therefore only representative of strokes in which a large artery is affected and does not present a well characterised infarct/peri-infarct region (Figure 4.2). Therefore, these models do not fully replicate the conditions observed in the penumbra following an ischaemic event.

In this chapter, focal ischaemia was achieved through the photothrombotic model of stroke. Results show a reproducible and localised infarct in the region corresponding to the motor and somatosensory frontal cortex (Figures 4.4 and 4.5). This was highly reproducible, facilitating comparison between animals. The ischaemic core was evident following PTS in all the brains analysed as this area was lost following sectioning of the brains (Figure 4.5). Therefore, this model allowed an excellent platform to characterise the evolution of tissue damage in the mouse PTS model of ischaemic stroke.

4.5.2 Neuronal death in the penumbra

In ischaemic stroke, necrotic cell death takes place rapidly in the infarcted core (Yuan 2009). Conversely, in the ischaemic penumbra, apoptosis is the main mechanism regulating cell death as a result of hypoxic insult to the brain (Namura *et al*., 1998; Ferrer and Planas 2003). Caspases are central players in apoptosis and their role in programmed cell death in neurological diseases (reviewed in McLaughlin 2004). Specifically, activation of caspase-3 is associated with the induction of apoptosis following ischaemia (Broughton *et al*., 2009) and a direct link between caspase 3 expression and infarct growth is evident in ischaemic stroke (Rosell *et al*., 2008). Furthermore, pharmacological inhibition or genetic disruption of caspase-3 expression have been found to be neuroprotective (Ma *et al*., 1998; Le *et al*., 2002) or promote neuroregenerative responses (Fan *et al*., 2014). Data presented here demonstrate discrete activation of caspase-3, therefore agreeing with previous literature and indicating that caspase-3-mediated apoptosis occurs in the peri-infarct zone following PTS (Figure 4.6).

The different mechanisms that promote neuronal death in the penumbra makes choosing a single marker, such as caspase-3, difficult to study the precise extent of the penumbra. Furthermore, due to the complex immunolabelling pattern of caspase-3, using this marker to assess the extent of the penumbra and its development in the following days represented a technical and conceptual challenge. Therefore, alternative markers of the penumbra were investigated.

4.5.3 HSP70 can define the penumbra

There is a complex relationship between apoptotic and necrotic cellular death in the ischaemic core and penumbra, however other fundamental cellular adaptations, such as the activation of the UPR and HSP70, are exclusive to the penumbra (Sharp *et al*., 2013; Yang and Paschen 2016). A global reduction in protein synthesis and induction of HSP70 is representative of the early cellular response to focal ischaemia (Zhang *et al*., 2006). Permanent abolition of cerebral protein synthesis occurs in the ischaemic core and is associated with cell death, whereas recovery of protein synthesis is known to promote cell survival (Kokubo *et al*., 2003). The expression of inducible HSP70 (HSP70i or simply HSP70), which is involved in protein folding following stress, is therefore considered to be a biomarker of penumbral tissue (Brea *et al*., 2015).

HSP70 immunolabelling in the peri-infarct zone (Figure 4.7) agree with previous literature in which the expression of HSP70 was localised in the proximity of the ischaemic core (Popp *et al*., 2009; Sharp *et al*., 2013; Agulla *et al*., 2014). In more distant areas from the infarct and the contralateral hemisphere, the expression was significantly reduced to basal levels. In neurons, HSP70 follows a time-dependent localisation as in the early stages following an ischaemic insult it is expressed in the cytoplasm, extending to dendrites and finally to axons in the later stages (Ferrer and Planas 2003). However, differences in region-specific HSP70 immunolabelling within the neuron were not observed under the conditions herein (Figure 4.7) and were not part of the investigation.

HSP70 was validated as a specific marker of stressed cells in the mouse PTS and expression was significantly up-regulated in the region extending 200 μm from the ischaemic core five days following PTS (Figure 4.16). This spatial location of the penumbra is in agreement with a previous study by *Brown* et al. (2008) using mice and the PTS model. Here, dendritic spine length was used as a tool to measure neuronal stress in the peri-infarct zone and also identified an area of neuronal stress 200 μm from the ischaemic core.

Although many studies have investigated HSP70 expression in the peri-infarct region, this study allowed the spatiotemporal characterisation of HSP70 for the first time and provided an analysis of the precise extent of the penumbra in the PTS model and its development in the days following the injury. Therefore, through HSP70 immunolabeling, the penumbra was exclusively distinguished from healthy neuronal tissue, representing a critical and necessary methodology in order to identify mechanisms of neuronal damage specific to this region (Figure 4.16). This knowledge will allow future development of neuroprotective strategies to potentially target and rescue neuronal tissue in this region and prevent its recruitment into the ischaemic core.

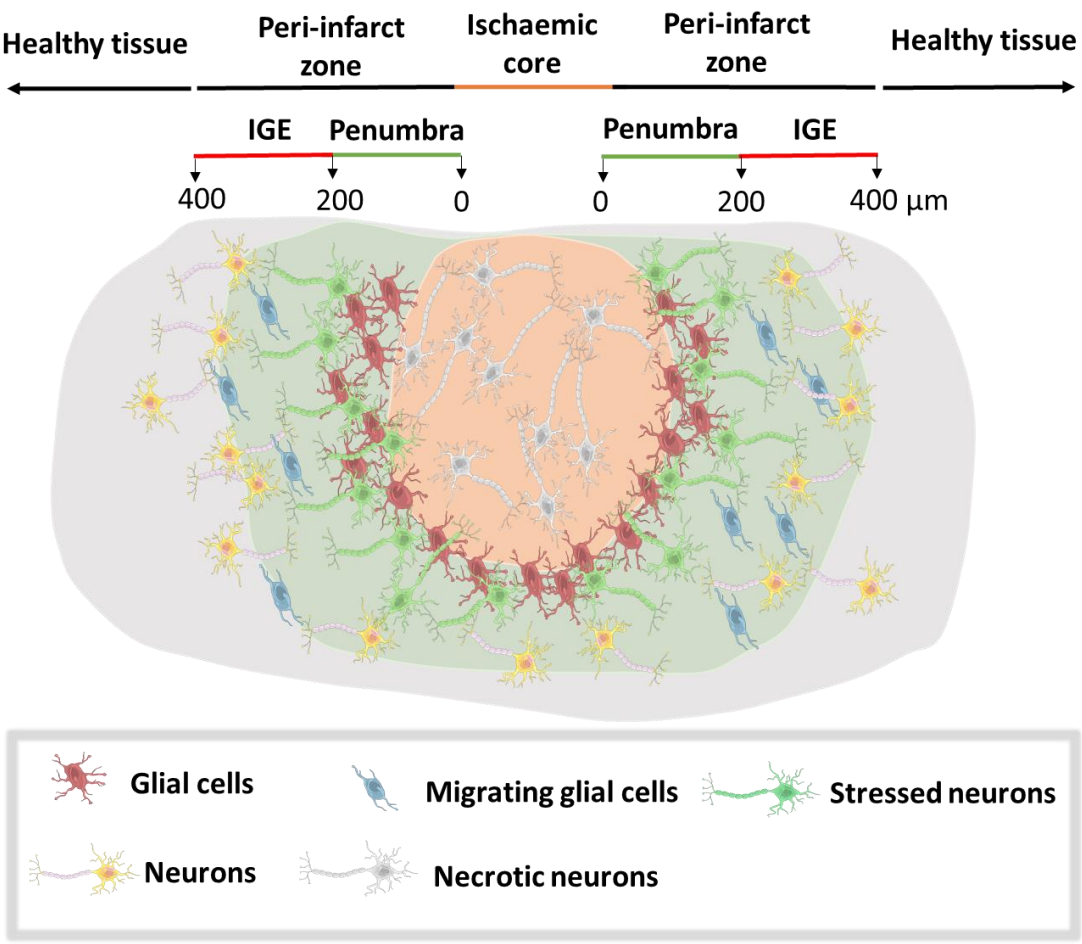

Figure 4.16. Model representing the regions that surround the ischaemic core in mouse PTS. The ischaemic core, in which necrosis takes place, is surrounded by the peri-infarct zone and healthy tissue. The peri-infarct zone is subdivided into the penumbra (0-200 µm from the ischaemic core) containing stressed neurons and the glial scar. The area of increased glial enrichment (IGE) (200-400 µm from the ischaemic core) is composed of glial cells with increased reactivity and potentially cells migrating to the glial scar.

4.5.4 The glial scar as a marker of the penumbra

GFAP staining allowed the identification of the glial scar surrounding the ischaemic core and revealed its rapid formation one day following PTS (Figures 4.8, 4.10, 4.11, 4.12). This is in agreement with previous findings, as in human patients, through PET scans, an initial microglial response was detected under 72 hours of a subacute ischaemic stroke and this persisted in the peri-infarct zone up to 30 days post-stroke (Price *et al*., 2006). In rats, microglial activation has been reported to take place within 24 hours following transient global ischaemia (Gehrmann *et al*., 1992), although phagocytic microglia were prominent eight to 12 weeks after stroke through electron microscopy in a gerbil model of MCAO (Ito *et al*., 2007). In the mouse model of PTS, elevated GFAP immunolabelling was identified one day following ischaemia in cortex, and then decreased from day seven through to day 60 post-injury (Haupt *et al*., 2007). A more recent study of PTS in mice found a significant upregulation of GFAP-positive cells in the cortex two days following the injury, peaking at day four (Li *et al*., 2014). They also analysed proliferating glial cells ($GFAP^+$ $BrdU^+$) in the peri-infarct region, and indicated that astrogliosis mostly occurs due to upregulation of GFAP expression from existing and migratory glial cells rather than proliferating glial cells. A focal cerebral ischaemia model in mice revealed that most astrocyte proliferation occurs within 200 μm of the edge of the infarct (Barreto *et al*., 2011). However, the cumulative percentage of proliferating microglial cells over a week was modest at 11.4% and the percentage of proliferating astrocytes declined sharply with distance. This study indicated that only astrocytes within the glial boundary resume proliferation following stroke, while

astrocytes further out display reactive changes but largely without proliferation. Overall, these previous findings are in agreement with the results of this chapter, indicating that the glial scar forms rapidly following stroke and that its presence is sustained in the days following the insult.

The investigation of glial scar formation incorporated a spatial analysis that complemented the previously well documented time-dependent formation analysis of the glial scar (Li *et al*., 2014). The temporal analysis is in agreement with previous studies that indicated rapid glial scar formation following stroke and extends this investigation by incorporating spatial dynamics of glial reactivity. Two distinct areas of glial reactivity were observed in the PTS model (Figure 4.16); **i)** a well-defined glial scar with a significant increase in GFAP immunolabelling, representing reactive astrocytes, in the region up to 200 μm from the ischaemic core, and **ii)** an area with a decrease in GFAP immunolabelling and reduced level of structural intricacy in the area between 200 and 400 μm from the ischaemic core (Figure 4.12, Figure 4.13). The lack of proliferating cells in this region shown by others (Barreto *et al*., 2011) and the fact that neural stem cells can migrate to the peri-infarct region where they can differentiate into reactive astroglia (Faiz *et al*., 2015) suggest that this area could represent a migratory zone to the area surrounding the injury.

The exact role of the glial scar is still under debate as both beneficial and detrimental roles have been observed (Carmichael *et al*., 2016). However, current thinking suggests that the glial scar is beneficial in the early

responses to ischaemic injury to seal and confine the damage (Rolls *et al*., 2009), but it is detrimental in the long term as it prevents axonal regeneration in the area (Carmichael *et al*., 2016).

The analysis of HSP70 spatiotemporal immunolabelling and acknowledging the glial scar as a marker of the penumbra (Zamanian *et al*., 2012; Li *et al*., 2014), provide strong evidence for the existence of penumbral tissue located up to 200 μm from the ischaemic core in mouse brain following PTS under the aforementioned experimental conditions (Figure 4.16). In summary, this research provided evidence for the molecular subdivision of the peri-infarct zone into the penumbra and an area of increased glial enrichment (IGE) and precisely characterise the extent of each region.

4.5.5. Neuronal loss in the penumbra

Brain ischaemia induces selective neuronal loss in the penumbra, being particularly relevant in the cortex, striatum and CA1 layer of the hippocampus (Pulsinelli *et al*., 1982). NeuN staining is considered to be the best method to quantify neuronal loss although it presents some limitations as some neurons may still stain for NeuN yet already be dead (Baron *et al*., 2014). Although avoiding neuronal loss in the penumbra is a logical and well documented beneficial therapeutic strategy, some degree of neuronal loss is known to be beneficial in order to promote plastic reorganisation, a process that underlies recovery (Neher *et al*., 2013; Baron *et al*., 2014).

Neuronal loss takes place in the penumbra and this loss increases progressively in the days following the PTS (Figure 4.15). This has great relevance as it shows that affected penumbral areas are recruited to the infarct core. There is an increase in neuronal damage in the days following the insult, a time window that is outside the therapeutic treatments currently used (Green and Shuaib 2006). Therefore, this area of the brain has a potential to be salvaged and it is of critical necessity to understand the mechanisms that lead to the recruitment of this area into the infarct core. This will allow the development of neuroprotective strategies with a therapeutic window that accompanies the reality of stroke patients, which do not normally benefit from the strategies of revascularisation due to its limited 4.5 hours window (del Zoppo *et al*., 2009). Current strategies rely on the rapid revascularisation of the affected area through thrombolytic agents, such as recombinant tissue plasminogen activator (rt-PA) or mechanical thrombolytic devices (Holmes *et al*., 2015; Akbik *et al*., 2016). Neuroprotective and neurorehabilitation strategies are needed, especially at the sub-acute and chronic phases of stroke, for which no effective therapies are currently available, probably due to a lack of understanding and characterisation of penumbral dynamics.

In summary, the assessment of the extent and evolution of the penumbra in the days following PTS, provides an excellent tool to study mechanisms of neuronal damage in this area and the potential for the development of therapeutic strategies specific to the penumbra. These results provide a strategy to discriminate between penumbra and healthy tissue within the peri-

infarct zone and a method to quantify this specific response. Furthermore, the increasing neuronal loss observed up to five days following the insult, emphasises the potential of this area to be salvaged. Therefore, a platform in which to study penumbra-specific molecular events involved in the spreading of the damage was created.

5. Chloride co-transporters represent a valid therapeutic target to reduce neuronal loss in stroke

5.1 Introduction

Stroke is a leading cause of death and disability worldwide (Thrift *et al*., 2014; Mozaffarian *et al*., 2016). The interruption of blood flow to the brain creates an infarct that continues to develop in the hours and days following ischaemic injury (Chapter 4; Baron *et al*., 2014). Increasing the volume of saved penumbral tissue, can improve neuronal recovery (Heiss 2010). Furthermore, one third of patients suffer from secondary damage of penumbral tissue augmenting the neurological impairment for which there are no current therapies (Roger *et al*., 2011). It is therefore imperative to develop novel therapeutics that could ameliorate the damage caused by the ensuing neuronal loss in the penumbra and promote neurorehabilitation (Martín-Aragón Baudel *et al*., 2017).

5.1.1 Excitotoxicity in the development of the penumbra

The ischaemic core is the brain region immediately impacted by rapid and irreversible damage and is subsequently considered as a non-salvageable tissue (Astrup *et al*., 1981). The penumbra, area immediately surrounding the

ischaemic core, is only partially metabolically compromised but it can be readily recruited into a core-like state due to excitotoxicity (Olney 1969; Hinzman *et al*., 2015). This is a consequence of the inability of collateral blood supply to sustain the high glucose and oxygen demands of the penumbral tissue, leading to the deterioration of neuronal ionic gradients (Dreier and Reiffurth 2015). Ionic dysregulation results in excessive activation of NMDA and AMPA receptors and increased intracellular calcium, which ultimately leads to caspase activation and free radical formation (Szydlowska and Tymianski 2010) among other ionic dysfunctions (Chapter 1). Substantial release of excitatory neurotransmitters produce continuous peri-infarct depolarisations (PIDs) (Nedergaard and Hansen 1993) that spread outwards from the ischaemic core, depleting the glucose and ATP pool, and preventing neurons from repolarising (Feuerstein *et al*., 2010; Dreier and Reiffurth 2015). The penumbra has the potential to be salvaged and it is therefore necessary to determine the underlying molecular mechanisms responsible for the damage that could provide novel therapeutic targets.

In the previous chapter, molecular characterisation of the peri-infarct region following photothrombotic stroke in mice was performed. This provided a defined platform to elucidate the extent of the penumbra and assess neuronal loss within this region in the days following the insult. The resulting penumbra in this model extended 200 μm from the ischaemic core and a significant neuronal loss was observed within one day and continued over the five days monitored following the insult. The aim of the following study was to

investigate the pattern of expression of the cation chloride co-transporters (CCCs) in the penumbra in order to extend the molecular characterisation and discern their potential validity as neuroprotective targets.

5.1.2 Chloride cotransporters mediate GABAergic inhibitory tone

Synaptic activity is responsible for information processing in the CNS. Synaptic activation of $GABA_AR$ usually inhibits post-synaptic neuronal firing, whereas release of glutamate promotes action potential emission. $GABA_AR$ are transmembrane ligand-gated ion channels. $GABA_AR$ activation generates an inhibitory post-synaptic current that depends upon the electrochemical gradient within the neuron relative to extracellular [Cl^-] (Kaila 1994). Cation chloride cotransporters are the key players in the regulation of intracellular chloride concentration in neurons (Kaila *et al*., 2014). The CCC family of proteins includes two Na^+–K^+–$2Cl^-$ cotransporters, NKCC1 and NKCC2 (encoded by *Slc12a2* and *Slc12a1* respectively), a Na^+–Cl^- cotransporter (NCC; encoded by *Slc12a3*) and four K^+– Cl^- cotransporters, KCC1, KCC2, KCC3 and KCC4 (encoded by *Slc12a4*, *Slc12a5*, *Slc12a6* and *Slc12a7* respectively).

NKCC1 and KCC2 are the principal chloride cotransporters in the brain, mediating electroneutral chloride import and export respectively (Kaila *et al*., 2014). However, the expression of KCC1, KCC3 and KCC4 has also been documented in neurons (Blaesse *et al*., 2009) and the expression of NKCC2, long-believed to have brain-independent functions, has recently been

demonstrated to be involved in neuronal osmoregulation (Konopacka *et al*., 2015). In mature neurons, KCC2 activity is increased in comparison to NKCC1, mediating a low $[Cl^-]_i$ (Figure 5.1). Therefore, upon $GABA_A$ receptor activation leads to chloride influx into cells, promoting hyperpolarisation.

In mammalian brain during development, and the first two post-natal weeks, the expression pattern of the CCCs in neurons is altered, with expression of NKCC1 being greater than KCC2 resulting in high $[Cl^-]_i$. Upon GABA binding to its receptor, chloride effluxes and thus, $GABA_AR$-ergic response is depolarising (Figure 5.1) (Rivera *et al*., 1999; Yamada *et al*., 2004). $GABA_AR$-dependent depolarisation has been shown to lead to post-synaptic neuronal excitation by promoting the activation of voltage-gated calcium channels, triggering action potentials and generating giant depolarising potentials (Ben-Ari 2001). Such a response is observed in all neurons of the CNS although its precise timing can vary between different brain regions and neuronal subtypes (Ben-Ari *et al*., 2007; Wang and Kriegstein 2009). GABA-mediated excitation promotes neuronal proliferation, migration and targeting (Blaesse and Schmidt 2015). In other pathological situations, the gene expression patterns of CCCs also resembles early development (Figure 5.1). These include, cerebral oedema, traumatic and ischaemic brain injury, temporal lobe epilepsy, schizophrenia, Andermann syndrome, Bartter syndrome and cancer (Uyanik *et al*., 2006; Kaila *et al*., 2014; Kahle *et al*., 2015). The activity of NKCC1 and KCC2 is therefore important in dictating the $GABA_AR$-mediated response (Succol *et al*., 2012).

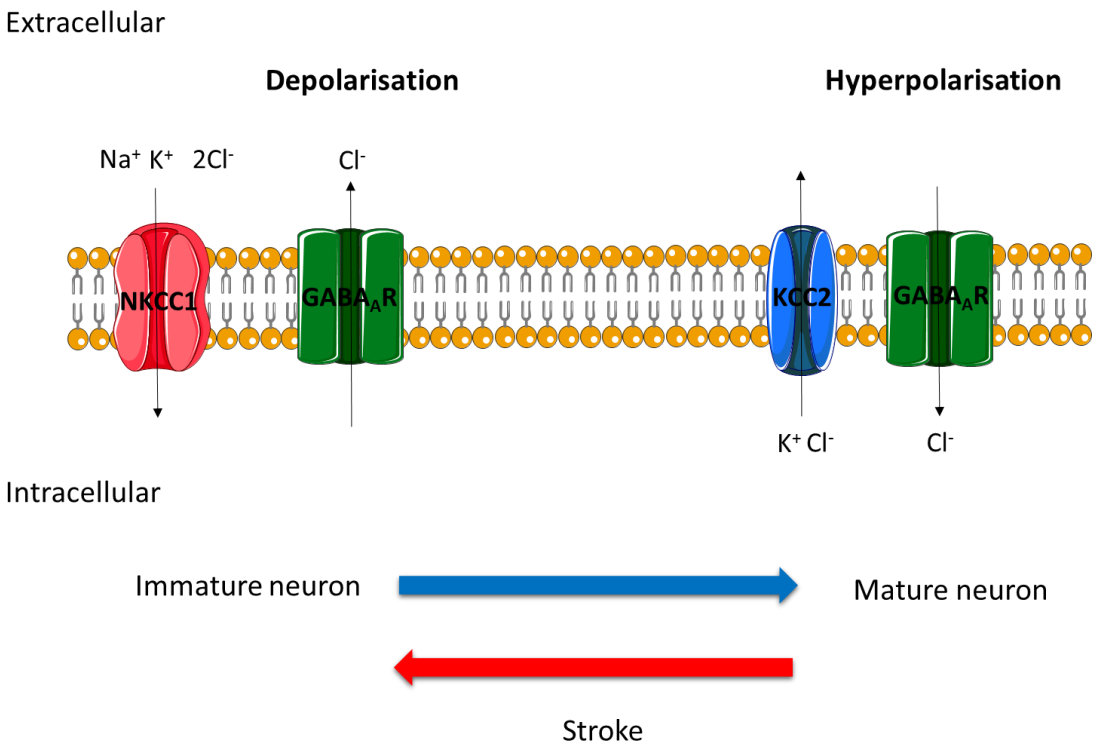

Figure 5.1. NKCC1 and KCC2 dictate the GABA$_A$R response. NKCC1 is responsible for transport of chloride into the cell in immature neurons, whereas KCC2 which extrudes chloride, is up-regulated during CNS development and in mature neurons promoting hyperpolarising, or depolarising GABA$_A$R-mediated currents respectively. In stroke and other pathological situations this chloride homeostasis is reversed towards a temporary immature-like state.

5.1.3 Cation chloride cotransporters as potential therapeutic targets in stroke

The switch in NKCC1 and KCC2 expression might augment the excitotoxic damage that promotes development of the penumbra into a core-like state in the days following an ischaemic event by diminishing, or even reversing, $GABA_AR$-mediated inhibition (Rivera *et al*., 2002; Jaenisch *et al*., 2016; Martín-Aragón Baudel *et al*., 2017). GABA has been shown to be neuroprotective and able to reduce excitotoxic-derived neuronal death in the acute phase of stroke (Figure 5.2; Lyden and Hedges 1992; Green *et al*., 2000). However, $GABA_AR$ agonists administered during the acute phase of stroke failed to improve the outcome of stroke patients (Lyden *et al*., 2002; Liu and Wang 2013). This could be due to the lack of suitable preclinical animal models (Chapter 4) and $GABA_AR$ subtype-specific compounds (Clarkson 2012). In contrast, reducing GABA-mediated inhibition in the long term following stroke (rehabilitation post-stroke), is beneficial for functional recovery and improves brain plasticity (Figure 5.2; Clarkson *et al*., 2010; Hiu *et al*., 2016). Recently, the contribution of NKCC1 and KCC2 in the spreading depolarisations that are responsible for post-stroke injury was revealed (Steffensen *et al*., 2015). The promising results obtained in preclinical models and the relative failure of $GABA_AR$-specific compounds in clinical trials suggests that that therapies targeting chloride co-transporters could represent a potential novel strategy to reduce the damage associated with stroke (Figure 5.2).

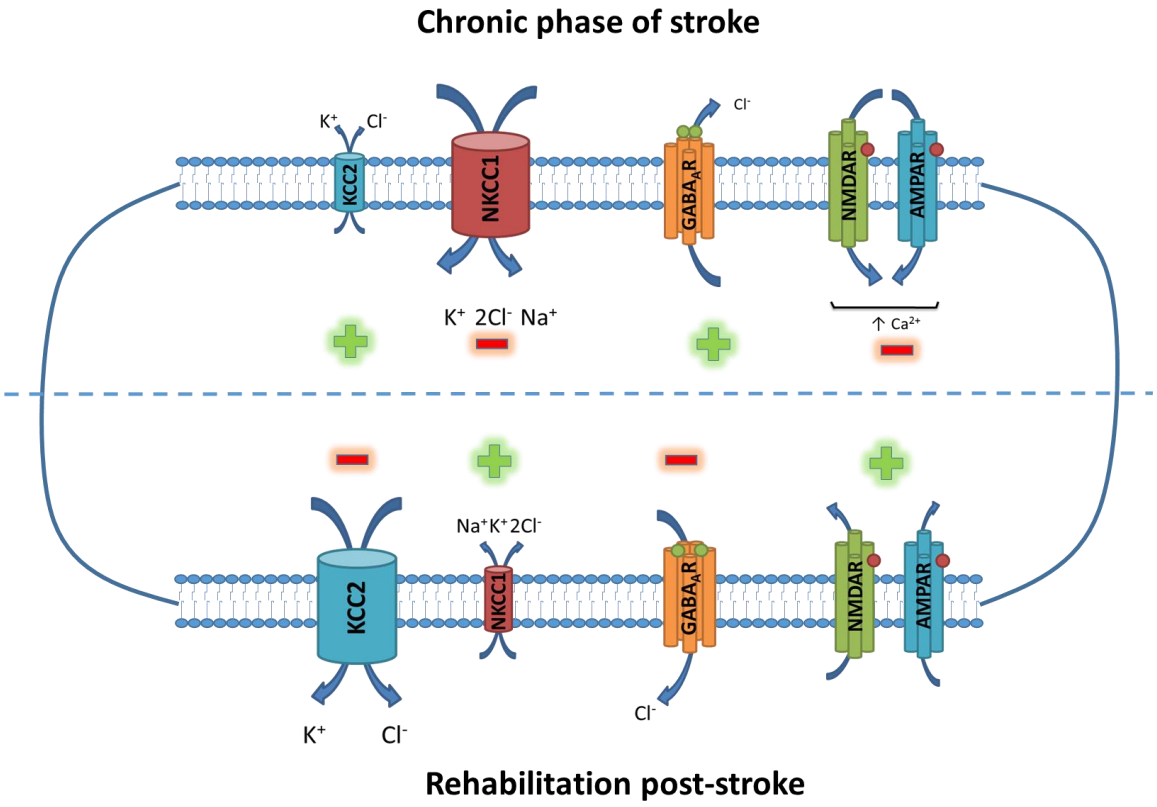

Figure 5.2 Schematic representation of potential positive and negative therapeutic strategies in stroke. During the chronic phase of stroke, the reversal of the chloride gradient mediated by the CCCs could be targeted with positive (+) or negative (-) modulators of KCC2 and NKCC1 activity/expression respectively. This would promote $GABA_AR$-mediated inhibition and counteract NMDA and AMPA-mediated excitotoxicity. Conversely, in the long term, post-stroke, an opposed strategy could promote neurorehabilitation.

It is hypothesised that after a stroke event, KCC2 is down-regulated while NKCC1 is up-regulated, modifying neuronal $[Cl^-]_i$ balance, and rendering $GABA_A$ receptors excitatory (Figure 5.1). This phenomenon, coupled with the substantial release of glutamate, and NMDA and AMPA receptor activation, constitutes the excitotoxicity that ultimately leads to neuronal death

(Szydlowska and Tymianski 2010). Different therapies, used after either the initial event, or in the long term, acting on CCCs and/or $GABA_A$ receptors could promote neuroprotection or neurogenesis and, subsequent, rehabilitation (Figure 5.2).

5.1.3.1 NKCC1 in ischaemia

NKCC1 activity has been shown to be up-regulated in peri-infarct cortex following middle cerebral artery occlusion (MCAO) in mice (Yan *et al*., 2003; Begum *et al*., 2015). In addition, NKCC1-null mice have been shown to exhibit less grey and white matter damage following MCAO (Chen *et al*., 2005). The kinase with no lysine kinase 3 (WNK3) directly stimulates NKCC1 activity by phosphorylating NKCC1 (Alessi *et al*., 2014). WNK3 knockout mice subjected to MCAO have been shown to present reduced brain damage and improved recovery after stroke (Begum *et al*., 2015).

Bumetanide acts as an antagonist of NKCC1 channels at low concentrations (2-10 μM) whereas at higher concentrations it inhibits both NKCC1 and KCC2 activity (Payne *et al*., 2003). At doses that solely block NKCC1 activity, different studies have shown that bumetanide administration following MCAO promotes neurogenesis and increases behavioural recovery 28 days following the insult (Xu *et al*., 2016). It also decreases oedema formation three hours and up to two days after the insult (Wang *et al*., 2014). However, this effect could be due to the expression of NKCC1 in the luminal side of endothelial cells in the blood brain barrier (BBB), which is known to decrease

oedema formation (O'Donnell *et al*., 2004). NKCC1 has a role in the formation of ionic oedema as it transports sodium into endothelial cells, which is then expelled by the Na^+-K^+ ATPase, therefore controlling volume regulation (Brillault *et al*., 2008). However, the implication of NKCC1 in neuronal loss following stroke in the ischaemic penumbra has not been adequately addressed.

5.1.3.2 KCC2 in ischaemia

KCC2 expression has been shown to be downregulated following ischaemia in a model of MCAO in rats (Jaenisch *et al*., 2010). Application of exogenous glutamate to cortical neurons, to mimic excitotoxicity (Figure 1.1), also resulted in KCC2 downregulation (Jaenisch *et al*., 2016). Functional downregulation of KCC2 in vitro was also observed following different neuronal stressors, such as oxidative stress, BDNF-induced stress and hyperexcitability (Wake *et al*., 2007). Little research into the change in the expression of KCC2 following PTS has been undertaken. In spinal motoneurons, KCC2 expression was downregulated seven days following stroke but not at three or 21 days (Toda *et al*., 2014). However, data was not in the context of KCC2 participation in the development of the penumbra.

No therapeutic agents specifically targeting KCC2 that can cross the BBB and with a long half-life are available for human use. Bumetanide and furosemide can inhibit KCCs activity, however they can also inhibit NKCC1 at higher concentrations (Austin and Delpire 2011). Therefore, specific KCC2 inhibitors are required to further elucidate KCC2 function. KCC2-specific

agonists have been identified recently by Gagnon et al. (2013). The KCC2-selective analogue CLP257, and its prodrug CLP290, lower the $[Cl^-]_i$ and restore impaired chloride transport to alleviate hypersensitivity in a rat model of neuropathic pain (Gagnon *et al*., 2013) and modulate the epileptic response in an *in vitro* model of ictogenesis (Hamidi and Avoli 2015). A selective KCC2 inhibitor, VU0463271, has recently been developed (Delpire *et al*., 2012) and been shown to induce epileptiform discharges both *in vitro* and *in vivo (*Sivakumaran *et al*., 2015) and increase the duration of seizure–like events (Kelley *et al*., 2016). These studies highlight the importance of KCC2 in regulating neuronal chloride concentration and mediating GABAergic activity in different pathologies and the critical necessity for specific compounds able to cross the BBB and specifically target KCC2.

The combined effects of NKCC1 and KCC2 are thought to be involved in the excitotoxic events that take place rapidly after stroke (Jantzie *et al.,* 2015, Beck *et al.,* 2003) but also in promoting neurorehabilitation in the days following the insult (Tanaka *et al.,* 2009). The joint assessment of KCC2 expression, having a role opposed to NKCC1, will further the understanding of the chloride gradient and thus $GABA_AR$-mediated activity in neurons after PTS. Additionally, it will expand the knowledge of the molecular events that ultimately dictate neuronal fate during the days following stroke. In this study, expression of the chloride co-transporters, NKCC1 and KCC2, mediators of the $GABA_AR$-mediated response was assessed in: **i)** neuronal-like PC12 and NT2 cells following hypoxia in a modular chamber *in vitro* and **ii)** in the penumbral cortex following photothrombotic stroke in mice. Neuronal loss

was assessed *in vivo* in the penumbra and compared with mice treated with bumetanide and CLP257.

5.2 Aims

Aim 1. To characterise expression of the (N)KCC family of proteins in the neuronal-like differentiated PC12 and NT2 cells following acute hypoxia.

Aim 2. To quantify spatial and temporal expression of NKCC1 and KCC2 in the penumbra following PTS in mice.

Aim 3. To assess the impact of NKCC1 and KCC2 modulation by bumetanide (NKCC1 antagonist) and CLP257 (KCC2 agonist) on neuronal loss in the established penumbra.

5.3 Research Questions

RQ1. Does an ischaemic-like episode reverse the expression of the cation chloride cotransporters *in vitro* and *in vivo*?

RQ2. Do drugs that specifically target the cation chloride cotransporters prevent neuronal loss in the penumbra following ischaemic stroke?

5.4 Results

5.4.1 The expression of CCCs in neuronal-like PC12 and NT2 cells is modified following hypoxia

A model for generating differentiated neuronal-like cells using the pluripotent cell lines PC12 and NT2 was developed in Chapter 3. Using an *in vitro* hypoxic modular chamber, eight hours of acute hypoxic insult (1% O_2) was established as the time point that induces damage and changes in hypoxic-responsive genes and proteins. The activity of the CCCs is fundamental in mediating the $GABA_AR$-mediated response (Succol *et al*., 2012). Following hypoxic insults such as stroke, the alteration in the expression of some of these transporters has been demonstrated (Yan *et al*., 2003; Jaenisch *et al*., 2010; Begum *et al*., 2015). Therefore, an *in vitro* model of hypoxia with the neuron-like PC12 and NT2 cells, provided a platform to analyse the changes in expression of this family of transporters.

5.4.1.1 *In vitro* gene expression profile of the CCCs following hypoxia.

The expression of the CCCs genes, *Slc12a2* (NKCC1), *Slc12a4* (KCC1), *Slc12a5* (KCC2), *Slc12a6* (KCC3) and *Slc12a7* (KCC4) was assessed following acute hypoxia in differentiated PC12 and NT2 cell lines via qPCR. Expression of the chloride exporter genes *Slc12a4-7* showed a significant downregulation following hypoxic insult in both PC12 and NT2 cells. In contrast, the expression of the chloride importer *Slc12a2* was relatively unchanged (Figure 5.3).

Following acute hypoxia in PC12 cells, a significant 7.5-fold decrease in *Slc12a5* (KCC2) (p = 0.04) mRNA abundance and a 3.4-fold decrease for *Slc12a6* (KCC3) (p = 0.006) were observed (Figure 5.3 A). However, *Slc12a4* (KCC1) and *Slc12a7* (KCC4) mRNA was not significantly downregulated (*Slc12a4*: 6.3-fold change, p = 0.08; *Slc12a7*: 12.5-fold change, p = 0.12).

NT2 cells showed a similar variation in mRNA for the CCCs following acute hypoxia (Figure 5.3 B). The expression of the chloride exporters *Slc12a4-7* (KCC4-7), was significantly downregulated following acute hypoxia, whereas only a small 1.3-fold decrease in the gene expression of the chloride importer *Slc12a2* (NKCC1) was observed. A significant 1.84-fold decrease in mRNA (p = 0.04) was observed for *Slc12a4* (KCC1), 2-fold change for *Slc12a6* (KCC3; p = 0.02), 2.2-fold change for *Slc12a7* (KCC4; p = 0.004). Interestingly, a non-significant 1.6-fold downregulation was observed for *Slc12a5* (KCC2; p = 0.06).

In summary, the expression profile of the CCCs genes is modified following acute hypoxia in neuronal-like PC12 and NT2 cells. In particular, significant downregulation in mRNA encoding chloride exporters KCC1-4 was observed whilst the expression of the chloride importer NKCC1, was not significantly altered following the insult. Changes in mRNA levels do not always translate into changes in protein expression, therefore protein expression following hypoxia was analysed via immunoblotting.

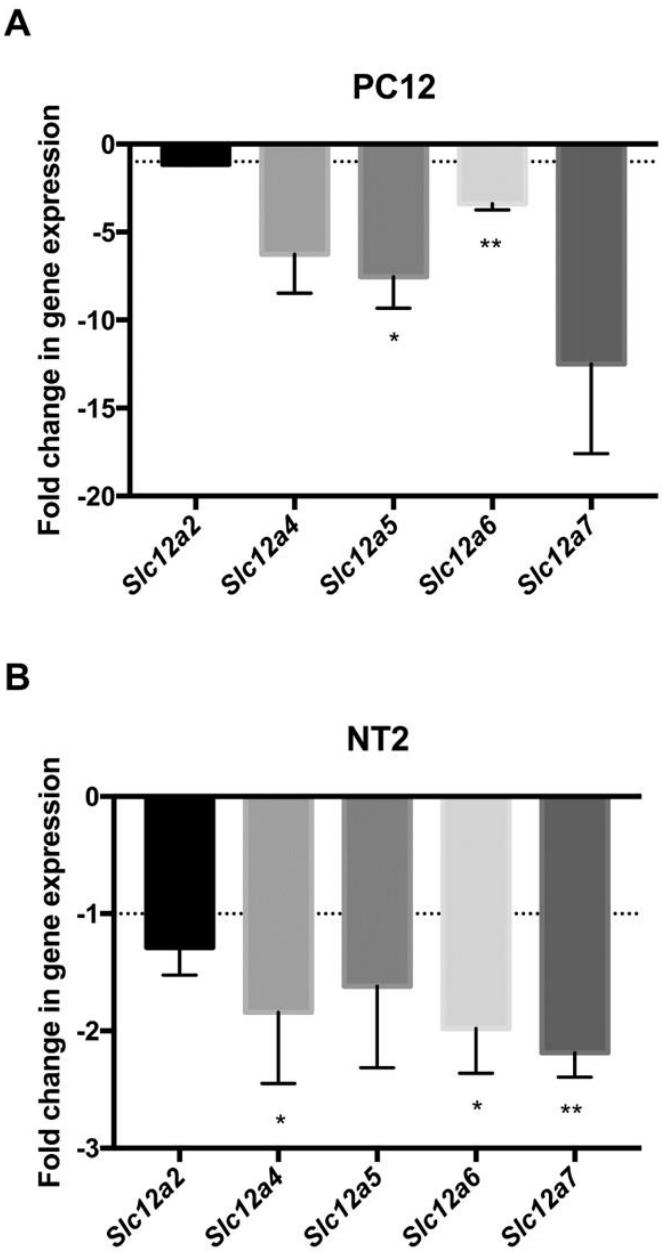

Figure 5.3. Hypoxia downregulates expression of all chloride extruder genes but not in the chloride importer in PC12 and NT2 cells. Relative mRNA expression of *Slc12a2* (NKCC1) and *Slc12a4-7* (KCC1-4) was analysed in PC12 (**A**) and NT2 (**B**) cells after 8 hours of hypoxia relative to the reference gene; *TOP1* for PC12 and *ACTB* for NT2. Results are expressed as the mean fold change ± SEM (n=3). Two-tailed unpaired Student's *t* test.

5.4.1.2 Immune detection of the CCCs in response to hypoxia

The neuron-specific chloride exporter KCC2 and the chloride importer NKCC1 are the most important members of the CCC family of proteins in the mammalian brain (Kaila *et al*., 2014) so were analysed at protein level in PC12 and NT2 cells following acute hypoxia.

Prominent NKCC1 expression was detected in PC12 and NT2 (Figure 5.4). Expression of NKCC1 was not altered by hypoxia in PC12 cells (Figure 5.4). Staining intensity of NKCC1 was, however, increased in differentiated NT2 cells following 4 and 8 hours of hypoxia (Figure 5.4). Equal loading of protein, as shown by actin immunoblot, indicates NKCC1 is upregulated by acute hypoxia in NT2 cells. Note that the band corresponding to NKCC1 has an expected size of 130 KDa, however the band detected in PC12 cells was smaller (~115 KDa). This could be due to the antibody having been synthesised to recognise a human epitope (NT2 cells) and, therefore, not being specific for a rat epitope (PC12 cells).

A marked basal expression of KCC2 was observed in PC12 and NT2 cells in normoxic conditions. KCC2 protein expression was dramatically affected by hypoxic insult in differentated PC12 and NT2 cells (Figure 5.5). The band corresponding to KCC2 was not observed in PC12 cells following hypoxia and an intense decrease in the expression of the chloride exporter was observed in NT2 cells. These results suggest that the chloride exporter KCC2 expression is downregulated by acute hypoxia.

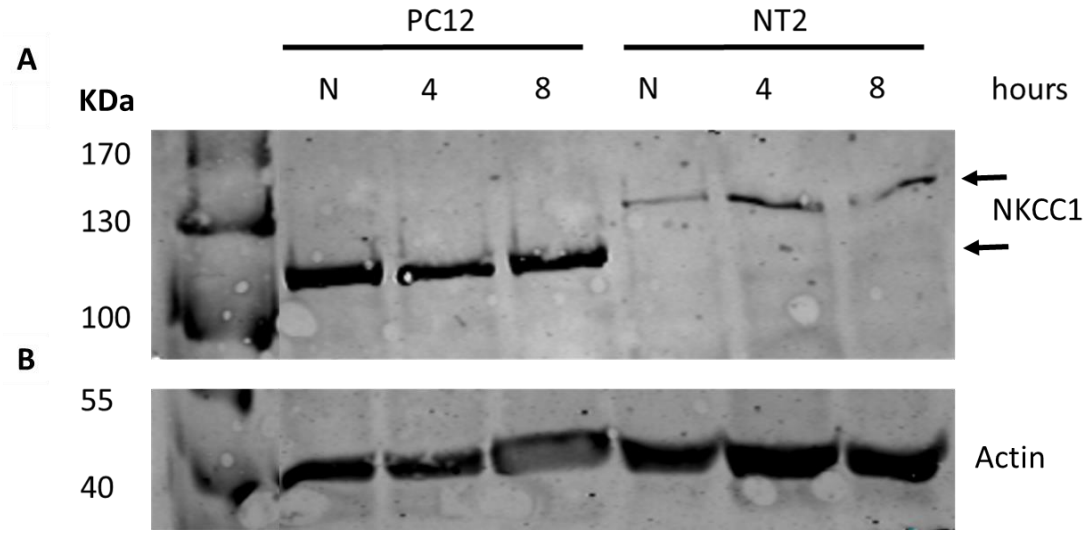

Figure 5.4. Analysis of chloride importer NKCC1 expression following acute hypoxia in PC12 and NT2 cells. Representative immunoblot analysis showing: **A.** NKCC1 protein expression in differentiated PC12 and NT2 cells under normoxic (N) or hypoxic conditions for 4 and 8 hours. **B.** Immunoblotting with actin was used to verify equal protein loading.

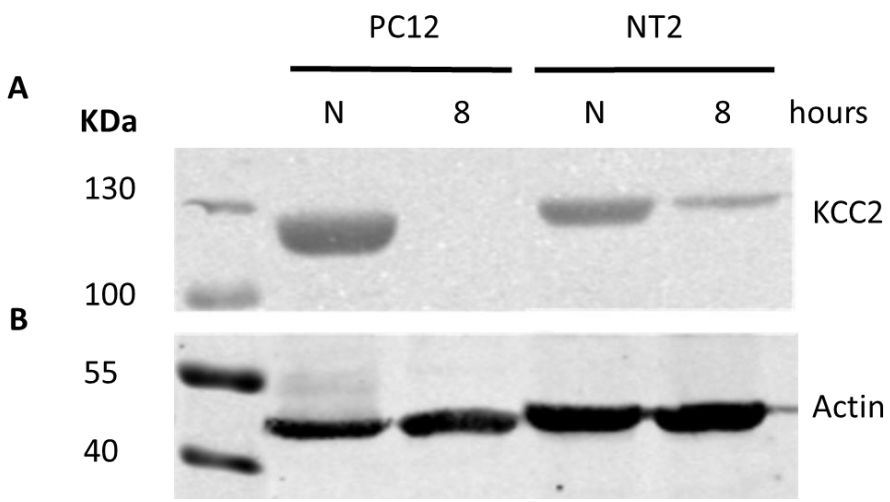

Figure 5.5 The impact of hypoxia on KCC2 expression in hypoxic neuronal-like PC12 and NT2 cells. Representative immunoblot analysis showing: **A.** KCC2 protein expression in differentiated PC12 and NT2 cells under normoxic (N) or hypoxic conditions for 8 hours. **B.** Immunoblotting with actin was used to verify equal protein loading.

Previous literature has focused on the expression of KCC2 and NKCC1 as principal mediators of the $GABA_AR$-mediated response whereas less attention has been payed into the function of the remaining chloride exporters, KCC1, KCC3 and KCC4 in CNS pathologies and adaptation to hypoxic insult. mRNA quantification showed downregulation of chloride exporter expression following hypoxia (Figure 5.3), therefore their protein expression was analysed via immunoblotting.

Changes in protein expression of KCC3 and KCC4 following hypoxia (Figure 5.6) were not as obvious as for NKCC1 and KCC2 (Figure 5.4 and 5.5). The band corresponding to KCC3 showed no difference in intensity following acute hypoxia in both cell lines analysed (Figure 5.6 A). A decrease in KCC4 immunolabeling was observed after four hours of hypoxic insult and staining was even less robust after 8 hours in PC12 cells (Figure 5.6 B). KCC4 expression was not detected in NT2 cells due to a lack of human-specific antibody. In summary, a small downregulation in the chloride exporter KCC4 expression in PC12 cells was observed following acute hypoxia whereas changes were not detected in KCC3 expression.

These results suggest that chloride trafficking might be modified in neuronal-like cells following hypoxia due to changes in the expression of the CCCs, as a decrease in the expression of the chloride exporters (KCC1-4) in both the mRNA and protein was observed. The chloride importer NKCC1 protein expresion was upregulated in NT2 cells, but significant changes in the mRNA

abundance for PC12 and NT2 cells, and PC12 cells protein expression, were not observed.

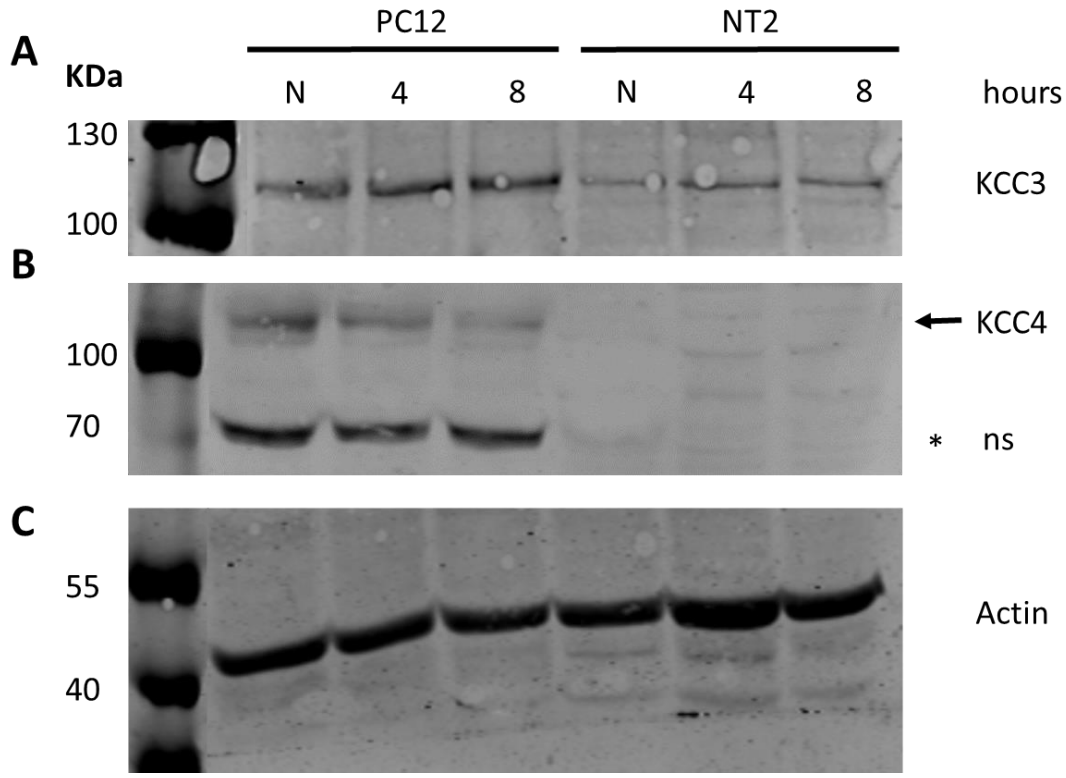

Figure 5.6 Analysis of the chloride exporters KCC3 and KCC4 expression following hypoxia in PC12 and NT2 cells. Representative immunoblot analysis showing KCC3 (**A**) and KCC4 (**B**) protein expression in differentiated PC12 and NT2 cells under normoxic (N) or hypoxic conditions for 4 or 8 hours. Ns: non-specific. Immunoblotting with actin was used to verify equal protein loading (**C**).

5.4.2 Analysing the expression of NKCC1 and KCC2 *in vivo* in the peri-infarct region following photothrombotic stroke

In Chapter 4, the penumbra was assessed and defined in a photothrombotic stroke (PTS) model in mouse. In the 200 µm region surrounding the ischaemic core, an increase in neuronal stress and recruitment of glial cells was identified (Figure 4.16). This was taken to define the penumbra, as neuronal stress and glial reactivity are two well-defined hallmarks of the region (Popp *et al*., 2009; Barreto *et al*., 2011). Increased glial reactivity was also identified in the region between 200 and 400 µm from the ischaemic core (Figure 4.16), which was named area of increased glial enrichment (IGE). Furthermore, significant neuronal loss was observed within the penumbra following PTS demonstrating that the damage in this tissue continues to increase in the days after the ischaemic insult.

The goal of this study was to analyse the pattern of NKCC1 and KCC2 expression in the now defined penumbral cortex following PTS. The results observed in the *in vitro* model indicated a decrease in KCC2 at the mRNA and protein levels as an adaptation to hypoxia in neuron-like cells. Thus, this could potentially contribute to excitotoxic neuronal injury following an ischaemic event. Therefore, expression of NKCC1 and KCC2, the two principal mediators of neuronal chloride trafficking, was assessed via immunostaining of brain sections encompassing the penumbra following PTS.

Immunostaining for NKCC1 and KCC2 was performed in 40 µm mouse brain slices in untreated mice at at one, three and five days following PTS (Figure 5.7). Five serial images encompassing 30 µm across the z-axis were taken per brain slice. Regions of 200 µm length and 200 µm width were marked on the brain cortex and aligned at the edge of the ischaemic core representing the penumbra (Figure 5.7 red box). The IGE area was analysed in regions of 200 µm length and 200 µm width aligned at the edge of the penumbral cortex (Figure 5.7 blue box). This procedure was repeated in matching regions of the contralateral hemisphere.

Confocal microscopy images of the injury at low magnification (x 10) revealed defined NKCC1 staining in the area surrounding the ischaemic core (Figure 5.7 A). As expected, KCC2 staining was ubiquitous in the brain (Figure 5.7 A). Higher magnification images were taken in the penumbra and IGE area (Figure 5.7 B and C, red and blue box respectively). A high number of NKCC1-positive cells was observed in the penumbra and the staining was defined at the perisomatic and dendritic membrane (Figure 5.7 B, white arrows). In the IGE area, NKCC1-positive cells were less prominent and the staining intensity was decreased (Figure 5.7 C, white arrows). KCC2 staining was more diffuse as it stained perisomatic, dendritic and axonal membranes, creating higher background noise. Therefore, only perisomatic membrane staining, which identified individual cells was considered to be KCC2-positive (Figure 5.7 B and C, yellow arrows). A higher number of KCC2-positive cells could be visually distinguished in the IGE zone when compared to the penumbra in the cortex (Figure 5.7 B and C). Therefore, visual observations

indicated a reversal in the expression of the chloride importer NKCC1 and the chloride exporter KCC2 in the penumbra compared to more remote, healthy areas.

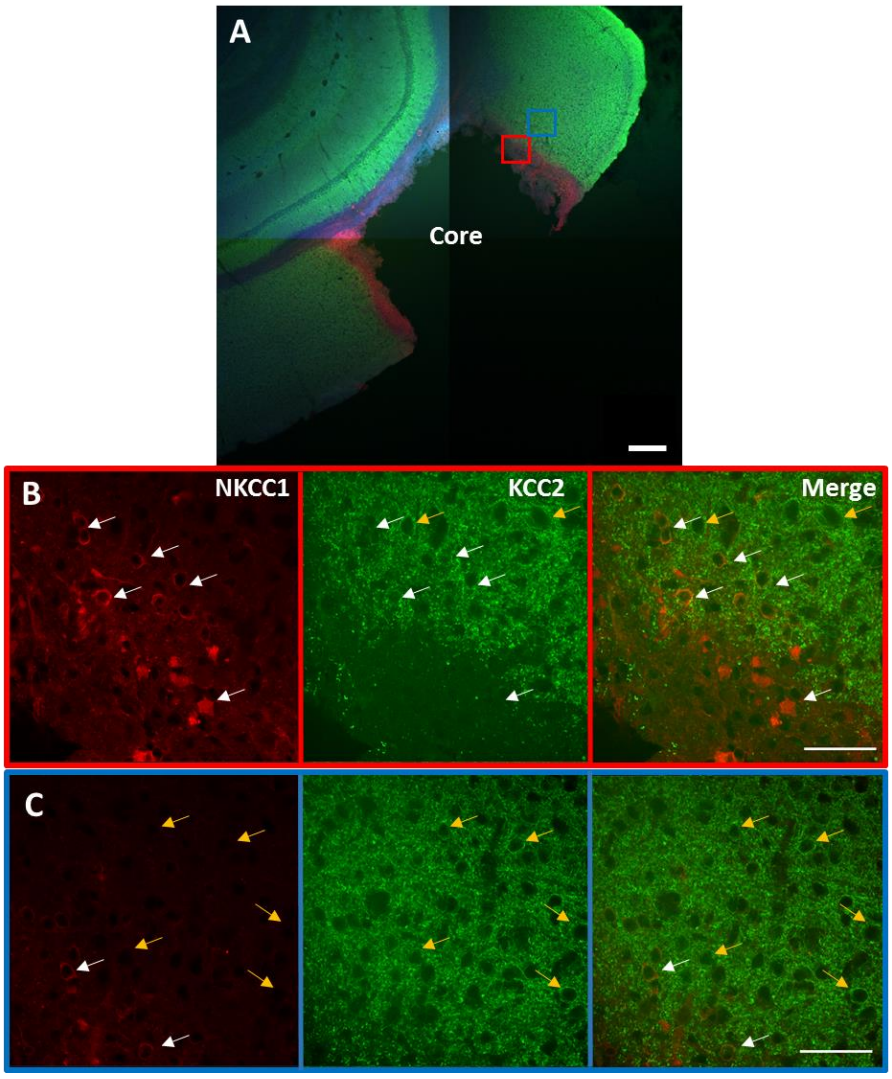

Figure 5.7 NKCC1 and KCC2 expression is altered in the penumbra following PTS. Representative mouse brain images three days after PTS displaying NKCC1 (red) and KCC2 (green) immunolabeling. **A**: General overview of the marking for NKCC1 and KCC2 at x 10 magnification. Red box represents an area of the penumbra, blue box the IGE zone. **B**: Detailed (x 63) magnification of the penumbra. **C**: Detailed (x 63) magnification of IGE area. White arrows represent NKCC1-positive cells, yellow arrows represent KCC2-positive cells. Scale bar represent 200 µm (A) and 50 µm (B and C).

5.4.2.1 Analysing the expression of NKCC1 and KCC2 in the penumbra following PTS

Brains of mice were analysed at one, three and five days following PTS and compared to untreated mice. Furthermore, three different mice per time point and nine different brain slices per mouse were analysed for statistical significance

In the damaged ipsilateral hemisphere, the penumbra comprised a significantly higher number of NKCC1-positive cells compared to KCC2-positive cells at at one, three and five days following PTS (Figure 5.8 A). One day post-PTS, 58.7% of DAPI-positive cells were NKCC1-positive compared to 25.5% KCC2-positive cells ($p < 0.001$). Three days following PTS, 53.1% of the cells were NKCC1-positive and 26.5% KCC2-positive ($p = 0.004$) and five days after the insult 58.6% were NKCC1-positive and 21.6% KCC2-positive ($p <0.001$).

In the undamaged contralateral hemisphere, regions of cortex that matched the location of the penumbra in the ipsilateral hemisphere were analysed. In this area, the expression of NKCC1 and KCC2 was reversed, with a significantly higher number of KCC2-positive cells than NKCC1-positive cells at one, three and five days following the insult (Figure 5.8 B, $p < 0.001$). At days at one, three and five days 63.5 ± 1 % of the cells were KCC2-positive and NKCC1-positive cells remained unchanged at 24 ± 0.5 %.

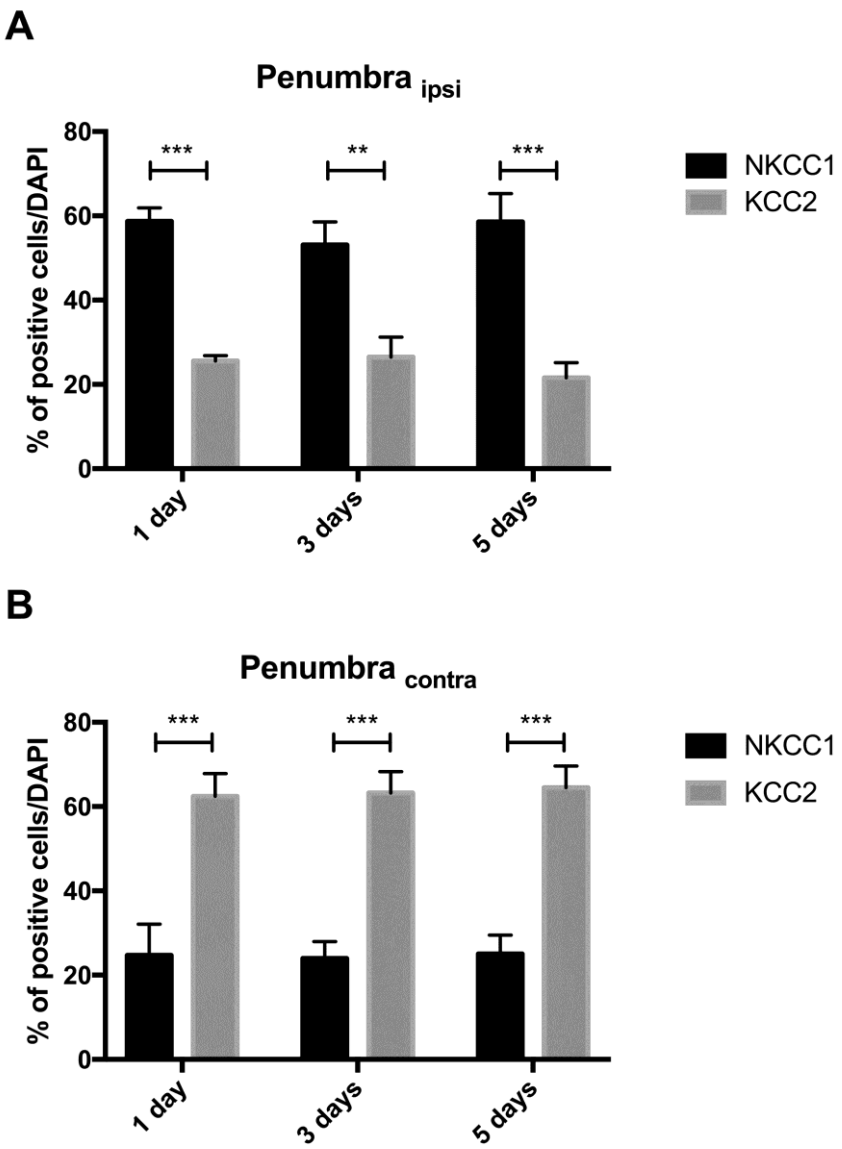

Figure 5.8 NKCC1 expression is more abundant than KCC2 in the penumbra following the injury. The expression of NKCC1 and KCC2 was analysed in the penumbra in the ipsilateral (**A**, ipsi) and contralateral (**B**, contra) hemispheres. Results were normalised as a percentage of total DAPI-positive cells for each marker and represented as the mean ± SEM (n=3). Two-way ANOVA with Sidak's multiple comparisons test.

This data strongly indicate that there was a higher number of NKCC1-positive cells in the penumbra compared to KCC2 positive cells and that this pattern opposes that of the contralateral hemisphere, where the population of KCC2-positive cells is significantly greater than the amount of NKCC1 positive cells. However, no temporal changes were observed indicating that the reversal in the expression of these transporters takes place before one day following PTS and is maintained beyond five days following the insult.

In order to compare expression of NKCC1 and KCC2 independently between the ipsilateral and contralateral hemispheres, a different analysis was performed (Figure 5.9). Here, expression of each transporter in the ipsilateral penumbra was compared to matching regions in the contralateral hemisphere. This permitted a clear distinction between the ipsilateral and contralateral hemispheres and provided a tool to examine differences created by the injury with a matching control without damage but within the same animal. This approach negates variation between individuals. Figure 5.9 panel A, revealed highly significant differences ($p < 0.001$) in the expression of NKCC1 between the ipsilateral penumbra, where a high percentage of cells were NKCC1-positive, and the cortex of the contralateral hemisphere where, in comparison, the number of NKCC1-positive cells was reduced. Highly significant differences ($p < 0.001$) in KCC2 expression between ipsilateral and contralateral hemispheres were also observed in the penumbra following PTS (Figure 5.9 B). However, the pattern of KCC2 expression was reversed, with a significantly higher number of KCC2-positive cells in the contralateral hemisphere compared to the ipsilateral hemisphere.

The results indicate that there was a reversal in the expression of the CCCs, NKCC1 and KCC2 in the penumbra following PTS.

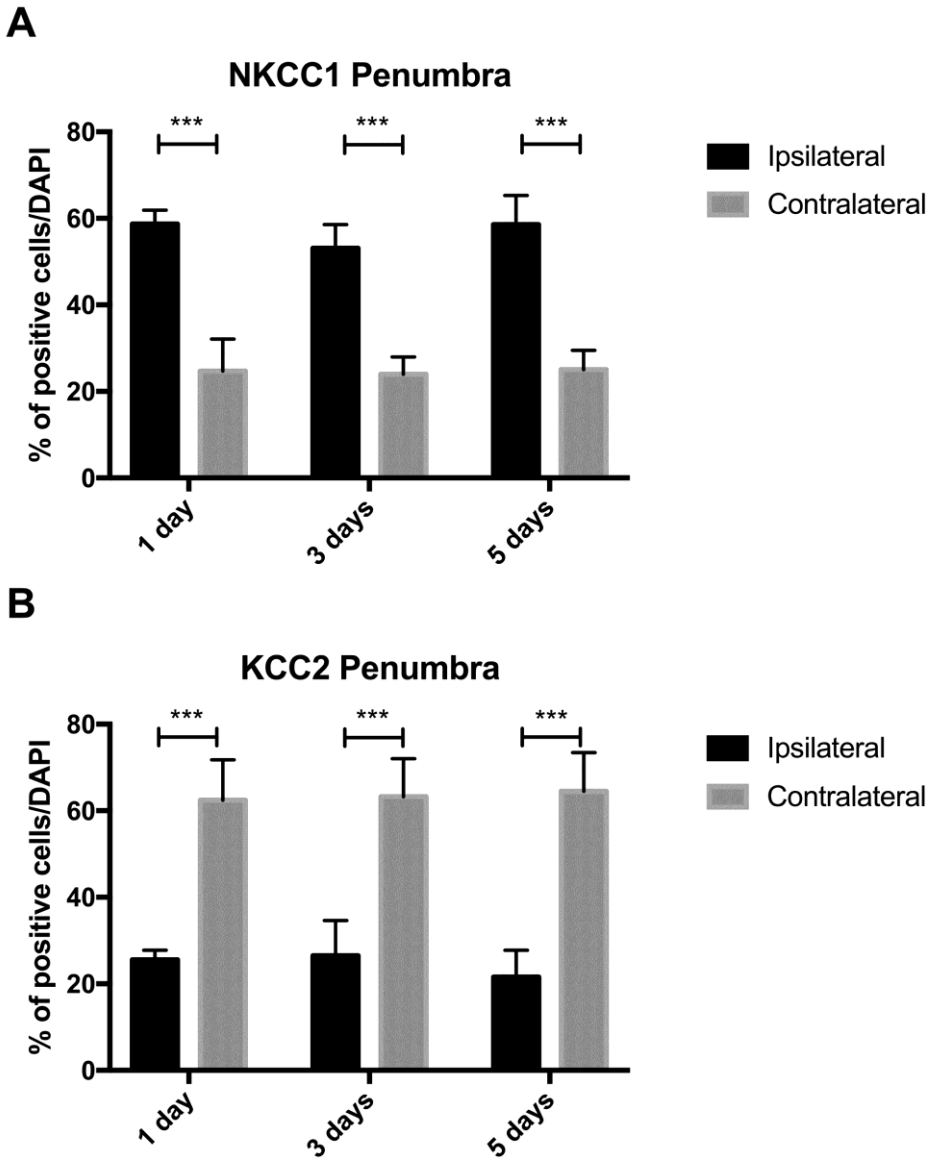

Figure 5.9 Distinct differences in NKCC1 and KCC2 expression in the penumbra following PTS. The expression of NKCC1 (**A**) and KCC2 (**B**) was analysed in the penumbra in the ipsilateral and contralateral hemispheres. Results were normalised as a percentage of total DAPI-positive cells for each marker and represented as the mean ± SEM (n=3). Two-way ANOVA with Sidak's multiple comparisons test.

5.4.2.2 Analysis of NKCC1 and KCC2 expression in the IGE area following PTS

In chapter 4 a region displaying increased glial reactivity, referred to as the increased glial enrichment (IGE) area was identified between 200 and 400 μm from the ischaemic core. In order to analyse the expression of the cation chloride cotransporters, NKCC1 and KCC2, in this transitional area and further understand chloride homeostasis within it, an identical analysis as per section 5.4.2.1 was performed in the IGE zone.

In the IGE zone, significant differences between NKCC1- and KCC2-positive cells were observed in both the ipsilateral and contralateral hemispheres (Figure 5.10). In the IGE zone of the ipsilateral hemisphere (Figure 5.10 A), one day following PTS, 32.9% of DAPI-positive cells were NKCC1-positive, whereas 54% were KCC2 positive ($p = 0.02$). Three days following the insult 23.5% of DAPI-positive cells were NKCC1-positive and 65% KCC2-positive ($p < 0.001$) and after five days 24% NKCC1-positive and 64.4% KCC2-positive ($p < 0.001$).

Similar results were obtained in the contralateral hemisphere: at day one, 26% of cells were NKCC1-positive and 63.1% KCC2-positive, at day three the percentage of NKCC1-positive cells decreased to 22.5% and 65.1% KCC2-positive and at five days 25.1% NKCC1-positive and 66.2% KCC2-positive. The differences between NKCC1 and KCC2 expression were highly significant at all time points following the injury ($p < 0.001$). KCC2-positive cells were therefore significantly more abundant than NKCC1-positive in the

IGE area in the ipsilateral hemisphere compared to matching regions in the contralateral hemisphere cortex.

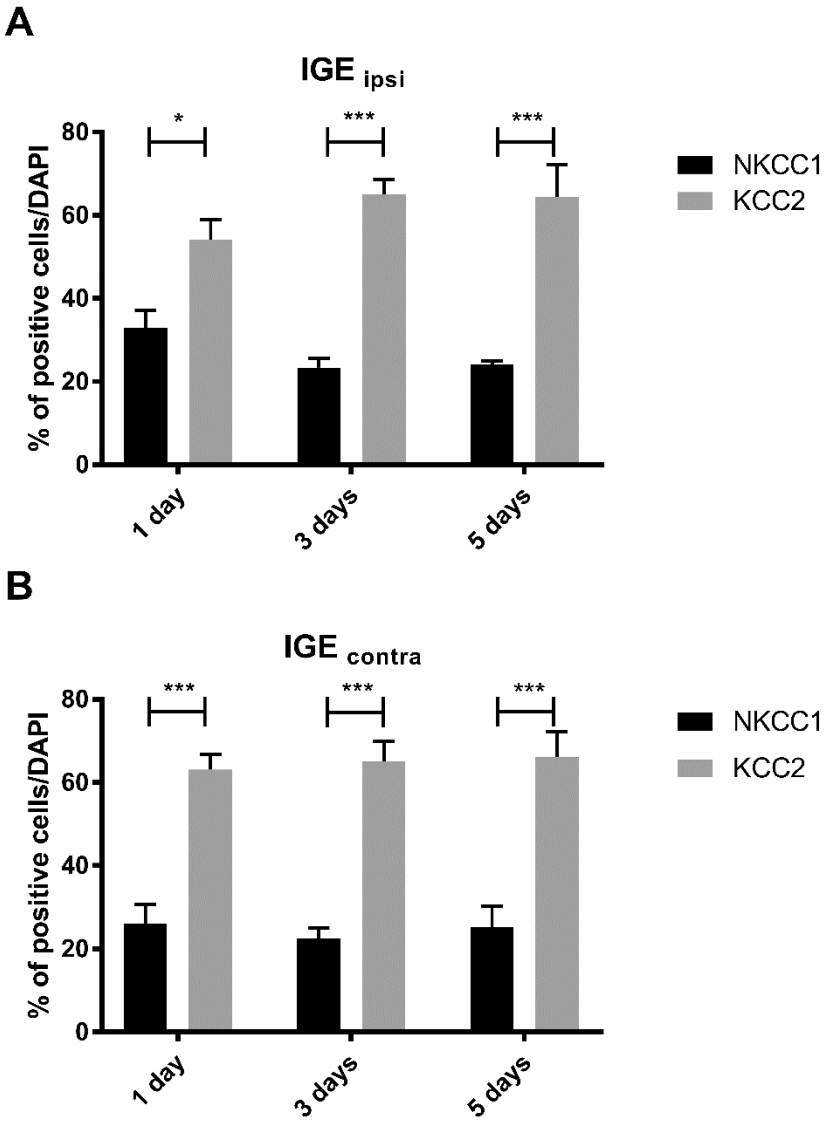

Figure 5.10 KCC2 expression is more abundant than NKCC1 in the IGE area following PTS. Expression of NKCC1 and KCC2 was analysed in the penumbra in the ipsilateral (ipsi) and contralateral (contra) hemispheres at at one, three and five days post-injury. Results were normalised as a percentage of total DAPI-positive cells for each transporter and represented as the mean ± SEM (n=3). Two-way ANOVA with Sidak's multiple comparisons test.

Transporter-specific differences between the ipsilateral hemisphere and matching regions of the contralateral hemisphere were assessed in the IGE zone (Figure 5.11). Differences were not observed in the percentage of NKCC1-positive cells in the IGE zone between the ipsilateral and contralateral hemispheres (Figure 5.11 A). Furthermore, time-dependent differences were not observed in the expression pattern of NKCC1 in the days following the injury. The percentage of KCC2-positive cells was also very similar in the ipsilateral and contralateral hemisphere and significant differences were not observed (Figure 5.11 B). As for NKCC1 time-dependent differences were not observed in the days following the PTS. Therefore, expression of NKCC1 and KCC2 between the IGE area was very similar in the damaged (ipsilateral) and healthy (contralateral) hemispheres.

Interestingly, the results shown in Figures 5.10 and 5.11 reveal that, in contrast to the penumbra, the expression of the CCCs, NKCC1 and KCC2, is not affected in the IGE zone. Furthermore, the pattern of expression of these transporters is very similar to healthy areas of the brain (contralateral hemisphere). Therefore, this area is further confirmed as a non-penumbral region where there is an increase in glial reactivity but where potential ionic imbalance is not extended to, or at least not mediated by changes in the expression of the chloride transporters NKCC1 and KCC2.

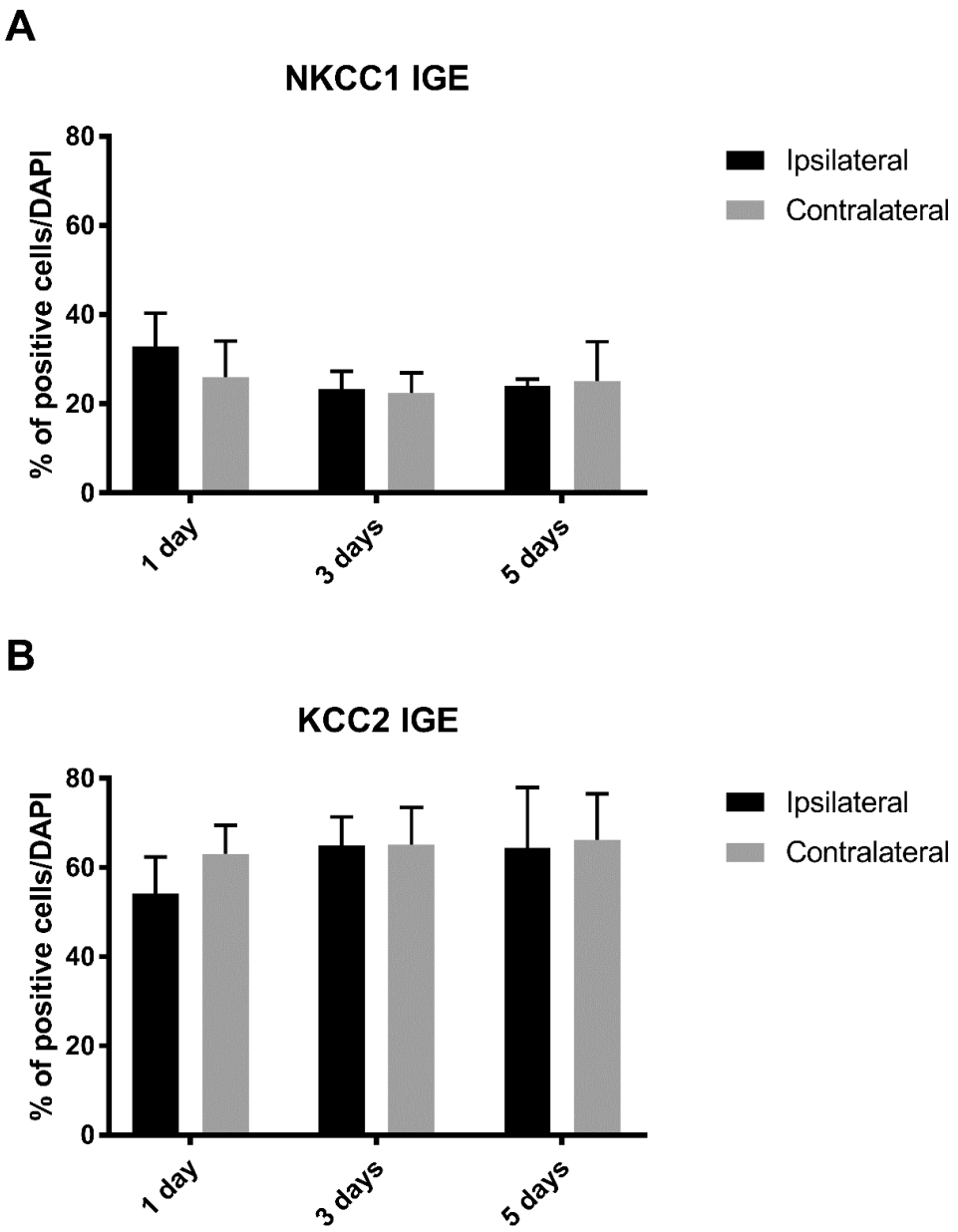

Figure 5.11 NKCC1 and KCC2 expression is not affected by PTS in the IGE area when compared to healthy tissue. The expression of NKCC1 (**A**) and KCC2 (**B**) was analysed in the IGE area in the ipsilateral and contralateral hemispheres at one, three and five days post-PTS. Results were normalised as a percentage of total DAPI-positive cells for each transporter and represented as the mean ± SEM (n=3). Two-way ANOVA with Sidak's multiple comparisons test.

In summary, analysis of NKCC1 and KCC2 expression in the area surrounding the ischaemic core following PTS indicated: **i)** a strong induction of NKCC1 expression in the penumbra following the injury; **ii)** A concurrent decrease in the number of neurons expressing KCC2 in the penumbra; **iii)** The zone with increased glial reactivity (IGE), hypothesised to be a glial migration zone, displays an almost identical pattern of NKCC1 and KCC2 expression in matching, unaffected contralateral hemisphere; **iv)** Expression of NKCC1 or KCC2 was unchanged in the days following the injury in any of the areas analysed. Together, this indicates rapid (before one day) and sustained reversal in NKCC1 and KCC2 expression occurs in the penumbra following PTS. The striking differences in NKCC1 and KCC2 expression induced by ischaemia strongly suggest that chloride trafficking is modified and could be contributing to an ionic imbalance in neurons of the penumbra up to five days and beyond following the injury.

The clear alteration in expression of NKCC1 and KCC2 in the penumbra after PTS might represent a reversal in the chloride trafficking across neuronal membranes, therefore modifying neuronal $[Cl^-]_i$ (Figure 5.1). This shift could modify $GABA_AR$-mediated activity rendering it depolarising (Succol *et al*., 2012) and, therefore, contributing to the excitotoxicity that terminates in neuronal damage in the penumbra (Szydlowska and Tymianski 2010). In light of the data, NKCC1 and KCC2 represented very attractive neuroprotective targets for modulation in order to rescue the salvageable penumbral tissue at risk of infarction following PTS. Accordingly, the next study was aimed to

investigate whether the modulation of CCCs channel function, using CCCs-specific ligands, would impact on neuronal loss following PTS.

5.4.3 Modulation of NKCC1 and KCC2 activity reduces neuronal loss in the penumbra following PTS

Specific drugs that target NKCC1 and KCC2 are needed in order to modulate their activity and test their validity as neuroprotective targets in different pathologies. The neuroprotective potential of NKCC1 and KCC2 was analysed by treating mice with transporter-specific modulators and measuring subsequent neuronal loss in the defined penumbra following PTS.

5.4.3.1 CLP257 as a neuroprotective modulator of KCC2 activity

CLP257 is a specific KCC2 agonist (Gagnon *et al*., 2013) and has been shown to strengthen KCC2 activity and recover loss of neuronal inhibition as well as pain hypersensitivity in a rat model of neuropathic pain (Gagnon *et al*., 2013). It therefore represents a novel strategy to restore the normal chloride gradient in the penumbra after PTS. KCC2 mRNA and protein were downregulated in neuronal-like PC12 and NT2 cells following acute hypoxia *in vitro* (Figures 5.3 and 5.5) and a substantial decrease in the number of neurons expressing KCC2 was observed in the penumbra following PTS *in vivo* (Figure 5.8 and 5.9).

CLP257 was administered intraperitoneally to mice at 100mg/kg 1 hour following the photothrombotic insult as described previously (Gagnon *et al*.,

2013). For days three and five post PTS, a second dose was administered to mice 24 hours following the PTS insult. In Chapter 4, NeuN immunostaining following PTS revealed neuronal loss taking place in the penumbra increasing up to 5 days following the insult (Figure 4.15). Brain slices were immunostained with NeuN and DAPI and images obtained as explained in section 5.4.2.1. Untreated, vehicle and CLP257-treated mice were examined. The vehicle used with the drug treatments (0.1% DMSO in NaCl) was used as a control to eliminate any possible interference of the solvent on the drug effects.

Analysis of NeuN-positive staining of cells in the penumbra (Figure 5.12, A, red boxes), healthy cortex in the peri-infarct region (Figure 5.12, A, yellow boxes) and an area matching the location of the penumbra in the contralateral hemisphere (Figure 5.12, C) was analysed at one, three and five days following PTS (Figure 5.12). NeuN immunolabeling was homogeneous in the brain (Figure 5.12, A, top panel), although a decrease in the total number of cells, as well as an increase in DAPI-positive NeuN-negative cells, was observed in the penumbral cortex at all time points following the PTS (Figure 5.12, A, red boxes).

NeuN- and DAPI-positive cells were counted in the different regions and analysed to quantify neuronal loss in the penumbra and contralateral hemisphere following PTS and were expressed as a ratio of NeuN/DAPI. One day following the insult the NeuN/DAPI ratio was 0.66 in untreated mice, 0.60 in vehicle control and increased to 0.74 in CLP256-treated animals (Figure

5.12 B, p = 0.74). Three days after PTS the ratio in untreated animals was 0.59, 0.58 in vehicle-treated and 0.55 in CLP257-treated mice (Figure 5.12 B). Finally, five days following PTS, the NeuN/DAPI ratio was 0.42 in untreated mice, 0.46 in vehicle-treated and 0.53 in CLP257-treated (Figure 5.12 B). The vehicle used for the drug administration did not induce any changes on neuronal loss (Figure 5.12 B). Significant changes in neuronal loss were not observed following CLP257 treatment. A small increase in neuronal numbers was observed at one and five days following the insult compared to the vehicle and untreated animals in CLP257-treated mice. Therefore, this result indicates that CLP257, under the conditions of this investigation, did not decrease neuronal loss in the penumbra up to five days following PTS in mice.

In the contralateral hemisphere, changes in neuronal loss were not observed following vehicle or drug treatment (Figure 5.12 C). Furthermore, the NeuN/DAPI ratio was very similar, 0.87 ± 0.02, indicating that the contralateral hemisphere did not suffer from any effect following the drug treatments and therefore functioned as a valid control.

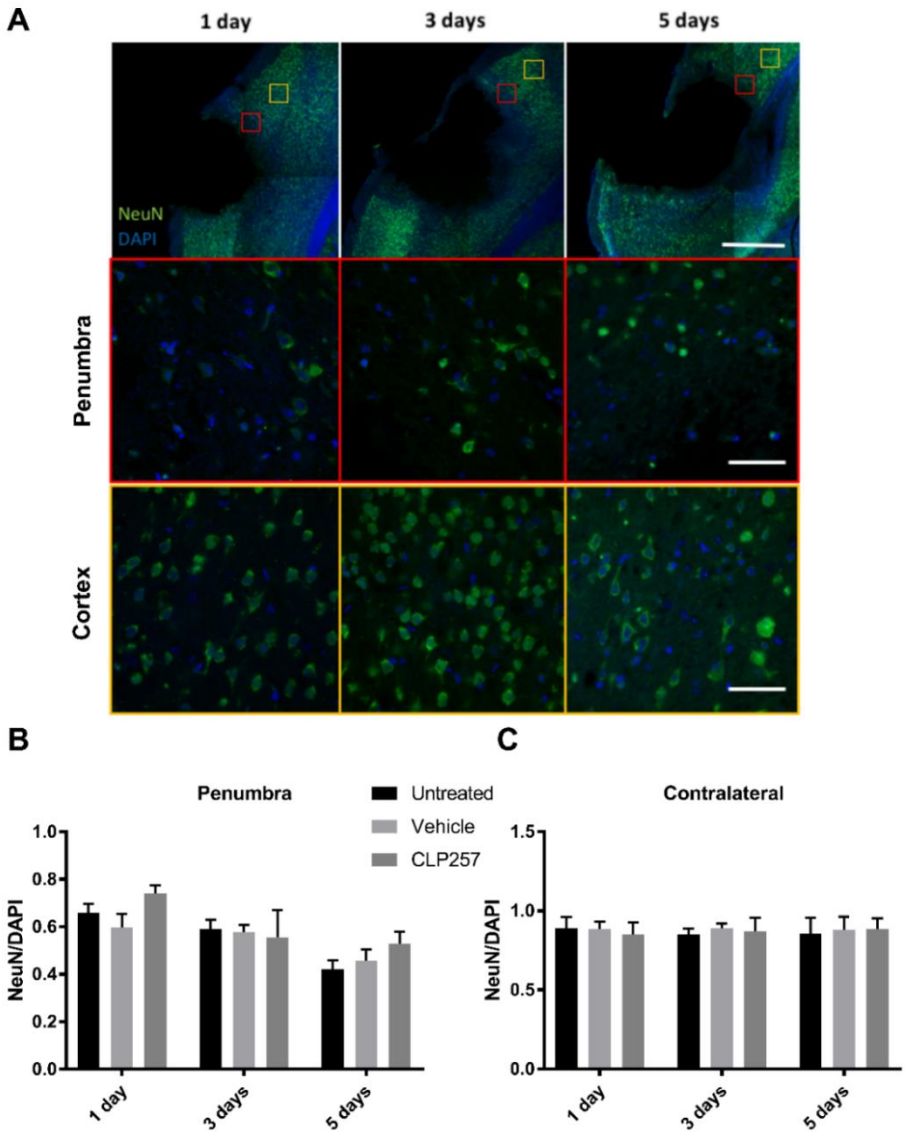

Figure 5.12 CLP257 treatment following PTS does not affect neuronal loss in the penumbra. A. Representative images of untreated, vehicle-treated and CLP257-treated mice analysed for NeuN (green) and DAPI (blue) staining in the penumbra (red boxes), healthy cortex (yellow boxes). Scale bar represents 500 µm (top panel) and 50 µm (bottom panels). The NeuN/DAPI ratio was represented in the penumbra (**B**) and contralateral hemisphere (**C**) at one, three and five days following PTS. Results are represented as the mean ± SEM (n=3). Two-way ANOVA with Sidak's multiple comparisons test.

5.4.3.1 Bumetanide as a neuroprotective modulator of NKCC1 activity

Bumetanide is an NKCC1-specific antagonist at low concentration (< 10 μM) (Dzhala *et al*., 2005). The results shown earlier in this chapter indicate that NKCC1 and KCC2 expression was modified following ischaemic insults. In the hypoxic *in vitro* model, NKCC1 levels were not modified at mRNA level (Figure 5.3) but there was an increase in the protein levels following acute hypoxia in NT2 cells (Figure 5.4). In the *in vivo* PTS model, the ischaemic penumbra revealed a significant increase in NKCC1-positive cells in the days following the insult (Figures 5.8 and 5.9). Bumetanide has been shown to be effective in reducing neonatal seizures in different animal models (Kahle and Staley 2008) and to be protective in preterm hypoxic brain injury (Jantzie *et al*., 2015), situations in which high expression of NKCC1 was observed. Hence, given the over-expression of NKCC1 observed in the penumbra (Figures 5.8 and 5.9), bumetanide was postulated to be effective in reducing excitotoxicity by facilitating $GABA_AR$-mediated hyperpolarisation. It was hypothesised that the antagonising actions of bumetanide would inhibit NKCC1-mediated chloride import and therefore, upon $GABA_AR$ activation, the higher concentrations of extracellular chloride would lead to chloride influx in the cell. This could eventually induce hyperpolarising action potentials, mitigating the excitotoxic effect that ensues in the penumbra following stroke.

Untreated, vehicle and bumetanide-treated mice were analysed by NeuN immunostaining of brain sections following PTS. Analysis of the number of NeuN-positive cells in the penumbra (Figure 5.13, A, red boxes), healthy

cortex in the peri-infarct region (Figure 5.13, A, yellow boxes) and an area matching the location of the penumbra in the contralateral hemisphere (Figure 5.13, C) was assessed at one, three and five days following PTS (Figure 5.13). NeuN immunolabeling was, as expected, homogeneous in the brain (Figure 5.13, A, top panel), although a decrease in total number of cells, and an increase in DAPI-positive NeuN-negative cells, was observed in the penumbral cortex at one, three and five days following PTS (Figure 5.13, A, red boxes).

By counting the number of NeuN and DAPI-positive cells in the penumbra and contralateral hemispheres, neuronal survival following PTS was determined (Figure 5.13 B and C). In the penumbra, one day following PTS, the NeuN/DAPI ratio was 0.66, 0.60 in the vehicle control and 0.71 in the bumetanide-treated mice (Figure 5.13 B). Three days following PTS the ratio of neurons in the penumbra was reduced to 0.59 in untreated mice, 0.58 in vehicle control and a significantly higher 0.76 ratio ($p = 0.01$) was observed in bumetanide-treated animals. Five days after PTS, the ratio of NeuN/DAPI in untreated mice in the penumbra was reduced to 0.42, 0.46 in the vehicle control and a significantly higher 0.68 ratio ($p < 0.001$) in bumetanide-treated mice. The vehicle control had no effect on untreated mice indicating that the vehicle did not interfere with the drug effects. However, treatment with bumetanide promoted neuronal survival three and five days following PTS (Figure 5.13 B).

An interesting observation was that the ischaemic core is always lost during the tissue handling, however, one of the bumetanide-treated mice analysed one day following the ischaemic insult did not lose the ischaemic core during the sample preparation (Figure 5.13 A). Whether this was an isolated event or produced by maintenance of tissue integrity due to reduced neuronal loss could not be ascertained.

In the contralateral hemisphere, changes in neuronal loss were not observed following vehicle or drug treatment (Figure 5.13 C). Furthermore, the NeuN/DAPI ratio was very similar in the different groups analysed, 0.88 ± 0.04, indicating that, as expected, the contralateral hemisphere did not suffer from any effect following the drug and vehicle treatments and therefore functioned as a valid control.

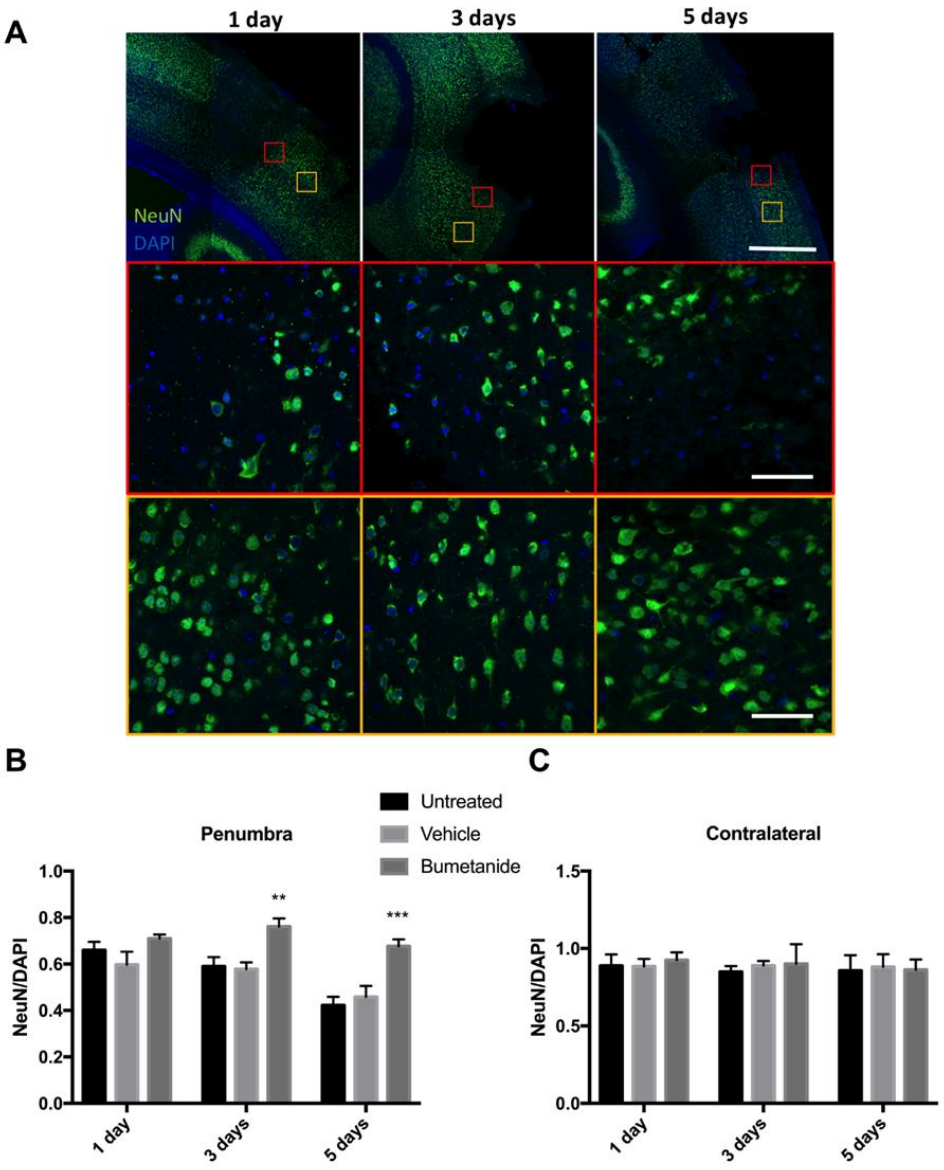

Figure 5.13 Bumetanide treatment reduces neuronal loss in the penumbra following PTS. (**A**) Representative images of untreated, vehicle-treated and bumetanide-treated mice at one, three and five days following PTS were analysed for NeuN (green) and DAPI (blue) staining in the penumbra (red boxes), healthy cortex (yellow boxes). Scale bar represent 500 µm (top panel) and 50 µm (bottom panels). The NeuN/DAPI ratio was represented in the penumbra (**B**) and contralateral hemisphere (**C**). Results are represented as the mean ± SEM (n=3). Two-way ANOVA with Sidak's multiple comparisons test.

In summary, the analysis of KCC2 and NKCC1 modulation on neuronal loss following PTS revealed two main findings: **i)** there is a reversal in the expression of the CCC family of proteins following hypoxic insults in both *in vitro* and *in vivo* models. The expression of the chloride exporters was downregulated at both the mRNA and protein level following hypoxic insults while the expression of the chloride importer NKCC1 was upregulated; **ii)** Treatment with bumetanide, an NKCC1 antagonist reduced neuronal loss three and five days following the insult in a photothrombotic model of stroke in mice.

The aim of this study was to assess the impact of NKCC1 and KCC2 modulation on neuronal loss in the established penumbra following treatment with the NKCC1 antagonist bumetanide and the KCC2 agonist CLP257. Treatment with bumetanide resulted in an increase in neuronal survival in the penumbra following PTS in mice (Figure 5.13). The fundamental role of NKCC1 in inducing excitatory GABAergic neurotransmission makes it an attractive target to curtail neuronal excitotoxicity following stroke. Bumetanide produced significant increases in the number of surviving neurons compared to the untreated and vehicle control mice three and five days following PTS (Figure 5.13). Therefore, the protective efficacy of bumetanide in reducing the neuronal loss in the days following PTS suggests that NKCC1 inhibition may have clinical application in stroke patients. This is highly important as its usage one, and 24 hours following PTS induced neuronal survival 3 and 5 days following the insult, representing an available

therapeutic agent with the potential to increase the therapeutic window of current stroke treatments.

5.5 Discussion

In this chapter, a reversal in the pattern of expression of the chloride exporters, KCC1-4 and NKCC1, importer of the CCC family of proteins, was observed following hypoxia in neuronal-like cells *in vitro* and in the penumbra following an *in vivo* mouse model of PTS. Furthermore, blockage of NKCC1 activity with bumetanide rescued neuronal loss within the penumbra.

5.5.1 Implications of the reversal in the expression of the CCCs following hypoxic insults

CCCs are the master regulators of chloride homeostasis in the brain and this chloride balance is responsible for $GABA_AR$-mediated postsynaptic activity (Kaila *et al*., 2014). Therefore CCCs modulate $GABA_AR$-mediated activity and modifications in their regulation and expression have been shown to be involved in the development of various CNS pathologies (reviewed by Kahle *et al*., 2015, Figure 5.1). However CCCs also have $GABA_AR$-independent functions, in neuronal volume regulation, synaptogenesis, dendritic spine formation, interactions with trophic factors and intracellular molecular cascades (Blaesse *et al*., 2009).

A reversal in the chloride gradient mediated by NKCC1 upregulation and simultaneous KCC1-4 downregulation, promotes a shift in the GABAergic potential towards a less hyperpolarising or even depolarising state (Rivera *et al*., 1999; Figure 5.1). The inhibitory tone of GABA is essential for the correct development of signal transmission within the brain. Downregulation of the chloride exporters KCC1-4 expression was observed in the *in vitro* model of hypoxia at mRNA and protein levels (Figures 5.3, 5.5 and 5.6) alongside an upregulation of NKCC1 at protein level (Figure 5.4). This adaptation to hypoxia is similar to embryogenesis, where a reversal in the expression pattern of NKCC1 and KCC2 renders $GABA_AR$-mediated responses depolarising (Rivera *et al*., 1999). This depolarisation increases the intracellular levels of Ca^{2+}, activating downstream signalling cascades, which in turn promote the release of trophic factors and promote neuronal proliferation and synaptogenesis (Ben-Ari *et al*., 2007). Therefore, the *in vitro* response to hypoxia observed in this chapter could represent an adaptation of neurons to revert to earlier in development phenotypes and thus, potentially proliferative states. This adaptive response is, to a certain extent, similar to the adaptations observed following acute hypoxia in neuronal-like cells in Chapter 3. However, this strategy could also contribute to further depleting the energetic pool following hypoxia. Most importantly, $GABA_AR$-mediated depolarisation could contribute to excitotoxicity, which is responsible for the expansion of the penumbra and its recruitment into the core (Szydlowska and Tymianski 2010).

Inhibition of the KCCs using a non-specicific inhibitor, [(dihydroindenyl)oxy]alkanoic acid (DIOA), and KCC1-targetted knockdown with siRNA, both enhanced NGF-mediated neurite outgrowth in PC12 cells (Nagao et al., (2012). NGF treatment of PC12 cells was shown to inhibit KCC1 expression but not KCC2-4. NKCC1 is up-regulated following NGF treatment of PC12 cells and NKCC1 knock-down diminished neurite outgrowth (Nakajima *et al*., 2007). These results indicate that the chloride balance is fundamental for neurite elongation and that when CCCs expression is reversed, neurite outgrowth is enhanced. Although these two studies do not analyse the effect of hypoxia in PC12 cells, they provide an insight into the role of CCCs in neurite elongation and how this could parallel the results obtained in following hypoxia in Chapter 3. This is that reversal of CCCs expression could lead to immature adaptive responses (Figure 5.1) and that this temporary return to an immature phenotype may be protective to re-establish neuronal networks.

Analysis of CCC expression in the *in vitro* model of hypoxia demonstrated that changes in the expression of these cotransporters are observed following acute hypoxic insults in neuronal-like cells. This has a great significance as it provides a platform to further investigate $GABA_AR$-dependent, and $GABA_AR$-independent roles of the CCCs following hypoxia that could be translated to *in vivo* models. However, changes in CCCs expression and function may, or may not occur in neurons within the brain *in vivo*, and these findings were therefore replicated in a model of PTS in mice in order to determine their clinical relevance.

In vitro findings were confirmed *in vivo* as a highly significant increase in the expression of NKCC1 and decrease in the expression of KCC2 were observed in the penumbra of mice at one, three and five days following PTS (Figures 5.8 and 5.9). Although changes in CCCs expression do not necessarily determine changes in the activity of these transporters, the extraordinary reversal in expression observed in the penumbra compared to healthy or contralateral cortex, strongly suggest a modification in the chloride gradient promoted by NKCC1 and KCC2. A direct relationship between changes in the expression of KCC2 and NKCC1 in neuronal $[Cl^-]_i$ has been previously demonstrated (Dzhala *et al*., 2010; Gagnon *et al*., 2013). This strongly suggests that alterations in the expression of the CCCs such as those observed herein, could potentially reflect changes in $[Cl^-]_i$, and therefore influence $GABA_AR$-mediated potential (Succol *et al*., 2012).

Several studies have addressed the expression of NKCC1 and KCC2 following stroke. NKCC1 has been shown to be upregulated in the peri-infarct cortex following MCAO (Yan *et al*., 2003; Begum *et al*., 2015) and KCC2 downregulated under the same model (Jaenisch *et al*., 2010; Jaenisch *et al*., 2016). Only one study has shown KCC2 to be downregulated following PTS in individual motoneurons (Toda *et al*., 2014). However, studies that address the expression of both NKCC1 and KCC2 in a clearly-identified penumbra following PTS are seriously lacking. Therefore, understanding the pattern of expression of the CCCs in a precisely defined penumbra represented an unmet need for the development of this field of research.

The results described in this chapter show a reversal in the expression of both NKCC1 and KCC2, primary regulators of neuronal chloride trafficking in mammalian CNS, in a molecularly and precisely characterised penumbra, located up to 200 μm from the ischaemic core. Furthermore, changes in the expression of NKCC1 and KCC2 were not observed in the IGE zone. This is highly important as previous studies were targeted at a loosely defined peri-infarct zone, which could lead to the misinterpretation of results (Yan *et al*., 2003; Jaenisch *et al*., 2010; Begum *et al*., 2015; Jaenisch *et al*., 2016). Studies aimed at a vaguely defined peri-infarct area could in fact represent a combination of healthy tissue and the penumbra.

5.5.2 KCC2 as a target for neuroprotection

KCC2 expression was downregulated in the penumbra in the days following PTS, therefore the aim of this study was to rescue KCC2 activity through a specific KCC2 agonist (Gagnon *et al*., 2013). Neuronal loss was not significantly improved with the treatment of CLP257 following PTS, although a small increase in neuronal numbers was observed one and five days after the experimental stroke (Figure 5.12). The mechanism of action of CLP257 is thought to be a result of an increase in the trafficking of existing KCC2 protein complexes to the plasma membrane (Gagnon *et al*., 2013).

Successful experiments with CLP257 in rescuing KCC2 activity have been achieved *in vitro* through electrophysiological recordings in spinal cord slices in a peripheral nerve injury model *(*Gagnon *et al*., 2013), cortex slices in an ictogenesis model (Hamidi and Avoli 2015) and hippocampal slices in a

model of Alzheimer's (Chen *et al*., 2017); but also *in vivo* via intraperitoneal injection in peripheral nerve injury animals (Gagnon *et al*., 2013) and in a neuropathic pain model (Lavertu *et al*., 2014). However, due to the poor pharmacokinetics of CLP257 the maximum efficacy of this drug was achieved two hours post injection (Gagnon *et al*., 2013) or with an attached chamber that perfused the drug for 30 minutes (Lavertu *et al*., 2014). Poor pharmacokinetics and short half-life might therefore be responsible for the results obtained in our model. However, the photothrombotic model of stroke presents the advantage of instantly disrupting the BBB (Schoknecht *et al*., 2014), therefore giving greater access to drugs to neuronal tissue that otherwise would not be able to cross this barrier and exert their potentially beneficial effects. Therefore this model is useful in order to screen the potential of such drugs.

An improved version of CLP257, CLP290, has been developed which presents an improved plasma concentration (Gagnon *et al*., 2013). However, this drug was not commercially available at the time of designing this study. It would be interesting to repeat this study with CLP290 in order to maximise the potential of KCC2 modulation and increase the drug's exposure. The ability of novel drugs which possess a longer half-life and cross the BBB to reach their target location within the brain is a big limitation to reach clinical relevance. Therefore, more effort should be addressed into finding such compounds.

5.5.3 NKCC1 as a target for neuroprotection

Expression of NKCC1 was shown to be dramatically upregulated in the penumbra 1, 3 and 5 days following PTS (Figures 5.8 and 5.9). Furthermore, this upregulation was suggested to occur rapidly (before one day) and maintained up to 5 days and beyond after stroke. NKCC1 expression affects $GABA_AR$ polarity by increasing neuronal $[Cl^-]_i$ (Dzhala *et al*., 2010). This shift in chloride equilibrium potential renders $GABA_AR$ responses depolarising (Rivera *et al*., 1999) reversing normal GABA-mediated postsynaptic inhibitory tone. Therefore, NKCC1 is believed to participate in the spreading depolarisations and excitotoxicity that follows an ischaemic stroke in the penumbra (Beck *et al*., 2003; Steffensen *et al*., 2015; Martín-Aragón Baudel *et al*., 2017). In this study, it was hypothesised that treatment with bumetanide, an NKCC1 antagonist, could inhibit reversed chloride transport and subsequently reduce $GABA_AR$-mediated depolarisation thereby decreasing neuronal loss associated with excitotoxicity.

Treatment with bumetanide 1 and 24 hours following PTS decreased neuronal loss in the penumbra three and five days after stroke (Figure 5.13). These results highlight the role of NKCC1 upregulation in the penumbra in mediating neuronal loss, as pharmacological inhibition of its activity resulted in a significant increase in neuronal survival. Furthermore, the beneficial effect of bumetanide was observed three and five days following the insult, time points at which a second dose of bumetanide was injected at 24 hours. This underlines the potential of this drug to provide a longer therapeutic window than current pharmacological or mechanical strategies focused on

thrombolysis (Holmes *et al*., 2015; Akbik *et al*., 2016). These results support the idea that rescuing the penumbra could provide stroke victims with a longer therapeutic window therefore increasing the selection criteria for patients outside the current 4.5 hours therapeutic window for thrombolytic strategies.

It could be argued that the protective role of bumetanide could be due to a reduction in oedema formation. Oedema formation is secondary damage produced after stroke that contributes to neuronal loss and mortality (Sandoval and Witt 2008). This is caused by an increase in Na^+ and water transport from the blood across the BBB to the brain (Betz 1996). A number of findings have revealed a role for NKCC1 in participating in Cl^- and Na^+ transport in BBB endothelial cells in the hours following an ischaemic event (Spatz *et al*., 1997; Wallace *et al*., 2012). Bumetanide decreased oedema formation in a permanent MCAO model in rats (O'Donnell *et al*., 2004), however, in this model, reperfusion does not take place, which is responsible for the breakdown of the BBB (Yang and Betz 1994). BBB breakdown takes place ~4 hours after the onset of ischemia (Betz 1996) and the protective effects of bumetanide observed 3 and 5 days following PTS took place when a second dose of was injected 24 hours after PTS. Furthermore, the BBB is immediately disrupted following PTS (Schoknecht *et al*., 2014) and therefore, the beneficial effects of bumetanide cannot be attributed to a decrease in oedema formation mediated by reducing NKCC1 activity.

Drugs able to restore low neuronal $[Cl^-]_i$ and therefore $GABA_AR$-mediated inhibition in different neuronal types and pathological conditions, may provide novel therapies for different CNS disorders. High $[Cl^-]_i$ and $GABA_AR$-mediated excitatory actions have been observed in different pathological conditions such as Autism Spectrum Disorders (ASD), seizures, spinal chord lesions, chronic pain, Down's syndrome, brain trauma and ischaemic stroke (Pizzarelli and Cherubini 2011; Ben-Ari 2014; Kaila *et al*., 2014). Bumetanide has been shown effective in many animal models and case studies for the treatment of these pathologies and is considered a safe compound with minimal side effects (Ben-Ari *et al*., 2016). This drug is currently under a phase one clinical trial for the treatment of neonatal seizures (Pilot Study of Bumetanide for Newborn Seizures Trial). However, another recent phase 1/2 trial for the treatment of seizures in newborn infants with hypoxic ischaemic encephalopathy (NEMO trial), found that bumetanide, administered with phenobarbital ($GABA_AR$ agonist), failed to improve seizure control and presents some side-effects (Pressler *et al*., 2015). However, newborn seizures present unique characteristics in comparison to other brain disorders where bumetanide still can be considered as a novel and promising therapeutic (Ben-Ari *et al*., 2016).

High concentrations of bumetanide are needed to reach beneficial outcomes in brain pathologies, increasing undesirable side-effects such as diuresis (Wang *et al*., 2015). This is because of the non-selective action of bumetanide on both NKCC1 and NKCC2, which is highly expressed and plays an important function in the kidney (Brandt *et al*., 2010). Bumetanide

also presents poor brain penetration through the BBB (Römermann *et al*., 2017) and a short half-life which together, accounts for a poor neuronal accumulation (Löscher *et al*., 2013). Therefore, novel, NKCC1-specific compounds with enhanced half-life and increased brain penetration are needed. To that end, derivatives of bumetanide are currently being developed (Lykke *et al*., 2016) which may bring some hope for the successful translation of the results here presented to clinical therapies.

There is a great body of evidence suggesting a role for NKCC1 in the development of injury following stroke and its potential as a neuroprotective target (Yan *et al*., 2003; Chen *et al*., 2005; Begum *et al*., 2015; Xu *et al*., 2016). Therefore, a different strategy to inhibit NKCC1 activity, other than direct pharmacological inhibition of this transporter, could reside in the modulation of its regulation. However, the precise mechanisms that lead to NKCC1 activation following stroke are yet to be fully ascertained. A chloride sensing kinase, WNK3, is well expressed in the brain and thought to be responsible for NKCC1 activation (de los Heros *et al*., 2006). NKCC1 activation occurs by the association and phosphorylation of WNK 3 with SPAK/OSR1 (Ste20/SPS1-related proline-alanine-rich protein kinase / oxidative stress-responsive 1), which in turn phosphorylates a cluster of conserved threonine residues in NKCC1 (Kahle *et al*., 2008). WNK3 knockout mice as well as genetic inhibition of WNK3 or siRNA knockdown of SPAK/OSR1, resulted in decreased infarct volume in the MCAO model of stroke and increased resistance to ischaemic insults *in vitro* (Begum *et al*.,

2015). These promising results open a novel strategy to achieve neuroprotection by targeting NKCC1 regulation.

The failure of $GABA_AR$ agonists in the treatment of stroke (Cheng *et al*., 2004; Clarkson 2012) combined with the promising preclinical findings obtained by modulating the expression/activity of the CCCs, makes targeting NKCC1 and KCC2 very attractive candidates for the treatment of a great number of brain-derived pathologies, and as neuroprotective targets following stroke (Martín-Aragón Baudel *et al*., 2017). Special attention should be focused on combined therapies that potentiate both KCC2 activity/expression and NKCC1 downregulation/blockade in the acute phase of ischaemic stroke in the penumbra (Figure 5.2).

As well as in the penumbra, this molecular response is observed during early mammalian brain development, where KCC2 levels are down-regulated and contribute to $GABA_AR$–mediated depolarising response (Rivera *et al*., 1999). Neuronal excitation is responsible for growth and arborisation (Deisseroth *et al*., 2004) therefore KCC2 downregulation after hypoxia links with results discussed in Chapter 3. This is that neurons respond to hypoxia by promoting proliferative adaptations to hypoxic insults and that this response might be enhanced by KCC2 downregulation and NKCC1 upregulation.

5.5.4 Neurorehabilitation

A different strategy in stroke intervention is based on promoting neuronal recovery in the days to months after ischaemic stroke. The classic approach to promote neurorehabilitation involves physical, occupational, and cognitive therapies (Dobkin 2004, 2008). However, drug treatments that enhance brain repair and plasticity post-stroke are not yet available. This strategy could open a different and enlarged therapeutic window as brain reorganisation in the peri-infarct zone has been shown to take place over weeks following the insult (Brown *et al*., 2009).

Recent evidence suggests that, as opposed to during the acute phase of stroke, promoting excitation via glutamate receptors and suppression of $GABA_AR$–mediated inhibition could promote stroke recovery in the long term (Clarkson *et al*., 2010; Clarkson *et al*., 2011). This functional gain relies on the modulation of motor learning and memory pathways (Krakauer 2006), which is in turn is based on increasing neuronal excitability (Clarkson and Carmichael 2009). Extrasynaptic $GABA_ARs$ respond to ambient levels of GABA, which are known to be substantially increased following ischaemic events (Schwartz *et al*., 1995; Hutchinson *et al*., 2002) and produce long lasting tonic inhibition (Glykys and Mody 2007). Moreover, dampening $GABA_AR$-mediated extrasynaptic tonic inhibition has been shown to enhance long-term functional recovery (Clarkson *et al*., 2010). This demonstrates that many of the molecular mechanisms involved in learning and memory could represent potential targets for neurorehabilitation following stroke.

Strategies that focus on promoting neurorehabilitation via $GABA_AR$s in the penumbra following ischaemic stroke would also benefit from careful consideration of $GABA_AR$ subtype-specific modulators. Tonic $GABA_AR$s in cortex contain either *α5* or *δ* subunits (Glykys and Mody 2007). Reduced tonic inhibition through the specific modulation of *α5* and *δ* subunit-containing receptors, results in enhanced cognitive performance, long term potentiation and neuronal excitability (Collinson *et al*., 2002; Atack *et al*., 2006; Dawson *et al*., 2006). There is a great controversy on the specificity of *δ* subunit-specific modulators, the neurosteroids tetrahydrodeoxycorticosterone (THDOC) or gaboxadol and tracazolate as the most sensitive and specific agonists for the *δ* subunit (Zheleznova *et al*., 2009; Lewis *et al*., 2010). L655,708, an *α5*-specific antagonist, has been shown to reduce infarct size and improve motor recovery, in the long-term, when chronically administered starting three days post-stroke (Clarkson *et al*., 2010). However, when administered immediately following stroke, infarct size was increased, emphasising the importance of timing during the neuroprotective and subsequent neurorehabilitation phases of stroke (Figure 5.2). The lack of consideration of subtype-specific $GABA_AR$ modulators, combined with ill-timed administration might also explain the failure of compounds that broadly act on synaptic $GABA_AR$s in stroke research.

Cation chloride cotransporters, mediators of the GABAergic response, could therefore present a beneficial target in promoting neuronal recovery in the long-term following stroke (Figure 5.2, Martín-Aragón Baudel *et al*., 2017). This action would be opposed to the one discussed in this chapter which was

based on promoting neuroprotection and it would rely on decreasing $GABA_AR$-mediated tonic inhibition. NKCC1 potentiators and KCC2 antagonists would therefore increase neuronal $[Cl^-]_i$ and facilitate $GABA_AR$ hyperpolarisation promoting functional recovery after stroke (Figure 5.1).

A specific KCC2 antagonist, VU0463271, has been developed by Delpire and colleagues (2012) and used to induce epileptiform discharges (Sivakumaran *et al*., 2015). It has also been used to demonstrate the critical role of KCC2 in regulating seizure event duration (Kelley *et al*., 2016). Therefore, this compound could restore impaired neuronal inhibition in the recovery phase following stroke. Increasing the activity of NKCC1 or upregulating its expression could, in turn, represent an alternative strategy to promote neurorehabilitation (Figure 5.2). Although specific NKCC1 agonists are not available yet, different strategies have been shown to potentiate its activation through the stimulation of the WNK3/SPAK/OSR1 system (Gagnon and Delpire 2010; Kahle *et al*., 2010; Nugent *et al*., 2012). These strategies could potentially participate in potentiating neuronal recovery. Therefore, future effort should be directed in finding novel and more specific CCCs modulators.

5.6 Summary

In this chapter, the expression of the (N)KCC family of proteins in the neuronal-like cells PC12 and NT2 following hypoxia and following PTS in mice was characterised. Downregulation of the chloride exporters (KCCs) was observed in both *in vitro* and *in vivo* models whereas the chloride importer NKCC1 was upregulated. This reversal in expression of chloride transporters has been previously shown to affect GABAergic polarity and augment penumbral excitotoxicity. Following treatment with bumetanide, an NKCC1 antagonist, neuronal loss was reduced in the penumbra. These results highlight the potential of CCCs as neuroprotective targets and encourage further research to discover novel CCCs modulators that could reduce the burden associated with neuronal loss following stroke.

6. General discussion and future directions

6.1 Summary of findings

The main findings of this investigation can be summarised as follows:

1. HIF-2α is the predominant driver of adaptation to acute hypoxia *in vitro* in neuronal-like PC12 and NT2 cells. Interestingly, these adaptations promote a regression to undifferentiated states. Preferential activation of HIF-2α dependant adaptation could therefore promote neuronal recovery and potentially reduce damage associated with ischaemic insult. Therapeutic manipulation of endogenous pathways driving neuronal adaptation to hypoxic stress could represent exciting possibilities to promote neurogenesis in the penumbra and enhance recovery following ischaemic stroke.

2. For the first time, the penumbra following PTS in mouse brain has been fully analysed and the extent quantified over time using molecular markers. The peri-infarct zone following PTS can be anatomically and molecularly subdivided into the penumbra, located 200 μm from the infarct, and IGE zone in the area between 200 and 400 μm from the ischaemic core. The precise characterisation of the penumbra in the PTS model is highly significant, as it allows the study of molecular mechanisms of damage intrinsic to the heterogeneous penumbra. Furthermore, a continuing neuronal loss was observed up to five days following PTS, showing that the penumbra is progressively deteriorating. Therefore, this model provides a platform to

study the potential development of novel therapies targeted at rescuing this tissue from infarction.

3. A significant reversal in expression of the CCCs was observed after acute hypoxia *in vitro* and in the penumbra in mice following PTS *in vivo*. A striking upregulation of NKCC1 expression was observed in the penumbra, alongside a concurrent reduction of KCC2 expression *in vivo*. The combined activity of NKCC1 and KCC2 regulates neuronal chloride trafficking and subsequently $GABA_AR$ polarity. The clear reversal in expression indicates a potential mechanism by which GABA-mediated depolarisation can contribute to excitotoxicity in the penumbra following stroke and accounts for the relative failure of $GABA_A$-R targeting therapies in the treatment of ischaemic stroke.

4. Modulating NKCC1 activity with the antagonist bumetanide significantly increases neuronal survival up to five days following PTS. Bumetanide was administered at 1 and 24 hours following the insult. Neuronal recovery was evident in the long-term (up to five days), providing potential for a novel therapeutic strategy with an increased secondary therapeutic window and an unexplored neuroprotective target compared to current strategies.

Overall, the findings of this investigation provide two different platforms on which to study ischaemic stroke and two different and novel strategies to potentially reduce the personal, social and economic burden that stroke causes. However, these findings open a door for further investigation into the precise mechanisms by which HIF-2α–mediated adaptation to hypoxia could

be directed into a therapeutic strategy and how CCC-mediated neuroprotection and rehabilitation could be translated for use in human patients.

6.2 Neuronal dedifferentiation as an adaptation to hypoxia to promote neuronal recovery

Many molecular similarities can be observed between neurodevelopment and CNS tissue repair. In different neuropathologies, such as stroke, amyotrophic lateral sclerosis, Huntington's disease or Alzheimer's disease, evidence shows that the reversal of molecular events, which promote survival in mature neurons, are seen during neurodegeneration (reviewed by Kole *et al*., 2013). In the peri-infarct cortex surrounding the ischaemic core, neurons lose their perineuronal net, which are specialized extracellular matrix structures responsible for synaptic stabilisation in the adult brain and its loss promotes synaptic plasticity (Wang and Fawcett 2012; Yang *et al*., 2015). Furthermore, neurons within the peri-infarct area show modified intracortical inhibition (Clarkson *et al*., 2010), and become growth-factor dependent (Sist *et al*., 2014). These characteristics are mirrored in neurodevelopment, where neuronal plasticity is essential for the correct formation of new connections (Egorov and Draguhn 2013; Carmichael 2016).

The findings of this investigation have revealed two different adaptations to hypoxia that also share similarities to neurodevelopment. First, the *in vitro* findings on HIF-2α-mediated regression to dedifferentiated states, and

second, *in vivo* and *in vitro* findings of a reversal in the expression of CCCs that could be responsible for a $GABA_AR$-mediated change in polarity and excitability in neurons of the penumbra.

Hypoxia has previously been shown to downregulate neuronal markers *(*Jögi *et al*., 2002) and participate in brain development and neurogenesis (Simon and Keith 2008). In particular, HIF-2α is expressed during murine development, participating in sympathetic nervous system formation (Nilsson *et al*., 2005). HIF-2α signalling in neuroblastoma cells promotes the maintenance of an immature, neural crest-like phenotype (Pietras *et al*., 2009). Expression of neural crest genes is increased by hypoxia, and may drive towards a more immature phenotype in neuroblastoma cells (Jögi *et al*., 2002). HIF-2α regulates several genes involved in proliferation and regeneration, including the *OCT4* transcription factor which maintains stem-like characteristics (Nichols *et al*., 1998) and neural stem cell pluripotency (Forristal *et al*., 2010; Kim *et al*., 2009). Therefore, the results of this work further support previous literature and indicate that neurons try to adapt to hypoxic insults by dedifferentiating into more immature phenotypes and that this response is suggested to be HIF-2α-driven.

Significant alteration in CCC expression after acute hypoxia *in vitro* and following PTS in mice *in vivo*, also points towards an immature-like neuronal phenotype as a protective adaptation to hypoxia. However, in the short-term, CCC-mediated reversal of $GABA_AR$ polarity towards an excitatory response, might be detrimental for neuroprotection. This response would be beneficial

in the long-term following a stroke to promote neurorehabilitation (Clarkson *et al*., 2010), however, in the short term, it might contribute to the excitotoxicity-mediated recruitment of the penumbra into the infarcted core, and thus, accelerate neuronal loss (Szydlowska and Tymianski 2010; Steffensen *et al*., 2015). This hypothesis is strengthened by the results on NKCC1 blockage with bumetanide that led to increased neuronal survival in the penumbra following PTS.

It is therefore conceivable that these two molecular adaptations induced by hypoxia might share some common regulatory modulation. However, although some molecular manipulations aimed at promoting immature phenotypes and neuronal proliferation, might be beneficial, it could also lead to deleterious events.

6.3 A potential link between HIF and the CCCs

It was interesting to consider that there may be a link between the HIF response and CCC expression/activity after ischaemia. There is a paucity of evidence in the literature of a direct link between the HIF-response in the regulation of the CCCs. To date, only one study in epithelial cells has provided direct evidence of the CCCs being regulated by HIF-1α, where microarray analysis identified NKCC1 mRNA repression by hypoxia and further experiments identified a HIF-1α binding site in the NKCC1 5′-UTR, confirming HIF-1α-mediated repression of NKCC1 *in vivo* (Ibla *et al*., 2006).

However, the mechanism by which HIF-1α might induce NKCC1 repression has not yet been elucidated. Although this investigation was conducted in epithelial cells, it provides an insight into potential regulatory mechanisms of NKCC1 facilitated by the HIF response in neurons. The findings in Chapter 3, revealed a preferential HIF-2α-mediated response to acute hypoxia in neuronal-like cells that could potentially explain the lack of significant changes in NKCC1 mRNA abundance in Chapter 5. However, HIF-1α expression has been identified in the penumbra as a driver of a wide range of cellular adaptations to hypoxia (Shi 2009), and therefore the striking increase in NKCC1expression in the penumbra following PTS in mice remains controversial. This suggests that HIF-1α-mediated repression might be tissue specific and therefore not repress NKCC1 expression in neurons. In agreement with this hypothesis, Lu et al. (2015) recently revealed a correlation between HIF-1α and NKCC1 expression following traumatic brain injury (TBI) and propose HIF-1α as a key player in neuronal NKCC1 upregulation after TBI-induced severe brain oedema.

Although a direct link between the HIF response and reversed CCC expression is yet to be confirmed, some indirect evidence suggests shared regulatory mechanisms between these two events. Repressor Element-1 Silencing Transcription factor (REST), is a transcriptional repressor that has been demonstrated to regulate over 200 genes and is involved in mediating cellular adaptation to hypoxia (Cavadas *et al*., 2017). REST is widely expressed during embryogenesis in the brain, expression decreases during maturation, conferring neurons with a mature phenotype (Ooi and Wood

2007). Interestingly, it is also well expressed following ischaemia in neurons (Calderone *et al*., 2003), giving further credence to the notion of cells transiently reverting back to an immature phenotype. KCC2 (Yeo *et al*., 2009) and HIF-1α, but not HIF-2α (Cavadas *et al*., 2015) are amongst the genes regulated by REST, which represses their expression. REST promotes HIF-1α downregulation in response to prolonged hypoxia, which prevents the deleterious consequences that prolonged activation of the HIF pathway can cause (Cavadas *et al*., 2015). Following ischaemic stroke, there is a prolonged situation of hypoxia in the penumbra (Spratt *et al*., 2011) and therefore, it is conceivable that, as it has been shown following global ischaemia (Calderone *et al*., 2003), REST could be activated in this therapeutically critical zone. Consequently, REST could potentially be responsible for the observed KCC2 downregulation in the penumbra, which as shown in this investigation together with an increase in NKCC1 expression, has deleterious consequences for neuronal survival. Therefore, it would be interesting to further investigate the role of REST following stroke in regulating KCC2 expression and its potential as neuroprotective target or as a promoter of neurorehabilitation.

6.4 Impact, clinical relevance and future directions

6.4.1 Dedifferentiation and proliferation

In Chapter 3, preferential HIF-2α-mediated adaptation in PC12 and NT2 cells following acute hypoxia was demonstrated. Furthermore, the adaptations mediated by this transcription factor were suggested to regulate dedifferentiation and regression to immature phenotypes. However, to ratify these findings and reveal the potential of HIF-2α-mediated responses as a neuroprotective/neurorehabilitative strategy, further investigation would be required.

Additional markers of dedifferentiation and immature neuronal phenotypes such as expression of the pluripotency factors *Oct4*, *Sox2*, and *Nanog* (Boyer *et al*., 2005) could be used. These transcription factors are essential in development and characteristic of embryonic stem cells (Aoi *et al*., 2008). Furthermore, to study the role of HIF-2α in regulating the process of dedifferentiation after ischaemia, knock-down of HIF-2α via siRNA, or CRISPR/Cas9-mediated knock out, would reveal its role in promoting the expression of markers of dedifferentiation and stem cell-ness. Fully differentiated PC12 and NT2 cells do not proliferate, and therefore it would be interesting to analyse if acute hypoxia stimulates regain of cell division. Simple proliferation assays such Alamar blue or tetrazolium salts in the long term following acute hypoxia would therefore indicate if neurons adapt to hypoxia by promoting proliferation. These experiments combined with HIF2-

α genetic knockdown would ultimately indicate the potential involvement of HIF-2α-mediated adaptations in promoting neurorehabilitation following stroke.

In order to confirm *in vitro* findings, the results on HIF-2α-mediated adaptation should be investigated in the PTS model in mouse. Analysing expression and nuclear localisation of the HIF family of transcription factors would yield useful information regarding their activity in the penumbra. Furthermore, the expression of immature neuronal markers such as doublecortin, a microtubule-associated phosphoprotein that promotes neurite extension and cell migration (Spampanato *et al*., 2012) or beta III tubulin, a cytoskeletal protein used to label immature neurons (Menezes and Luskin 1994), could be employed to see immature phenotypic changes in neuronal populations in the penumbra following PTS. The analysis of these markers would also link with results from Chapter 5, which showed an increase in NKCC1 expression and a decrease in KCC2 expression following ischaemic insults and which is a hallmark of premature neuronal phenotypes.

Finally, to assess neuronal proliferation in the penumbra and potential restructuring following PTS, cell proliferation indicators such as 5-Bromo-2'-deoxyuridine (BrdU) (Wen-Lei Li *et al*., 2008), would indicate a regenerative response in the post-ischaemic brain. Comparing the potential neurogenesis response in the penumbra after PTS with conditional knockout mice deficient for HIF-2α (Smeyne *et al*., 2015) and strategies aimed at potentiating HIF-2α-mediated adaptations such as erythropoietin production or exogenous

administration of erythropoietin, may reveal the benefit of these strategies in the long-term functional recovery from ischemic stroke.

Data in Chapter 4 revealed a defined area of increased glial enrichment (IGE), within the penumbra lying between 200 and 400 μm from the ischaemic core. Whilst, involvement of the immune response in the development of the damage following PTS was outside the scope of this investigation, employing GFAP immunolabelling as a hallmark of the penumbra revealed some interesting findings. Although a compact and homogeneous glial accumulation was observed in the immediate vicinity of the ischaemic core, conforming the glial scar, further GFAP labelling was also observed in independent glial cells in more remote areas from the penumbra, conforming what has henceforth been described in this investigation as the IGE zone. Therefore, it would be interesting to elucidate the origin of these cells and their function in the IGE zone, whether they represent locally activated glial cells, and if they proliferate or migrate from adjacent healthy tissue.

6.4.2 Neuroprotection vs. neurorehabilitation

Current neuroprotective therapies in ischaemic stroke rely solely on rapid reperfusion strategies. However, due to a limited therapeutic window (4.5 h), secondary effects and extensive exclusion criteria (Fugate and Rabinstein 2015), less than 10% of all patients with acute ischaemic stroke receive the intravenous plasminogen activator alteplase in the UK (SSNAP 2016). It is therefore crucial to find novel therapeutic targets that could reduce neuronal

loss following reperfusion after an ischaemic incident and provide neuroprotection. The immediate effects of stroke were not the primary consideration in this work. The salvageable penumbra persists in mammalian brain days after stroke onset and continues to suffer recruitment to a core-like state (Dohmen *et al*., 2008, Foley *et al*., 2010). In the PTS model, neuronal loss continued up to day five after the stroke, highlighting the importance of understanding the evolution of the penumbra in the longer term after the ischaemic insult and the presence of a longer secondary therapeutic window. However, timing is critical, as many of the molecular processes that present as attractive candidates to achieve neuroprotection are deleterious in the long term to promote neurorehabilitation and vice versa. Therefore, greater emphasis should be placed into understanding the precise timing in the development of damage following stroke. This study is the first to properly characterise the heterogeneous penumbra from a molecular point of view.

The work herein focused on a potentially new and relatively unexplored therapeutic window aimed at achieving neuroprotection in the subacute phase of stroke. Physiological imaging in human studies have found that viable tissue within the penumbra at risk of infarction can be found up to 48 hours following stroke onset (Leigh *et al*., 2017, Schlaug *et al*., 1999) and this was confirmed in the PTS model in mouse. However, an in-depth investigation identifying the precise timing of ionic dysregulation within the penumbra in the days following stroke and its precise contribution to excitotoxicity and peri-infarct depolarisations (PIDs) has yet to be ascertained. Results showed no differences at the three time points analysed

when considering neuronal stress (HSP70), glial reactivity (GFAP) or ionic dysregulation (NKCC1 and KCC2 reversal in expression). This indicates that, from a molecular perspective, neurons within the penumbra become quickly stressed and remain in this state where they are at risk of infarction, beyond five days following the insult. Therefore, it would be interesting to examine both longer (beyond five days) and shorter (below 24 hours) time points in order to further clarify the precise timing of the onset of penumbral risk and its decline over time. The data herein presents a novel potential therapeutic window below one and beyond five days following stroke to counteract excitotoxicity, but it would be particularly interesting to understand when this therapeutic opportunity ends. The temporal nature of the evolving penumbra is highly important, as a secondary therapeutic window represents a crossover between neuroprotection and neurorehabilitation, where potential neuroprotective strategies, such as counteracting neuronal excitement could be deleterious during the neurorehabilitation process.

A great example of this dichotomy, is the reversed expression of NKCC1 and KCC2 in the penumbra following PTS in mice. The striking switch in expression strongly suggests modification of neuronal $[Cl^-]_i$ that would subsequently affect $GABA_AR$ polarity, rendering it depolarising beyond five days following PTS. This reversal is present during development and other CNS pathologies (Rivera *et al.,* 1999) in order to promote GABA-mediated neuronal proliferation, arborisation and differentiation (Ben-Ari *et al*., 2007); therefore, following ischaemic stroke, modified chloride transport might be a strategy aimed at promoting an transient immature phenotype that would

encourage neurorehabilitation (Wake *et al*., 2007). Although, an increased tonic $GABA_AR$-mediated inhibition is observed in the long-term following an ischaemic event and blocking this inhibitory tone has been shown to promote and facilitate neuronal rehabilitation (Clarkson *et al*., 2010). Conversely, it could be speculated that modification of GABAergic tone, could augment excitotoxicity and thus, be detrimental for neuroprotection, as evidenced by many studies that have detailed the relative failure of targeting $GABA_A$ receptors after stroke (Cheng *et al*., 2004; Clarkson 2012). Data demonstrated that modulation of the chloride transport by antagonism of NKCC1 following PTS was neuroprotective and prevented neuronal loss up to five days after the insult. Therefore, it would have been interesting to analyse the precise onset and duration of expression changes in NKCC1 and KCC2 reversal in a longer time-frame, where the neurorehabilitation phase of stroke begins. It would also be useful to determine more precisely the cycling of CCCs at the cell membranes, as just expression may not fully demonstrate the particular role of these transporters. Especially as KCC2 has been shown to rapidly cycle to and from the cell surface (Kahle *et al*., 2013). Furthermore, using NKCC1 agonists and KCC2 antagonists (separately and in combination) in a long-term study, would provide an opportunity to analyse the potential of CCC modulators in of promotion neurorehabilitation in the penumbra following ischaemic stroke. A long-term study was outwith the parameters of the current study.

6.4.3 Translating findings into mechanistic and functional studies

Modulating NKCC1 activity with bumetanide has proven to be a successful strategy to reduce neuronal loss in the penumbra in the first five days following PTS in mice (Chapter 5). Future work should aim at discerning the precise mechanism behind this protection. An obvious future direction would be to confirm if changes in the expression of CCCs translate into changes in neuronal $[Cl^-]_i$. As the electroneutrality of CCC transport does not easily allow direct measurement of their activity, indirect measurement methods of chloride movement have been developed (Ludwig *et al*., 2017). Genetically engineered chloride sensors such as Clomeleon, encode fluorophores sensitive to $[Cl^-]_i$ and allow visualisation of chloride movement in and out of cells elicited by activation of CCCs and $GABA_AR$ (Kuner and Augustine 2000). Clomeleon vectors could be transfected into cell lines such as PC12 or NT2 (Friedel *et al*., 2013) and transgenic mice expressing Clomeleon are available (Berglund *et al*., 2006). Using such transfected cells exposured to *in vitro* hypoxic insults (Chapter 3) or organotypic brain slice cultures submitted to oxygen and glucose deprivation (Pond 2006) would demonstrate if the reversal in expression observed in this study following acute hypoxia and PTS corresponds to a change in neuronal $[Cl^-]_i$. Furthermore, electrophysiological measurements would further detail if changes in $[Cl^-]$i affect $GABA_AR$-mediated post-synaptic activity. These experiments would discern whether treatment with CCC modulators can effectively modify $[Cl^-]_i$ and alter $GABA_AR$ polarity as a strategy to counteract excitotoxicity and promote neuroprotection in the salvageable penumbra in the days following ischaemic stroke.

References

Abeysinghe HCS, Bokhari L, Dusting GJ and Roulston CL (2014) Brain Remodelling following Endothelin-1 Induced Stroke in Conscious Rats. *PLoS ONE* 9(5): e97007.

Adragna NC, Ravilla NB, Lauf PK, Begum G, Khanna AR, Sun D and Kahle KT (2015) Regulated phosphorylation of the K-Cl cotransporter KCC3 is a molecular switch of intracellular potassium content and cell volume homeostasis. *Frontiers in Cellular Neuroscience* 9: 255.

Agulla J, Brea D, Campos F, Sobrino T, Argibay B, Al-Soufi W, Blanco M, Castillo J and Ramos-Cabrer P (2014) In vivo theranostics at the peri-infarct region in cerebral ischemia. *Theranostics* 4(1): 90–105.

Akbik F, Hirsch JA, Cougo-Pinto PT, Chandra R V., Simonsen CZ and Leslie-Mazwi T (2016) The Evolution of Mechanical Thrombectomy for Acute Stroke. *Current Treatment Options in Cardiovascular Medicine* 18(5): 32.

Albers GW, Goldstein LB, Hall D and Lesko LM (2001) Aptiganel hydrochloride in acute ischemic stroke: a randomized controlled trial. *JAMA* 286(21): 2673–82.

Alessi DR, Zhang J, Khanna A, Hochdörfer T, Shang Y and Kahle KT (2014) The WNK-SPAK/OSR1 pathway: master regulator of cation-chloride cotransporters. *Science Signaling* 7(334): re3.

An WG, Neckers LM, Kanekal M, Simon MC, Maltepe E and Blagosklonny M V. (1998) Stabilization of wild-type p53 by hypoxia-inducible factor 1α. *Nature* 392(6674): 405–408.

Anderson MA, Burda JE, Ren Y, Ao Y, O'Shea TM, Kawaguchi R, Coppola G, Khakh BS, Deming TJ and Sofroniew M V (2016) Astrocyte scar formation aids central nervous system axon regeneration. *Nature* 0(1): 1–20.

Andrews PW (1984) Retinoic acid induces neuronal differentiation of a cloned human embryonal carcinoma cell line in vitro. *Developmental Biology* 103(2): 285–293.

Angelica MD and Fong Y (2008) Expression of α5 integrin rescues fibronectin responsiveness in NT2N CNS neuronal cells. *Journal of Neuroscience Research* 141(4): 520–529.

Annunziato L, Boscia F and Pignataro G (2013) Ionic transporter activity in astrocytes, microglia, and oligodendrocytes during brain ischemia. *Journal of Cerebral Blood Flow and Metabolism* 33(7): 969–82.

Anuncibay-Soto B, Pérez-Rodríguez D, Llorente IL, Regueiro-Purriños M, Gonzalo-Orden JM and Fernández-López A (2014) Age-dependent modifications in vascular adhesion molecules and apoptosis after 48-h

reperfusion in a rat global cerebral ischemia model. *Age* 36(5): 9703.

Aoi T, Yae K, Nakagawa M, Ichisaka T, Okita K, Takahashi K, Chiba T and Yamanaka S (2008) Generation of Pluripotent Stem Cells from Adult Mouse Liver and Stomach Cells. *Science* 321(5889): 699–702.

Appelros P, Stegmayr B and Terent A (2009) Sex differences in stroke epidemiology: A systematic review. *Stroke* 40(4): 1082–1090.

Arion D and Lewis DA (2011) Altered expression of regulators of the cortical chloride transporters NKCC1 and KCC2 in schizophrenia. *Archives of General Psychiatry*. 68(1): 21–31.

Arvidsson A, Collin T, Kirik D, Kokaia Z and Lindvall O (2002) Neuronal replacement from endogenous precursors in the adult brain after stroke. *Nature Medicine* 8(9): 963–970.

Astrup J, Siesjö BK and Symon L (1981) Thresholds in cerebral ischemia - the ischemic penumbra. *Stroke* 12(6): 723–725.

Atack JR, Bayley PJ, Seabrook GR, Wafford KA, McKernan RM and Dawson GR (2006) L-655,708 enhances cognition in rats but is not proconvulsant at a dose selective for α5-containing GABAA receptors. *Neuropharmacology* 51(6): 1023–1029.

Austin TM and Delpire E (2011) Inhibition of KCC2 in mouse spinal cord neurons leads to hypersensitivity to thermal stimulation. *Anesthesia and Analgesia* 113(6): 1509–1515.

Back T, Ginsberg MD, Dietrich WD and Watson BD (1996) Induction of Spreading Depression in the Ischemic Hemisphere Following Experimental Middle Cerebral Artery Occlusion: Effect on Infarct Morphology. *Journal of Cerebral Blood Flow and Metabolism* 16(2): 202–213.

Badan I, Buchhold B, Hamm A, Gratz M, Walker LC, Platt D and Kessler C (2003) Accelerated Glial Reactivity to Stroke in Aged Rats Correlates With Reduced Functional Recovery. *Journal of Cerebral Blood Flow and Metabolism* 23 (7): 845–854.

Baranova O, Miranda LF, Pichiule P, Dragatsis I, Johnson RS and Chavez JC (2007) Neuron-specific inactivation of the hypoxia inducible factor 1 alpha increases brain injury in a mouse model of transient focal cerebral ischemia. *Journal of Neurosciences* 27(23): 6320–6332.

Barhwal K, Hota SK, Jain V, Prasad D, Singh SB and Ilavazhagan G (2009) Acetyl-l-carnitine (ALCAR) prevents hypobaric hypoxia-induced spatial memory impairment through extracellular related kinase-mediated nuclear factor erythroid 2-related factor 2 phosphorylation. *Neuroscience* 161(2): 501–514.

Baron JC (1996) Clinical use of positron emission tomography in cerebrovascular diseases. *Neurosurgery Clinics of Norh America.* 7(4): 653–664.

Baron JC, Yamauchi H, Fujioka M and Endres M (2014) Selective neuronal loss in ischemic stroke and cerebrovascular disease. *Journal of Cerebral Blood Flow and Metabolism* 34(1): 2–18

Barreto GE, Sun X, Xu L, Giffard RG, Pekny M, Nilsson M, Buffo A, Rite I, Tripathi P, Lepier A, Colak D, Sofroniew M, Sofroniew M, Vinters H, Cavanagh J, Latov N, Nilaver G, Zimmerman E, Johnson W, Silverman A, Ludwin S, Reier P, Janeczko K, Janeczko K, Schiffer D, Giordana M, Cavalla P, Vigliani M, Attanasio A, Schiffer D, Giordana M, Migheli A, Giaccone G, Pezzotta S, Fernaud-Espinosa I, Nieto-Sampedro M, Bovolenta P, Hajos F, Gerics B, Turai E, Hatten M, Liem R, Shelanski M, Mason C, Lindsay R, Ridet J, Malhotra S, Privat A, Gage F, Vaughn J, Pease D, Norenberg M, Liu Y, Namba T, Liu J, Suzuki R, Shioda S, Petito C, Morgello S, Felix J, Lesser M, Cahoy J, Emery B, Kaushal A, Foo L, Zamanian J, Gong S, Zheng C, Doughty M, Losos K, Didkovsky N, Han R, Ouyang Y, Xu L, Agrawal R, Patterson A, Dingman A, Lee S, Derugin N, Wendland M, Vexler Z, Alonso G, Myer D, Gurkoff G, Lee S, Hovda D, Sofroniew M, Popa-Wagner A, Badan I, Walker L, Groppa S, Patrana N, Dziewulska D, Burns K, Murphy B, Danzer S, Kuan C, Dihne M, Block F, Korr H, Topper R, Bushong E, Martone M, Jones Y, Ellisman M, Ogata K, Kosaka T, Halassa M, Fellin T, Takano H, Dong J, Haydon P, Broughton B, Reutens D and Sobey C (2011) Astrocyte Proliferation Following Stroke in the Mouse Depends on Distance from the Infarct. *PLoS ONE* 6(11): e27881.

Barteczek P, Li L, Ernst A-S, Böhler L-I, Marti HH and Kunze R (2017) Neuronal HIF-1α and HIF-2α deficiency improves neuronal survival and sensorimotor function in the early acute phase after ischemic stroke. *Journal of Cerebral Blood Flow and Metabolism* 37 (1): 291-306

Baxter PS, Bell KFS, Hasel P, Kaindl AM, Fricker M, Thomson D, Cregan SP, Gillingwater TH and Hardingham GE (2015) Synaptic NMDA receptor activity is coupled to the transcriptional control of the glutathione system. *Nature Communications* 6: 6761.

Beck J, Lenart B, Kintner DB and Sun D (2003) Na-K-Cl cotransporter contributes to glutamate-mediated excitotoxicity. *The Journal of Neuroscience* 23(12): 5061–5068.

Befani C, Mylonis I, Gkotinakou IM, Georgoulias P, Hu CJ, Simos G and Liakos P (2013) Cobalt stimulates HIF-1-dependent but inhibits HIF-2-dependent gene expression in liver cancer cells. *International Journal of Biochemistry and Cell Biology* 45(11): 2359–2368.

Begum G, Yuan H, Kahle KT, Li L, Wang S, Shi Y, Shmukler BE, Yang S Sen, Lin SH, Alper SL and Sun D (2015a) Inhibition of WNK3 Kinase Signaling Reduces Brain Damage and Accelerates Neurological Recovery

after Stroke. *Stroke* 46(7): 1956–1965.

Ben-Ari Y (2001) Developing networks play a similar melody. *Trends in Neurosciences*, 24(6): 353–360.

Ben-Ari Y (2002) Excitatory actions of gaba during development: the nature of the nurture. *Nature Reveiws Neuroscience* 3(9): 728–739.

Ben-Ari Y, Gaiarsa J, Tyzio R and Khazipov R (2007) GABA: a pioneer transmitter that excites immature neurons and generates primitive oscillations. *Physiological Reviews* 87(4): 1215–84.

Ben-Ari Y (2014) The GABA excitatory/inhibitory developmental sequence: A personal journey. *Neuroscience* 279: 187–219.

Ben-Ari Y, Damier P and Lemonnier E (2016) Failure of the Nemo Trial: Bumetanide Is a Promising Agent to Treat Many Brain Disorders but Not Newborn Seizures. *Frontiers in Cellular Neuroscience* 10: 90.

Benarroch EE (2013) Neocortical interneurons: Functional diversity and clinical correlations. *Neurology* 81(3): 273–280.

Bergeron M, Yu AY, Solway KE, Semenza GL and Sharp FR (1999) Induction of hypoxia-inducible factor-1 (HIF-1) and its target genes following focal ischaemia in rat brain. *The European Journal of Neuroscience* 11(12): 4159–4170.

Berglund K, Schleich W, Krieger P, Loo LS, Wang D, Cant NB, Feng G, Augustine GJ and Kuner T (2006) Imaging synaptic inhibition in transgenic mice expressing the chloride indicator, Clomeleon. *Brain Cell Biology* 35(4–6): 207–28.

Berra E, Roux D, Richard DE and Pouysségur J (2001) Hypoxia-inducible factor-1 alpha (HIF-1 alpha) escapes O(2)-driven proteasomal degradation irrespective of its subcellular localization: nucleus or cytoplasm. *EMBO Reports* 2(7): 615–620.

Besancon E, Guo S, Lok J, Tymianski M and Lo EH (2008) Beyond NMDA and AMPA glutamate receptors: emerging mechanisms for ionic imbalance and cell death in stroke. *Trends in Pharmacological Sciences* 29(5): 268–275.

Betz AL (1996) Alterations in cerebral endothelial cell function in ischemia. *Advances in Neurology* 71: 301–303.

Bierbower SM, Choveau FS, Lechleiter JD and Shapiro MS (2015) Augmentation of M-Type (KCNQ) Potassium Channels as a Novel Strategy to Reduce Stroke-Induced Brain Injury. *Journal of Neuroscience* 35(5): 2101–2111.

Blackman CF, Benane SG, House DE and Pollock MM (1993) Action of 50 Hz magnetic fields on neurite outgrowth in pheochromocytoma cells. *Bioelectromagnetics* 14(3): 273–86.

Blaesse P, Airaksinen MS, Rivera C and Kaila K (2009) Cation-Chloride Cotransporters and Neuronal Function. *Neuron* 61(6): 820–838.

Blaesse P and Schmidt T (2015) K-Cl cotransporter KCC2—a moonlighting protein in excitatory and inhibitory synapse development and function. *Pflugers Archiv European Journal of Physiology* 615–624.

Bliss TVP and L0mo T (1973) Long-lasting potentiation of synaptic transmission in the dentate area of the anaesthetized rabbit following stimulation of the perforant path. *Journal of Physiology* 232: 331–356.

Boccia ML, Petrusz P, Suzuki K, Marson L and Pedersen CA (2013) Immunohistochemical localization of oxytocin receptors in human brain. *Neuroscience* 253: 155–164.

Boettger T, Hübner CA, Maier H, Rust MB, Beck FX and Jentsch TJ (2002) Deafness and renal tubular acidosis in mice lacking the K-Cl co-transporter Kcc4. *Nature* 416(6883): 874–878.

Bonislawski DP, Schwarzbach EP and Cohen AS (2007) Brain injury impairs dentate gyrus inhibitory efficacy. *Neurobiology of Disease* 25(1): 163–169.

Bossenmeyer C, Chihab R, Muller S, Schroeder H and Daval J-L (1998) Hypoxiarreoxygenation induces apoptosis through biphasic induction of protein synthesis in cultured rat brain neurons. *Brain Research* 787: 107–116.

Bossenmeyer-Pourié C, Chihab R, Schroeder H and Daval JL (1999) Transient hypoxia may lead to neuronal proliferation in the developing mammalian brain: From apoptosis to cell cycle completion. *Neuroscience* 91(1): 221–231.

Boycott HE, Wilkinson JA, Boyle JP, Pearson HA and Peers C (2008) Differential involvement of TNFα in hypoxic suppression of astrocyte glutamate transporters. *Glia* 56(9): 998–1004.

Boyer LA, Lee TI, Cole MF, Johnstone SE, Levine SS, Zucker JP, Guenther MG, Kumar RM, Murray HL, Jenner RG, Gifford DK, Melton DA, Jaenisch R and Young RA (2005) Core Transcriptional Regulatory Circuitry in Human Embryonic Stem Cells. *Cell* 122(6): 947–956.

Brandt C, Nozadze M, Heuchert N, Rattka M and Loscher W (2010) Disease-Modifying Effects of Phenobarbital and the NKCC1 Inhibitor Bumetanide in the Pilocarpine Model of Temporal Lobe Epilepsy. *Journal of Neuroscience* 30(25): 8602–8612.

Brassai A, Suvanjeiev RG, B??n EG and Lakatos M (2015) Role of synaptic and nonsynaptic glutamate receptors in ischaemia induced neurotoxicity. *Brain Research Bulletin* 112: 1–6.

Brea D, Agulla J, Staes A, Gevaert K, Campos F, Sobrino T, Blanco M, Dávalos A, Castillo J, Ramos-Cabrer P, Murray CJ, Hossmann KA, Traystman RJ, Gomis M, Dávalos A, Dyken ML, Hachinski V, Lo EH, Ramos-Cabrer P, Campos F, Sobrino T, Castillo J, Hata R, Maeda K, Hermann D, Mies G, Hossmann KA, Ramos-Cejudo J, Rami A, Hill WD, Kokubo Y, Sanz O, Estrada A, Ferrer I, Planas A, Dhodda VK, Sailor KA, Bowen KK, Vemuganti R, Chen A, Liao WP, Lu Q, Wong WS, Wong PT, Datta A, Mariucci G, Tantucci M, Giuditta A, Ambrosini M V., Lee YJ, Corry PM, Ren C, Datta A, Ait-Belkacem R, Gevaert K, Vandekerckhove J, Gevaert K, Gilany K, Pardue S, Wang S, Miller MM, Morrison-Bogorad M, Datta A, Cristobal J De, Bederson JB, Agulla J, Brea D, Shevchenko A, Wilm M, Vorm O, Mann M and Gevaert K (2015) Study of Protein Expresion in Peri-Infarct Tissue after Cerebral Ischemia. *Scientific Reports* 5: 12030.

Brillault J, Lam TI, Rutkowsky JM, Foroutan S and O'Donnell ME (2008) Hypoxia effects on cell volume and ion uptake of cerebral microvascular endothelial cells. *AJP: Cell Physiology* 294(1): C88–C96.

Broughton BRS, Reutens DC and Sobey CG (2009) Apoptotic mechanisms after cerebral ischemia. *Stroke* 40(5): 331-339.

Brown CE, Wong C and Murphy TH (2008) Rapid morphologic plasticity of peri-infarct dendritic spines after focal ischemic stroke. *Stroke* 39(4): 1286–1291.

Brown CE, Aminoltejari K, Erb H, Winship IR and Murphy TH (2009) In Vivo Voltage-Sensitive Dye Imaging in Adult Mice Reveals That Somatosensory Maps Lost to Stroke Are Replaced over Weeks by New Structural and Functional Circuits with Prolonged Modes of Activation within Both the Peri-Infarct Zone and Distant Sites. *Journal of Neuroscience* 29(6): 1719–1734.

Brown IR (2007) Heat shock proteins and protection of the nervous system. *Annals of the New York Academy of Sciences* 1113:147–158.

Caldeira M V., Salazar IL, Curcio M, Canzoniero LMT and Duarte CB (2014) Role of the ubiquitin-proteasome system in brain ischemia: Friend or foe? *Progress in Neurobiology* 112: 50–69.

Calderone A, Jover T, Noh K, Tanaka H, Yokota H, Lin Y, Grooms SY, Regis R, Bennett MVL and Zukin RS (2003) Ischemic insults derepress the gene silencer REST in neurons destined to die. *The Journal of Neuroscience* 23(6): 2112–21.

Campen KA, Clark ZL, Olds MA, McNatty KP and Pitman JL (2016) The in-vitro effects of cAMP and cGMP modulators on inter-cellular dye transfer and gene expression levels in rat cumulus cell – oocyte complexes. *Molecular*

and Cellular Endocrinology 420: 46–56.

Cappelletti G, Galbiati M, Ronchi C, Maggioni MG, Onesto E and Poletti A (2007) Neuritin (cpg15) enhances the differentiating effect of NGF on neuronal PC12 cells. *Journal of Neuroscience Research* 2702–2713.

Carlén M, Meletis K, Göritz C, Darsalia V, Evergren E, Tanigaki K, Amendola M, Barnabé-Heider F, Yeung MSY, Naldini L, Honjo T, Kokaia Z, Shupliakov O, Cassidy RM, Lindvall O and Frisén J (2009) Forebrain ependymal cells are Notch-dependent and generate neuroblasts and astrocytes after stroke. *Nature Neuroscience* 12(3): 259–267.

Carmichael ST (2005) Rodent models of focal stroke: size, mechanism, and purpose. *NeuroRx : the journal of the American Society for Experimental NeuroTherapeutics* 2(3): 396–409.

Carmichael ST (2016a) Emergent properties of neural repair: Elemental biology to therapeutic concepts. *Annals of Neurology* 79(6): 895–906.

Carmichael ST (2016b) The 3 Rs of Stroke Biology: Radial, Relayed, and Regenerative. *Neurotherapeutics* 13(2): 348-359.

Carmichael ST, Kathirvelu B, Schweppe CA and Nie EH (2017) Molecular, cellular and functional events in axonal sprouting after stroke. *Experimental Neurology* 287(3): 384:394

Carreau A, El Hafny-Rahbi B, Matejuk A, Grillon C and Kieda C (2011) Why is the partial oxygen pressure of human tissues a crucial parameter? Small molecules and hypoxia. *Journal of Cellular and Molecular Medicine* 15(6): 1239–1253.

Casals JB, Pieri NCG, Feitosa MLT, Ercolin ACM, Roballo KCS, Barreto RSN, Bressan FF, Martins DS, Miglino MA and Ambrósio CE (2011) The use of animal models for stroke research: a review. *Comparative medicine* 61(4): 305–313.

Cavadas MAS, Mesnieres M, Crifo B, Manresa MC, Selfridge AC, Scholz CC, Cummins EP, Cheong A and Taylor CT (2015) REST mediates resolution of HIF-dependent gene expression in prolonged hypoxia. *Scientific Reports* 5: 17851.

Cavadas MAS, Cheong A and Taylor CT (2017) The regulation of transcriptional repression in hypoxia. *Experimental Cell Research*. 4827(17): 30076-30079

Chamboredon S, Ciais D, Desroches-Castan A, Savi P, Bono F, Feige J-J and Cherradi N (2011) Hypoxia-inducible factor-1{alpha} mRNA: a new target for destabilization by tristetraprolin in endothelial cells. *Molecular Biology of the Cell* 22(18): 3366–3378.

Chang JC, Shook LL, Biag J, Nguyen EN, Toga AW, Charles AC and Brennan KC (2010) Biphasic direct current shift, haemoglobin desaturation and neurovascular uncoupling in cortical spreading depression. *Brain* 133(4): 996–1012.

Chavez JC, Baranova O, Lin J and Pichiule P (2006) The transcriptional activator hypoxia inducible factor 2 (HIF-2/EPAS-1) regulates the oxygen-dependent expression of erythropoietin in cortical astrocytes. *The Journal of Neuroscience* 26(37): 9471–81.

Chelluboina B, Klopfenstein JD, Gujrati M, Rao JS and Veeravalli KK (2014) Temporal regulation of apoptotic and anti-apoptotic molecules after middle cerebral artery occlusion followed by reperfusion. *Molecular Neurobiology* 49(1): 50–65.

Chen C, Pore N, Behrooz A, Ismail-Beigi F and Maity A (2001) Regulation of glut1 mRNA by Hypoxia-inducible Factor-1: interaction between H-ras and hypoxia. *Journal of Biological Chemistry* 276(12): 9519–9525.

Chen H, Luo J, Kintner DB, Shull GE and Sun D (2005) Na(+)-dependent chloride transporter (NKCC1)-null mice exhibit less gray and white matter damage after focal cerebral ischemia. *Journal of Cerebral Blood Flow and Metabolism* 25(1): 54–66.

Chen H and Sun D (2005) The role of Na–K–Cl co–transporter in cerebral ischemia. *Neurological Research* 27(3): 280–286.

Chen M, Wang J, Jiang J, Zheng X and Justice NJ (2017) APP modulates KCC2 expression and function in hippocampal GABAergic inhibition. *eLife* 6: e20142

Chen Y, Vartiainen NE, Ying W, Chan PH, Koistinaho J and Swanson RA (2001) Astrocytes protect neurons from nitric oxide toxicity by a glutathione-dependent mechanism. *Journal of Neurochemistry* 77(6): 1601–1610.

Cheng YD, Al-Khoury L and Zivin JA (2004) Neuroprotection for ischemic stroke: two decades of success and failure. *NeuroRx : the journal of the American Society for Experimental NeuroTherapeutics* 1(1): 36–45.

Chiu BY, Chang CP, Lin JW, Yu JS, Liu WP, Hsu YC and Lin MT (2014) Beneficial effect of astragalosides on stroke condition using PC12 cells under oxygen glucose deprivation and reperfusion. *Cellular and Molecular Neurobiology* 34(6): 825–837.

Clarkson AN and Carmichael ST (2009) Cortical excitability and post-stroke recovery. *Biochemical Society Transactions* 37(Pt 6): 1412–1414.

Clarkson AN, Huang BS, Macisaac SE, Mody I and Carmichael ST (2010) Reducing excessive GABA-mediated tonic inhibition promotes functional recovery after stroke. *Nature* 468(7321): 305–309.

Clarkson AN, Overman JJ, Zhong S, Mueller R, Lynch G and Carmichael ST (2011) AMPA Receptor-Induced Local Brain-Derived Neurotrophic Factor Signaling Mediates Motor Recovery after Stroke. *Journal of Neuroscience* 31(10): 3766–3775.

Clarkson AN (2012) Perisynaptic GABA receptors the overzealous protector. *Advances in Pharmacological Sciences*. 1–8.

Clarkson AN, Parker K, Nilsson M, Walker FR and Gowing EK (2015) Combined ampakine and BDNF treatments enhance poststroke functional recovery in aged mice via AKT-CREB signaling. *Journal of Cerebral Blood Flow and Metabolism* 35(2): 1–8.

Cleary RT, Sun H, Huynh T, Manning SM, Li Y, Rotenberg A, Talos DM, Kahle KT, Jackson M, Rakhade SN, Berry G, Jensen FE, Ronen G, Buckley D, Penney S, Streiner D, Sankar R, Painter M, Scher M, Alvin J, Gaus L, Minnigh B, Painter M, Glykys J, Dzhala V, Kuchibhotla K, Feng G, Kuner T, Silverstein F, Jensen F, Rakhade S, Jensen F, Kahle K, Staley K, Blaesse P, Airaksinen M, Rivera C, Kaila K, Ari Y Ben, Sipila S, Huttu K, Yamada J, Afzalov R, Voipio J, Russell J, Galanopoulou A, Nunez J, McCarthy M, Rakhade S, Klein P, Huynh T, Hilario-Gomez C, Kosaras B, Dzhala V, Brumback A, Staley K, Dzhala V, Talos D, Sdrulla D, Brumback A, Mathews G, Ibla J, Khoury J, Kong T, Robinson A, Colgan S, Sullivan J, Witte M, Yamashita T, Myers C, Blumer J, Lopez-Samblas A, Adams J, Goldberg R, Modi M, Jensen F, Applegate C, Holtzman D, Belin T, Burchfiel J, Li Y, Cleary R, Kellogg M, Soul J, Berry G, Bittigau P, Sifringer M, Genz K, Reith E, Pospischil D, Ives J, Ikonomidou C, Bosch F, Miksa M, Bittigau P, Vockler J, Talos D, Fishman R, Park H, Folkerth R, Follett P, Jensen F, Wang C, Stafstrom C, Liu Z, Geary C, Rakhade S, Zhou C, Aujla P, Fishman R, Sucher N, Talos D, Sun H, Kosaras B, Joseph A, Folkerth R, Brandt C, Nozadze M, Heuchert N, Rattka M, Loscher W, Olney J, Painter M, Scher M, Stein A, Armatti S, Wang Z, Silverstein F, Jensen F, Inder T, Hellstrom-Westas L, Hirtz D, Cha B, Silveira D, Liu X, Hu Y, Holmes G, Koh S, Jensen F, Rossetti F, Rodrigues M, Oliveira J de, Garcia-Cairasco N, Mazarati A, Shin D, Sankar R, Raol Y, Lapides D, Keating J, Brooks-Kayal A, Cooper E, Talos D, Sun H, Zhou X, Fitzgerald E, Jackson M, Liu Y, Shangguan Y, Barks J, Silverstein F, Lemonnier E, Ben-Ari Y, Rivera C, Voipio J, Kaila K, Sipila S, Schuchmann S, Voipio J, Yamada J, Kaila K, Dzhala V, Kuchibhotla K, Glykys J, Kahle K, Swiercz W, Bragin D, Sanderson J, Peterson S, Connor J, Muller W, Flemmer A, Gimenez I, Dowd B, Darman R, Forbush B, Sullivan J, Witte M, Yamashita T, Myers C, Blumer J, Kim J, Kondratyev A, Tomita Y, Gale K, Glier C, Dzietko M, Bittigau P, Jarosz B and Korobowicz E (2013) Bumetanide Enhances Phenobarbital Efficacy in a Rat Model of Hypoxic Neonatal Seizures. *PLoS ONE*. 8(3): e57148.

Collinson N, Kuenzi FM, Jarolimek W, Maubach KA, Cothliff R, Sur C, Smith A, Otu FM, Howell O, Atack JR, McKernan RM, Seabrook GR, Dawson GR, Whiting PJ and Rosahl TW (2002) Enhanced learning and memory and altered GABAergic synaptic transmission in mice lacking the alpha 5 subunit

of the GABAA receptor. *The Journal of Neuroscience* 22(13): 5572–5580.

Connell BJ, Di Iorio P, Sayeed I, Ballerini P, Saleh MC, Giuliani P, Saleh TM, Rathbone MP, Su C and Jiang S (2013) Guanosine protects against reperfusion injury in rat brains after ischemic stroke. *Journal of Neuroscience Research* 91(2): 262–272.

Cook DJ, Teves L and Tymianski M (2012) Treatment of stroke with a PSD-95 inhibitor in the gyrencephalic primate brain - with comments. *Nature* 483(7388): 213–217.

Covello KL, Kehler J, Yu H, Gordan JD, Arsham AM, Hu CJ, Labosky PA, Simon MC and Keith B (2006) HIF-2?? regulates Oct-4: Effects of hypoxia on stem cell function, embryonic development, and tumor growth. *Genes and Development* 20(5): 557–570.

Cregg JM, DePaul MA, Filous AR, Lang BT, Tran A and Silver J (2014) Functional regeneration beyond the glial scar. *Experimental Neurology* 253: 197–207.

Dalen ML, Frøyland E, Saugstad OD, Mollnes TE and Rootwelt T (2009) Post-hypoxic hypothermia is protective in human NT2-N neurons regardless of oxygen concentration during reoxygenation. *Brain Research* 1259: 80–89.

Dales J, Beaufils N, Silvy M, Picard C, Pauly V, Pradel V, Formisano-Treziny C, Bonnier P, Giusiano S, Charpin C and Gabert J (2010) Hypoxia inducible factor 1alpha gene (HIF-1alpha) splice variants: potential prognostic biomarkers in breast cancer. *BMC Medicine* 8(1): 44–55.

Darbinian N (2013) Cultured Cell Line Models of Neuronal Differentiation: NT2, PC12. *Methods in Molecular Biology* 1078: 23-33.

Das KP, Freudenrich TM and Mundy WR (2004) Assessment of PC12 cell differentiation and neurite growth: a comparison of morphological and neurochemical measures. *Neurotoxicology and Teratology* 26(3): 397–406.

Datta PK, Bonner JF, Haas CJ and Fischer I (2013) Neuronal Cell Culture. *Neuronal Cell Culture: Methods and Protocols* 1078: 35–44.

Davis SM, Lees KR, Albers GW, Diener HC, Markabi S, Karlsson G and Norris J (2000) Selfotel in acute ischemic stroke : possible neurotoxic effects of an NMDA antagonist. *Stroke* 31(2): 347–354.

Dawson GR, Maubach KA, Collinson N, Cobain M, Everitt BJ, MacLeod AM, Choudhury HI, McDonald LM, Pillai G, Rycroft W, Smith AJ, Sternfeld F, Tattersall FD, Wafford KA, Reynolds DS, Seabrook GR and Atack JR (2006) An inverse agonist selective for alpha5 subunit-containing GABAA receptors enhances cognition. *The Journal of Pharmacology and Experimental Therapeutics* 316(3): 1335–1345.

DeGracia DJ and Hu BR (2007b) Irreversible Translation Arrest in the Reperfused Brain. *Journal of Cerebral Blood Flow and Metabolism* 27(5): 875–893.

Deisseroth K, Singla S, Toda H, Monje M, Palmer TD and Malenka RC (2004) Excitation-neurogenesis coupling in adult neural stem/progenitor cells. *Neuron* 42(4): 535–52.

Delpire E (2000) Cation-Chloride Cotransporters in Neuronal Communication. *News in Physiological Sciences* 15(6): 309-312.

Delpire E, Baranczak A, Waterson AG, Kim K, Kett N, Morrison RD, Scott Daniels J, David Weaver C and Lindsley CW (2012) Further optimization of the K-Cl cotransporter KCC2 antagonist ML077: Development of a highly selective and more potent in vitro probe. *Bioorganic and Medicinal Chemistry Letters* 22(14): 4532–4535.

Deng Y-H, He H-Y, Yang L-Q and Zhang P-Y (2016) Dynamic changes in neuronal autophagy and apoptosis in the ischemic penumbra following permanent ischemic stroke. *Neural Regeneration Research* 11(7): 1108–1114.

Ding J and Delpire E (2014) Deletion of KCC3 in parvalbumin neurons leads to locomotor deficit in a conditional mouse model of peripheral neuropathy associated with agenesis of the corpus callosum. *Behavioural Brain Research* 274: 128–136.

Dirnagl U and Endres M (2014) Found in Translation. *Stroke* 45(5).

Dobkin BH (2004) Strategies for stroke rehabilitation. *The Lancet Neurology* 3(9): 528–536.

Dobkin BH (2008) Training and exercise to drive poststroke recovery. *Nature Clinical Practice Neurology* 4(2): 76–85.

Doeppner TR, Nagel F, Dietz GP, Weise J, Tonges L, Schwarting S and Bahr M (2009) TAT-Hsp70-mediated neuroprotection and increased survival of neuronal precursor cells after focal cerebral ischemia in mice. *Journal of Cerebral Blood Flow and Metabolism* 29(6): 1187–1196.

Doeppner TR, Kaltwasser B, Fengyan J, Hermann DM and Bähr M (2013) TAT-Hsp70 induces neuroprotection against stroke via anti-inflammatory actions providing appropriate cellular microenvironment for transplantation of neural precursor cells. *Journal of Cerebral Blood Flow and Metabolism* 33(10): 1778–1788.

Doetsch F (2003) The glial identity of neural stem cells. *Nature Neuroscience* 6(11): 1127–1134.

Dohmen C, Sakowitz OW, Fabricius M, Bosche B, Reithmeier T, Ernestus

RI, Brinker G, Dreier JP, Woitzik J, Strong AJ and Graf R (2008) Spreading depolarizations occur in human ischemic stroke with high incidence. *Annals of Neurology* 63(6): 720–728.

Dowd B and Forbush B (2003) Pask (proline-alanine-rich STE20-related kinase), a regulatory kinase of the Na-K-Cl cotransporter (NKCC1). *Journal of Biological Chemistry* 278(30): 27347–27353.

Dreier JP (2011) The role of spreading depression, spreading depolarization and spreading ischemia in neurological disease. *Nature Medicine* 17(4): 439–447.

Dreier JP and Reiffurth C (2015) The Stroke-Migraine Depolarization Continuum. *Neuron* 86(4): 902–922.

Duan C (2016) Hypoxia-inducible factor 3 biology: complexities and emerging themes. *American Journal of Physiology. Cell Physiology* 310(4): C260-9.

Dzhala VI, Kuchibhotla K V., Glykys JC, Kahle KT, Swiercz WB, Feng G, Kuner T, Augustine GJ, Bacskai BJ and Staley KJ (2010) Progressive NKCC1-dependent neuronal chloride accumulation during neonatal seizures. *The Journal of Neuroscience* 30(35): 11745–61.

Dzhala VI, Talos DM, Sdrulla DA, Brumback AC, Mathews GC, Benke TA, Delpire E, Jensen FE and Staley KJ (2005) NKCC1 transporter facilitates seizures in the developing brain. *Nature medicine* 11(11): 1205–13.
Egorov A V. and Draguhn A (2013) Development of coherent neuronal activity patterns in mammalian cortical networks: Common principles and local hetereogeneity. *Mechanisms of Development* 130(6–8): 412–423.

Ehrenreich H, Weissenborn K, Prange H, Schneider D, Weimar C, Wartenberg K, Schellinger PD, Bohn M, Becker H, Wegrzyn M, Jahnig P, Herrmann M, Knauth M, Bahr M, Heide W, Wagner A, Schwab S, Reichmann H, Schwendemann G, Dengler R, Kastrup A, Bartels C and EPO Stroke Trial Group (2009) Recombinant Human Erythropoietin in the Treatment of Acute Ischemic Stroke. *Stroke* 40(12): e647–e656.

Einheber S, Zanazzi G, Ching W, Scherer S, Milner TA, Peles E and Salzer JL (1997) The Axonal Membrane Protein Caspr, a Homologue of Neurexin IV, Is a Component of the Septate-like Paranodal Junctions That Assemble during Myelination. *The Journal of Cell Biology* 139(6): 1495–1506.

Erker T, Brandt C, Töllner K, Schreppel P, Twele F, Schidlitzki A and Löscher W (2016) The bumetanide prodrug BUM5, but not bumetanide, potentiates the antiseizure effect of phenobarbital in adult epileptic mice. *Epilepsia* 57(5):698-705.

European Agency for the Evaluation of Medicinal Products (2002). Summary information on a referral opinion following an arbitration pursuant to Article

29 of Directive 2001/83/EC, for Actilyse International Non-Proprietary Name (INN): Alteplase: Background information and Annex I. Available at : http://www.ema.europa.eu/docs/en_GB/document_library/Referrals_document/Actilyse_29/WC500010327.pdf. [Accessed: November 2016].

Faiz M, Sachewsky N, Gascó S, Bang KWA, Morshead CM and Nagy A (2015) Adult Neural Stem Cells from the Subventricular Zone Give Rise to Reactive Astrocytes in the Cortex after Stroke Cell Stem Cell Adult Neural Stem Cells from the Subventricular Zone Give Rise to Reactive Astrocytes in the Cortex after Stroke. *Cell Stem Cell* 17: 624–634.

Fan W, Dai Y, Xu H, Zhu X, Cai P, Wang L, Sun C, Hu C, Zheng P and Zhao BQ (2014) Caspase-3 modulates regenerative response after stroke. *Stem Cells* 32(2): 473–486.

Ferrer I and Planas AM (2003) Signaling of cell death and cell survival following focal cerebral ischemia: life and death struggle in the penumbra. *Journal of Neuropathology and Experimental Neurology* 62(4): 329–39.

Feuerstein D, Manning A, Hashemi P, Bhatia R, Fabricius M, Tolias C, Pahl C, Ervine M, Strong AJ and Boutelle MG (2010a) Dynamic metabolic response to multiple spreading depolarizations in patients with acute brain injury: an online microdialysis study. *Journal of Cerebral Blood Flow and Metabolism* 30(7): 1343–55.

Fields R and Lancaster M (1993) Dual-attribute continuous monitoring of cell proliferation/cytotoxicity. *American Biotechnology Laboratory* 11(4): 48–50.
Fields RD, Woo DH and Basser PJ (2015) Glial Regulation of the Neuronal Connectome through Local and Long-Distant Communication. *Neuron* 86(2): 374–386.

Fiumelli H, Briner A, Puskarjov M, Blaesse P, Belem BJ, Dayer AG, Kaila K, Martin J-L and Vutskits L (2013) An ion transport-independent role for the cation-chloride cotransporter KCC2 in dendritic spinogenesis in vivo. *Cerebral Cortex* 23(2): 378–88.

Fluri F, Schuhmann MK and Kleinschnitz C (2015) Animal models of ischemic stroke and their application in clinical research. *Drug Design, Development and Therapy* 9: 3445–54.

Foley LM, Hitchens TK, Barbe B, Zhang F, Ho C, Rao GR and Nemoto EM (2010) Quantitative Temporal Profiles of Penumbra and Infarction During Permanent Middle Cerebral Artery Occlusion in Rats. *Translational Stroke Research* 1(3): 220–229.

Forristal CE, Wright KL, Hanley NA, Oreffo ROC and Houghton FD (2010) Hypoxia inducible factors regulate pluripotency and proliferation in human embryonic stem cells cultured at reduced oxygen tensions. *Reproduction* 139(1): 85–97.

Frendl A and Csiba L (2011) Pharmacological and non-pharmacological recanalization strategies in acute ischemic stroke. *Frontiers in Neurology* 2: 1–11.

Friedel P, Bregestovski P and Medina I (2013) Improved method for efficient imaging of intracellular Cl(-) with Cl-Sensor using conventional fluorescence setup. *Frontiers in Molecular Neuroscience* 6: 7.

FRONTIER trial. Field Randomization of NA-1 Therapy in Early Responders (2014). Available at: https://clinicaltrials.gov/ct2/show/NCT02315443. [Accessed: December 2016].

Frøyland E, Skjæret C, Wright MS, Dalen ML, Cvancarova M, Kasi C and Rootwelt T (2008) Inflammatory receptors and pathways in human NT2-N neurons during hypoxia and reoxygenation. Impact of acidosis. *Brain Research* 1217: 37–49.

Fugate JE and Rabinstein AA (2015) Absolute and Relative Contraindications to IV rt-PA for Acute Ischemic Stroke. *The Neurohospitalist* 5(3): 110–121.

Gagnon KB and Delpire E (2010) Multiple pathways for protein phosphatase 1 (PP1) regulation of Na-K-2Cl cotransporter (NKCC1) function: The N-terminal tail of the Na-K-2Cl cotransporter serves as a regulatory scaffold for Ste20-related proline/alanine-rich kinase (SPAK) and PP1. *Journal of Biological Chemistry* 285(19): 14115–14121.

Gagnon KB and Delpire E (2013) Physiology of SLC12 transporters: lessons from inherited human genetic mutations and genetically engineered mouse knockouts. *American Journal of Physiology. Cell Physiology* 304(8): C693-714.

Gagnon M, Bergeron MJ, Lavertu G, Castonguay A, Tripathy S, Bonin RP, Perez-Sanchez J, Boudreau D, Wang B, Dumas L, Valade I, Bachand K, Jacob-Wagner M, Tardif C, Kianicka I, Isenring P, Attardo G, Coull JAM and De Koninck Y (2013) Chloride extrusion enhancers as novel therapeutics for neurological diseases. *Nature Medicine* 19(11): 1524–8.

Galbán S and Gorospe M (2009) Factors interacting with HIF-1α mRNA: novel therapeutic targets. *Current Pharmaceutical Design* 15(33): 3853–3860.

Gao L, Lyons AR and Greenfield LJ (2004) Hypoxia alters GABAA receptor function and subunit expression in NT2-N neurons. *Neuropharmacology* 46(3): 318–330.

Gehrmann J, Bonnekoh P, Miyazawa T, Hossmann K a and Kreutzberg GW (1992) Immunocytochemical study of an early microglial activation in ischemia. *Journal of Cerebral Blood Flow and Metabolism* 12(2): 257–69.

Gerelsaikhan T and Turner RJ (2000) Membrane topology and function of the secretory Na+-K+-2Cl- cotransporter (NKCC1). *Journal of Korean Medical Science*.Supplement: S3-4

Giaccia A, Siim BG and Johnson RS (2003) HIF-1 as a target for drug development. *Nature Reviews Drug Discovery* 2(10): 803–811.

Giffard RG, Han R-Q, Emery JF, Duan M and Pittet JF (2008) Regulation of apoptotic and inflammatory cell signaling in cerebral ischemia: the complex roles of heat shock protein 70. *Anesthesiology* 109(2): 339–48.

Glykys J and Mody I (2007) Activation of GABAA Receptors: Views from Outside the Synaptic Cleft. *Neuron* 56(5): 763–770.

Go AS, Mozaffarian D, Roger VL, Benjamin EJ, Berry JD, Blaha MJ, Dai S, Ford ES, Fox CS, Franco S, Fullerton HJ, Gillespie C, Hailpern SM, Heit JA, Howard VJ, Huffman MD, Judd SE, Kissela BM, Kittner SJ, Lackland DT, Lichtman JH, Lisabeth LD, Mackey RH, Magid DJ, Marcus GM, Marelli A, Matchar DB, McGuire DK, Mohler ER, Moy CS, Mussolino ME, Neumar RW, Nichol G, Pandey DK, Paynter NP, Reeves MJ, Sorlie PD, Stein J, Towfighi A, Turan TN, Virani SS, Wong ND, Woo D and Turner MB (2014) *Heart Disease and Stroke Statistics - 2014 Update: A report from the American Heart Association*. *Circulation* 129(3): e28-e292

Goldberg M, Dunning S and Bunn H (1988) Regulation of the erythropoietin gene: evidence that the oxygen sensor is a heme protein. *Science* 242(4884): 1412–1415.

Gonzalez-Perez A, Gaist D, Wallander M-A, McFeat G and Garcia-Rodriguez LA (2013) Mortality after hemorrhagic stroke: data from general practice (The Health Improvement Network). *Neurology* 81(6): 559–565.

Gould E (2007) How widespread is adult neurogenesis in mammals? *Nature Reviews Neuroscience* 8(6): 481–488.

Goyal M, Demchuk AM, Menon BK, Eesa M, Rempel JL, Thornton J, Roy D, Jovin TG, Willinsky RA, Sapkota BL, Dowlatshahi D, Frei DF, Kamal NR, Montanera WJ, Poppe AY, Ryckborst KJ, Silver FL, Shuaib A, Tampieri D, Williams D, Bang OY, Baxter BW, Burns PA, Choe H, Heo J-H, Holmstedt CA, Jankowitz B, Kelly M, Linares G, Mandzia JL, Shankar J, Sohn S-I, Swartz RH, Barber PA, Coutts SB, Smith EE, Morrish WF, Weill A, Subramaniam S, Mitha AP, Wong JH, Lowerison MW, Sajobi TT and Hill MD (2015) Randomized Assessment of Rapid Endovascular Treatment of Ischemic Stroke. *New England Journal of Medicine* 372(11): 1019–1030.

Grau CM and Greene LA (2012) Use of PC12 cells and rat superior cervical ganglion sympathetic neurons as models for neuroprotective assays relevant to parkinson's disease. *Methods in Molecular Biology* 846: 201–211.

Green AR, Hainsworth AH and Jackson DM (2000) GABA potentiation: a logical pharmacological approach for the treatment of acute ischaemic

stroke. *Neuropharmacology* 39(9): 1483–94.

Green AR and Shuaib A (2006) Therapeutic strategies for the treatment of stroke. *Drug Discovery Today* 11(15–16): 681–693.

Greene LA, Tischlert AS and Kuffler SW (1976) Establishment of a noradrenergic clonal line of rat adrenal pheochromocytoma cells which respond to nerve growth factor. *Cell Biology* 73(7): 2424–2428.

Grupke S, Hall J, Dobbs M, Bix GJ and Fraser JF (2015) Understanding history, and not repeating it. Neuroprotection for acute ischemic stroke: From review to preview. *Clinical Neurology and Neurosurgery*. 129: 1–9.

Guillemain I (2000) Human NT2 Neurons Express a Large Variety of Neurotransmission Phenotypes In Vitro. *The Journal of Comparative Neurology* 395: 380–395.

Guo K, Searfoss G, Krolikowski D, Pagnoni M, Franks C, Clark K, Yu KT, Jaye M and Ivashchenko Y (2001) Hypoxia induces the expression of the pro-apoptotic gene BNIP3. *Cell Death and Differentiation* 8(4): 367–376.

Gursoy-Ozdemir Y, Qiu J, Matsuoka N, Bolay H, Bermpohl D, Jin H, Wang X, Rosenberg GA, Lo EH and Moskowitz MA (2004) Cortical spreading depression activates and upregulates MMP-9. *Journal of Clinical Investigation* 113(10): 1447–1455.

Haas M (1994) The Na-K-Cl cotransporters. *The American Journal of Physiology* 267(4 Pt 1): C869-85.

Haase VH (2013) Regulation of erythropoiesis by hypoxia-inducible factors. *Blood Reviews* 27(1): 41–53.

Haile Y, Fu W, Shi B, Westaway D, Baker G, Jhamandas J and Giuliani F (2014) Characterization of the NT2-derived neuronal and astrocytic cell lines as alternative in vitro models for primary human neurons and astrocytes. *Journal of Neuroscience Research* 92(9): 1187–1198.

Hakim AM (1998) Ischemic penumbra: the therapeutic window. *Neurology* 51(3 Suppl 3): S44-6.

Hamidi S and Avoli M (2015) KCC2 function modulates in vitro ictogenesis. *Neurobiology of Disease*. 79: 51–58.

Han D, Lerner AG, Walle L Vande, Upton J-P, Xu W, Hagen A, Backes BJ, Oakes SA and Papa FR (2009) IRE1α Kinase Activation Modes Control Alternate Endoribonuclease Outputs to Determine Divergent Cell Fates. *Cell* 138(3): 562-575.

Hankey GJ (2006) Potential new risk factors for ischemic stroke: What is their potential? *Stroke* 37: 2181–2188.

Hardingham GE and Bading H (2010) Synaptic versus extrasynaptic NMDA receptor signalling: implications for neurodegenerative disorders. *Nature Reviews Neuroscience* 11(10): 682–96.

Hartings JA, Rolli ML, Lu X-CM and Tortella FC (2003) Delayed secondary phase of peri-infarct depolarizations after focal cerebral ischemia: relation to infarct growth and neuroprotection. *The Journal of Neuroscience* 23(37): 11602–11610.

Hartmann A-M and Nothwang HG (2014) Molecular and evolutionary insights into the structural organization of cation chloride cotransporters. *Frontiers in Cellular Neuroscience* 8: 470.

Harvey AJ, Kind KL and Thompson JG (2007) Regulation of gene expression in bovine blastocysts in response to oxygen and the iron chelator desferrioxamine. *Biology of Reproduction* 77(1): 93–101.

Hata R, Maeda K, Hermann D, Mies G and Hossmann K-A (2000) Evolution of Brain Infarction After Transient Focal Cerebral Ischemia in Mice. *Journal of Cerebral Blood Flow and Metabolism* 20(6): 937–946.

Haupt C, Witte OW and Frahm C (2007) Up-regulation of Connexin43 in the glial scar following photothrombotic ischemic injury. *Molecular and Cellular Neuroscience* 35(1): 89–99.

Hebert SC, Mount DB and Gamba G (2004) Molecular physiology of cation-coupled Cl- cotransport: The SLC12 family. *Pflugers Archiv European Journal of Physiology* 447(5): 580–593.

Heikkil M, Pasanen A, Kivirikko KI and Myllyharju J (2011) Roles of the human hypoxia-inducible factor (HIF)-3α variants in the hypoxia response. *Cellular and Molecular Life Sciences* 68(23): 3885–3901.

Heiss WD (2010) The concept of the penumbra: Can it be translated to stroke management? *International Journal of Stroke* 5(4): 290–295.

Helton R, Cui J, Scheel JR, Ellison JA, Ames C, Gibson C, Blouw B, Ouyang L, Dragatsis I, Zeitlin S, Johnson RS, Lipton SA and Barlow C (2005) Brain-specific knock-out of hypoxia-inducible factor-1alpha reduces rather than increases hypoxic-ischemic damage. *The Journal of neuroscience* 25(16): 4099–4107.

Hill EJ, Jiménez-González C, Tarczyluk M, Nagel DA, Coleman MD and Parri HR (2012) NT2 derived neuronal and astrocytic network signalling. *PLoS ONE* 7(5): 1–10.

Hill MD, Martin RH, Mikulis D, Wong JH, Silver FL, terBrugge KG, Milot G, Clark WM, MacDonald RL, Kelly ME, Boulton M, Fleetwood I, McDougall C, Gunnarsson T, Chow M, Lum C, Dodd R, Poublanc J, Krings T, Demchuk AM, Goyal M, Anderson R, Bishop J, Garman D and Tymianski M (2012)

Safety and efficacy of NA-1 in patients with iatrogenic stroke after endovascular aneurysm repair (ENACT): A phase 2, randomised, double-blind, placebo-controlled trial. *The Lancet Neurology* 11(11): 942–950.

Hinman JD, Rasband MN and Carmichael ST (2013) Remodeling of the axon initial segment after focal cortical and white matter stroke. *Stroke* 44(1): 182–189.

Hinzman JM, DiNapoli VA, Mahoney EJ, Gerhardt GA and Hartings JA (2015) Spreading depolarizations mediate excitotoxicity in the development of acute cortical lesions. *Experimental Neurology* 267: 243–253.

Hirsch D, Steiner J and Dawson T (1993) Neurotransmitter release regulated by nitric oxide in PC-12 cells and brain synaptosomes. *Current Biology* 3(11): 749–754.

Hiu T, Farzampour Z, Paz JT, Wang EHJ, Badgely C, Olson A, Micheva KD, Wang G, Lemmens R, Tran K V., Nishiyama Y, Liang X, Hamilton SA, O'Rourke N, Smith SJ, Huguenard JR, Bliss TM and Steinberg GK (2016) Enhanced phasic GABA inhibition during the repair phase of stroke: A novel therapeutic target. *Brain* 139(2): 468–480.

Hoehn BD, Palmer TD and Steinberg GK (2005) Neurogenesis in rats after focal cerebral ischemia is enhanced by indomethacin. *Stroke* 36(12): 2718–2724.

Holloway PM and Gavins FNE (2016) Modeling Ischemic Stroke in Vitro: Status Quo and Future Perspectives. *Stroke* 47(2): 561–569.

Holmes M, Davis S and Simpson E (2015a) Alteplase for the Treatment of Acute Ischaemic Stroke: A NICE Single Technology Appraisal; an Evidence Review Group Perspective. *PharmacoEconomics* 33(3): 225–233.

Holmquist-Mengelbier L, Fredlund E, Löfstedt T, Noguera R, Navarro S, Nilsson H, Pietras A, Vallon-Christersson J, Borg A, Gradin K, Poellinger L and Påhlman S (2006) Recruitment of HIF-1alpha and HIF-2alpha to common target genes is differentially regulated in neuroblastoma: HIF-2alpha promotes an aggressive phenotype. *Cancer Cell* 10(5): 413–23.

Hota KB, Hota SK, Srivastava RB and Singh SB (2012) Neuroglobin regulates hypoxic response of neuronal cells through Hif-1α- and Nrf2-mediated mechanism. *Journal of Cerebral Blood Flow and Metabolism* 32(6): 1046–60.

Huang L, Wu ZB, ZhuGe Q, Zheng W, Shao B, Wang B, Sun F and Jin K (2014) Glial scar formation occurs in the human brain after ischemic stroke. *International Journal of Medical Sciences* 11(4): 344–348.

Huberfeld G, Wittner L, Clemenceau S, Baulac M, Kaila K, Miles R and Rivera C (2007) Perturbed chloride homeostasis and GABAergic signaling in

human temporal lobe epilepsy. *The Journal of Neuroscience* 27(37): 9866–9873.

Hübner CA, Stein V, Hermans-Borgmeyer I, Meyer T, Ballanyi K and Jentsch TJ (2001) Disruption of KCC2 reveals an essential role of K-Cl cotransport already in early synaptic inhibition. *Neuron* 30(2): 515–24.

Hui AS, Bauer AL, Striet JB, Schnell PO and Czyzyk-Krzeska MF (2006) Calcium signaling stimulates translation of HIF-alpha during hypoxia. *The FASEB Journal* 20(3): 466–75.

Hyde TM, Lipska BK, Ali T, Mathew S V, Law AJ, Metitiri OE, Straub RE, Ye T, Colantuoni C, Herman MM, Bigelow LB, Weinberger DR and Kleinman JE (2011) Expression of GABA Signaling Molecules KCC2, NKCC1, and GAD1 in Cortical Development and Schizophrenia. *Journal of Neuroscience* 31(30): 11088–11095.

Iadecola C and Anrather J (2011) The immunology of stroke: from mechanisms to translation. *Nature Medicine* 17(7): 796–808.

Ibla J, Khoury J, Kong T, Robinson A and Colgan S (2006) Transcriptional repression of Na-K-2Cl cotransporter NKCC1 by hypoxia-inducible factor-1. *American Journal of Physiology. Cell Physiology* 291(2): 9.

Instrum R and Sun HS (2013) Restoring neuroprotection through a new preclinical paradigm: translational success for NA-1 in stroke therapy. *Acta Pharmacol Sin* 34(1): 3–5.

Ito U, Nagasao J, Kawakami E and Oyanagi K (2007) Fate of Disseminated Dead Neurons in the Cortical Ischemic Penumbra. *Stroke* 38(9): 2577-2583

Iwai M, Cao G, Yin W, Stetler RA, Liu J and Chen J (2007) Erythropoietin promotes neuronal replacement through revascularization and neurogenesis after neonatal hypoxia/ischemia in rats. *Stroke* 38(10): 2795–2803.

Jaenisch N, Witte OW and Frahm C (2010) Downregulation of potassium chloride cotransporter KCC2 after transient focal cerebral ischemia. *Stroke* 41(3).

Jaenisch N, Liebmann L, Guenther M, Hübner CA, Frahm C and Witte OW (2016) Reduced tonic inhibition after stroke promotes motor performance and epileptic seizures. *Scientific Reports* 6: 26173.

Jantzie LL, Hu MY, Park H-K, Jackson MC, Yu J, Maxwell JR and Jensen FE (2015) Chloride cotransporter NKCC1 inhibitor bumetanide protects against white matter injury in a rodent model of periventricular leukomalacia. *Pediatric Research* 77(4): 554–62.

Jeon C-Y, Jin J-K, Koh Y-H, Chun W, Choi I-G, Kown H-J, Kim Y-S and Park J-B (2010) Neurites from PC12 cells are connected to each other by

synapse-like structures. *Synapse* 64(10): 765-772.

Jeromel M, Milosevic Z V., Kocijancic IJ, Lovric D, Svigelj V and Zvan B (2013) Mechanical revascularization for acute ischemic stroke: A single-center, retrospective analysis. *Cardiovascular and Interventional Radiology* 36(2): 338–345.

Jochmanov I, Yang C, Zhuang Z and Pacak K (2013) Hypoxia-inducible factor signaling in pheochromocytoma: Turning the rudder in the right direction. *Journal of the National Cancer Institute* 105(17): 1270–1283.

Jögi A, Øra I, Nilsson H, Lindeheim A, Makino Y, Poellinger L, Axelson H and Påhlman S (2002) Hypoxia alters gene expression in human neuroblastoma cells toward an immature and neural crest-like phenotype. *Proceedings of the National Academy of Sciences of the United States of America* 99(10): 7021–6.

Juin P, Pelletier M, Oliver L, Tremblais K, Grégoire M, Meflah K and Vallette FM (1998) Induction of a caspase-3-like activity by calcium in normal cytosolic extracts triggers nuclear apoptosis in a cell-free system. *The Journal of Biological Chemistry* 273(28): 17559–64.

Kaelin WG and Ratcliffe PJ (2008) Oxygen Sensing by Metazoans: The Central Role of the HIF Hydroxylase Pathway. *Molecular Cell* 30(4): 393–402.

Kahle KT, Rinehart J, de Los Heros P, Louvi A, Meade P, Vazquez N, Hebert SC, Gamba G, Gimenez I and Lifton RP (2005) WNK3 modulates transport of Cl- in and out of cells: implications for control of cell volume and neuronal excitability. *Proceedings of the National Academy of Sciences of the United States of America* 102(46): 16783–16788.

Kahle KT, Ring AM and Lifton RP (2008) Molecular Physiology of the WNK Kinases. *Annual Review of Physiology* 70(1): 329–355.

Kahle KT and Staley KJ (2008) The bumetanide-sensitive Na-K-2Cl cotransporter NKCC1 as a potential target of a novel mechanism-based treatment strategy for neonatal seizures. *Neurosurgical Focus* 25(3): E22.

Kahle KT, Staley KJ, Nahed B V, Gamba G, Hebert SC, Lifton RP and Mount DB (2008) Roles of the cation-chloride cotransporters in neurological disease. *Nature clinical practice. Neurology* 4(9): 490–503.

Kahle KT, Simard JM, Staley KJ, Nahed B V., Jones PS and Sun D (2009) Molecular Mechanisms of Ischemic Cerebral Edema: Role of Electroneutral Ion Transport. *Physiology* 24(4): 257–265.

Kahle KT, Rinehart J and Lifton RP (2010) Phosphoregulation of the Na-K-2Cl and K-Cl cotransporters by the WNK kinases. *Biochimica et Biophysica Acta*. Howard Hughes Medical Institute 1802(12): 1150–1158.

Kahle KT, Deeb TZ, Puskarjov M, Silayeva L, Liang B, Kaila K and Moss SJ (2013) Modulation of neuronal activity by phosphorylation of the K-Cl cotransporter KCC2. *Trends in Neurosciences* 36(12): 726–737.

Kahle KT, Khanna AR, Alper SL, Adragna NC, Lauf PK, Sun D and Delpire E (2015) K-Cl cotransporters, cell volume homeostasis, and neurological disease. *Trends in Molecular Medicine* 21(8): 513–523.

Kaila K (1994) Ionic basis of GABAA receptor channel function in the nervous system. *Progress in Neurobiology* 42(4): 489–537.

Kaila K, Price TJ, Payne JA, Puskarjov M and Voipio J (2014) Cation-chloride cotransporters in neuronal development, plasticity and disease. *Nature Reviews. Neuroscience* 15(10): 637–654.

Kalogeris T, Baines CP, Krenz M and Korthuis RJ (2012) Cell biology of ischemia/reperfusion injury. *International Review of Cell and Molecular Biology* 298: 229–317.

Kaluz S, Kaluzová M, Liao SY, Lerman M and Stanbridge EJ (2009b) Transcriptional control of the tumor- and hypoxia-marker carbonic anhydrase 9: A one transcription factor (HIF-1) show? *Biochimica et Biophysica Acta - Reviews on Cancer* 1795(2): 162–172.

Karlócai MR, Wittner L, Tóth K, Maglóczky Z, Katarova Z, Rásonyi G, Erőss L, Czirják S, Halász P, Szabó G, Payne JA, Kaila K and Freund TF (2016) Enhanced expression of potassium-chloride cotransporter KCC2 in human temporal lobe epilepsy. *Brain Structure and Function* 221(7): 3601–3615.

Ke Q and Costa M (2006) Hypoxia-Inducible Factor-1 (HIF-1). *Molecular Pharmacology* 70(5): 1469–1480.

Keith B, Johnson RS and Simon MC (2012) HIF1α and HIF2α: sibling rivalry in hypoxic tumour growth and progression. *Nature reviews Cancer* 12(1): 9–22.

Kelley MR, Deeb TZ, Brandon NJ, Dunlop J, Davies PA and Moss SJ (2016) Compromising KCC2 transporter activity enhances the development of continuous seizure activity. *Neuropharmacology* 108: 103–110.

Keysar SB and Jimeno A (2010) More than markers: biological significance of cancer stem cell-defining molecules. *Molecular Cancer Therapeutics* 9(9): 2450–2457.

Khanna A, Kahle KT, Walcott BP, Gerzanich V and Simard JM (2014) Disruption of Ion Homeostasis in the Neurogliovascular Unit Underlies the Pathogenesis of Ischemic Cerebral Edema. *Translational Stroke Research* 5(1): 3–16.

Kidwell CS (2013) MRI biomarkers in acute ischemic stroke: a conceptual

framework and historical analysis. *Stroke* 44(2): 570–578.

Kim GW, Sugawara T and Chan PH (2000) Involvement of oxidative stress and caspase-3 in cortical infarction after photothrombotic ischemia in mice. *Journal of Cerebral Blood Flow and Metabolism* 20(12): 1690–1701.

Kim JB, Sebastiano V, Wu G, Araúzo-Bravo MJ, Sasse P, Gentile L, Ko K, Ruau D, Ehrich M, van den Boom D, Meyer J, Hübner K, Bernemann C, Ortmeier C, Zenke M, Fleischmann BK, Zaehres H and Schöler HR (2009) Oct4-Induced Pluripotency in Adult Neural Stem Cells. *Cell* 136(3): 411–419.

Kim JW, Tchernyshyov I, Semenza GL and Dang C V. (2006) HIF-1-mediated expression of pyruvate dehydrogenase kinase: A metabolic switch required for cellular adaptation to hypoxia. *Cell Metabolism* 3(3): 177–185.

Kitagawa T, Tsuruhara Y, Hayashi M, Endo T and Stanbridge EJ (1995) A tumor-associated glycosylation change in the glucose transporter GLUT1 controlled by tumor suppressor function in human cell hybrids. *Journal of Cell Science* 3735–43.

Kluver, H., and Barrera E (1953) A method for the combined staining of cells and fibers in the Nervous system. *Journal of Neuropathology and Experimental Neurology* 12(4): 400–403.

Koh MY, Spivak-Kroizman TR and Powis G (2008) HIF-1 regulation: not so easy come, easy go. *Trends in Biochemical Sciences* 33(11): 526–534.

Koh MY and Powis G (2012) Passing the baton: The HIF switch. *Trends in Biochemical Sciences* 37(9): 364–372.

Kokubo Y, Liu J, Rajdev S, Kayama T, Sharp FR and Weinstein PR (2003) Differential cerebral protein synthesis and heat shock protein 70 expression in the core and penumbra of rat brain after transient focal ischemia. *Neurosurgery* 53(1): 186-190.

Kole AJ, Annis RP and Deshmukh M (2013) Mature neurons: equipped for survival. *Cell Death and Disease* 4(6): e689.

Kondziolka D, Steinberg GK, Wechsler L, Meltzer CC, Elder E, Gebel J, Decesare S, Jovin T, Zafonte R, Lebowitz J, Flickinger JC, Tong D, Marks MP, Jamieson C, Luu D, Bell-Stephens T and Teraoka J (2005) Neurotransplantation for patients with subcortical motor stroke: a phase 2 randomized trial. *Journal of Neurosurgery* 103(1): 38–45.

Konopacka A, Qiu J, Yao ST, Greenwood MP, Greenwood M, Lancaster T, Inoue W, Mecawi A de S, Vechiato FM V, de Lima JBM, Coletti R, Hoe SZ, Martin A, Lee J, Joseph M, Hindmarch C, Paton J, Antunes-Rodrigues J, Bains J and Murphy D (2015) Osmoregulation requires brain expression of the renal Na-K-2Cl cotransporter NKCC2. *The Journal of Neuroscience* 35(13): 5144–55.

Koumenis C (2006) 'Translating' Tumor Hypoxia: Unfolded Protein Response (UPR)-Dependent and UPR-Independent Pathways. *Molecular Cancer Research* 4(7): 423–436.

Kovalevich J and Langford D (2013) Considerations for the use of SH-SY5Y neuroblastoma cells in neurobiology. *Methods in Molecular Biology* 1078: 9–21.

Krakauer J (2006) Motor learning: its relevance to stroke recovery and neurorehabilitation. *Current Opinion in Neurology* 19(1): 84-90.

Krutsay M (1970) [Nissl staining with cresyl violet]. *Zeitschrift für medizinische Labortechnik* 11(2): 75–6.

Krzyżanowska W, Pomierny B, Filip M and Pera J (2014) Glutamate transporters in brain ischemia: to modulate or not? *Acta Pharmacologica Sinica* 35(4): 444–462.

Kumar GK, Overholt JL, Bright GR, Hui KY, Lu H, Gratzl M and Prabhakar NR (1998) Release of dopamine and norepinephrine by hypoxia from PC-12 cells. *The American Journal of Physiology* 274(6 Pt 1): C1592-600.

Kuner T and Augustine GJ (2000) A genetically encoded ratiometric indicator for chloride: capturing chloride transients in cultured hippocampal neurons. *Neuron* 27(3): 447–459.

De La Rosa X, Santalucía T, Fortin PY, Purroy J, Calvo M, Salas-Perdomo A, Justicia C, Couillaud F and Planas AM (2013) In vivo imaging of induction of heat-shock protein-70 gene expression with fluorescence reflectance imaging and intravital confocal microscopy following brain ischaemia in reporter mice. *European Journal of Nuclear Medicine and Molecular Imaging* 40(3): 426–438.

Labat-gest V and Tomasi S (2013) Photothrombotic ischemia: a minimally invasive and reproducible photochemical cortical lesion model for mouse stroke studies. *Journal of Visualized Experiments* (76).

Lahiani A, Zahavi E, Netzer N, Ofir R, Pinzur L, Raveh S, Arien-Zakay H, Yavin E and Lazarovici P (2015) Human PLacental eXpanded (PLX) mesenchymal-like adherent stromal cells confer neuroprotection to nerve growth factor (NGF)-differentiated PC12 cells exposed to ischemia by secretion of IL-6 and VEGF. *Biochimica et Biophysica Acta - Molecular Cell Research* 1853(2): 422–430.

Lalonde CC and Mielke JG (2014) Selective vulnerability of hippocampal sub-fields to oxygen–glucose deprivation is a function of animal age. *Brain Research* 1543: 271–279.

Lan A, Liao X, Mo L, Yang C, Yang Z, Wang X, Hu F, Chen P, Feng J, Zheng D and Xiao L (2011) Hydrogen sulfide protects against chemical hypoxia-

induced injury by inhibiting ROS-activated ERK1/2 and p38mapk signaling pathways in PC12 cells. *PLoS ONE* 6(10): e25921

Larkin MA, Blackshields G, Brown NP, Chenna R, Mcgettigan PA, McWilliam H, Valentin F, Wallace IM, Wilm A, Lopez R, Thompson JD, Gibson TJ and Higgins DG (2007) Clustal W and Clustal X version 2.0. *Bioinformatics* 23(21): 2947–2948.

Lau A and Tymianski M (2010) Glutamate receptors, neurotoxicity and neurodegeneration. *Pflugers Archiv European Journal of Physiology* 460(2): 525–542.

Lavertu G, Côté SL and De Koninck Y (2014) Enhancing K-Cl co-transport restores normal spinothalamic sensory coding in a neuropathic pain model. *Brain*. Oxford University Press 137(3): 724–738.

Le DA, Wu Y, Huang Z, Matsushita K, Plesnila N, Augustinack JC, Hyman BT, Yuan J, Kuida K, Flavell RA and Moskowitz MA (2002) Caspase activation and neuroprotection in caspase-3-deficient mice after in vivo cerebral ischemia and in vitro oxygen glucose deprivation. *Proceedings of the National Academy of Sciences of the United States of America*. 99(23): 15188–93.

Lee K-H, Ryu CJ, Hong HJ, Kim J and Lee EH (2005) cDNA Microarray Analysis of Nerve Growth Factor-Regulated Gene Expression Profile in Rat PC12 Cells. *Neurochemistry Research* 30(4):533-40 .

Leigh R, Knutsson L, Zhou J and van Zijl PC (2017) Imaging the physiological evolution of the ischemic penumbra in acute ischemic stroke. *Journal of Cerebral Blood Flow & Metabolism* 1:271678X17700913

Leiser Y, Silverstein N, Blumenfeld A, Shilo D, Haze A, Rosenfeld E, Shay B, Tabakman R, Lecht S, Lazarovici P and Deutsch D (2011) The induction of tuftelin expression in PC12 cell line during hypoxia and NGF-induced differentiation. *Journal of Cellular Physiology* 226(1): 165–172.

Lemonnier E, Degrez C, Phelep M, Tyzio R, Josse F, Grandgeorge M, Hadjikhani N and Ben-Ari Y (2012) A randomised controlled trial of bumetanide in the treatment of autism in children. *Translational Psychiatry* 2(12): e202.

Leonzino M, Busnelli M, Antonucci F, Verderio C, Mazzanti M and Chini B (2016) The Timing of the Excitatory-to-Inhibitory GABA Switch Is Regulated by the Oxytocin Receptor via KCC2. *Cell Reports* 15(1): 96–103.

Lewis RW, Mabry J, Polisar JG, Eagen KP, Ganem B and Hess GP (2010) Dihydropyrimidinone Positive Modulation of δ-Subunit-Containing γ-Aminobutyric Acid Type A Receptors, Including an Epilepsy-Linked Mutant Variant. *Biochemistry* 49(23): 4841–4851.

Li H, Khirug S, Cai C, Ludwig A, Blaesse P, Kolikova J, Afzalov R, Coleman SK, Lauri S, Airaksinen MS, Keinänen K, Khiroug L, Saarma M, Kaila K and Rivera C (2007) KCC2 Interacts with the Dendritic Cytoskeleton to Promote Spine Development. *Neuron* 56(6): 1019–1033.

Li H, Zhang N, Lin H-Y, Yu Y, Cai Q-Y, Ma L and Ding S (2014a) Histological, cellular and behavioral assessments of stroke outcomes after photothrombosis-induced ischemia in adult mice. *BMC Neuroscience* 15: 58.

Li L, Lundkvist A, Andersson D, Wilhelmsson U, Nagai N, Pardo AC, Nodin C, Stahlberg A, Aprico K, Larsson K, Yabe T, Moons L, Fotheringham A, Davies I, Carmeliet P, Schwartz JP, Pekna M, Kubista M, Blomstrand F, Maragakis N, Nilsson M and Pekny M (2008) Protective role of reactive astrocytes in brain ischemia. *Journal of Cerebral Blood Flow and Metabolism* 28(3): 468–481.

Li L, Saliba P, Reischl S, Marti HH and Kunze R (2016) Neuronal deficiency of HIF prolyl 4-hydroxylase 2 in mice improves ischemic stroke recovery in an HIF dependent manner. *Neurobiology of Disease* 91: 221–235.

Li QF, Wang XR, Yang YW and Lin H (2006) Hypoxia upregulates hypoxia inducible factor (HIF)-3alpha expression in lung epithelial cells: characterization and comparison with HIF-1alpha. *Cell Research* 16(6): 548–58.

Li R, Wang Y, Yang Z, He Y, Zhao T, Fan M, Wang X, Zhu L and Wang X (2015) Hypoxia-inducible factor-1α regulates the expression of L-type voltage-dependent Ca(2+) channels in PC12 cells under hypoxia. *Cell Stress & Chaperones* 20(3): 507–16.

Li W-L, Yu SP, Ogle ME, Ding XS and Wei L (2008) Enhanced neurogenesis and cell migration following focal ischemia and peripheral stimulation in mice. *Developmental Neurobiology* 68(13): 1474–1486.

Li Z, Bao S, Wu Q, Wang H, Eyler C, Sathornsumetee S, Shi Q, Cao Y, Lathia J, McLendon RE, Hjelmeland AB and Rich JN (2009) Hypoxia-Inducible Factors Regulate Tumorigenic Capacity of Glioma Stem Cells. *Cancer Cell* 15(6): 501–513.

Liddelow SA and Barres BA (2016) Regeneration: Not everything is scary about a glial scar. *Nature* 532(7598): 182–183.

Lin KC, Lin HJ, Chang CP and Lin MT (2015) Decreasing or increasing heat shock protein 72 exacerbates or attenuates heat-induced cell death, respectively, in rat hypothalamic cells. *FEBS Open Bio* 5: 724–730.

Lindvall O and Kokaia Z (2015) Neurogenesis following stroke affecting the adult brain. *Cold Spring Harbor Perspectives in Biology* 7(11): 1–20.

Lipton S (2006) Paradigm shift in neuroprotection by NMDA receptor

blockade: memantine and beyond. *Nature reviews. Drug Discovery* 5(2): 160–170.

Liu J and Wang L-N (2013) Gamma aminobutyric acid (GABA) receptor agonists for acute stroke. *The Cochrane Database of Systematic Reviews*. 2(2): CD009622.

Liu S, Levine SR and Winn HR (2010) Targeting ischemic penumbra: part I - from pathophysiology to therapeutic strategy. *Journal of Experimental Stroke & Translational Medicine*. 3(1): 47–55.

Liu Z, Xie J, Wu T, Truong T, Auchus RJ and Huang CL (2011) Downregulation of NCC and NKCC2 cotransporters by kidney-specific WNK1 revealed by gene disruption and transgenic mouse models. *Human Molecular Genetics* 20(5): 855–866.

Llorente IL, Burgin TC, Pérez-Rodríguez D, Martínez-Villayandre B, Pérez-García CC and Fernández-López A (2013) Unfolded protein response to global ischemia following 48 h of reperfusion in the rat brain: the effect of age and meloxicam. *Journal of Neurochemistry* 127(5): 701–710.

Longstreth WT, Katz R, Tirschwell DL, Cushman M and Psaty BM (2010) Intravenous tissue plasminogen activator and stroke in the elderly. *The American journal of emergency medicine* 28(3): 359–363.

Lopes FM, Schroder R, Junior MLC da F, Zanotto-Filho A, Miller CB, Pires AS, Meurer RT, Colpo GD, Gelain DP, Kapczinski F, Moreira JCF, Fernandes M da C and Klamt F (2010) Comparison between proliferative and neuron-like SH-SY5Y cells as an in vitro model for Parkinson disease studies. *Brain Research* 1337: 85–94.

de los Heros P, Kahle KT, Rinehart J, Bobadilla NA, V zquez N, San Cristobal P, Mount DB, Lifton RP, Hebert SC and Gamba G (2006) WNK3 bypasses the tonicity requirement for K-Cl cotransporter activation via a phosphatase-dependent pathway. *Proceedings of the National Academy of Sciences* 103(6): 1976–1981.

Löscher W, Puskarjov M and Kaila K (2013) Cation-chloride cotransporters NKCC1 and KCC2 as potential targets for novel antiepileptic and antiepileptogenic treatments. *Neuropharmacology*. 69: 62–74.

Lu K-T, Huang T-C, Wang J-Y, You Y-S, Chou J-L, Chan MWY, Wo PYY, Amstislavskaya TG, Tikhonova MA and Yang Y-L (2015) NKCC1 mediates traumatic brain injury-induced hippocampal neurogenesis through CREB phosphorylation and HIF-1α expression. *Pflügers Archiv - European Journal of Physiology* 467(8): 1651–1661.

Lu KT, Huang TC, Wang JY, You YS, Chou JL, Chan MWY, Wo PYY, Amstislavskaya TG, Tikhonova MA and Yang YL (2015) NKCC1 mediates traumatic brain injury-induced hippocampal neurogenesis through CREB

phosphorylation and HIF-1α expression. *Pflugers Archiv European Journal of Physiology* 467(8): 1651–1661.

Ludwig A, Uvarov P, Soni S, Thomas-Crusells J, Airaksinen MS and Rivera C (2011) Early growth response 4 mediates BDNF induction of potassium chloride cotransporter 2 transcription. *The Journal of neuroscience : the official journal of the Society for Neuroscience* 31(2): 644–649.

Lyden PD and Hedges B (1992) Protective effect of synaptic inhibition during cerebral ischemia in rats and rabbits. *Stroke* 23(10): 1463-9-70.

Lyden PD, Shuaib A, Ng K, Levin K, Atkinson RP, Rajput A, Wechsler L, Ashwood T, Claesson L, Odergren T and Salazar-Grueso E (2002) Clomethiazole acute stroke study in ischemic stroke (CLASS-I): Final results. *Stroke* 33(1): 122–128.

Lykke K, Tollner K, Feit PW, Erker T, MacAulay N and Loscher W (2016) The search for NKCC1-selective drugs for the treatment of epilepsy: Structure-function relationship of bumetanide and various bumetanide derivatives in inhibiting the human cation-chloride cotransporter NKCC1A. *Epilepsy Behaviour* 59: 42–49.

Ma J, Endres M and Moskowitz MA (1998) Synergistic effects of caspase inhibitors and MK-801 in brain injury after transient focal cerebral ischaemia in mice. *British Journal of Pharmacology* 124(4): 756–62.

MacRae I (2011) Preclinical stroke research - Advantages and disadvantages of the most common rodent models of focal ischaemia. *British Journal of Pharmacology* 164(4): 1062–1078.

Magistretti PJ and Allaman I (2015) A Cellular Perspective on Brain Energy Metabolism and Functional Imaging. *Neuron* 86(4): 883–901.

Majmundar AJ, Wong WJ and Simon MC (2010) Hypoxia-inducible factors and the response to hypoxic stress. *Molecular Cell* 40(2): 294–309.

Manabat C, Han BH, Wendland M, Derugin N, Fox CK, Choi J, Holtzman DM, Ferriero DM and Vexler ZS (2003) Reperfusion differentially induces caspase-3 activation in ischemic core and penumbra after stroke in immature brain. *Stroke* 34(1): 207–213.

Marangos PJ and Schmechel DE (1987) Neuron Specific Enolase, A Clinically Useful Marker for Neurons and Neuroendocrine Cells. *Annual Review of Neuroscience*. 10(1): 269–295.

Margaill I, Parmentier S, Callebert J, Allix M, Boulu RG and Plotkine M (1996) Short Therapeutic Window for MK-801 in Transient Focal Cerebral Ischemia in Normotensive Rats. *Journal of Cerebral Blood Flow & Metabolism* 16(1): 107–113.

Martín-Aragón Baudel MAS, Poole AV. and Darlison MG (2017) Chloride co-transporters as possible therapeutic targets for stroke. *Journal of Neurochemistry* 140(2): 195–209.

Maurer MH, Geomor HK, Bürgers HF, Schelshorn DW and Kuschinsky W (2006) Adult neural stem cells express glucose transporters GLUT1 and GLUT3 and regulate GLUT3 expression. *FEBS Letters* 580(18): 4430–4434.

Mayer MP and Bukau B (2005) Hsp70 chaperones: cellular functions and molecular mechanism. *Cellular and Molecular Life Sciences* 62(6): 670–84.

Maynard MA, Evans AJ, Hosomi T, Hara S, Jewett MAS and Ohh M (2005) Human HIF-3alpha4 is a dominant-negative regulator of HIF-1 and is down-regulated in renal cell carcinoma. *FASEB journal* 19(11): 1396–406.

McBean DE and Kelly PA (1998) Rodent models of global cerebral ischemia: a comparison of two-vessel occlusion and four-vessel occlusion. *General Pharmacology* 30(4): 431–4.

Mccarthy MM (2009) Estradiol and the developing brain. *Physiology* 88(1): 91–124.

McLaughlin B (2004) The kinder side of killer proteases: caspase activation contributes to neuroprotection and CNS remodeling. *Apoptosis : an International Journal on Programmed Cell Death*. 9(2): 111–21.

Mehta A, Prabhakar M, Kumar P, Deshmukh R and Sharma PL (2013) Excitotoxicity: Bridge to various triggers in neurodegenerative disorders. *European Journal of Pharmacology* 698(1–3): 6–18.

Menezes J and Luskin M (1994) Expression of neuron-specific tubulin defines a novel population in the proliferative layers of the developing telencephalon. *Journal of Neuroscience* 14(9): 5399-5416.

Ming G li and Song H (2011) Adult Neurogenesis in the Mammalian Brain: Significant Answers and Significant Questions. *Neuron* 70(4): 687–702.

Monyer H, Burnashev N, Laurie DJ, Sakmann B and Seeburg PH (1994) Developmental and regional expression in the rat brain and functional properties of four NMDA receptors. *Neuron* 12(3): 529–40.

Morita Y, Callicott JH, Testa LR, Mighdoll MI, Dickinson D, Chen Q, Tao R, Lipska BK, Kolachana B, Law AJ, Ye T, Straub RE, Weinberger DR, Kleinman JE and Hyde TM (2014) Characteristics of the cation cotransporter NKCC1 in human brain: alternate transcripts, expression in development, and potential relationships to brain function and schizophrenia. *The Journal of Neuroscience* 34(14): 4929–40.

Morris GF, Bullock R, Marshall SB, Marmarou A, Maas A and Marshall LF (1999) Failure of the competitive *N* -methyl- d -aspartate antagonist Selfotel

(CGS 19755) in the treatment of severe head injury: results of two Phase III clinical trials. *Journal of Neurosurgery* 91(5): 737–743.

Mosmann T (1983) Rapid colorimetric assay for cellular growth and survival: application to proliferation and cytotoxicity assays. *Journal of Immunological Methods* 65(1–2): 55–63.

Mozaffarian D, Benjamin EJ, Go AS, Arnett DK, Blaha MJ, Cushman M, Das SR, Ferranti S De, Després JP, Fullerton HJ, Howard VJ, Huffman MD, Isasi CR, Jiménez MC, Judd SE, Kissela BM, Lichtman JH, Lisabeth LD, Liu S, MacKey RH, Magid DJ, McGuire DK, Mohler ER, Moy CS, Muntner P, Mussolino ME, Nasir K, Neumar RW, Nichol G, Palaniappan L, Pandey DK, Reeves MJ, Rodriguez CJ, Rosamond W, Sorlie PD, Stein J, Towfighi A, Turan TN, Virani SS, Woo D, Yeh RW and Turner MB (2016) Heart disease and stroke statistics-2016 update a report from the American Heart Association. *Circulation*, e38–e48.

Muir KW, Buchan A, von Kummer R, Rother J and Baron J-C (2006) Imaging of acute stroke. *The Lancet Neurology* 5(9): 755–768.

Mullen RJ, Buck CR and Smith AM (1992) NeuN, a neuronal specific nuclear protein in vertebrates. *Development* 116(1): 201–211.

Naeve GS, Ramakrishnan M, Kramer R, Hevroni D, Citri Y and Theill LE (1997) Neuritin: a gene induced by neural activity and neurotrophins that promotes neuritogenesis. *Proceedings of the National Academy of Sciences of the United States of America* 94(6): 2648–2653.

Nagao H, Nakajima KI, Niisato N, Hirota R, Bando H, Sakaguchi H, Hisa Y and Marunaka Y (2012) K-Cl-cotransporter 1 (KCC1) negatively regulates NGF-induced neurite outgrowth in PC12 cells. *Cellular Physiology and Biochemistry* 30(3): 538–551.

Nakajima K ichi, Miyazaki H, Niisato N and Marunaka Y (2007) Essential role of NKCC1 in NGF-induced neurite outgrowth. *Biochemical and Biophysical Research Communications* 359(3): 604–610.

Namura S, Zhu J, Fink K, Endres M, Srinivasan A, Tomaselli KJ, Yuan J and Moskowitz MA (1998) Activation and Cleavage of Caspase-3 in Apoptosis Induced by Experimental Cerebral Ischemia. *Journal of Neurosciences* 18(10): 3659–3668.

Naranjo-Suárez S, Castellanos MC, Álvarez-Tejado M, Vara A, Landázuri MO and Del Peso L (2003) Down-regulation of hypoxia-inducible factor-2 in PC12 cells by nerve growth factor stimulation. *Journal of Biological Chemistry* 278(34): 31895–31901.

Naruse M, Shibasaki K and Ishizaki Y (2015) FGF-2 signal promotes proliferation of cerebellar progenitor cells and their oligodendrocytic differentiation at early postnatal stage. *Biochemical and Biophysical*

Research Communications 463(4): 1091–1096.

Naruse M, Shibasaki K, Yokoyama S, Kurachi M and Ishizaki Y (2013) Dynamic Changes of CD44 Expression from Progenitors to Subpopulations of Astrocytes and Neurons in Developing Cerebellum. *PLoS ONE* 8(1): 1–12.

Nedergaard M and Hansen J (1993) Characterization of cortical depolarizations evoked in focal cerebral ischemia. *Journal of Cerebral Blood Flow and Metabolism* 13: 568–574.

Neelands TR, Greenfield LJ, Zhang J, Turner RS and Macdonald RL (1998) GABAA receptor pharmacology and subtype mRNA expression in human neuronal NT2-N cells. *The Journal of Neuroscience* 18(13): 4993–5007.

Neher JJ, Emmrich J V, Fricker M, Mander PK, Théry C and Brown GC (2013) Phagocytosis executes delayed neuronal death after focal brain ischemia. *Proceedings of the National Academy of Sciences of the United States of America* 110(43): E4098-107.

Nichols J, Zevnik B, Anastassiadis K, Niwa H, Klewe-Nebenius D, Chambers I, Schöler H and Smith A (1998) Formation of pluripotent stem cells in the mammalian embryo depends on the POU transcription factor Oct4. *Cell* 95(3): 379–91.

Nilsson H, Jögi A, Beckman S, Harris AL, Poellinger L and Påhlman S (2005) HIF-2α expression in human fetal paraganglia and neuroblastoma: Relation to sympathetic differentiation, glucose deficiency, and hypoxia. *Experimental Cell Research* 303(2): 447–456.

Nishitoh H (2012) CHOP is a multifunctional transcription factor in the ER stress response. *Journal of Biochemistry* 151(3): 217–219.

Nugent, BM, Valenzuela C, Simons T and McCarthy M (2012) Kinases SPAK and OSR1 are up regulated by estradiol and activate NKCC1 in the developing hypothalamus. *Journal of Neuroscience* 32(2): 593–598.

Nyiri G, Stephenson FA, Freund TF and Somogyi P (2003) Large variability in synaptic N-methyl-D-aspartate receptor density on interneurons and a comparison with pyramidal-cell spines in the rat hippocampus. *Neuroscience* 119(2): 347–363.

O'Collins VE, Macleod MR, Donnan GA, Horky LL, van der Worp BH and Howells DW (2006) 1,026 Experimental treatments in acute stroke. *Annals of Neurology* 59(3): 467–477.

O'Donnell ME, Tran L, Lam TI, Liu XB and Anderson SE (2004) Bumetanide inhibition of the blood-brain barrier Na-K-Cl cotransporter reduces edema formation in the rat middle cerebral artery occlusion model of stroke. *Journal of Cerebral Blood Flow and Metabolism* 24(9): 1046–1056.

Ohh M, Park CW, Ivan M, Hoffman MA, Kim TY, Huang LE, Pavletich N, Chau V and Kaelin WG (2000) Ubiquitination of hypoxia-inducible factor requires direct binding to the beta-domain of the von Hippel-Lindau protein. *Nature Cell Biology* 2(7): 423–427.

Olney JW (1969) Brain lesions, obesity, and other disturbances in mice treated with monosodium glutamate. *Science* 164(880): 719–721.

Olney JW and Sharpe LG (1969) Brain lesions in an infant rhesus monkey treated with monsodium glutamate. *Science* 166(3903): 386–388.

Olsen TS, Larsen B, Herning M, Skriver EB and Lassen NA (1983) Blood flow and vascular reactivity in collaterally perfused brain tissue. Evidence of an ischemic penumbra in patients with acute stroke. *Stroke* 14(3): 332–341.

Ooi L and Wood IC (2007) Chromatin crosstalk in development and disease: lessons from REST. *Nature Reviews Genetics* 8(7): 544–554.

Oyadomari S and Mori M (2004) Roles of CHOP/GADD153 in endoplasmic reticulum stress. *Cell Death and Differentiation* 11(4): 381–389.

Pamenter ME, Perkins GA, McGinness AK, Gu XQ, Ellisman MH, Haddad GG, Branston N, Symon L, Crockard H, Pasztor E, Olsen T, Larsen B, Herning M, Skriver E, Lassen N, Lo E, Candelario-Jalil E, Broughton B, Reutens D, Sobey C, Rami A, Kogel D, Sharp F, Lu A, Tang Y, Millhorn D, Galluzzi L, Maiuri M, Vitale I, Zischka H, Castedo M, Hansen A, Benchoua A, Guegan C, Couriaud C, Hosseini H, Sampaio N, Yao H, Shu Y, Wang J, Brinkman B, Haddad G, Anderson R, Tan W, Martin H, Meyer F, Rami A, Hossmann K, Anderson R, Tan W, Meyer F, Yao H, Sun X, Gu X, Wang J, Haddad G, Yao H, Felfly H, Wang J, Zhou D, Haddad G, Lehnardt S, Massillon L, Follett P, Jensen F, Ratan R, Pamenter M, Ali S, Tang Q, Finley J, Gu X, Pamenter M, Ryu J, Hua S, Perkins G, Mendiola V, Karaman M, Herrgard S, Treiber D, Gallant P, Atteridge C, Chae H, Kang J, Byun J, Han K, Kim D, Roberton A, Holloway C, Knight I, Beechey R, Morimoto B, Jr DK, Leist M, Single B, Castoldi A, Kuhnle S, Nicotera P, Akanda N, Elinder F, Dagda R, Gusdon A, Pien I, Strack S, Green S, Ju W, Kim K, Lindsey J, Angert M, Patel A, Boulares A, Yakovlev A, Ivanova V, Stoica B, Wang G, Chaitanya G, Steven A, Babu P, Fadok V, Voelker D, Campbell P, Cohen J, Bratton D, Koopman G, Reutelingsperger C, Kuijten G, Keehnen R, Pals S, Karbowski M, Youle R, Banasiak K, Cronin T, Haddad G, Matsushita K, Matsuyama T, Kitagawa K, Matsumoto M, Yanagihara T, Tanida I, Ueno T, Kominami E, Kroemer G, Jaattela M, Puyal J, Vaslin A, Mottier V, Clarke P, Barone F, Lazebnik Y, Takahashi A, Moir R, Goldman R, Poirier G, Hattori K, Kajimura M, Hishiki T, Nakanishi T, Kubo A, Kalinowska M, Garncarz W, Pietrowska M, Garrard W, Widlak P, Wang J, Wei Q, Wang C, Hill W, Hess D, Morin D, Pires F, Plin C, Tillement J, Repici M, Centeno C, Tomasi S, Forloni G, Bonny C, Maiuri M, Zalckvar E, Kimchi A, Kroemer G, Yao H, Takasawa R, Fukuda K, Shiokawa D, Sadanaga-Akiyoshi F, Culmsee C, Zhu C, Landshamer S, Becattini B, Wagner E, Weinstein P, Hong S, Sharp F, Krupinski J, Lopez E, Marti E, Ferrer I, Rami A, Langhagen A, Steiger S,

Ferrer I, Friguls B, Dalfo E, Justicia C, Planas A, Kroemer G, El-Deiry W, Golstein P, Peter M, Vaux D, Graham S, Chen J, Fink S, Cookson B, Yakovlev A, Faden A, Gelot A, Villapol S, Villemeur TB de, Renolleau S, Charriaut-Marlangue C, Xu L, Sapolsky R, Giffard R, Zoppo G del, Zoppo G del, Frankowski H, Gu Y, Osada T, Kanazawa M, Zhang J, Chung T and Oldenburg K (2012) Autophagy and Apoptosis Are Differentially Induced in Neurons and Astrocytes Treated with an In Vitro Mimic of the Ischemic Penumbra. *PLoS ONE* 7(12): e51469.

Pannasch U, Vargová L, Reingruber J, Ezan P, Holcman D, Giaume C, Syková E and Rouach N (2011) Astroglial networks scale synaptic activity and plasticity. *Proceedings of the National Academy of Sciences of the United States of America* 108(20): 8467–72.

Papandreou I, Cairns RA, Fontana L, Lim AL and Denko NC (2006) HIF-1 mediates adaptation to hypoxia by actively downregulating mitochondrial oxygen consumption. *Cell Metabolism* 3(3): 187–197.

Papers JBC, M DOI, Alvarez-Tejado M, Naranjo-sua S, Carrera AC, Landa MO, Peso L, Naranjo-Suarez S, Jiménez C, Carrera AC, Landázuri MO and del Peso L (2001) Hypoxia Induces the Activation of the Phosphatidylinositol 3-Kinase / Akt Cell Survival Pathway in PC12 Cells. *Biochemistry* 276(25): 22368–22374.

Papp E, Rivera C, Kaila K and Freund TF (2008) Relationship between neuronal vulnerability and potassium-chloride cotransporter 2 immunoreactivity in hippocampus following transient forebrain ischemia. *Neuroscience* 154(2): 677–689.

Paris S, Denis H, Delaive E, Dieu M, Dumont V, Ninane N, Raes M and Michiels C (2005) Up-regulation of 94-kDa glucose-regulated protein by hypoxia-inducible factor-1 in human endothelial cells in response to hypoxia. *FEBS Letters* 579(1): 105–114.

Paxinos G and Franklin KBJ (2013) *Paxinos and Franklin's the Mouse Brain in Stereotaxic Coordinates. 4th Edition*.

Payne J a, Stevenson J and Donaldson L (1996) Molecular characterization of putative K - Cl cotransporter in rat brain, Journal of *Biological Chemistry* 271(27): 16245–16252.

Payne JA, Rivera C, Voipio J and Kaila K (2003b) Cation–chloride co-transporters in neuronal communication, development and trauma. *Trends in Neurosciences* 26(4): 199–206.

Pedersen ED, Frøyland E, Kvissel AK, Pharo AM, Skålhegg BS, Rootwelt T and Mollnes TE (2007) Expression of complement regulators and receptors on human NT2-N neurons-Effect of hypoxia and reoxygenation. *Molecular Immunology* 44(9): 2459–2468.

Pellegrino C, Gubkina O, Schaefer M, Becq H, Ludwig A, Mukhtarov M, Chudotvorova I, Corby S, Salyha Y, Salozhin S, Bregestovski P and Medina I (2011) Knocking down of the KCC2 in rat hippocampal neurons increases intracellular chloride concentration and compromises neuronal survival. *The Journal of Physiology* 589(10): 2475–2496.

Pereira ER, Frudd K, Awad W and Hendershot LM (2014) Endoplasmic reticulum (ER) stress and hypoxia response pathways interact to potentiate hypoxia-inducible factor 1 (HIF-1) transcriptional activity on targets like vascular endothelial growth factor (VEGF). *The Journal of Biological Chemistry* 289(6): 3352–64.

Pfeffer CK, Stein V, Keating DJ, Maier H, Rinke I, Rudhard Y, Hentschke M, Rune GM, Jentsch TJ and Hübner CA (2009) NKCC1-dependent GABAergic excitation drives synaptic network maturation during early hippocampal development. *The Journal of Neuroscience* 29(11): 3419–30.

Piechotta K, Lu J and Delpire E (2002) Cation chloride cotransporters interact with the stress-related kinases Ste20-related proline-alanine-rich kinase (SPAK) and oxidative stress response 1 (OSR1). *Journal of Biological Chemistry* 277(52): 50812–50819.

Pietras A, Hansford LM, Johnsson AS, Bridges E, Sjölund J, Gisselsson D, Rehn M, Beckman S, Noguera R, Navarro S, Cammenga J, Fredlund E, Kaplan DR and Påhlman S (2009) HIF-2alpha maintains an undifferentiated state in neural crest-like human neuroblastoma tumor-initiating cells. *Proceedings of the National Academy of Sciences of the United States of America* 106(39): 16805–16810.

Pilot Study of Bumetanide for Newborn Seizures Trial (2009) Available at: https://clinicaltrials.gov/ct2/show/NCT00830531. [Accessed: April 2017]

Pizzarelli R and Cherubini E (2011) Alterations of GABAergic signaling in autism spectrum disorders. *Neural plasticity* 2011: 297153.

Pleasure SJ, Page C and Lee VM (1992) Pure, postmitotic, polarized human neurons derived from NTera 2 cells provide a system for expressing exogenous proteins in terminally differentiated neurons. *The Journal of Neuroscience* 12(5): 1802–1815.

Ploughman M, Windle V, MacLellan CL, White N, Dor JJ and Corbett D (2009) Brain-derived neurotrophic factor contributes to recovery of skilled reaching after focal ischemia in rats. *Stroke* 40(4): 1490–1495.

Podrygajlo G, Tegenge MA, Gierse A, Paquet-Durand F, Tan S, Bicker G and Stern M (2009) Cellular phenotypes of human model neurons (NT2) after differentiation in aggregate culture. *Cell and Tissue Research* 336(3): 439–452.

Pond BB (2006) The Chloride Transporter Na+-K+-Cl- Cotransporter

Isoform-1 Contributes to Intracellular Chloride Increases after In Vitro Ischemia. *Journal of Neuroscience* 26(5): 1396–1406.

Popa-Wagner A, Carmichael ST, Kokaia Z, Kessler C and Walker LC (2007) The response of the aged brain to stroke: too much, too soon? *Current Neurovascular Research* 4(3): 216–27.

Popp A, Jaenisch N, Witte OW and Frahm C (2009) Identification of Ischemic Regions in a Rat Model of Stroke. *PLoS ONE* 4(3): e4764.

Porter a G and Jänicke RU (1999) Emerging roles of caspase-3 in apoptosis. *Cell Death and Differentiation* 6(2): 99–104.

Pressler RM, Boylan GB, Marlow N, Blennow M, Chiron C, Cross JH, de Vries LS, Hallberg B, Hellström-Westas L, Jullien V, Livingstone V, Mangum B, Murphy B, Murray D, Pons G, Rennie J, Swarte R, Toet MC, Vanhatalo S and Zohar S (2015) Bumetanide for the treatment of seizures in newborn babies with hypoxic ischaemic encephalopathy (NEMO): an open-label, dose finding, and feasibility phase 1/2 trial. *The Lancet Neurology* 14(5): 469–477.

Price CJS, Wang D, Menon DK, Guadagno J V., Cleij M, Fryer T, Aigbirhio F, Baron JC and Warburton EA (2006) Intrinsic activated microglia map to the peri-infarct zone in the subacute phase of ischemic stroke. *Stroke* 37(7): 1749–1753.

Pulsinelli WA, Brierley JB and Plum F (1982) Temporal profile of neuronal damage in a model of transient forebrain ischemia. *Annals of Neurology* 11(5): 491–498.

Puskarjov M, Ahmad F, Kaila K and Blaesse P (2012) Activity-Dependent Cleavage of the K-Cl Cotransporter KCC2 Mediated by Calcium-Activated Protease Calpain. *Journal of Neuroscience* 32(33): 11356–11364.

Puskarjov M, Ahmad F, Khirug S, Sivakumaran S, Kaila K and Blaesse P (2015) BDNF is required for seizure-induced but not developmental up-regulation of KCC2 in the neonatal hippocampus. *Neuropharmacology* 88: 103–109.

Puskarjov M, Kahle KT, Ruusuvuori E and Kaila K (2014) Pharmacotherapeutic targeting of cation-chloride cotransporters in neonatal seizures. *Epilepsia*, 806–818.

Rajdev S, Hara K, Kokubo Y, Mestril R, Dillmann W, Weinstein PR and Sharp FR (2000) Mice overexpressing rat heat shock protein 70 are protected against cerebral infarction. *Annals of Neurology* 47(6): 782–91.

Ralph GS, Parham S, Lee SR, Beard GL, Craigon MH, Ward N, White JR, Barber RD, Rayner W, Kingsman SM, Mundy CR, Mazarakis ND and Krige D (2004) Identification of Potential Stroke Targets by Lentiviral Vector Mediated Overexpression of HIF-1?? and HIF-2?? in a Primary Neuronal

Model of Hypoxia. *Journal of Cerebral Blood Flow & Metabolism* 24(2): 245–258.
Rami A and Kögel D (2008) Apoptosis meets autophagy-like cell death in the ischemic penumbra: Two sides of the same coin? *Autophagy* 4(4): 422–6.

Ramos-Cabrer P, Campos F, Sobrino T and Castillo J (2011) Targeting the ischemic penumbra. *Stroke* 42(1): S7-11.

Rankin EB, Biju MP, Liu Q, Unger TL, Rha J, Johnson RS, Simon MC, Keith B and Haase VH (2007) Hypoxia-inducible factor-2 (HIF-2) regulates hepatic erythropoietin in vivo. *Journal of Clinical Investigation* 117(4): 1068–1077.

Rao JN, Madasu Y and Dominguez R (2014) Mechanism of actin filament pointed-end capping by tropomodulin. *Science* 345(6195): 463–7.

Ratan RR, Siddiq A, Smirnova N, Karpisheva K, Haskew-Layton R, McConoughey S, Langley B, Estevez A, Huerta PT, Volpe B, Roy S, Sen CK, Gazaryan I, Cho S, Fink M and LaManna J (2007) Harnessing hypoxic adaptation to prevent, treat, and repair stroke. *Journal of Molecular Medicine* 85(12): 1331–1338.

Raval RR, Lau KW, Tran MGB, Sowter HM, Mandriota SJ, Li J-L, Pugh CW, Maxwell PH, Harris AL and Ratcliffe PJ (2005) Contrasting properties of hypoxia-inducible factor 1 (HIF-1) and HIF-2 in von Hippel-Lindau-associated renal cell carcinoma. *Molecular and Cellular Biology* 25(13): 5675–86.

Reischl S, Li L, Walkinshaw G, Flippin LA, Marti HH, Kunze R, Zhao Y, Rempe D, Dirnagl U, Iadecola C, Moskowitz M, Gelderblom M, Leypoldt F, Steinbach K, Behrens D, Choe C, Sandoval K, Witt K, Siddiq A, Aminova L, Ratan R, Bernaudin M, Marti H, Roussel S, Divoux D, Nouvelot A, Rabie T, Marti H, Sun F, Guo X, Sun Y, Jin K, Xie L, Childs J, Mao X, Wang Y, Kilic E, Kilic U, Weber B, Bassetti C, Li Y, Lu Z, Ogle M, Wei L, Liu K, Sun T, Wang P, Liu Y, Zhang L, Kaelin W, Ratcliffe P, Myllyharju J, Koivunen P, Rabie T, Kunze R, Marti H, Kunze R, Zhou W, Veltkamp R, Wielockx B, Breier G, Montesano R, Pepper M, Mohle-Steinlein U, Risau W, Wagner E, Davis J, Maher P, Milosevic J, Adler I, Manaenko A, Schwarz S, Walkinshaw G, Greenberg D, Jin K, Baranova O, Miranda L, Pichiule P, Dragatsis I, Johnson R, Nagel S, Papadakis M, Chen R, Hoyte L, Brooks K, Ogle M, Gu X, Espinera A, Wei L, Siddiq A, Ayoub I, Chavez J, Aminova L, Shah S, Karuppagounder S, Ratan R, Erez N, Stambolsky P, Shats I, Milyavsky M, Kachko T, Henze A, Riedel J, Diem T, Wenner J, Flamme I, Schneider C, Krischke G, Keller S, Walkinshaw G, Arend M, Kaur C, Ling E, Chen R, Nagel S, Papadakis M, Bishop T, Pollard P, Bauer A, Burgers H, Rabie T, Marti H, Rosenstein J, Krum J, Ruhrberg C, Fischer S, Clauss M, Wiesnet M, Renz D, Schaper W, Schoch H, Fischer S, Marti H, Zhang Z, Zhang L, Jiang Q, Zhang R, Davies K, Antonetti D, Barber A, Hollinger L, Wolpert E, Gardner T, Esser S, Lampugnani M, Corada M, Dejana E, Risau W, Valable S, Montaner J, Bellail A, Berezowski V, Brillault J, Bernaudin M, Bellail A, Marti H, Yvon A, Vivien D, Martinez-Estrada O, Rodriguez-Millan E, Vicente EG, Reina M, Vilaro S, Helton R, Cui J, Scheel J, Ellison J, Ames C, Yan J, Zhou

B, Taheri S, Shi H, Zlokovic B, Zlokovic B, Sagare A, Bell R and Zlokovic B (2014) Inhibition of HIF prolyl-4-hydroxylases by FG-4497 Reduces Brain Tissue Injury and Edema Formation during Ischemic Stroke. *PLoS ONE* 9(1): e84767.

Resende RR, Majumder P, Gomes KN, Britto LRG and Ulrich H (2007) P19 embryonal carcinoma cells as in vitro model for studying purinergic receptor expression and modulation of N-methyl-d-aspartate-glutamate and acetylcholine receptors during neuronal differentiation. *Neuroscience* 146(3): 1169–1181.

Rivera C, Li H, Thomas-Crusells J, Lahtinen H, Viitanen T, Nanobashvili A, Kokaia Z, Airaksinen MS, Voipio J, Kaila K and Saarma M (2002) BDNF-induced TrkB activation down-regulates the K+-Cl- cotransporter KCC2 and impairs neuronal Cl- extrusion. *The Journal of Cell Biology* 159(5): 747–52.

Rivera C, Voipio J, Payne JA, Ruusuvuori E, Lahtinen H, Lamsa K, Pirvola U, Saarma M and Kaila K (1999a) The K+/Cl- co-transporter KCC2 renders GABA hyperpolarizing during neuronal maturation. *Nature* 397(6716): 251–255.

Roger VL, Go AS, Lloyd-Jones DM, Adams RJ, Berry JD, Brown TM, Carnethon MR, Dai S, De Simone G, Ford ES, Fox CS, Fullerton HJ, Gillespie C, Greenlund KJ, Hailpern SM, Heit JA, Michael Ho P, Howard VJ, Kissela BM, Kittner SJ, Lackland DT, Lichtman JH, Lisabeth LD, Makuc DM, Marcus GM, Marelli A, Matchar DB, McDermott MM, Meigs JB, Moy CS, Mozaffarian D, Mussolino ME, Nichol G, Paynter NP, Rosamond WD, Sorlie PD, Stafford RS, Turan TN, Turner MB, Wong ND and Wylie-Rosett J (2011) Heart disease and stroke statistics-2011 update: A report from the American Heart Association. *Circulation* 123(4): e18–e209.

Rolls A, Shechter R and Schwartz M (2009) The bright side of the glial scar in CNS repair. *Nature Reviews Neuroscience* 10(3): 235–241.

Römermann K, Fedrowitz M, Hampel P, Kaczmarek E, Töllner K, Erker T, Sweet DH and Löscher W (2017) Multiple blood-brain barrier transport mechanisms limit bumetanide accumulation, and therapeutic potential, in the mammalian brain. *Neuropharmacology* 117: 182–194.

Ron D (2002) Translational control in the endoplasmic reticulum stress response. *Journal of Clinical Investigation* 110(10): 1383–1388.

Rosell A, Cuadrado E, Alvarez-Sabín J, Hernández-Guillamon M, Delgado P, Penalba A, Mendioroz M, Rovira A, Fernández-Cadenas I, Ribó M, Molina CA and Montaner J (2008) Caspase-3 is related to infarct growth after human ischemic stroke. *Neuroscience Letters* 430(1): 1–6.

Rossi DJ, Oshima T and Attwell D (2000) Glutamate release in severe brain ischaemia is mainly by reversed uptake. *Nature* 403(1): 316–321.

Roussel BD, Kruppa AJ, Miranda E, Crowther DC, Lomas DA and Marciniak SJ (2013) Endoplasmic reticulum dysfunction in neurological disease. *The Lancet. Neurology* 12(1): 105–18.

Saka Ö, Mcguire A and Wolfe C (2009) Cost of stroke in the United Kingdom. *Age and Ageing* 38(1): 27–32.

Sandoval KE and Witt KA (2008) Blood-brain barrier tight junction permeability and ischemic stroke. *Neurobiology of Disease* 32(2): 200–219.
Sanin V, Heeß C, Kretzschmar HA and Schüller U (2013) Recruitment of neural precursor cells from circumventricular organs of patients with cerebral ischaemia. *Neuropathology and Applied Neurobiology* 39(5): 510–518.

Sanz-Clemente A, Nicoll RA and Roche KW (2013) Diversity in NMDA Receptor Composition. *The Neuroscientist* 19(1): 62–75.

Saver JL (2006) Time is brain--quantified. *Stroke* 37(1): 263–266.

Schepens B, Tinton SA, Bruynooghe Y, Beyaert R and Cornelis S (2005) The polypyrimidine tract-binding protein stimulates HIF-1α IRES-mediated translation during hypoxia. *Nucleic Acids Research* 33(21): 6884–6894.

Schlaug G, Benfield A, Baird AE, Siewert B, Lövblad KO, Parker RA, Edelman RR and Warach S (1999) The ischemic penumbra Operationally defined by diffusion and perfusion MRI. *Neurology* 53(7): 1528–1537.

Schmidt-Kastner R (2015) Genomic approach to selective vulnerability of the hippocampus in brain ischemia-hypoxia. *Neuroscience* 309: 259–279.

Schofield CJ and Ratcliffe PJ (2004) Oxygen sensing by HIF hydroxylases. *Nature Reviews Molecular Cell Biology* 5(5): 343–354.

Schoknecht K, David Y and Heinemann U (2015) The blood-brain barrier-Gatekeeper to neuronal homeostasis: Clinical implications in the setting of stroke. *Seminars in Cell and Developmental Biology* 38: 35–42.

Schoknecht K, Prager O, Vazana U, Kamintsky L, Harhausen D, Zille M, Figge L, Chassidim Y, Schellenberger E, Kovács R, Heinemann U and Friedman A (2014) Monitoring stroke progression: in vivo imaging of cortical perfusion, blood-brain barrier permeability and cellular damage in the rat photothrombosis model. *Journal of cerebral blood flow and metabolism* 34(11): 1791–801.

Schwab BL, Guerini D, Didszun C, Bano D, Ferrando-May E, Fava E, Tam J, Xu D, Xanthoudakis S, Nicholson DW, Carafoli E and Nicotera P (2002) Cleavage of plasma membrane calcium pumps by caspases: a link between apoptosis and necrosis. *Cell Death and Differentiation* 9(8): 818–831.

Schwartz RD, Yu X, Katzman MR, Haydenhixson DM and Perry JM (1995) Diazepam, Given Postischemia, Protects Selectively Vulnerable Neurons In

the Rat Hippocampus and Striatum. *Journal of Neuroscience* 15(1 Pt2): 529–539.
Sedmak G, Jovanov-Milošević N, Puskarjov M, Ulamec M, Krušlin B, Kaila K, Judaš M, Jovanov-Miloševi N, Puskarjov M, Ulamec M, Krušlin B, Kaila K and Judaš M (2015) Developmental Expression Patterns of KCC2 and Functionally Associated Molecules in the Human Brain. *Cerebral Cortex* 26(12): 4574-4589.

Semenza GL (2003) Targeting HIF-1 for cancer therapy. *Nature Reviews Cancer* 3(10): 721–732.

Semenza GL (2012) Hypoxia-inducible factors in physiology and medicine. *Cell* 148(3): 399–408.

Sentinel Stroke National Audit Programme (SSNAP) Annual Report (2016) Available at: http://annualreport.ssnap.org/2015-16SSNAPAnnualReport/html5/index.html?page=1&noflash. [Accessed on February 2017].

Sharp FR and Bernaudin M (2004) HIF1 and oxygen sensing in the brain. *Nature Reviews Neuroscience* 5(6): 437–448.

Sharp FR, Zhan X and Liu D-Z (2013) Heat shock proteins in the brain: role of Hsp70, Hsp 27, and HO-1 (Hsp32) and their therapeutic potential. *Translational Stroke Research* 4(6): 685–692.

Shen C-C, Yang Y-C, Chiao M-T, Cheng W-Y, Tsuei Y-S and Ko J-L (2010) Characterization of endogenous neural progenitor cells after experimental ischemic stroke. *Current Neurovascular Research* 7(1): 6–14.

Shevtsov MA, Nikolaev BP, Yakovleva LY, Dobrodumov A V, Dayneko AS, Shmonin AA, Vlasov TD, Melnikova E V, Vilisov AD, Guzhova I V, Ischenko AM, Mikhrina AL, Galibin O V, Yakovenko I V and Margulis BA (2014) Neurotherapeutic activity of the recombinant heat shock protein Hsp70 in a model of focal cerebral ischemia in rats. *Drug Design, Development and Therapy* 8: 639–650.

Shi H (2009) Hypoxia inducible factor 1 as a therapeutic target in ischemic stroke. *Current Medicinal Chemistry* 16(34): 4593–600.

Shin HK, Dunn AK, Jones PB, Boas D a, Moskowitz M a and Ayata C (2006) Vasoconstrictive neurovascular coupling during focal ischemic depolarizations. *Journal of Cerebral Blood Flow and Metabolism* 26(8): 1018–1030.

Silver J and Miller JH (2004) Regeneration beyond the glial scar. *Nature Reviews Neuroscience* 5(2): 146–156.

Simard CF, Bergeron MJ, Frenette-Cotton R, Carpentier G a, Pelchat M-E, Caron L and Isenring P (2007) Homooligomeric and heterooligomeric

associations between K+-Cl- cotransporter isoforms and between K+-Cl- and Na+-K+-Cl- cotransporters. *The Journal of Biological Chemistry* 282(25): 18083–18093.

Simmons DA, Rex CS, Palmer L, Pandyarajan V, Fedulov V, Gall CM and Lynch G (2009) Up-regulating BDNF with an ampakine rescues synaptic plasticity and memory in Huntington's disease knockin mice. *Proceedings of the National Academy of Sciences of the United States of America* 106(12): 4906–4911.

Simon MC and Keith B (2008) The role of oxygen availability in embryonic development and stem cell function. *Nature Reviews Molecular Cell Biology* 9(4): 285–296.

Simpson IA, Dwyer D, Malide D, Moley KH, Travis A and Vannucci SJ (2008) The facilitative glucose transporter GLUT3: 20 years of distinction. *American journal of physiology. Endocrinology and Metabolism* 295(2): E242-53.

Sims NR and Muyderman H (2010) Mitochondria, oxidative metabolism and cell death in stroke. *Biochimica et Biophysica Acta (BBA) - Molecular Basis of Disease* 1802(1): 80–91.

Sist B, Fouad K and Winship IR (2014) Plasticity beyond peri-infarct cortex: Spinal up regulation of structural plasticity, neurotrophins, and inflammatory cytokines during recovery from cortical stroke. *Experimental Neurology* 252: 47–56.

Sivakumaran S, Cardarelli R a., Maguire J, Kelley MR, Silayeva L, Morrow DH, Mukherjee J, Moore YE, Mather RJ, Duggan ME, Brandon NJ, Dunlop J, Zicha S, Moss SJ and Deeb TZ (2015) Selective Inhibition of KCC2 Leads to Hyperexcitability and Epileptiform Discharges in Hippocampal Slices and In Vivo. *Journal of Neuroscience* 35(21): 8291–8296.

Smeyne M, Sladen P, Jiao Y, Dragatsis I and Smeyne RJ (2015) HIF1α is necessary for exercise-induced neuroprotection while HIF2α is needed for dopaminergic neuron survival in the substantia nigra pars compacta. *Neuroscience* 295: 23–38.

Sofroniew M V. (2009) Molecular dissection of reactive astrogliosis and glial scar formation. *Trends in Neurosciences* 32(12): 638–647.

Sofroniew M V. and Vinters H V. (2010) Astrocytes: Biology and pathology. *Acta Neuropathologica* 119(1): 7–35.

Spampanato J, Sullivan RK, Turpin FR, Bartlett PF and Sah P (2012) Properties of Doublecortin Expressing Neurons in the Adult Mouse Dentate Gyrus. *PLoS ONE* 7(9): e41029.

Spatz M, Kawai N, Merkel N, Bembry J and McCarron RM (1997) Functional properties of cultured endothelial cells derived from large microvessels of

human brain. *The American Journal of Physiology* 272(1 Pt 1): C231-9.

Spratt NJ, Donnan GA, McLeod DD and Howells DW (2011) 'Salvaged' stroke ischaemic penumbra shows significant injury: studies with the hypoxia tracer FMISO. *Journal of Cerebral Blood Flow and Metabolism* 31(3): 934–943.

Steffensen AB, Sword J, Croom D, Kirov SA and MacAulay N (2015) Chloride Cotransporters as a Molecular Mechanism underlying Spreading Depolarization-Induced Dendritic Beading. *The Journal of neuroscience* 35(35): 12172–12187.

Steinberg GK, Yoon EJ, Kunis DM, Sun GH, Maier CM and Grant GA (1995) Neuroprotection by N-methyl-D-aspartate antagonists in focal cerebral ischemia is dependent on continued maintenance dosing. *Neuroscience* 64(1): 99–107.

Strober W (2001) Trypan Blue Exclusion Test of Cell Viability. *Current Protocols in Immunology* 3.

Stroke Association (2017) State of the nation. Available at: https://www.stroke.org.uk/sites/default/files/stroke_statistics_2015.pdf. [Accessed March 2017].

Su G, Kintner DB and Sun D (2002) Contribution of Na(+)-K(+)-Cl(-) cotransporter to high-[K(+)](o)- induced swelling and EAA release in astrocytes. *American journal of physiology. Cell Physiology* 282(5): C1136-46.

Succol F, Fiumelli H, Benfenati F, Cancedda L and Barberis A (2012) Intracellular chloride concentration influences the GABAA receptor subunit composition. *Nature Communications*. 3: 738.

Sun D and Kahle KT (2014) Dysregulation of Diverse Ion Transport Pathways Controlling Cell Volume Homoestasis Contribute to Neuroglial Cell Injury Following Ischemic Stroke. *Translational Stroke Research* 5(1): 1–2.

Swanson RA, Ying W and Kauppinen TM (2004) Astrocyte influences on ischemic neuronal death. *Current Molecular Medicine* 4(2): 193–205.

Szydlowska K and Tymianski M (2010) Calcium, ischemia and excitotoxicity. *Cell Calcium* 47(2): 122–129.

Tabakman R, Lazarovici P and Kohen R (2002) Neuroprotective effects of carnosine and homocarnosine on pheochromocytoma PC12 cells exposed to ischemia. *Journal of Neuroscience Research* 68(4): 463–469.

Takano T, Oberheim NA, Cotrina ML and Nedergaard M (2009) Astrocytes and ischemic injury. *Stroke* 40(3 SUPPL. 1): 8–13.

Thornton B and Basu C (2011) Real-time PCR (qPCR) primer design using free online software. *Biochemistry and Molecular Biology Education* 39(2): 145–154.

Thrift AG, Cadilhac DA, Thayabaranathan T, Howard G, Howard VJ, Rothwell PM and Donnan GA (2014) Global Stroke Statistics. *International Journal of Stroke* 9(1): 6–18.

Toda T, Ishida K, Kiyama H, Yamashita T and Lee S (2014) Down-regulation of KCC2 expression and phosphorylation in motoneurons, and increases the number of in primary afferent projections to motoneurons in mice with post-stroke spasticity. *PLoS ONE* 9(12): e114328.

Töllner K, Brandt C, Töpfer M, Brunhofer G, Erker T, Gabriel M, Feit PW, Lindfors J, Kaila K and Löscher W (2014) A novel prodrug-based strategy to increase effects of bumetanide in epilepsy. *Annals of Neurology* 75(4): 550–562.

Tornberg J, Voikar V, Savilahti H, Rauvala H and Airaksinen MS (2005) Behavioural phenotypes of hypomorphic KCC2-deficient mice. *European Journal of Neuroscience* 21(5): 1327–1337.

Towbin H, Staehelin T, Gordon J. (1979) Electrophoretic transfer of proteins from polyacrylamide gels to nitrocellulose sheets: procedure and some applications. *Proceedings of the National Academiy of Sciences* 76(9):4350-4354.

Tsai PT, Ohab JJ, Kertesz N, Groszer M, Matter C, Gao J, Liu X, Wu H and Carmichael ST (2006) A Critical Role of Erythropoietin Receptor in Neurogenesis and Post-Stroke Recovery. *Journal of Neuroscience* 26(4): 1269–1274.

Tymianski M (2010) Can molecular and cellular neuroprotection be translated into therapies for patients?: Yes, but not the way we tried it before. *Stroke* 41(10 SUPPL. 1): S87-90.

Uchida T, Rossignol F, Matthay MA, Mounier R, Couette S, Clottes E and Clerici C (2004) Prolonged hypoxia differentially regulates hypoxia-inducible factor (HIF)-1α and HIF-2α expression in lung epithelial cells: Implication of natural antisense HIF-1α. *Journal of Biological Chemistry* 279(15): 14871–14878.

Usoskin D, Furlan A, Islam S, Abdo H, Lönnerberg P, Lou D, Hjerling-Leffler J, Haeggström J, Kharchenko O, Kharchenko P V, Linnarsson S and Ernfors P (2014) Unbiased classification of sensory neuron types by large-scale single-cell RNA sequencing. *Nature Neuroscience* 18(1): 145–153. Uvarov P, Pruunsild P, Timmusk T and Airaksinen MS (2005) Neuronal K+/Cl- co-transporter (KCC2) transgenes lacking neurone restrictive silencer element recapitulate CNS neurone-specific expression and developmental up-regulation of endogenous KCC2 gene. *Journal of Neurochemistry* 95(4):

1144–1155.

Uvarov P, Ludwig A, Markkanen M, Rivera C and Airaksinen MS (2006) Upregulation of the neuron-specific K+/Cl- cotransporter expression by transcription factor early growth response 4. *The Journal of neuroscience : the official journal of the Society for Neuroscience* 26(52): 13463–13473.

Uvarov P, Ludwig A, Markkanen M, Pruunsild P, Kaila K, Delpire E, Timmusk T, Rivera C and Airaksinen MS (2007) A novel N-terminal isoform of the neuron-specific K-Cl cotransporter KCC2. *Journal of Biological Chemistry* 282(42): 30570–30576.

Uwechue NM, Marx M-C, Chevy Q and Billups B (2012) Activation of glutamate transport evokes rapid glutamine release from perisynaptic astrocytes. *The Journal of Physiology* 590(10): 2317–2331.

Uyanik G, Elcioglu N, Penzien J, Gross C, Yilmaz Y, Olmez A, Demir E, Wahl D, Scheglmann K, Winner B, Bogdahn U, Topaloglu H, Hehr U and Winkler J (2006) Novel truncating and missense mutations of the KCC3 gene associated with Andermann syndrome. *Neurology* 66(7): 1044–1048.

Vandesompele J, De Preter K, Pattyn F, Poppe B, Van Roy N, De Paepe A and Speleman F (2002) Accurate normalization of real-time quantitative RT-PCR data by geometric averaging of multiple internal control genes. *Genome Biology* 3(7): 32

Vannucci SJ, Maher F and Simpson IA (1997) Glucose transporter proteins in brain: delivery of glucose to neurons and glia. *Glia* 21(1): 2–21.

Vannucci SJ, Reinhart R, Maher F, Bondy C a, Lee WH, Vannucci RC and Simpson I a (1998) Alterations in GLUT1 and GLUT3 glucose transporter gene expression following unilateral hypoxia-ischemia in the immature rat brain. *Brain research. Developmental Brain Research* 107(2): 255–64.

Vibat CR, Holland MJ, Kang JJ, Putney LK and O'Donnell ME (2001) Quantitation of Na+-K+-2Cl- cotransport splice variants in human tissues using kinetic polymerase chain reaction. *Analytical Biochemistry* 298(2): 218–230.

Viitanen T, Ruusuvuori E, Kaila K and Voipio J (2010) The K+-Cl cotransporter KCC2 promotes GABAergic excitation in the mature rat hippocampus. *The Journal of Physiology* 588(9): 1527–1540.

Wahl AS, Buchthal B, Rode F, Bomholt SF, Freitag HE, Hardingham GE, Rønn LCB and Bading H (2009) Hypoxic/ischemic conditions induce expression of the putative pro-death gene Clca1 via activation of extrasynaptic N-methyl-d-aspartate receptors. *Neuroscience* 158(1): 344–352.

Wake H, Watanabe M, Moorhouse AJ, Kanematsu T, Horibe S, Matsukawa

N, Asai K, Ojika K, Hirata M and Nabekura J (2007) Early Changes in KCC2 Phosphorylation in Response to Neuronal Stress Result in Functional Downregulation. *Journal of Neuroscience* 27(7): 1642–1650.

Wallace BK, Jelks KA and O'Donnell ME (2012) Ischemia-induced stimulation of cerebral microvascular endothelial cell Na-K-Cl cotransport involves p38 and JNK MAP kinases. *American Journal of Physiology. Cell physiology* 302(3): C505-17.

Wang D and Fawcett J (2012) The perineuronal net and the control of CNS plasticity. *Cell and Tissue Research* 349(1): 147–160.

Wang DD and Kriegstein AR (2008) GABA regulates excitatory synapse formation in the neocortex via NMDA receptor activation. *The Journal of Neuroscience* 28(21): 5547–5558.

Wang DD and Kriegstein AR (2009) Defining the role of GABA in cortical development. *Journal of Physiology* 587(9): 1873–1879.

Wang G, Huang H, He Y, Ruan L and Huang J (2014a) Bumetanide protects focal cerebral ischemia-reperfusion injury in rat. *International Journal of Clinical and Experimental Pathology* 7(4): 1487–1494.

Wang S, Zhang XQ, Song CG, Xiao T, Zhao M, Zhu G and Zhao CS (2015) In vivo effects of bumetanide at brain concentrations incompatible with NKCC1 inhibition on newborn DGC structure and spontaneous EEG seizures following hypoxia-induced neonatal seizures. *Neuroscience* 286: 203–215.

Wardlaw JM, Murray V, Berge E, Del Zoppo G, Sandercock P, Lindley RL and Cohen G (2012) Recombinant tissue plasminogen activator for acute ischaemic stroke: An updated systematic review and meta-analysis. *The Lancet* 379(9834): 2364–2372.

Watson BD, Dietrich WD, Busto R, Wachtel MS and Ginsberg MD (1985) Induction of reproducible brain infarction by photochemically initiated thrombosis. *Annals of Neurology* 17(5): 497–504.

Weisova P, Concannon CG, Devocelle M, Prehn JHM and Ward MW (2009) Regulation of Glucose Transporter 3 Surface Expression by the AMP-Activated Protein Kinase Mediates Tolerance to Glutamate Excitation in Neurons. *Journal of Neuroscience* 29(9): 2997–3008.

Wenz M, Hartmann AM, Friauf E and Nothwang HG (2009) CIP1 is an activator of the K+-Cl- cotransporter KCC2. *Biochemical and Biophysical Research Communications* 381(3): 388–392.

Wey H-Y, Desai VR and Duong TQ (2013) A review of current imaging methods used in stroke research. *Neurological Research* 35(10): 1092–102.

Witte OW, Bidmon H-J, Schiene K, Redecker C and Hagemann G (2000)

Functional differentation of multiple perilesional zones after focal cerebral ischaemia. *J Cereb Flow Metab* 20: 1149–1165.

Woo N-S, Lu J, England R, McClellan R, Dufour S, Mount DB, Deutch AY, Lovinger DM and Delpire E (2002) Hyperexcitability and epilepsy associated with disruption of the mouse neuronal-specific K-Cl cotransporter gene. *Hippocampus* 12(2): 258–268.

Woodruff TM, Thundyil J, Tang S-C, Sobey CG, Taylor SM, Arumugam T V, Seshadri S, Beiser A, Kelly-Hayes M, Kase C, Au R, Kannel W, Wolf P, Beal C, Mergenthaler P, Dirnagl U, Meisel A, Mattson M, Duan W, Pedersen W, Culmsee C, Murray V, Norrving B, Sandercock P, Terent A, Wardlaw J, Wester P, Uyttenboogaart M, Keyser J De, Luijckx G, Arumugam T, Granger D, Mattson M, Legos J, Barone F, Sicard K, Fisher M, Braeuninger S, Kleinschnitz C, McBean D, Kelly P, Howells D, Porritt M, Rewell S, O'Collins V, Sena E, Worp H van der, Traystman R, Macleod M, Majno G, Joris I, Broughton B, Reutens D, Sobey C, Ginsberg M, Dirnagl U, Iadecola C, Moskowitz M, Lipton P, Zheng Z, Yenari M, Mehta S, Manhas N, Rahubir R, Mattson M, Culmsee C, Yu Z, Martin H, Wang Y, Won S, Kim D, Gwag B, Arundine M, Tymianski M, Mattson M, Suh S, Shin B, Ma H, Hoecke M Van, Brennan A, Yenari M, Swanson R, Choi K, Kim J, Kim G, Choi C, Allen C, Bayraktutan U, Love S, Neumar R, Hall E, Im J, Kim D, Paik S, Han P, Stoll G, Jander S, Schroeter M, Dawson V, Dawson T, Kukreja R, Xi L, Bhardwaj A, Northington F, Ichord R, Hanley D, Traystman R, Koehler R, Yamamoto E, Tamamaki N, Nakamura T, Kataoka K, Tokutomi Y, Dong Y, Fukuda M, Matsuba S, Ogawa H, Kim-Mitsuyama S, Ridder D, Schwaninger M, Chong Z, Li F, Maiese K, Luo J, Sun D, Weinstein P, Hong S, Sharp F, Kiewert C, Mdzinarishvili A, Hartmann J, Bickel U, Klein J, Sumbria R, Klein J, Bickel U, Mattson M, Ishikawa M, Zhang J, Nanda A, Granger D, Tuttolomondo A, Raimondo D Di, Sciacca R di, Pinto A, Licata G, Okun E, Griffioen K, Lathia J, Tang S, Mattson M, Arumugam T, Wang Q, Tang X, Yenari M, Gelderblom M, Leypoldt F, Steinbach K, Behrens D, Choe C, Siler D, Arumugam T, Orthey E, Gerloff C, Tolosa E, Magnus T, Zoppo G del, Milner R, Mabuchi T, Hung S, Wang X, Berg G, Koziol J, Jin R, Yang G, Li G, Zoppo G del, Hallenbeck J, Yilmaz G, Granger D, Barone F, Schmidt D, Hillegass L, Price W, White R, Feuerstein G, Clark R, Lee E, Griswold D, Sarau H, Price C, Menon D, Peters A, Ballinger J, Barber R, Balan K, Lynch A, Xuereb J, Fryer T, Guadagno J, Warburton E, Stowe A, Adair-Kirk T, Gonzales E, Perez R, Shah A, Park T, Gidday J, Matsuo Y, Onodera H, Shiga Y, Nakamura M, Ninomiya M, Kihara T, Kogure K, Hudome S, Palmer C, Roberts R, Mauger D, Housman C, Towfighi J, Yilmaz G, Arumugam T, Stokes K, Granger D, Cheng A, Arumugam T, Liu D, Khatri R, Mustafa K, Kwak S, Ling H, Gonzales C, Xin O, Jo D, Guo Z, Mark R, Mattson M, Tang S, Arumugam T, Xu X, Cheng A, Mughal M, Jo D, Lathia J, Siler D, Chigurupati S, Ouyang X, Magnus T, Camandola S, Mattson M, Arumugam T, Okun E, Tang S, Thundyil J, Taylor S, Woodruff T, Arumugam T, Chan S, Jo D, Yilmaz G, Tang S, Cheng A, Gleichmann M, Okun E, Dixit V, Chigurupati S, Mughal M, Ouyang X, Miele L, Magnus T, Poosala S, Granger D, Mattson M, Thundyil J, Tang S, Okun E, Shah K, Karamyan V, Li Y, Woodruff T, Taylor S, Jo D, Mattson M, Arumugam T, Choi Y, Gwon A, Jeong H, Park J, Baik S,

Arumugam T, Jo D, Cimino A, Balduini W, Carloni S, Gelosa P, Guerrini U, Tremoli E, Sironi L, Uchiyama Y, Koike M, Shibata M, Nagel S, Papadakis M, Hoyte L, Buchan A, Titova E, Ostrowski R, Zhang J, Tang J, Durukan A, Tatlisumak T, Woolsey T, Rovainen C, Cox S, Henegar M, Liang G, Liu D, Moskalenko Y, Sui J, Wei L, Kitagawa K, Matsumoto M, Yang G, Mabuchi T, Yagita Y, Hori M, Yanagihara T, Krakovsky M, Rogatsky G, Zarchin N, Mayevsky A, Ordy J, Thomas G, Volpe B, Dunlap W, Colombo P, Klocke R, Tian W, Kuhlmann M, Nikol S, Swan J, Evans M, Meldrum B, Herrmann M, Stern M, Vollenweider F, Nitsch C, Yonekura I, Kawahara N, Nakatomi H, Furuya K, Kirino T, Panahian N, Yoshida T, Huang P, HedleyWhyte E, Dalkara T, Fishman M, Moskowitz M, Bottiger B, Teschendorf P, Krumnikl J, Vogel P, Galmbacher P, Schmitz B, Motsch J, Martin E, Gass P, Koizumi J, Yoshida Y, Nakazawa T, Ooneda G, Memezawa H, Minamisawa H, Smith M, Siesjo B, Kawamura S, Yasui N, Shirasawa M, Fukasawa H, Arumugam T, Tang S, Lathia J, Cheng A, Mughal M, Chigurupati S, Magnus T, Chan S, Jo D, Ouyang X, Fairlie D, Granger D, Vortmeyer A, Basta M, Mattson M, Arumugam T, Selvaraj P, Woodruff T, Mattson M, McAuley M, Taguchi A, Kasahara Y, Nakagomi T, Stern D, Fukunaga M, Ishikawa M, Matsuyama T, Mdzinarishvili A, Geldenhuys W, Abbruscato T, Bickel U, Klein J, Schyf C Van der, Zhang L, Zhang Z, Zhang R, Lu M, Krams M, Chopp M, Watson B, Dietrich W, Busto R, Wachtel M, Ginsberg M, Zhao W, Ginsberg M, Prado R, Belayev L, Bacigaluppi M, Comi G, Hermann D, Acker T, Acker H, Martin R, Lloyd H, Cowan A, Taoufik E, Probert L, Yuan J, Rambani K, Vukasinovic J, Glezer A, Potter S, Zimmer J, Gahwiler B, Noraberg J, Poulsen F, Blaabjerg M, Kristensen B, Bonde C, Montero M, Meyer M, Gramsbergen J, Zimmer J, Bonde C, Noraberg J, Zimmer J, Bonde C, Noraberg J, Noer H, Zimmer J, Montero M, Poulsen F, Noraberg J, Kirkeby A, Beek J van, Leist M, Zimmer J, Cui H, Matsumoto K, Murakami Y, Hori H, Zhao Q, Obi R, Crain S, Raine C, Bornstein M, Gahwiler B, Stoppini L, Buchs P, Muller D, Mattson M, Barger S, Begley J, Mark R, Bledi Y, Domb A, Linial M, Hertz L, Peng L, Lai J, Yu A, Wong H, Yung H, Lau L, Saura J, Giulian D, Baker T, Yoshida T, Takeuchi M, Okun E, Arumugam T, Tang S, Gleichmann M, Albeck M, Sredni B, Mattson M, Ishikawa M, Cooper D, Arumugam T, Zhang T, Nanda A, Granger D, Russell J, Cooper D, Tailor A, Stokes K, Granger D, Ritter L, Orozco J, Coull B, McDonagh P, Lathia J, Chigurupati S, Thundyil J, Selvaraj P, Mughal M, Woodruff T, Chan S, Karamyan V, Mattson M, Arumugam T, Arumugam T, Phillips T, Cheng A, Morrell C, Mattson M, Wan R, Bederson J, Pitts L, Tsuji M, Nishimura M, Davis R, Bartkowski H, Li Y, Chopp M, Chen J, Wang L, Gautam S, Xu S, Zhang Z, Thompson R, Zhou N, MacVicar B, Deryck M, Arumugam T, Salter J, Chidlow J, Ballantyne C, Kevil C, Granger D, Dijkhuizen R, Nicolay K, Sung J, Cho E, Min W, Kim M, Kim M, Jung E, Koh P, Focking M, Besselmann M, Trapp T, Harrison D, Bond B, Siniscalchi A, Zona C, Sancesario G, D'Angelo E, Zeng Y, Mercuri N, Bernardi G, Badiola N, Malagelada C, Llecha N, Hidalgo J, Comella J, Sabria J, Rodriguez-Alvarez J, Mosmann T, Malagelada C, Xifro X, Minano A, Sabria J, Rodriguez-Alvarez J, Eckert B, Frey J, Tsirka S, Worp H van der, Macleod M, Kollmar R, Froehler M, Ovbiagele B, Inzitari D, Poggesi A, Danton G, Dietrich W, Cohan S, Zhang L, Andou Y, Masuda S, Mitani A, Kataoka K, Schurr A, Yam P, Dunn L, Graham D, Dewar D, McCulloch J, Kermer P, Klocker N, Bahr M, Yu Z, Bruce-Keller A, Goodman Y, Mattson M, Sydserff

S, Borelli A, Green A, Cross A, Iwashita A, Maemoto T, Nakada H, Shima I, Matsuoka N, Hisajima H, Lees K, Zivin J, Ashwood T, Davalos A, Davis S, Diener H, Grotta J, Lyden P, Shuaib A, Hardemark H, Wasiewski W, Shuaib A, Lees K, Lyden P, Grotta J, Davalos A, Davis S, Diener H, Ashwood T, Wasiewski W, Emeribe U, Legos J, Tuma R, Barone F, Prunell G, Arboleda V, Troy C, Hara H, Friedlander R, Gagliardini V, Ayata C, Fink K, Huang Z, ShimizuSasamata M, Yuan J, Moskowitz M, Robertson G, Crocker S, Nicholson D, Schulz J, Goussev A, Zhang Z, Anderson D, Chopp M, Zhang R, Chopp M, Jiang N, Tang W, Prostak J, Manning A, Anderson D, Schneider D, Berrouschot J, Brandt T, Hacke W, Ferbert A, Norris S, Polmar S, Schafer E, Furuya K, Takeda H, Azhar S, McCarron R, Chen Y, Ruetzler C, Wolcott K, DeGraba T, Rothlein R, Hugli T, Zoppo G del, Hallenbeck J, Krams M, Lees K, Hacke W, Grieve A, Orgogozo J, Ford G, Barone F, Irving E, May A, Lee J, Kassis S, Kumar S, Badger A, White R, McVey M, Legos J, Erhardt J, Nelson A, Ohlstein E, Hunter A, Ward K, Smith B, Adams J, Parsons A, Jiang X, Namura S, Nagata I, Hinsbergh V van, Koolwijk P, Beech J, Reckless J, Mosedale D, Grainger D, Williams S, Menon D, Loane D, Pocivavsek A, Moussa C, Thompson R, Matsuoka Y, Faden A, Rebeck G, Burns M, Dalakas M, Arumugam T, Woodruff T, Lathia J, Selvaraj P, Mattson M, Taylor S, Endres M, Laufs U, Rodriguez-Yanez M, Agulla J, Rodriguez-Gonzalez R, Sobrino T, Castillo J, Hernandez-Perera O, Perez-Sala D, Navarro-Antolin J, Sanchez-Pascuala R, Hernandez G, Diaz C, Lamas S, Holschermann H, Schuster D, Parviz B, Haberbosch W, Tillmanns H, Muth H, Marti-Fabregas J, Gomis M, Arboix A, Aleu A, Pagonabarraga J, Belvis R, Cocho D, Roquer J, Rodriguez A, Garcia M, Molina-Porcel L, Diaz-Manera J, Marti-Vilalta J, Alvarez-Sabin J, Huertas R, Quintana M, Rubiera M, Delgado P, Ribo M, Molina C and Montaner J (2011) Pathophysiology, treatment, and animal and cellular models of human ischemic stroke. *Molecular Neurodegeneration* 6(1): 11.

Wu D and Yotnda P (2011) Induction and testing of hypoxia in cell culture. *Journal of visualized experiments : JoVE* (54): e2899.

Wu H, Shao A, Zhao M, Chen S, Yu J, Zhou J, Liang F, Shi L, Dixon BJ, Wang Z, Ling C, Hong Y and Zhang J (2016) Melatonin attenuates neuronal apoptosis through up-regulation of K(+) -Cl(-) cotransporter KCC2 expression following traumatic brain injury in rats. *Journal of Pineal Research* 61(2): 241–50.

Xu L, Xiong X, Ouyang Y, Barreto G and Giffard R (2011) Heat shock protein 72 (Hsp72) improves long term recovery after focal cerebral ischemia in mice. *Neuroscience Letters* 488(3): 279–282.

Xu S-Y and Pan S-Y (2013) The failure of animal models of neuroprotection in acute ischemic stroke to translate to clinical efficacy. *Medical Science Monitor Basic Research* 19: 37–45.

Xu W, Mu X, Wang H, Song C, Ma W, Jolkkonen J and Zhao C (2016) Chloride Co-transporter NKCC1 Inhibitor Bumetanide Enhances Neurogenesis and Behavioral Recovery in Rats After Experimental Stroke.

Molecular Neurobiology 54(4): 2406-2414.

Yabe JT, Chan WKH, Wang FS, Pimenta A, Ortiz DD and Shea TB (2003) Regulation of the Transition From Vimentin to Neurofilaments During Neuronal Differentiation. *Cell Motility and the Cytoskeleton* 56(3): 193–205.

Yamada J, Okabe A, Toyoda H, Kilb W, Luhmann HJ and Fukuda A (2004) Cl- uptake promoting depolarizing GABA actions in immature rat neocortical neurones is mediated by NKCC1. *The Journal of Physiology* 557(3): 829–841.

Yamashita T, Ohneda O, Nagano M, Iemitsu M, Makino Y, Tanaka H, Miyauchi T, Goto K, Ohneda K, Fujii-Kuriyama Y, Poellinger L and Yamamoto M (2008) Abnormal heart development and lung remodeling in mice lacking the hypoxia-inducible factor-related basic helix-loop-helix PAS protein NEPAS. *Molecular and cellular biology* 28(4): 1285–1297.

Yan Y, Dempsey RJ, Flemmer A, Forbush B and Sun D (2003) Inhibition of Na+-K+-Cl- cotransporter during focal cerebral ischemia decreases edema and neuronal damage. *Brain Research* 961(1): 22–31.

Yang GY and Betz AL (1994) Reperfusion-induced injury to the blood-brain barrier after middle cerebral artery occlusion in rats. *Stroke* 25(8): 1658-1665.

Yang S, Cacquevel M, Saksida LM, Bussey TJ, Schneider BL, Aebischer P, Melani R, Pizzorusso T, Fawcett JW and Spillantini MG (2015) Perineuronal net digestion with chondroitinase restores memory in mice with tau pathology. *Experimental Neurology* 265: 48–58.

Yang W and Paschen W (2016) Unfolded protein response in brain ischemia: A timely update. *Journal of Cerebral Blood Flow & Metabolism* 36(12): 2044-2050.

Yeo M, Berglund K, Augustine G and Liedtke W (2009) Novel repression of Kcc2 transcription by REST-RE-1 controls developmental switch in neuronal chloride. *The Journal of Neuroscience* 29(46): 14652–14662.

Yepes M, Roussel BD, Ali C and Vivien D (2009) Tissue-type plasminogen activator in the ischemic brain: more than a thrombolytic. *Trends in Neurosciences* 32(1): 48–55.

Young W, Rappaport ZH, Chalif DJ and Flamm ES (1987) Regional brain sodium, potassium, and water changes in the rat middle cerebral artery occlusion model of ischemia. *Stroke* 18(4): 751–759.

Yu S, Cheng Q, Li L, Liu M, Yang Y and Ding F (2014) 2-(4-Methoxyphenyl)ethyl-2-acetamido-2-deoxy-d-pyranoside confers neuroprotection in cell and animal models of ischemic stroke through calpain1/PKA/CREB-mediated induction of neuronal glucose transporter 3. *Toxicology and Applied Pharmacology* 277(3): 259–269.

Yu S, Liu X, Shen Y, Xu H, Yang Y and Ding F (2016) Therapeutic benefits of combined treatment with tissue plasminogen activator and 2-(4-methoxyphenyl)ethyl-2-acetamido-2-deoxy-β-d-pyranoside in an animal model of ischemic stroke. *Neuroscience* 327:44-52.

Yu Y, Han Q, Ding X, Chen Q, Ye K, Zhang S, Yan S, Campbell BC V., Parsons MW, Wang S and Lou M (2016) Defining Core and Penumbra in Ischemic Stroke: A Voxel- and Volume-Based Analysis of Whole Brain CT Perfusion. *Scientific Reports* 10(6): 1–7.

Yuan J (2009a) Neuroprotective strategies targeting apoptotic and necrotic cell death for stroke. *Apoptosis* 14(4): 469–477.

Yuan Y, Hilliard G, Ferguson T and Millhorn DE (2003) Cobalt inhibits the interaction between hypoxia-inducible factor-alpha and von Hippel-Lindau protein by direct binding to hypoxia-inducible factor-alpha. *The Journal of Biological Chemistry* 278(18): 15911–15916.

Zador Z, Stiver S, Wang V and Manley GT (2009) Role of aquaporin-4 in cerebral edema and stroke. *Handbook of Experimental Pharmacology* (190): 159–170.

Zamanian JL, Xu L, Foo LC, Nouri N, Zhou L, Giffard RG and Barres BA (2012) Genomic analysis of reactive astrogliosis. *The Journal of Neuroscience* 32(18): 6391–6410.

Zauner A, Daugherty WP, Bullock MR, Warner DS, Selman WR and Dempsey RJ (2002) Brain oxygenation and energy metabolism: Part I - Biological function and pathophysiology. *Neurosurgery* 51 (2): 289–302.

Zhan X, Kim C and Sharp FR (2008) Very brief focal ischemia simulating transient ischemic attacks (TIAs) can injure brain and induce Hsp70 protein. *Brain Research* 1234: 183–197.

Zhang F, Liu CL and Hu BR (2006) Irreversible aggregation of protein synthesis machinery after focal brain ischemia. *Journal of Neurochemistry* 98(1): 102–112.

Zhang W, Zhang L, Hou W, Xu Y, Xu H, Lou F, Zhang Y and Wang Q (2009) Dynamic expression of glucose transporters 1 and 3 in the brain of diabetic rats with cerebral ischemia reperfusion. *Chinese Medical Journal* 122(17): 1996–2001.

Zhao H, Wang R, Wu X, Liang J, Qi Z, Liu X, Min L, Ji X and Luo Y (2015) Erythropoietin delivered via intra-arterial infusion reduces endoplasmic reticulum stress in brain microvessels of rats following cerebral ischemia and reperfusion. *Journal of Neuroimmune Pharmacology* 10(1): 153–161.

Zhao L, Yang Y-F, Gao Y-B, Wang S-M, Wang L-F, Zuo H-Y, Dong J, Xu X-P, Su Z-T, Zhou H-M, Zhu L-L and Peng R-Y (2014) Upregulation of HIF-1α

Via Activation of ERK and PI3K Pathway Mediated Protective Response to Microwave-Induced Mitochondrial Injury in Neuron-Like Cells. *Molecular Neurobiology* 50(3): 1024–1034.

Zhdanov A V., Dmitriev RI, Golubeva A V., Gavrilova SA and Papkovsky DB (2013) Chronic hypoxia leads to a glycolytic phenotype and suppressed HIF-2 signaling in PC12 cells. *Biochimica et Biophysica Acta* 1830(6): 3553–3569.

Zheleznova NN, Sedelnikova A and Weiss DS (2009) Function and modulation of delta-containing GABA(A) receptors. *Psychoneuroendocrinology* 34 Suppl 1: S67-73.

Zheng J, Zhang P, Li X, Lei S, Li W, He X, Zhang J, Wang N, Qi C, Chen X, Lu H and Liu Y (2013) Post-stroke estradiol treatment enhances neurogenesis in the subventricular zone of rats after permanent focal cerebral ischemia. *Neuroscience* 231: 82–90.

Zigova T, Barroso LF, Willing AE, Saporta S, McGrogan MP, Freeman TB and Sanberg PR (2000) Dopaminergic phenotype of hNT cells in vitro. *Developmental Brain Research* 122(1): 87–90.

del Zoppo GJ, Saver JL, Jauch EC, Adams HP and American Heart Association Stroke Council (2009) Expansion of the Time Window for Treatment of Acute Ischemic Stroke With Intravenous Tissue Plasminogen Activator: A Science Advisory From the American Heart Association/American Stroke Association. *Stroke* 40(8): 2945–2948.

del Zoppo GJ, Sharp FR, Heiss W-D and Albers GW (2011) Heterogeneity in the penumbra. *Journal of Cerebral Blood Flow and Metabolism* 31(9): 1836–1851.

Appendix: Published work resulting from this thesis:

Martín-Aragón Baudel MAS, Poole AV. and Darlison MG (2017) Chloride co-transporters as possible therapeutic targets for stroke. *Journal of Neurochemistry* 140(2): 195–209.

Martín-Aragón Baudel MAS, Rae MT, Darlison MG, Poole AV, Fraser JA (2017) Preferential activation of HIF-2α adaptive signalling in neuronal-like cells in response to acute hypoxia. *PLoS One* 12(10): e0185664

PLOS ONE

RESEARCH ARTICLE

Preferential activation of HIF-2α adaptive signalling in neuronal-like cells in response to acute hypoxia

Miguel A. S. Martín-Aragón Baudel, Mick T. Rae, Mark G. Darlison, Amy V. Poole, Jennifer A. Fraser*

School of Applied Sciences. Edinburgh Napier University, Sighthill Campus, Edinburgh, United Kingdom

* j.fraser@napier.ac.uk

OPEN ACCESS

Citation: Martín-Aragón Baudel MAS, Rae MT, Darlison MG, Poole AV, Fraser JA (2017) Preferential activation of HIF-2α adaptive signalling in neuronal-like cells in response to acute hypoxia. PLoS ONE 12(10): e0185664. https://doi.org/10.1371/journal.pone.0185664

Editor: George Simos, University of Thessaly Faculty of Medicine, GREECE

Received: June 28, 2017

Accepted: September 16, 2017

Published: October 2, 2017

Data Availability Statement: All relevant data are within the paper.

Funding: The authors received no specific funding for this work. Reagents and consumables used in this work were provided through Edinburgh Napier University's internal postgraduate student research budget.

Competing interests: The authors have declared that no competing interests exist.

Abstract

Stroke causes severe neuronal damage as disrupted cerebral blood flow starves neurons of oxygen and glucose. The hypoxia inducible factors (HIF-1α and HIF-2α) orchestrate oxygen homeostasis and regulate specific aspects of hypoxic adaptation. Here we show the importance of HIF-2α dependant signalling in neuronal adaptation to hypoxic insult. PC12 and NT2 cells were differentiated into neuronal-like cells using NGF and retinoic acid, and exposed to acute hypoxia (1% O_2). Gene and protein expression was analysed by qPCR and immunoblotting and the neuronal-like phenotype was examined. PC12 and NT2 differentiation promoted neurite extension and expression of neuronal markers, NSE and KCC2. Induction of HIF-1α mRNA or protein was not detected in hypoxic neuronal-like cells, however marked induction of HIF-2α mRNA and protein expression was observed. Induction of HIF-1α target genes was also not detected in response to acute hypoxia, however significant induction of HIF-2α transcriptional targets was clearly evident. Furthermore, hypoxic insult dramatically reduced both neurite number and length, and attenuated expression of neuronal markers, NSE and KCC2. This correlated with an increase in expression of the neural progenitor and stem cell-like markers, CD44 and vimentin, suggesting HIF-2α molecular mechanisms could potentially promote regression of neuronal-like cells to a stem-like state and trigger neuronal recovery following ischaemic insult. Our findings suggest the HIF-2α pathway predominates over HIF-1α signalling in neuronal-like cells following acute hypoxia.

Introduction

Blockage of cerebral arteries starves neurons of oxygen and glucose, triggering a cascade of events leading to irreversible cell death [1]. The tissue surrounding the blockage is partially perfused, therefore neurons here are vulnerable, yet salvageable, and must adapt to survive, to prevent further loss of neuronal tissue [2].

The hypoxia inducible factors (HIFs) are master regulators of oxygen homeostasis and critical for adaptation to hypoxic insult [3]. The HIF alpha subunit exist as three isoforms; HIF-1α,

-2α and -3α. HIF-1α and 2α are structurally similar and share common transcriptional targets, including *Slc2A1* and *VEGF* [4,5]. HIF-1α and -2α also regulate distinct subsets of genes and elicit different cellular fates. *HIF-1α* regulates *Pdk* and *LdhA* expression to maintain metabolism, and can activate *Bnip3* to trigger apoptosis, whilst *HIF-2α* promotes angiogenesis, cell division and tissue regeneration by regulating the expression of *EPO*, *Cyclin D1* and the stem cell marker, *Oct4*, respectively [4,6]. By contrast, HIF-3α exists in several alternatively spliced forms and may negatively regulate HIF-1α and -2α [7–9].

There has been considerable interest in the importance of HIF regulated pathways in the pathogenesis of stroke yet their role in stroke pathophysiology, particularly *HIF-1α*, is controversial. Targeted knockout of neuronal *HIF-1α* increased ischaemic damage, infarct volume and mortality following transient cerebral artery occlusion [10], whilst indirect induction of *HIF*, via genetic ablation of *Phd2*, reduced infarct size and improved sensorimotor function following transient ischaemia [11], suggesting *HIF-1α* mediated adaptation may be neuroprotective. However, neuronal-specific knockdown of *HIF-1α* and *HIF-2α* expression was shown to decrease infarct size and improve neuronal survival in the early acute stages of middle cerebral artery occlusion [12], suggesting *HIF* signalling could contribute to stroke-associated damage.

HIF-1α and *-2α* display temporal differences in signalling[6]; *HIF-1α* appears to be involved in adaptation to acute hypoxia whilst *HIF-2α* mediates adaptation to chronic hypoxic stress [13]. The timescale of HIF signalling may therefore be critical for effective recovery from stroke. Indeed, whilst ablation of neuronal *HIF-1α* and *HIF-2α* is reported to be beneficial in the hours following stroke, loss of *HIF-1α* and *-2α* correlated with increased apoptosis and reduced sensorimotor function in later stages [12]. This may be due to the importance of angiogenesis in stroke-associated neurogenesis [14,15] and *HIF's* key role in tuning *VEGF* signalling and angiogenesis [5,16]. These studies highlight the intricacies of HIF signalling, and their potential importance in neuroprotection and recovery from stroke damage.

Adaptation is central to neuronal recovery and stroke repair, however therapies promoting neuronal repair and regeneration are currently lacking. Fully understanding the adaptive mechanisms triggered in response to stroke is essential to develop novel therapeutics to enhance neuronal repair and regeneration, and limit the damage and disability associated with stroke [17].

In this study, neuronal cell lines were used as a model to study the molecular changes occurring in response to acute hypoxic stress. We observed preferential activation of HIF-2α dependant adaptive mechanisms in neuronal-like cells in response to acute hypoxia and an absence of HIF-1α dependant signalling. We also observed increased expression of neural progenitor stem cell-like markers, thought to be transcriptionally regulated by HIF-2α. Together, these findings underscore the importance of HIF-2α signalling in neuronal adaptation following acute hypoxic stress and highlight the potential for neuronal repair and regeneration.

Experimental procedures

Cell culture

PC12, NT2 and MCF7 cell lines were obtained from the American Type Culture Collection (ATCC). NT2 and MCF7 cells were maintained in Dulbecco's Modified Eagle's Media (DMEM, Gibco) supplemented with 10% (v/v) heat-inactivated foetal bovine serum (FBS, Sigma) and 1% (v/v) penicillin-streptomycin (Sigma). PC12 culture media was also supplemented with 5% (v/v) heat-inactivated horse serum (Sigma). Cells were grown at 37˚C in 5% (v/v) CO_2 atmosphere under high humidity.

PC12 and NT2 differentiation

PC12 cells were cultured on poly-L-lysine (0.1 mg/mL, Sigma) coated 6-well plates at a density of $2x10^6$ cells/well. After 24 hours, media was replaced with differentiation media (200 nM nerve growth factor (NGF; Sigma, Cat no: N0513), 1% (v/v) horse serum (Sigma) and 1% (v/v) penicillin-streptomycin in DMEM), and replenished every 2–3 days. NT2 cells were differentiated into a neuronal population by the method by Pleasure *et al*., (1992)[18]. Briefly, cells were seeded at 1 $x10^6$ in a T75 flask and grown in complete culture media containing all-trans-retinoic acid (ATRA, Sigma, 10 μM); media was replaced twice per week. After 4 weeks of ATRA treatment, NT2 cells were sub-cultured and grown for a further 2 weeks in media containing cytosine arabinoside (1 μM) and fluorodeoxyuridine (10 μM); media was replenished every 3–4 days. Cell morphology was analysed via bright field microscopy and images were captured using an inverted microscope and camera (Zeiss, Primovert and Axiocam) at 20x magnification.

AlamarBlue. Cells were seeded at 10^5 cells/well in a 96-well plate. After 24 hours, media was removed and 100 μL fresh media was added per well. AlamarBlue (ThermoFisher) was added to a final concentration of 10% (v/v). Negative controls contained media only without cells. Absorbance was measured at 550 nm and 600 nm using a plate reader (Elisa Reader LT-5000MS, LabTech International Ltd., Uckfield, UK) and data analysed using Manta software. Normoxic cells were taken to represent 100% mitochondrial activity and results were expressed as a percentage of mitochondrial activity compared to normoxic conditions.

Trypan blue staining. Cell number was determined using a Neubauer bright line haemocytometer and trypan blue (Sigma) staining. Following trypsinisation, cells were resuspended in complete media and diluted 1:1 (v/v) with trypan blue. The number of viable and non-viable cells were counted using a haemocytometer and the average viable:non-viable ratio was recorded as the total viable cells/mL. The percentage of viable cells (%) was calculated as: [1.00 –(number of trypan blue positive cells/number of total cells)] × 100.

Experimental hypoxia

Acute hypoxia was induced in PC12 and NT2 cells following differentiation. MCF7 cells were seeded 24 hours prior to the induction of hypoxia at a density of 2 $x10^6$ cells/well in a 6 well dish. Cells were placed in a modular hypoxic chamber (Billups-Rothenberg, Inc.) and hypoxia was induced following the method by Wu and Yotnda (2011)[19]. Briefly, the chamber was sealed and flushed with 1% O_2 gas mixture at a flow rate of 20 L/minute for 10 minutes then incubated at 37˚C in a 5% CO_2 incubator. After 1 hour, the chamber was purged again with 1% O_2 gas mixture at 20 L/minute for a further 10 minutes then incubated at 37˚C in a 5% CO_2 incubator for the remainder of the experimental exposure. The pH of the media remained stable using these hypoxic conditions.

RNA extraction and analysis

Cells were harvested on ice by scraping into ice cold PBS and collected by centrifugation at 4˚C at 3000 rpm in a benchtop centrifuge. RNA was extracted using Tri reagent (Ambion) at a ratio of 1 mL per $1x10^6$ cells following the manufacturer's instructions. RNA concentrations were determined using a NanoDrop spectrophotometer (ThermoFisher Scientific). RNA purity and integrity was assessed by Bioanalyzer (Agilent) and only samples with an RNA integrity number (RIN) >7 were used for downstream analysis. cDNA was synthesised using the nanoScript 2 Reverse Transcription premix kit (Primer Design) according to the manufacturer's instructions using a thermal cycler (Applied Biosystems Light Cycler 480).

Table 1. The forward (F) and reverse (R) oligonucleotides used in this study.

Target gene	Sequence 5'-3'	Species specificity
CA9	F:AGGGTGTCATCTGGACTGTG, R:TGTGTGGCTCGGAAGTTCAG	Human/Rat
Caspr1	F:TGACTCTGAACTTGGAGGGTCGTG, R:TATAGCGCATCCATGTGCCAGTCT	Human/Rat
CD44	F:GGATCAGGCATTGATGATGATGA, R:TTGGGTTCCACTGGGTCC	Human/Rat
CHOP	F: AGCTGGAAGCCTGGTATGAGG, R: GTGCTTGTGACCTCTGCTGG	Human/Rat
Grp78	F:TATGGTGCTGCTGTCCAGG, R:CTGAGACTTCTTGGTAGGCAC	Human/Rat
HIF-1α	F:GTACCCTAACTAGCCGAGGAAGAA, R:GTGAATGTGGCCTGTGCAGT, F:GCATCTCCACCTTCTACCC, R: CTCTTTCCTGCTCTGTCTG,	Human [21], Rat [22]
HIF-2α	F:ACCTGGAAGGTCTTGCACTGC, R:TCACACATGATGATGAGGCAGG	Human/Rat
HIF-3α	F:AGGATTGCAGAAGTGGCTGG, R:ATACTGCCCTGTTACTGCCTG	Human/Rat
NEFH	F:AGGAGTGGTTCCGAGTGAG, R:GGAGATAACTGAGTACCGGC	Human/Rat
Nrn1	F:GCATCTGGTGAATAATCGCTCACG, R:ACTGAAGGAGGCGACGACAATAGC	Human/Rat
PDI	F:TGCCCAAGAGTGTGTCTGAC, R:CTGGTTGTCGGTGTGGTC	Human/Rat
Ptbp2	F:TTTGTCCGGTTCGGCAATGG, R:GGACTACTGAGAACACTGCCTG	Human/Rat
SLC2A1	F:GCTGTGCTTATGGGCTTCTC, R:CACATACATGGGCACAAAGC, F:CCTTGCCTGAGACCAGTTGAA, R: ACAGCAGGGCAGGAGTGTC	Human, Rat [23]
SLC2A3	F:CAATGCTCCTGAGAAGATCATAAAGG, R:GAATTGCGCCTGCCAAAG, F:CGCCTGATTATTGGCATCTT, R: TCCAAACCAAAGACCTGAGC	Human, Rat [24]
Tmod1	F:GCTCTTGCTGAAATGCTGAA, R:AAGGCTGGCTCTGGTTGTC	Human/Rat
Vimentin	F:AGATTCAGGAACAGCATGTCC, R:AGCCTCAGAGAGGTCAGC	Human/Rat

https://doi.org/10.1371/journal.pone.0185664.t001

Quantitative real-time PCR (qPCR)

Oligonucleotides were obtained from MWG Eurofins (UK) and are listed in Table 1. qPCR reactions (20 μL) containing 300 nM oligonucleotides, 1X PrimerDesign Precision qPCR Mastermix, and 25 ng of cDNA in RNAse/DNAse free DEPC-H_2O. Controls included reactions containing cDNA from a reaction without reverse transcriptase (negative control) and cDNA replaced with nuclease-free water (template negative). Reactions were performed in triplicate using a StepOne™ Real Time PCR system (Applied Biosystems) under standard conditions and analysed using StepOne™ Software, V2.2. Stable reference genes were identified via Genorm analysis (PrimerDesign, UK) from a panel of 12 human or rat reference genes. Gene stability was calculated with *qbase+* software (Biogazelle). Expression of target genes were analysed relative to topoisomerase (*TOP1*) in PC12 cells and beta actin (*ACTB*) in NT2 and MCF7 cells and quantified using the 2–[delta][delta]Ct method [20].

Immunostaining

Cells were lysed in NP-40 lysis buffer (50 mM Tris, pH 8, 150 mM NaCl, 5mM EDTA, 1% NP-40) containing 1X Halt™ protease inhibitor cocktail (ThermoFisher) for 30 minutes on ice and clarified by centrifugation at 4˚C at 13000 rpm for 5 minutes. Protein concentrations were estimated by bicinchoninic acid assay (BCA) analysis[25] and samples were prepared in reducing Laemmli buffer (Sigma) and boiled before use. Twenty micrograms of cell lysate was resolved via 8, 10 or 12% SDS-polyacrylamide gel, transferred to 0.45 μm nitrocellulose membrane (Millipore) and blocked with 5% (w/v) non-fat milk (Marvel) in TBS-tween (0.1% v/v) for 1 hour. Protein expression was analysed via immunoblotting using anti-NSE (AbCam, #AB16808), anti-KCC2 (Merck Millipore, #07–432), anti-actin (Santa Cruz, #SC-1615), anti-HIF1α (BD Sciences, #610958; Abcam, #ab1), anti-HIF-2α (1:500, R&D Systems, #AF2886), anti-HIF-3α (Acris antibodies, #AP20606PU-N), anti-CD44 (CST, #5640) or anti-Vimentin

(BD Sciences, #550513) at a dilution of 1:1000 in 3% non-fat milk in 1x TBS-tween (0.1% v/v). Anti-goat 680LT (LI-COR, #925–68024), anti-rabbit 680LT (LI-COR, #925–68021) and anti-rabbit 800 CW (LI-COR, #925–32280) IRDye conjugated secondary antibodies, were used at a dilution of 1:10000 in 5% (w/v) non-fat milk in 1x TBS-tween (0.1% v/v) containing 0.01% SDS. Membranes were imaged using a LI-COR Odyssey imaging system (LI-COR, Cambridge, UK) and analysed using Image Studio v2.0.

Statistical analysis

All analyses were conducted using GraphPad Prism v7.0 (GraphPad Software Inc). Results are shown as the mean ± SEM, where n = 3. For single comparisons, significance was determined using unpaired Student's *t-test*; for multiple comparisons relative to untreated values, significance was determined using ANOVA with Dunnett's correction; $^{*}p<0.05$; $^{**}p\leq0.01$; $^{***}p\leq0.001$.

Results

Characterising the *in vitro* changes associated with the neuronal-like phenotype

PC12 cells were treated with 200 nM NGF and differentiation into neuronal-like cells was assessed morphologically. NGF treatment of PC12 cells rapidly initiated signs of differentiation. Untreated cells presented with round cell bodies, however after 3 days NGF treatment, PC12 cells developed neurite-like projections (Fig 1A). After 8 days, PC12 cells displayed a typical neuronal-like morphology with long projections and interlaced axon-like structures (Fig 1A, white arrow).

The relative expression of neuronal markers during PC12 cell differentiation was assessed by qPCR. *Neuritin 1 (Nrn1)* and *tropomodulin 1 (Tmod1)* expression was significantly increased ($p = 0.004$ and $p<0.001$ compared to untreated cultures) in PC12 cells after 8 days of NGF treatment (Fig 1B). By contrast, *contactin associated protein 1 (Caspr1)* expression was downregulated ($p = 0.4331$) by NGF treatment (Fig 1B). As *Nrn1*, and *Tmod1* are characteristically expressed in neurons[26,27], their upregulation supports the morphological neuronal-like changes in PC12 cells (Fig 1A).

Human NT2 cells differentiate into neuronal-like cells following all-trans-retinoic acid (ATRA) treatment[28]. NT2 cells started to produce axonal-like structures one week after ATRA treatment (data not shown), and these structures became thicker and longer after extended culture in ATRA (Fig 1C). NT2 cells also displayed longer projections and a typical neuronal morphology; ganglion-like clusters (Fig 1C, central panel, black arrow) and interlaced axon-like structures (Fig 1C, right panel, white arrow), as observed in primary neuronal cultures[29]. A homogenous population of neuronal-like cells was produced by sub-culturing NT2 in the presence of mitotic inhibitor, cytosine β-D-arabinofuranoside (C-Ara), to remove non-differentiated cells.

Nrn1, *Tmod1* and *Caspr1* expression was also assessed in NT2 cells (Fig 1D). Like PC12 cells, expression of *Nrn1* and *Tmod1* significantly increased ($p<0.001$) in NT2 cells during differentiation (Fig 1D). By contrast, *Caspr1* expression was significantly downregulated ($p = 0.004$) by ATRA treatment (Fig 1D). These results support the observed phenotypic changes in NT2 (Fig 1C) and are characteristic of neuronal differentiation [30,31].

Given the current interested in the chloride co-transporters (CCC) and their potential role in neuronal adaptation to ischaemic stroke [32], expression of neuron-specific enolase (NSE) [33] and the neuronal specific chloride co-transporter, KCC2 [34], were analyzed by

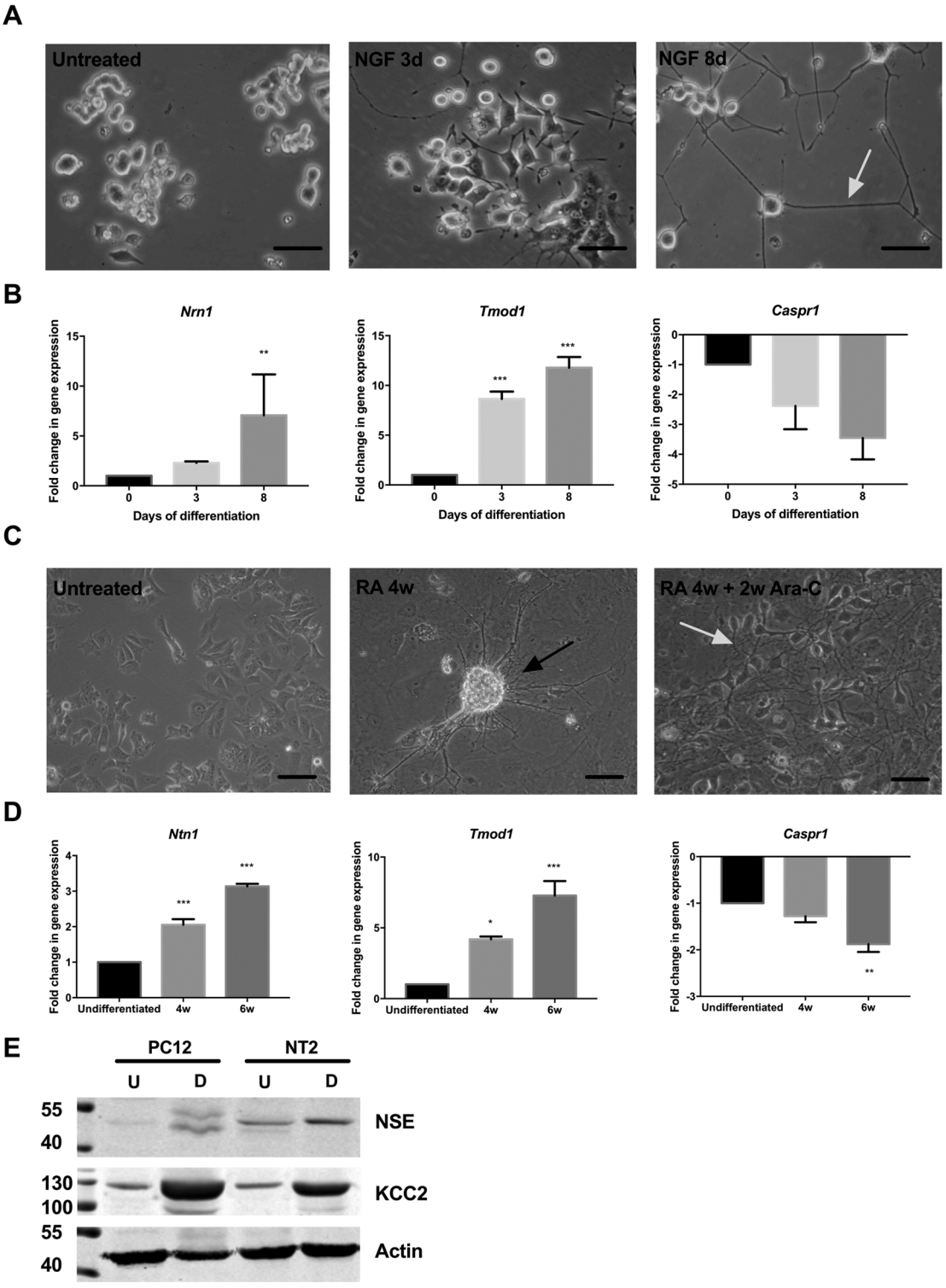

Fig 1. Characterising PC12 and NT2 morphology, gene and protein expression following differentiation into neuronal-like cells. A: Representative bright-field microscopy images of PC12 cell morphology after 3 and 8 days in the presence of NGF, (20x magnification). **B:** Relative *Nrn1*, *Tmod1* and *Caspr1* mRNA expression in differentiated PC12 cells was analysed by qPCR. **C:** Representative bright-field microscopy images of NT2 cell morphology were taken 4 weeks after treatment with all-trans-retinoic acid (ATRA 4w) and a further 2 weeks after treatment with cytosine arabinoside (Ara-C) (ATRA 4w + 2w Ara-C); (20x magnification). **D:** Relative *Nrn1*, *Tmod1* and *Caspr1* mRNA expression

in differentiated NT2 cells was analysed by qPCR. **E:** Representative immunoblot analysis showing NSE and KCC2 protein expression in undifferentiated (U) and differentiated (D) PC12 and NT2 cells. Equal protein loading was assessed by immunoblotting for actin. **A** and **C:** Scale bar represents 50 μm; white arrows indicate interlaced axon-like structures and black arrows indicate ganglion-like clusters. **B** and **D**: Data is presented as the mean ± SEM; n = 3; **p≤0.01, ***p≤0.001.

https://doi.org/10.1371/journal.pone.0185664.g001

immunoblotting (Fig 1E). Low basal KCC2 and NSE expression was detected in both PC12 and NT2 cells (Fig 1E) and a striking increase in expression of both markers was observed upon differentiation, particularly KCC2. Together, these data indicate differentiation of PC12 and NT2 cells induces changes in morphological, gene and protein expression, consistent with a neuronal-like phenotype.

Determining PC12 and NT2's response to hypoxia

Mitochondrial activity was analysed in differentiated PC12 and NT2 cells, 2, 4, 8 and 24 hours after hypoxia via alamarBlue to determine a suitable exposure time for hypoxia (Fig 2A). Induction of hypoxia and the hypoxic response is well characterised in MCF7 cells [35,36], so these were included as a positive control throughout this study to verify acute hypoxic conditions were achieved. Little reduction in activity was observed 2 hours post-hypoxia, however a dramatic reduction in activity ($p<0.001$) was observed after 4 hr in all cell lines (Fig 2A). PC12 and MCF7 cells showed an intense decrease in activity at 4, 8 and 24 hr (Fig 2A), whilst NT2 cells were more resistant to hypoxic insult at these time points (Fig 2A).

The effect of acute hypoxia on viability of differentiated PC12 and NT2 cells was also assessed by their ability to exclude trypan blue dye. Eight hours of acute hypoxia significantly decreased PC12, NT2 and MCF7 cell viability ($p<0.001$); using this method, NT2 cells were more sensitive than PC12 cells to hypoxic insult (Fig 2B). Longer exposure to acute hypoxia (24 hours) resulted in a large number of detached cells (data not shown). Therefore, eight hours hypoxic insult was used in all subsequent experiments (unless otherwise stated) as it maintained sufficient viable cellular material for analysis. Detached cells were removed and only viable cells were analysed.

Increased HIF-2α stability is observed in hypoxic neuronal-like PC12 and NT2 cells

Neuronal-like PC12 and NT2 cell adaptation to acute hypoxic stress was investigated by assessing *HIF-1α*, *HIF-2α* and *HIF-3α* gene expression. MCF7 cells were included as a positive control to verify acute hypoxia was successfully induced. *HIF-1α* mRNA expression was detected in all three cell lines, however a significant reduction in *HIF-1α* expression ($p = 0.008$) was observed in PC12 cells following hypoxia, and only a small increase in expression ($p = 0.02$) was observed in NT2 cells (Fig 3A). By contrast, and in keeping with work by others [35], MCF7 cell displayed a dramatic 11.3-fold up-regulation of *HIF-1α* mRNA ($p<0.001$), 8 hr after hypoxia (Fig 3A). Hypoxia triggered a significant increase ($p<0.001$) in *HIF-2α* mRNA expression in differentiated PC12 and NT2 cells (Fig 3A, 2.4- and 2.6- fold respectively) whilst *HIF-2α* expression in hypoxic MCF7 cells was significantly decreased ($p<0.001$). *HIF-3α* mRNA showed relatively stable levels of expression in PC12 and NT2 cells and was relatively unchanged in response to hypoxia (Fig 3A). By contrast, *HIF-3α* mRNA was upregulated ($p = 0.0037$) in MCF7 cells by hypoxic insult (Fig 3A).

HIF-1α protein undergoes post-translational stabilisation in response to hypoxic stress [37] (summarised in Fig 4). HIF-1α expression was analysed by immunoblotting using commercially available antibodies recognising distinct HIF-1α epitopes (400–550 aa and 610–727 aa).

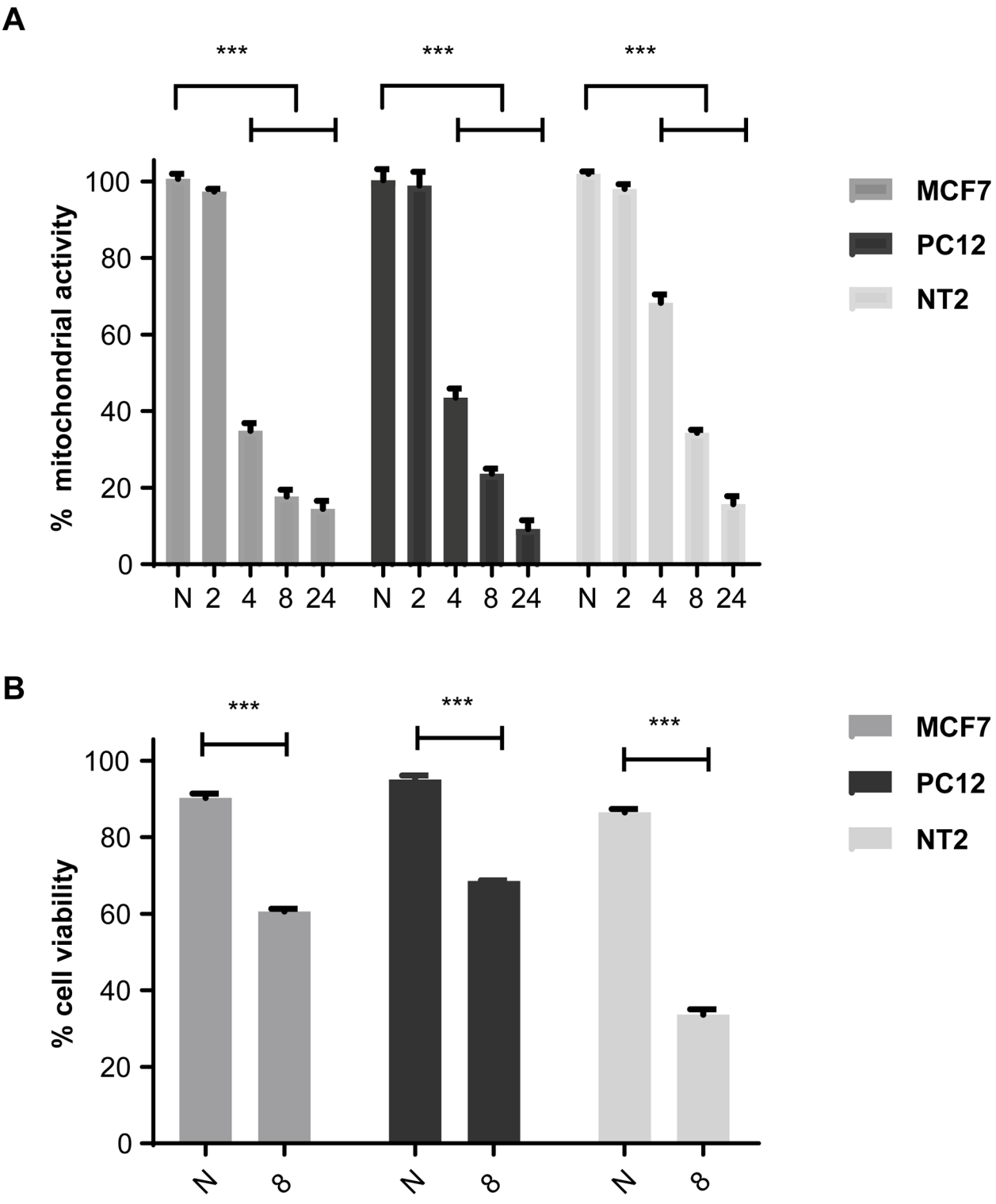

Fig 2. The effect of hypoxia on neuronal-like PC12 and NT2 cells. A: MCF7, PC12 and NT2 mitochondrial activity was analysed using alamarBlue 2, 4, 8 and 24 hours after exposure to hypoxia and expressed as a percentage of normoxic cell activity. **B:** MCF7, PC12 and NT2 cell viability was analysed via trypan blue staining 8 hours after exposure to hypoxia (8) and compared to staining of normoxic (N) cells. Data is expressed as mean ± SEM; n = 3; ***$p \leq 0.001$.

https://doi.org/10.1371/journal.pone.0185664.g002

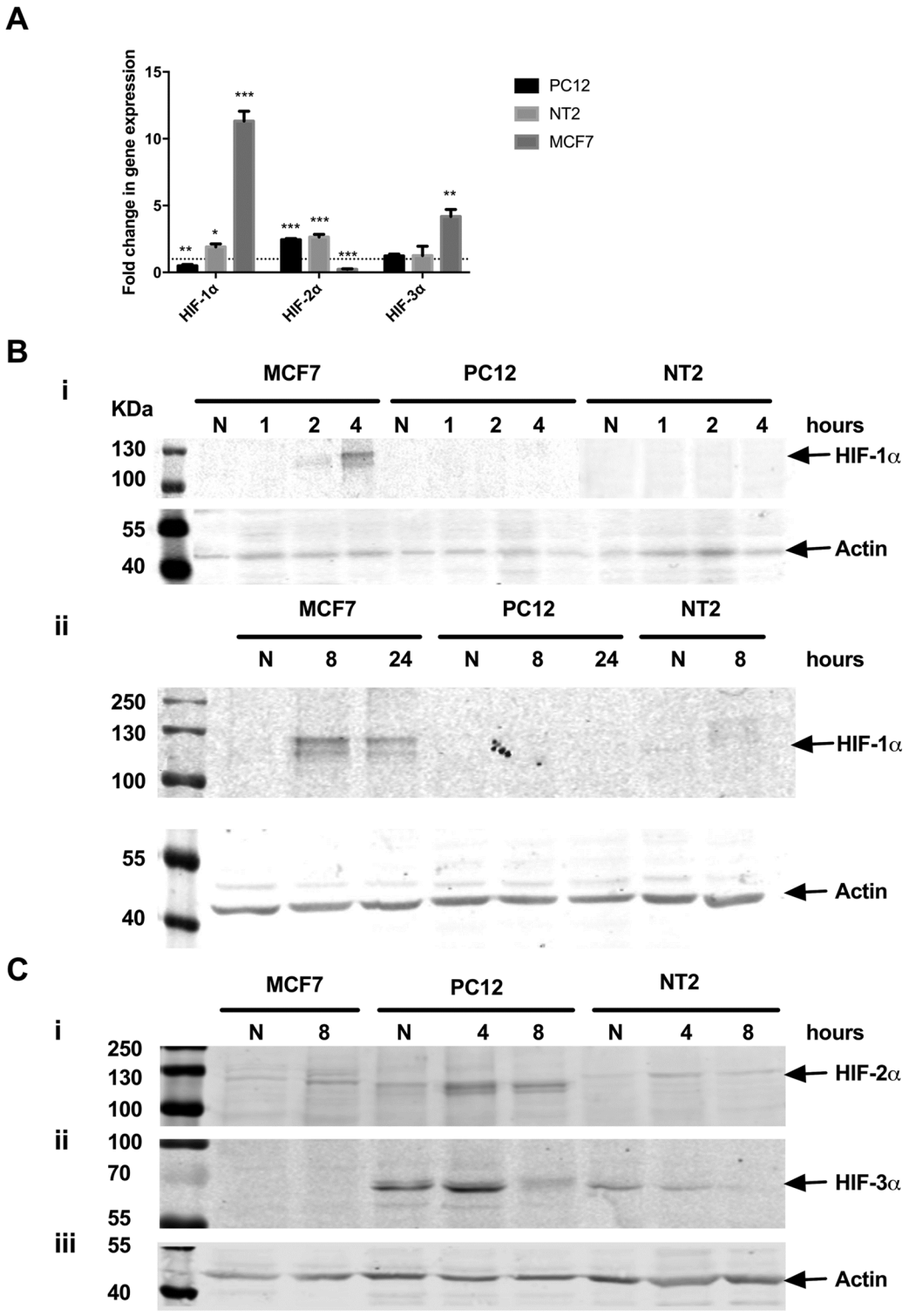

Fig 3. Increased HIF-2α stability is observed in neuronal-like PC12 and NT2 cells following hypoxia. A: Relative *HIF1-3α* mRNA expression was analysed in MCF7 and differentiated PC12 and NT2 cells exposed to 8 hours of hypoxia by qPCR. Data is expressed as mean ± SEM; n = 3; *p<0.05, **p≤0.01, ***p≤0.001. The dotted line represents basal gene expression. **B-C:** Representative immunoblots of HIF-1α (**B**), HIF-2α (**Ci**), HIF-3α (**Cii**) protein expression in MCF7 and differentiated PC12 and NT2 cells, 1, 2, 4, 8 or 24 hours after exposure to hypoxia. **B** and **C**: Equal protein loading was assessed by immunoblotting for actin.

https://doi.org/10.1371/journal.pone.0185664.g003

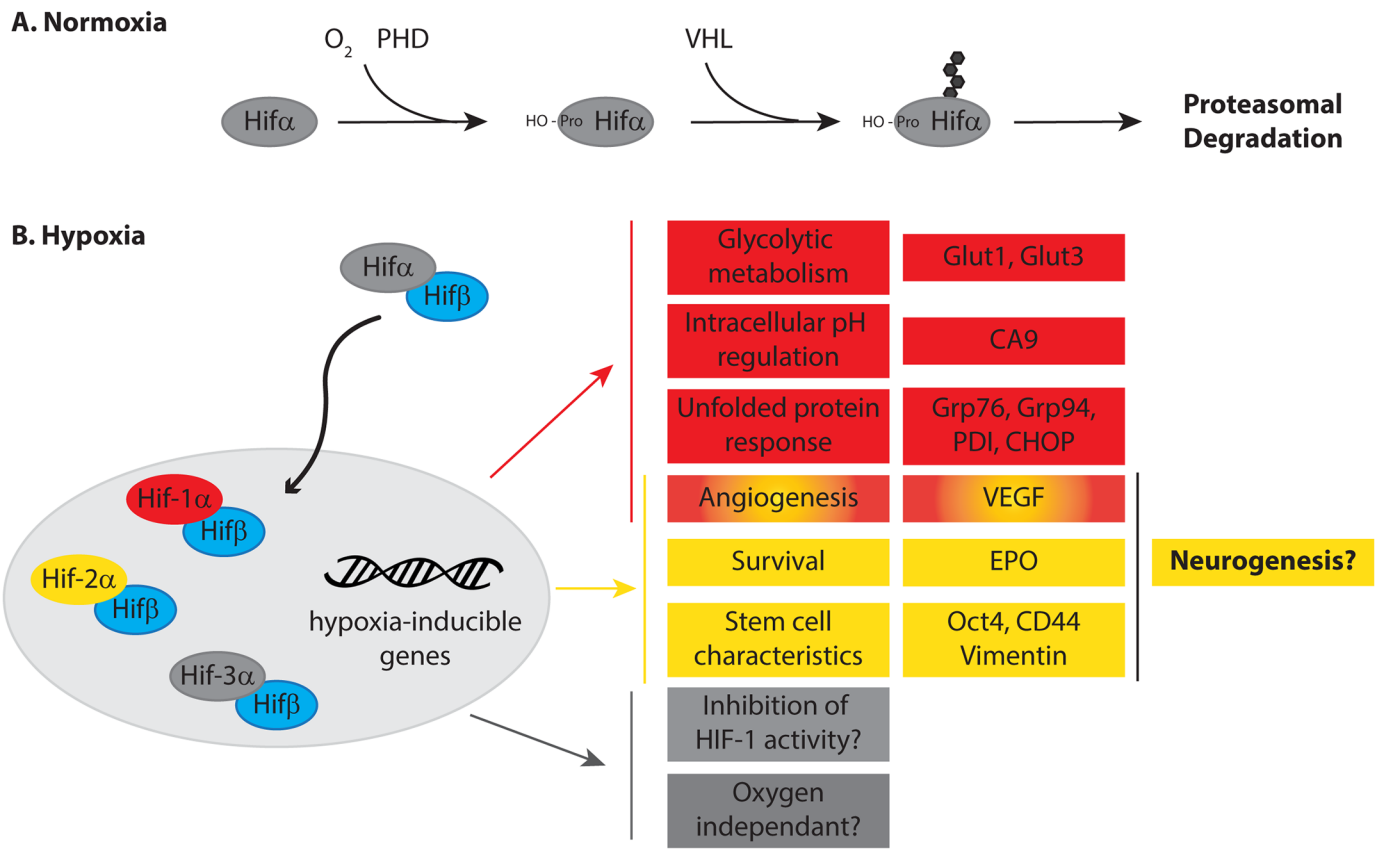

Fig 4. HIF mediated adaptation to hypoxic stress. A: Under physiological oxygen concentrations, HIF-1α/2α are hydroxylated by prolyl hydroxylases (PHD), promoting HIF-1α/2α binding to the E3 ligase, von Hippel-Lindau protein (pVHL), and their ubiquitination [3]. This maintains very low basal expression of HIF-1α/2α due to rapid proteasomal degradation. **B:** Under hypoxic conditions, PHD activity is inhibited [38]. This stabilises HIF-1α/2α expression, enhancing binding to HIFβ and translocation to the nucleus and transcription of various hypoxia-responsive genes[3]. HIF-1α and -2α share regulation of several genes, yet also regulate distinct subsets [4,6]. HIF-3α function is not yet fully understood. Abbreviations: CHOP, CCAAT-enhancer-binding protein homologous protein; EPO, Erythropoietin; Grp, Glucose regulated protein; HIF: Hypoxia Inducible Factor; PDI, protein disulphide isomerase; PHD, Prolyl hydroxylase; VEGF, Vascular epithelial growth factor; VHL, Von Hippel Lindau.

https://doi.org/10.1371/journal.pone.0185664.g004

A variety of conditions and antibody dilutions were tested however, HIF-1α induction in response to hypoxia was not detected in differentiated PC12 at any of the time points analysed (Fig 3B) and only a very slight increase in HIF-1α expression was detected in differentiated NT2 cells. By contrast, HIF-1α induction was clearly detected in MCF7 cells (Fig 3B, panel i and ii) after 2 hours of hypoxia and reached a maximum induction after 4–8 hours (Fig 3B, panel ii). HIF-1α induction in MCF7 verifies the validity of the experimental conditions and antibodies used here.

Bands corresponding to HIF-2α were readily detected in PC12, NT2 and MCF7 cells and their intensity increased after 4 hours of hypoxia (Fig 3C, panel i). HIF-3α expression was evident in both neuronal-like cell lines under normoxic conditions (Fig 3C, panel ii) however, a differential response to hypoxia was observed between PC12 and NT2 cells. HIF-3α expression was initially induced by hypoxia in PC12 cells yet reduced below basal expression at 8 hours (Fig 3D). By contrast, the intensity of HIF-3α expression progressively decreased in NT2 cells after 4 hours of hypoxia (Fig 3D). HIF-3α expression was not detected in MCF7 cells under either normoxic or hypoxic conditions.

Together, these findings suggest that under the experimental conditions tested here, HIF-1α is not stabilised in response to acute hypoxia in the neuronal-like cell models examined. The observed induction of HIF-2α and HIF-3α mRNA and protein expression suggests neuronal-like cells may activate different arms of the hypoxic adaptive machinery and HIF-2α mediated signalling may predominate over HIF-1α signalling in hypoxic neuronal-like cells.

Hypoxic adaption via HIF-2α predominates in neuronal-like cells

To further analyse potential differences in hypoxic adaptation in neuronal-like cells, regulators of *HIF-1α* and *HIF-1α* signalling were investigated. *Ptbp2* (poly pyrimidine track binding protein 2), binds the internal ribosome entry site in *HIF-1α*'s 5′-UTR, promoting efficient HIF-1α translation and up-regulation during hypoxia [39]. Carbonic anhydrase, isoform 9 (*Ca9*) contains a hypoxia-responsive element in its promoter [40] and is dramatically up-regulated following hypoxia via HIF-1α transcriptional regulation [41].

Ptbp2 and *Ca9* gene expression was analysed by qPCR (Fig 5A). Increased *Ptbp2* expression was observed in hypoxic neuronal-like PC12 ($p = 0.0069$) and NT2 cells ($p<0.001$), while little change in *Ptbp2* expression was observed in hypoxic MCF7 cells (Fig 5A). By contrast, *Ca9* expression remained relatively unchanged in hypoxic PC12 and NT2 cells (Fig 5A) yet was significantly upregulated in MCF7 cells ($p<0.001$). This is in keeping with HIF-1α dependant regulation of *Ca9* expression [41] and the observed lack of HIF-1α induction in neuronal-like cells (Fig 3).

Slc2A1 and Slc2A3 encode the glucose transporters, GLUT1 and 3, and their expression is regulated by HIF-1α and HIF-2α [42]. *Slc2A1* expression was significantly increased in neuronal-like PC12 ($p = 0.007$) and NT2 cells ($p = 0.004$), and MCF7 cells in response to hypoxia (Fig 5A). A small but significant increase in *Slc2A3* expression was also detected in neuronal-like PC12 ($p = 0.02$) and NT2 cells ($p = 0.01$) following hypoxia (Fig 5A) however *Slc2A3* expression was not detected in MCF7 cells or induced by hypoxic insult (Fig 5A), in keeping with GLUT3's status as a neuronal specific glucose transporter [43].

Hypoxic neuronal-like cells are more resistant to ER stress

Hypoxic stress triggers accumulation of misfolded proteins in the endoplasmic reticulum (ER) [44]. The unfolded protein response (UPR) serves to redress ER homeostasis by fine-tuning protein translation and enhancing folding capacity [45]. Growing evidence suggests HIF and UPR dependent pathways interact to coordinate gene expression, metabolism and cell survival [46].

Expression of UPR markers, *Grp78*, *PDI* and *CHOP*, was measured via qPCR in neuronal-like PC12 and NT2 cells, 8 hours after hypoxic insult (Fig 5B). *Grp78* expression was unchanged by hypoxia in PC12 and NT2 cells yet was significantly increased ($p = 0.0086$) in MCF7 cells (Fig 5B). *CHOP* expression was also unchanged by hypoxia in NT2 cells yet was significantly reduced in hypoxic PC12 cells ($p = 0.0039$) and increased in hypoxic MCF7 cells ($p = 0.0064$) (Fig 5B). *PDI* expression was relatively unchanged in hypoxic PC12 cells but showed a small but significant reduction ($p = 0.0260$) in hypoxic NT2 cells (Fig 5B). Collectively, this suggests neuronal-like cells present a higher resistance to ER stress following acute hypoxia under our experimental conditions.

Hypoxic adaption in neuronal-like cells drives expression of genes associated with a neuronal progenitor phenotype

Whilst HIF-1α and -2α share target genes, HIF-2α regulates gene expression independently of HIF-1α and promotes different aspects of hypoxic adaptation [6] (Fig 4). HIF-2α regulates

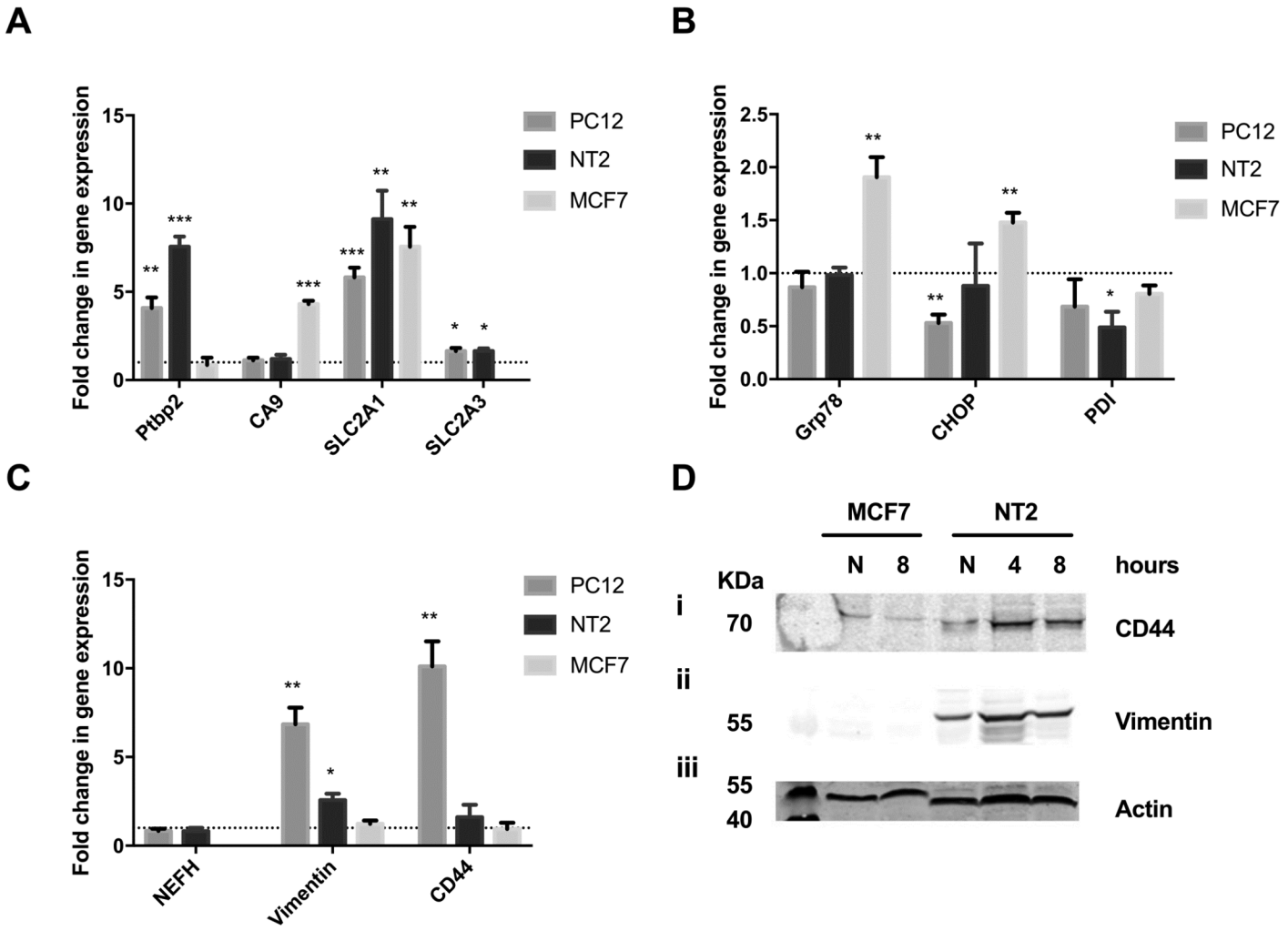

Fig 5. HIF-2α dependant pathways are preferentially activated in differentiated PC12 and NT2 cells following hypoxia. Relative expression of HIF-1α related target genes (*Ptbp2*, *CA9*, *SLC2A1* and *SLC2A3*) (**A**); UPR related genes (*Grp78*, *CHOP* and *PDI*) (**B**); and HIF-2α related target genes (*NEFH*, *Vimentin* and *CD44*) (**C**), were analysed in MCF7 and differentiated PC12 and NT2 cells, 8 hours after hypoxia, using qPCR. Data is expressed as mean ± SEM; n = 3; *p<0.05, **p≤0.01, ***p≤0.001. The dotted line represents basal gene expression. **D:** Representative immunoblots showing induction of CD44 (**i**) and vimentin (**ii**) protein expression in normoxic (N) or hypoxic (4 or 8 hours hypoxia) MCF7 and differentiated NT2 cells. Equal protein loading was assessed by immunoblotting for actin (**iii**).

https://doi.org/10.1371/journal.pone.0185664.g005

expression of stem cell markers [47] and maintains the undifferentiated state, via expression of neural crest and stem cell-associated genes [48]. Vimentin and CD44 are highly expressed in neuronal precursor cells [49,50], however expression declines during development as neurons become post-mitotic. In post-mitotic neurons, vimentin is replaced by neurofilaments [51].

Expression of the neuronal marker, neurofilament heavy chain (*NEFH*) [52] was evident in differentiated PC12 and NT2 cells yet undetected in MCF7 cells (Fig 5C); basal expression was also unaffected by hypoxic insult in PC12 and NT2 cells. *Vimentin* expression was significantly upregulated in PC12 ($p = 0.0033$) and NT2 cells ($p = 0.0119$) following hypoxia (Fig 5C). *CD44* expression was also dramatically increased in hypoxic PC12 cells ($p = 0.003$), whilst expression was only modestly effected in hypoxic NT2 cells (1.6-fold increase; $p = 0.43$; Fig 5C). *Vimentin* and *CD44* expression were not significantly altered in hypoxic MCF7 cells (Fig 5C).

CD44 and vimentin expression was also analysed by immunoblotting. CD44 and vimentin expression were readily detected in normoxic NT2 cells and markedly induced by hypoxia (Fig 5D). CD44 expression was unchanged in hypoxic MCF7 cells (Fig 5D), however vimentin was not detected in MCF7 cells in either normoxic or hypoxic conditions (Fig 5D). Together, these findings show strong induction of HIF-2α regulated genes in hypoxic neuronal-like cells and suggest the HIF-2α dependant cellular regeneration arm of the adaptive hypoxic response predominates over the HIF-1α arm in neuronal-like cells following acute hypoxia.

Hypoxia promotes a regression to undifferentiated states in neuronal-like cells

Neuron specific markers, NSE and KCC2 were dramatically induced following neuronal differentiation of PC12 and NT2 cells (Fig 1E). NSE and KCC2 expression was assessed by immunoblotting to determine whether hypoxia could reverse the expression of these neuronal markers. The dramatic increase in NSE expression was attenuated following hypoxia in differentiated PC12 cells, whereas NSE expression remained unchanged by hypoxia in differentiated NT2 cells (Fig 6A, panel i). The striking induction of KCC2 expression observed following differentiation was also dramatically reversed in hypoxic PC12 cells after as little as 8 hours of hypoxic insult and severely reduced in hypoxic NT2 cells (Fig 6A, panel ii).

Differentiated PC12 and NT2 display neurite-like processes and gangliar-like structures (Figs 1F and 6B). The neuronal-like morphology was dramatically modified in as little as 8 hours of hypoxic insult (Fig 6B); the number of differentiated PC12 and NT2 cells presenting

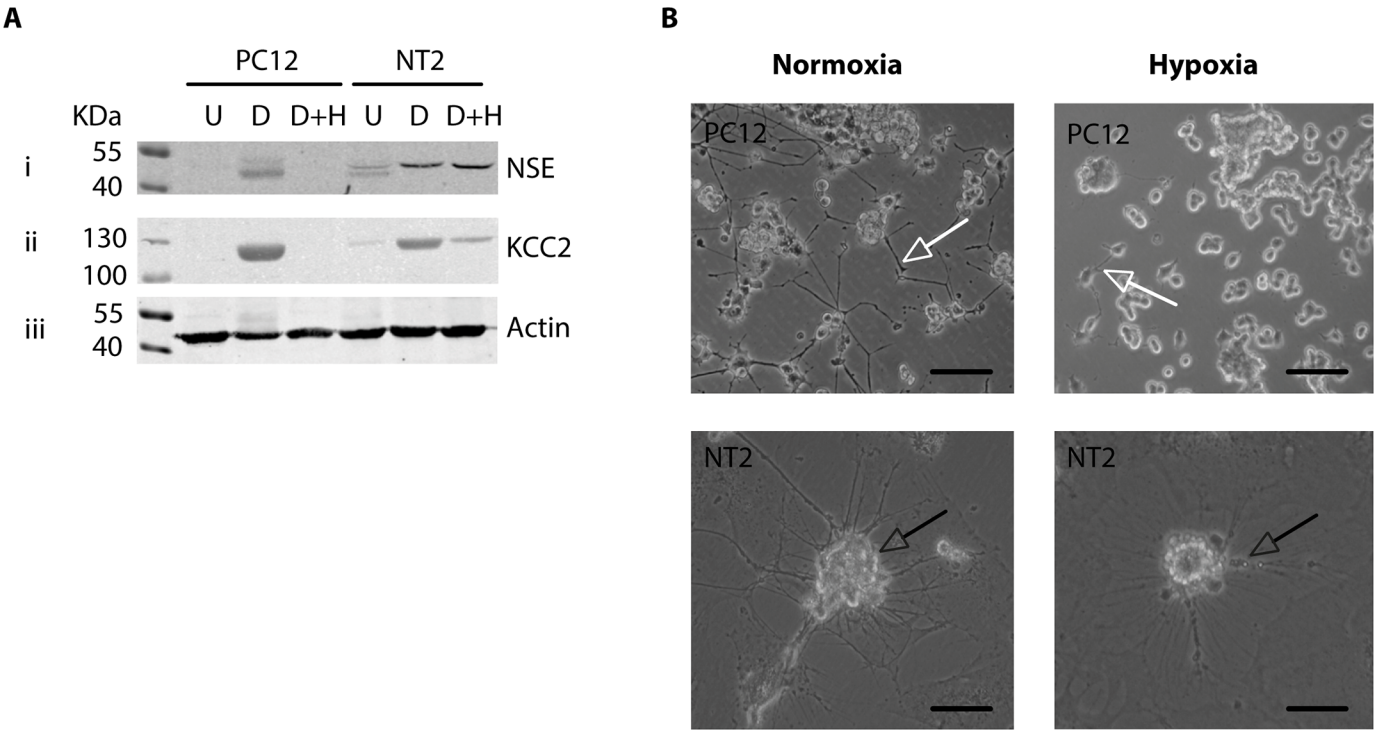

Fig 6. Hypoxia promotes a regression of neuronal-like cells to undifferentiated states. A: Representative immunoblots showing the change in NSE (**i**) and KCC2 (**ii**) protein expression in normoxic (N), differentiated (D) or differentiated and hypoxic (D+H, 8 hours) PC12 and NT2 cells. Equal protein loading was assessed by immunoblotting for actin (**iii**). **B:** Representative bright-field microscopy images of differentiated PC12 and NT2 morphology after exposure to 8 hours of normoxia or hypoxia (20x magnification). Scale bar represents 50 μm. White arrows indicate interlaced axon-like structures and black arrows indicate ganglion-like clusters.

https://doi.org/10.1371/journal.pone.0185664.g006

with neurites was dramatically reduced and the length of neurites was evidently shortened. These results combined with the observed HIF-2α dependant induction of neural progenitor cell markers (Fig 5B and 5D) suggest adaptations promoted by HIF-2α following acute hypoxic insult could drive neuronal-like cells into a more immature phenotype.

Discussion

Stroke is the second leading cause of death and disability worldwide [53]. PC12 and NT2 cells have been extensively used as models to study neuronal differentiation and neurological pathologies, including stroke [54–56]. Furthermore, NT2 cells are currently undergoing phase 1 and 2 clinical trials as neuronal grafts for stroke patients [57,58]. Whilst these cells are not primary neurons, differentiated PC12 and NT2 cells are a valid and commonly used source of neuronal-like cells, and an excellent model to study the hypoxic molecular adaptations that occur *in vivo*, following stroke.

Numerous studies have investigated the role of HIF-1α in neuronal adaptation to hypoxia [59,60] (Fig 4). HIF-2α and HIF-3α signalling have received less attention, however, recent work demonstrates HIF-2α is an essential component of hypoxic adaptation [6]. Likely, these pathways are complimentary and co-ordinated signalling of both HIF-1α and HIF-2α is required to promote survival and adaption following hypoxic insult (Fig 4). To our knowledge, this is the first study to dissect the importance of HIF dependant adaptation and downstream signalling in differentiated neuronal-like cells following hypoxia.

HIF-1α expression and induction following hypoxia has been reported in PC12 and NT2 cells [61,62] and neuroblastoma cells [59], therefore our observed lack of HIF-1α induction and signalling following acute hypoxia, as well as through chemical induction of hypoxia, using colbalt chloride (data not shown), was surprising. However, closer scrutiny reveals fundamental methodological differences with these studies which may account for the absence of HIF-1α induction, such as employing undifferentiated cells [62,63], culturing cells on uncoated plates [64], using different exposure times [65] or oxygen concentrations that confer mild hypoxia [62]. Interestingly, we observed consistent, preferential induction of HIF-2α over HIF-1α expression in differentiated PC12 and NT2 cells when acute hypoxia was induced, for 8 hours, with slightly different gas mixtures (1% O_2/99% N_2 and 1% O_2/5% CO_2/99% N_2, data not shown). Our model utilises fully differentiated post-mitotic neuronal-like cells, and is therefore potentially more representative of neuronal cell function than undifferentiated cells.

Despite the lack of HIF-1α induction in PC12 and NT2 cells, acute hypoxic conditions were achieved. MCF7 cells were used as a positive control as they show intense HIF-1α expression following acute hypoxia [35,36]. Hypoxia was induced simultaneously with NT2 and PC12 cells and rapid HIF-1α stabilisation and intense activation of *HIF-1α* signalling was observed in control MCF7 cells, confirming acute hypoxia was established. Marked induction of *Ptbp2 and Slc2A1* was observed in hypoxic PC12 and NT2 cells; genes thought to be specifically regulated by HIF-1α [66]. However, many HIF-1α specific genes have also been shown to be regulated by HIF-2α, including *Slc2A1* (GLUT-1)[67], underscoring the potential importance of HIF-2α signalling in hypoxic adaptation of neuronal-like cells.

Surprisingly, neuronal-like PC12 and NT2 cells are refractory to HIF-1α stabilisation in response to acute hypoxia and activation of HIF-1α signalling was absent. Instead, significant induction of *HIF-2α* mRNA and stabilisation of HIF-2α and HIF-3α protein was evident in hypoxic PC12 and NT2 cells. HIF-1α, HIF-2α expression is detected in undifferentiated neuroblastoma cells [59] however HIF-1α expression appears to be dominant and HIF-2α induction was only observed in certain cells under complete anoxia (0% O_2). These findings suggest the HIF-2α arm of the hypoxic adaptive response may predominate over HIF-1α dependant

mechanisms in differentiated neuronal-like cells and underscore the need to use differentiated neuronal *in vitro* models as a platform to investigate the molecular changes occurring following ischaemic stroke.

HIF-2α regulates several genes involved in proliferation and regeneration, including the *OCT4* transcription factor which maintains stem-like characteristics [68] and neural stem cell pluripotency [69,70]. HIF-2α signalling also maintains cells in an undifferentiated state. Expression of neural crest genes is increased by hypoxia, and may drive a more immature phenotype in neuroblastoma cells [59]. Increased expression of the stem cell marker, CD44 and early neuronal progenitor marker, vimentin, was readily observed in hypoxic neuronal-like cells and were accompanied by loss of neuronal markers, NSE and KCC2, and neuronal morphology. HIF-2α dependant hypoxic adaptation therefore may promote regression of neuronal-like cells to a more undifferentiated, and thus potentially transient, proliferative, state prior to repair. In doing so, HIF-2α signalling may have some utility in triggering neuronal repair, recovery and regeneration following acute hypoxic insult (Fig 4). Indeed exogenous administration of the HIF-2α target, EPO, can promote angiogenesis and neurogenesis following neonatal ischaemia in rats [71]. Preferentially activating the HIF-2α dependant arm of the hypoxic adaptive response could therefore represent a novel strategy to minimise damage associated with ischaemic stroke and promote neural repair and regeneration.

In the adult brain, neurogenesis occurs in the subventricular and hippocampal subgranular zones and to a lesser extent, the striatum and cerebral cortex [72]. Neural stem cell proliferation is dramatically increased following stroke [51,73] and progenitor cells can migrate to sites of infarct [74], however the vast majority of these immature neurons fail to survive, likely due to unfavourable environmental conditions or lack of functional connections [51,75]. Transient hypoxia can increase the number of mitotic neurons and expression of proliferative markers in cultured embryonic rat cortical neurons [76] whilst mild hypoxia favours proliferation and differentiation of neural spheres [77]. Together, these studies suggest sub-lethal hypoxic insult could potentially promote self-renewal *in vivo*. In the heart, chronic stabilisation of HIF-1α and HIF-2α protects against ischaemia reperfusion injury in adult mice [78] and systemic hypoxia promotes cardiomyocyte proliferation [79]. This suggests hypoxic stress may also act as a driving force for proliferation and a potential therapeutic tool in regenerative medicine.

The role of HIF in the pathophysiology of ischaemic stroke and its impact on neuronal survival remains controversial. *In vivo* global and focal ischaemia models provide conflicting results as genetic manipulation of neuronal *HIF-1α* has been reported to be both neuroprotective and detrimental [10,80]. HIF-1α overexpression has also been associated with dendritic overgrowth and abnormal patterning of cortical neurons [81]. Activation of HIF-1α dependant signalling may therefore be potentially deleterious to neurons in ischaemic stroke. Combined loss of HIF-1α and HIF-2α has been found to be detrimental for functional recovery after ischaemic stroke but surprisingly beneficial in the early stroke phase [12]. This suggests partial compensatory mechanism exist between the two transcription factors.

Ischaemic neuronal injury is a multifunctional process [1,2]. Spatial and temporal factors combined with the intensity of ischaemic challenge will all impact upon HIF dependant adaptation and whether downstream signalling promotes neuroprotection, ischaemia induced cell death or neuroproliferation. These areas require significantly greater research and specific therapeutic agents targeting HIF-1α and HIF-2α are needed to delineate the intricacies of HIF signalling and understand their therapeutic potential.

Due to the potential of small populations of neural stem cells to regenerate neuronal tissue and drive repair and recovery of damaged regions of brain tissue, understanding the mechanisms involved in promoting self-repair and how non-neurogenic areas in the brain can revert to neural stem/progenitor cells is crucial. Our results show the HIF-2α arm of the hypoxic

adaptive response may predominate over the HIF-1α arm in neuronal-like cells and suggest this could promote regression to a more dedifferentiated state. Whilst caution must be taken in extrapolating *in vitro* findings to an *in vivo* setting, it is possible that preferential activation of HIF-2α dependant adaptations in the small population of neuronal cells surviving the transient hypoxia of a stroke could drive expression of stem-like genes and promote the dedifferentiation of these cells. These dedifferentiated cells could then promote the self-renewal and growth of neuronal cells in the hours to days following a stroke. Ultimately, this could promote the repair of damaged neuronal tissue and reduce the long-term damage associated with ischaemic insult. Therapeutic manipulation of endogenous pathways driving neuronal adaptation to hypoxic stress could represent exciting possibilities to enhance repair and recovery of the stroke damaged brain and promote neurogenesis, and ultimately reduce stroke-associated disability.

Acknowledgments

Sadly, Professor Darlison passed away before the submission of the final version of this manuscript. As corresponding author, Dr Fraser accepts responsibility for the integrity and validity of the data collected and analysed.

Author Contributions

Conceptualization: Miguel A. S. Martín-Aragón Baudel, Mark G. Darlison, Amy V. Poole, Jennifer A. Fraser.

Formal analysis: Miguel A. S. Martín-Aragón Baudel, Mick T. Rae, Amy V. Poole, Jennifer A. Fraser.

Investigation: Miguel A. S. Martín-Aragón Baudel, Jennifer A. Fraser.

Methodology: Miguel A. S. Martín-Aragón Baudel, Jennifer A. Fraser.

Project administration: Amy V. Poole, Jennifer A. Fraser.

Supervision: Mick T. Rae, Mark G. Darlison, Amy V. Poole, Jennifer A. Fraser.

Validation: Miguel A. S. Martín-Aragón Baudel, Jennifer A. Fraser.

Visualization: Miguel A. S. Martín-Aragón Baudel, Mick T. Rae, Mark G. Darlison, Amy V. Poole, Jennifer A. Fraser.

Writing – original draft: Miguel A. S. Martín-Aragón Baudel, Jennifer A. Fraser.

Writing – review & editing: Miguel A. S. Martín-Aragón Baudel, Mick T. Rae, Mark G. Darlison, Amy V. Poole, Jennifer A. Fraser.

References

1. Astrup J, Siesjö BK, Symon L. Thresholds in cerebral ischemia—the ischemic penumbra. Stroke. 12: 723–5. Available: http://www.ncbi.nlm.nih.gov/pubmed/6272455 PMID: 6272455
2. Liu S, Levine SR, Winn HR. Targeting ischemic penumbra: part I—from pathophysiology to therapeutic strategy. J Exp Stroke Transl Med. NIH Public Access; 2010; 3: 47–55.
3. Semenza GL. Hypoxia-inducible factors in physiology and medicine. Cell. 2012. pp. 399–408. https://doi.org/10.1016/j.cell.2012.01.021 PMID: 22304911
4. Hu C-J, Wang L-Y, Chodosh LA, Keith B, Simon MC. Differential roles of hypoxia-inducible factor 1alpha (HIF-1alpha) and HIF-2alpha in hypoxic gene regulation. Mol Cell Biol. 2003; 23: 9361–74. Available: http://www.ncbi.nlm.nih.gov/pubmed/14645546 https://doi.org/10.1128/MCB.23.24.9361-9374.2003

5. Keith B, Johnson RS, Simon MC. HIF1α and HIF2α: sibling rivalry in hypoxic tumour growth and progression. Nat Rev Cancer. 2012; 12: 9–22. https://doi.org/10.1038/nrc3183 PMID: 22169972
6. Koh MY, Powis G. Passing the baton: The HIF switch. Trends in Biochemical Sciences. 2012. pp. 364–372. https://doi.org/10.1016/j.tibs.2012.06.004 PMID: 22818162
7. Maynard MA. Human HIF-3 4 is a dominant-negative regulator of HIF-1 and is down-regulated in renal cell carcinoma. FASEB J. Federation of American Societies for Experimental Biology; 2005; 19: 1396–1406. https://doi.org/10.1096/fj.05-3788com PMID: 16126907
8. Yamashita T, Ohneda O, Nagano M, Iemitsu M, Makino Y, Tanaka H, et al. Abnormal heart development and lung remodeling in mice lacking the hypoxia-inducible factor-related basic helix-loop-helix PAS protein NEPAS. Mol Cell Biol. American Society for Microbiology; 2008; 28: 1285–1297. https://doi.org/10.1128/MCB.01332-07 PMID: 18070924
9. Yang S, Wu C, Xiong Z, Fang X. Progress on hypoxia-inducible factor-3: Its structure, gene regulation and biological function (Review). Mol Med Rep. 2015; 12: 2411–6. PMID: 25936862
10. Baranova O, Miranda LF, Pichiule P, Dragatsis I, Johnson RS, Chavez JC. Neuron-Specific Inactivation of the Hypoxia Inducible Factor 1 Increases Brain Injury in a Mouse Model of Transient Focal Cerebral Ischemia. J Neurosci. 2007; 27: 6320–6332. https://doi.org/10.1523/JNEUROSCI.0449-07.2007 PMID: 17554006
11. Reischl S, Li L, Walkinshaw G, Flippin LA, Marti HH, Kunze R. Inhibition of HIF prolyl-4-hydroxylases by FG-4497 reduces brain tissue injury and edema formation during ischemic stroke. Baud O, editor. PLoS One. Public Library of Science; 2014; 9: e84767. https://doi.org/10.1371/journal.pone.0084767 PMID: 24409307
12. Barteczek P, Li L, Ernst A-S, Bo hler L-I, Marti HH, Kunze R. Neuronal HIF-1 and HIF-2 deficiency improves neuronal survival and sensorimotor function in the early acute phase after ischemic stroke. J Cereb Blood Flow Metab. 2016; https://doi.org/10.1177/0271678X15624933 PMID: 26746864
13. Holmquist-Mengelbier L, Fredlund E, Löfstedt T, Noguera R, Navarro S, Nilsson H, et al. Recruitment of HIF-1α and HIF-2α to common target genes is differentially regulated in neuroblastoma: HIF-2α promotes an aggressive phenotype. Cancer Cell. 2006; 10: 413–423. https://doi.org/10.1016/j.ccr.2006.08.026 PMID: 17097563
14. Shen Q, Goderie SK, Jin L, Karanth N, Sun Y, Abramova N, et al. Endothelial cells stimulate self-renewal and expand neurogenesis of neural stem cells. Science. 2004; 304: 1338–40. https://doi.org/10.1126/science.1095505 PMID: 15060285
15. Thored P, Wood J, Arvidsson A, Cammenga J, Kokaia Z, Lindvall O. Long-Term Neuroblast Migration Along Blood Vessels in an Area With Transient Angiogenesis and Increased Vascularization After Stroke. Stroke. 2007; 38: 3032–3039. https://doi.org/10.1161/STROKEAHA.107.488445 PMID: 17901386
16. Li L, Saliba P, Reischl S, Marti HH, Kunze R. Neuronal deficiency of HIF prolyl 4-hydroxylase 2 in mice improves ischemic stroke recovery in an HIF dependent manner. Neurobiol Dis. 2016; 91: 221–235. https://doi.org/10.1016/j.nbd.2016.03.018 PMID: 27001147
17. Adamson J, Beswick A, Ebrahim S. Is stroke the most common cause of disability? J Stroke Cerebrovasc Dis. 2004; 13: 171–7. https://doi.org/10.1016/j.jstrokecerebrovasdis.2004.06.003 PMID: 17903971
18. Pleasure SJ, Page C, Lee VM. Pure, postmitotic, polarized human neurons derived from NTera 2 cells provide a system for expressing exogenous proteins in terminally differentiated neurons. J Neurosci. 1992; 12: 1802–1815. PMID: 1578271
19. Wu D, Yotnda P. Induction and Testing of Hypoxia in Cell Culture. J Vis Exp. 2011; https://doi.org/10.3791/2899 PMID: 21860378
20. Livak KJ, Schmittgen TD. Analysis of Relative Gene Expression Data Using Real-Time Quantitative PCR and the 2−ΔΔCT Method. Methods. 2001; 25: 402–408. https://doi.org/10.1006/meth.2001.1262 PMID: 11846609
21. Dales J-P, Beaufils N, Silvy M, Picard C, Pauly V, Pradel V, et al. Hypoxia inducible factor 1α gene (HIF-1α) splice variants: potential prognostic biomarkers in breast cancer. BMC Med. BioMed Central; 2010; 8: 44. https://doi.org/10.1186/1741-7015-8-44 PMID: 20624301
22. Zhao L, Yang Y-F, Gao Y-B, Wang S-M, Wang L-F, Zuo H-Y, et al. Upregulation of HIF-1α Via Activation of ERK and PI3K Pathway Mediated Protective Response to Microwave-Induced Mitochondrial Injury in Neuron-Like Cells. Mol Neurobiol. 2014; 50: 1024–1034. https://doi.org/10.1007/s12035-014-8667-z PMID: 24627260
23. Campen KA, Clark ZL, Olds MA, McNatty KP, Pitman JL. The in-vitro effects of cAMP and cGMP modulators on inter-cellular dye transfer and gene expression levels in rat cumulus cell—oocyte complexes. Mol Cell Endocrinol. 2016; 420: 46–56. https://doi.org/10.1016/j.mce.2015.11.025 PMID: 26628038

24. Weisova P, Concannon CG, Devocelle M, Prehn JHM, Ward MW. Regulation of Glucose Transporter 3 Surface Expression by the AMP-Activated Protein Kinase Mediates Tolerance to Glutamate Excitation in Neurons. J Neurosci. 2009; 29: 2997–3008. https://doi.org/10.1523/JNEUROSCI.0354-09.2009 PMID: 19261894

25. Smith PK, Krohn RI, Hermanson GT, Mallia AK, Gartner FH, Provenzano MD, et al. Measurement of protein using bicinchoninic acid. Anal Biochem. 1985; 150: 76–85. https://doi.org/10.1016/0003-2697(85)90442-7 PMID: 3843705

26. Cappelletti G, Galbiati M, Ronchi C, Maggioni MG, Onesto E, Poletti A. Neuritin (cpg15) enhances the differentiating effect of NGF on neuronal PC12 cells. Journal of Neuroscience Research. 2007. pp. 2702–2713. https://doi.org/10.1002/jnr.21235 PMID: 17335086

27. Rao R V, Bredesen DE. Misfolded proteins, endoplasmic reticulum stress and neurodegeneration [Internet]. Current Opinion in Cell Biology. NIH Public Access; 2004. pp. 653–662. https://doi.org/10.1016/j.ceb.2004.09.012 PMID: 15530777

28. Andrews PW. Retinoic acid induces neuronal differentiation of a cloned human embryonal carcinoma cell line in vitro. Dev Biol. 1984; 103: 285–293. http://dx.doi.org/10.1016/0012-1606(84)90316-6 PMID: 6144603

29. Ray B, Bailey JA, Sarkar S, Lahiri DK. Molecular and immunocytochemical characterization of primary neuronal cultures from adult rat brain: Differential expression of neuronal and glial protein markers. J Neurosci Methods. 2009; 184: 294–302. https://doi.org/10.1016/j.jneumeth.2009.08.018 PMID: 19720084

30. Podrygajlo G, Tegenge MA, Gierse A, Paquet-Durand F, Tan S, Bicker G, et al. Cellular phenotypes of human model neurons (NT2) after differentiation in aggregate culture. Cell Tissue Res. Springer-Verlag; 2009; 336: 439–452. https://doi.org/10.1007/s00441-009-0783-0 PMID: 19377856

31. Haile Y, Fu W, Shi B, Westaway D, Baker G, Jhamandas J, et al. Characterization of the NT2-derived neuronal and astrocytic cell lines as alternative in vitro models for primary human neurons and astrocytes. J Neurosci Res. 2014; 92: 1187–1198. https://doi.org/10.1002/jnr.23399 PMID: 24801011

32. Martín-Aragón Baudel MAS, Poole A V, Darlison MG. Chloride co-transporters as possible therapeutic targets for stroke. J Neurochem. 2016; https://doi.org/10.1111/jnc.13901 PMID: 27861901

33. Schmechel D, Marangos P, Zis A, Brightman M, Goodwin F. Brain endolases as specific markers of neuronal and glial cells. Science (80-). 1978; 199.

34. Payne JA, Stevenson J, Donaldson L. Molecular characterization of putative K—Cl cotransporter in rat brain, J. Biol Chem. 1996; 271: 16245–16252. https://doi.org/10.1074/jbc.271.27.16245 PMID: 8663311

35. Du J, Xu R, Hu Z, Tian Y, Zhu Y, Gu L, et al. PI3K and ERK-induced Rac1 activation mediates hypoxia-induced HIF-1?? expression in MCF-7 breast cancer cells. Roy D, editor. PLoS One. Public Library of Science; 2011; 6: e25213. https://doi.org/10.1371/journal.pone.0025213 PMID: 21980400

36. Liu N, Xia W-Y, Liu S-S, Chen H-Y, Sun L, Liu M-Y, et al. MicroRNA-101 targets von Hippel-Lindau tumor suppressor (VHL) to induce HIF1α mediated apoptosis and cell cycle arrest in normoxia condition. Sci Rep. Nature Publishing Group; 2016; 6: 20489. https://doi.org/10.1038/srep20489 PMID: 26841847

37. Wang GL, Jiang BH, Rue EA, Semenza GL. Hypoxia-inducible factor 1 is a basic-helix-loop-helix-PAS heterodimer regulated by cellular O2 tension. Proc Natl Acad Sci U S A. National Academy of Sciences; 1995; 92: 5510–5514. https://doi.org/10.1073/pnas.92.12.5510

38. Kaelin WG, Ratcliffe PJ. Oxygen sensing by metazoans: the central role of the HIF hydroxylase pathway. Mol Cell. 2008; 30: 393–402. https://doi.org/10.1016/j.molcel.2008.04.009 PMID: 18498744

39. Schepens B, Tinton SA, Bruynooghe Y, Beyaert R, Cornelis S. The polypyrimidine tract-binding protein stimulates HIF-1?? IRES-mediated translation during hypoxia. Nucleic Acids Res. 2005; 33: 6884–6894. https://doi.org/10.1093/nar/gki1000 PMID: 16396835

40. Kaluz S, Kaluzová M, Liao SY, Lerman M, Stanbridge EJ. Transcriptional control of the tumor- and hypoxia-marker carbonic anhydrase 9: A one transcription factor (HIF-1) show? Biochimica et Biophysica Acta—Reviews on Cancer. 2009. pp. 162–172. https://doi.org/10.1016/j.bbcan.2009.01.001 PMID: 19344680

41. Grabmaier K, A de Weijert MC, Verhaegh GW, Schalken JA, Oosterwijk E. Strict regulation of CAIX (G250/MN) by HIF-1alpha in clear cell renal cell carcinoma. Oncogene. 2004; 23: 5624–31. https://doi.org/10.1038/sj.onc.1207764 PMID: 15184875

42. Christensen DR, Calder PC, Houghton FD, Evans MJ, Kaufman MH, Martin GR, et al. GLUT3 and PKM2 regulate OCT4 expression and support the hypoxic culture of human embryonic stem cells. Sci Rep. Nature Publishing Group; 2015; 5: 17500. https://doi.org/10.1038/srep17500 PMID: 26639784

43. Vannucci SJ, Maher F, Simpson IA. Glucose transporter proteins in brain: delivery of glucose to neurons and glia. Glia. 1997; 21: 2–21. Available: http://www.ncbi.nlm.nih.gov/pubmed/9298843 PMID: 9298843

44. Roussel BD, Kruppa AJ, Miranda E, Crowther DC, Lomas DA, Marciniak SJ. Endoplasmic reticulum dysfunction in neurological disease [Internet]. The Lancet Neurology. 2013. pp. 105–118. https://doi.org/10.1016/S1474-4422(12)70238-7 PMID: 23237905

45. Ron D. Translational control in the endoplasmic reticulum stress response [Internet]. Journal of Clinical Investigation. American Society for Clinical Investigation; 2002. pp. 1383–1388. https://doi.org/10.1172/JCI200216784

46. Pereira ER, Frudd K, Awad W, Hendershot LM. Endoplasmic Reticulum (ER) stress and Hypoxia response pathways interact to Potentiate Hypoxia-inducible Factor 1 (HIF-1) Transcriptional activity on targets like Vascular Endothelial Growth Factor (VEGF). J Biol Chem. American Society for Biochemistry and Molecular Biology; 2014; 289: 3352–3364. https://doi.org/10.1074/jbc.M113.507194 PMID: 24347168

47. Li Z, Bao S, Wu Q, Wang H, Eyler C, Sathornsumetee S, et al. Hypoxia-Inducible Factors Regulate Tumorigenic Capacity of Glioma Stem Cells. Cancer Cell. NIH Public Access; 2009; 15: 501–513. https://doi.org/10.1016/j.ccr.2009.03.018 PMID: 19477429

48. Pietras A, Hansford LM, Johnsson AS, Bridges E, Sjolund J, Gisselsson D, et al. HIF-2alpha maintains an undifferentiated state in neural crest-like human neuroblastoma tumor-initiating cells. Proc Natl Acad Sci U S A. National Academy of Sciences; 2009; 106: 16805–16810. https://doi.org/10.1073/pnas.0904606106 PMID: 19805377

49. Sanin V, Heeß C, Kretzschmar HA, Schüller U. Recruitment of neural precursor cells from circumventricular organs of patients with cerebral ischaemia. Neuropathol Appl Neurobiol. 2013; 39: 510–518. https://doi.org/10.1111/j.1365-2990.2012.01301.x PMID: 22985410

50. Naruse M, Shibasaki K, Ishizaki Y. FGF-2 signal promotes proliferation of cerebellar progenitor cells and their oligodendrocytic differentiation at early postnatal stage. Biochem Biophys Res Commun. 2015; 463: 1091–1096. https://doi.org/10.1016/j.bbrc.2015.06.063 PMID: 26079890

51. Arvidsson A, Collin T, Kirik D, Kokaia Z, Lindvall O. Neuronal replacement from endogenous precursors in the adult brain after stroke. Nat Med. 2002; 8: 963–970. https://doi.org/10.1038/nm747 PMID: 12161747

52. Usoskin D, Furlan A, Islam S, Abdo H, Lönnerberg P, Lou D, et al. Unbiased classification of sensory neuron types by large-scale single-cell RNA sequencing. Nat Neurosci. Nature Research; 2014; 18: 145–153. https://doi.org/10.1038/nn.3881 PMID: 25420068

53. WHO. The top 10 causes of death [Internet]. 2017 [cited 7 Jun 2017]. http://www.who.int/mediacentre/factsheets/fs310/en/

54. Meland MN, Herndon ME S C. Expression of alpha5 integrin rescues fibronectin responsiveness in NT2N CNS neuronal cells. J Neurosci Res. 2010; 88: 222–32. https://doi.org/10.1002/jnr.22171 PMID: 19598247

55. Lan A, Liao X, Mo L, Yang C, Yang Z, Wang X, et al. Hydrogen sulfide protects against chemical hypoxia-induced injury by inhibiting ROS-activated ERK1/2 and p38mapk signaling pathways in PC12 cells. PLoS One. 2011; 6. https://doi.org/10.1371/journal.pone.0025921 PMID: 21998720

56. Chiu BY, Chang CP, Lin JW, Yu JS, Liu WP, Hsu YC, et al. Beneficial effect of astragalosides on stroke condition using PC12 cells under oxygen glucose deprivation and reperfusion. Cell Mol Neurobiol. 2014; 34: 825–837. https://doi.org/10.1007/s10571-014-0059-4 PMID: 24807460

57. Kondziolka D, Steinberg GK, Wechsler L, Meltzer CC, Elder E, Gebel J, et al. Neurotransplantation for patients with subcortical motor stroke: a phase 2 randomized trial. J Neurosurg. 2005; 103: 38–45. https://doi.org/10.3171/jns.2005.103.1.0038 PMID: 16121971

58. Manley NC, Azevedo-pereira RL, Bliss TM, Steinberg GK. Cell Therapy for Brain Injury. 2015; 91–109. https://doi.org/10.1007/978-3-319-15063-5

59. Jögi A, Øra I, Nilsson H, Lindeheim A, Makino Y, Poellinger L, et al. Hypoxia alters gene expression in human neuroblastoma cells toward an immature and neural crest-like phenotype. Proc Natl Acad Sci U S A. National Academy of Sciences; 2002; 99: 7021–6. https://doi.org/10.1073/pnas.102660199 PMID: 12011461

60. Ratan RR, Siddiq A, Smirnova N, Karpisheva K, Haskew-Layton R, McConoughey S, et al. Harnessing hypoxic adaptation to prevent, treat, and repair stroke [Internet]. Journal of Molecular Medicine. Springer-Verlag; 2007. pp. 1331–1338. https://doi.org/10.1007/s00109-007-0283-1 PMID: 18043901

61. Frøyland E, Skjæret C, Wright MS, Dalen ML, Cvancarova M, Kasi C, et al. Inflammatory receptors and pathways in human NT2-N neurons during hypoxia and reoxygenation. Impact of acidosis. Brain Res. 2008; 1217: 37–49. https://doi.org/10.1016/j.brainres.2008.04.038 PMID: 18502402

62. Zhdanov A V., Dmitriev RI, Golubeva A V., Gavrilova SA, Papkovsky DB. Chronic hypoxia leads to a glycolytic phenotype and suppressed HIF-2 signaling in PC12 cells. Biochim Biophys Acta—Gen Subj. Elsevier B.V.; 2013; 1830: 3553–3569. https://doi.org/10.1016/j.bbagen.2013.02.016 PMID: 23462283

63. Hui AS, Bauer AL, Striet JB, Schnell PO, Czyzyk-Krzeska MF. Calcium signaling stimulates translation of HIF-alpha during hypoxia. FASEB J. 2006; 20: 466–75. https://doi.org/10.1096/fj.05-5086com PMID: 16507764

64. Naranjo-Suárez S, Castellanos MC, Álvarez-Tejado M, Vara A, Landázuri MO, Del Peso L. Down-regulation of hypoxia-inducible factor-2 in PC12 cells by nerve growth factor stimulation. J Biol Chem. 2003; 278: 31895–31901. https://doi.org/10.1074/jbc.M304079200 PMID: 12805361

65. Li R, Wang Y, Yang Z, He Y, Zhao T, Fan M, et al. Hypoxia-inducible factor-1α regulates the expression of L-type voltage-dependent Ca2+ channels in PC12 cells under hypoxia. Cell Stress Chaperones. Springer; 2015; 20: 507–516. https://doi.org/10.1007/s12192-015-0575-2 PMID: 25648081

66. Chen C, Pore N, Behrooz A, Ismail-Beigi F, Maity A. Regulation of glut1 mRNA by hypoxia-inducible factor-1: Interaction between H-ras and hypoxia. J Biol Chem. 2001; 276: 9519–9525. https://doi.org/10.1074/jbc.M010144200 PMID: 11120745

67. Harvey AJ, Kind KL, Thompson JG. Regulation of gene expression in bovine blastocysts in response to oxygen and the iron chelator desferrioxamine. Biol Reprod. Society for the Study of Reproduction; 2007; 77: 93–101. https://doi.org/10.1095/biolreprod.106.058826 PMID: 17329595

68. Nichols J, Zevnik B, Anastassiadis K, Niwa H, Klewe-Nebenius D, Chambers I, et al. Formation of pluripotent stem cells in the mammalian embryo depends on the POU transcription factor Oct4. Cell. 1998; 95: 379–391. https://doi.org/10.1016/S0092-8674(00)81769-9 PMID: 9814708

69. Forristal CE, Wright KL, Hanley NA, Oreffo ROC, Houghton FD. Hypoxia inducible factors regulate pluripotency and proliferation in human embryonic stem cells cultured at reduced oxygen tensions. Reproduction. Bioscientifica Ltd.; 2010; 139: 85–97. https://doi.org/10.1530/REP-09-0300 PMID: 19755485

70. Kim JB, Sebastiano V, Wu G, Araúzo-Bravo MJ, Sasse P, Gentile L, et al. Oct4-Induced Pluripotency in Adult Neural Stem Cells. Cell. 2009; 136: 411–419. https://doi.org/10.1016/j.cell.2009.01.023 PMID: 19203577

71. Iwai M, Cao G, Yin W, Stetler RA, Liu J, Chen J. Erythropoietin promotes neuronal replacement through revascularization and neurogenesis after neonatal hypoxia/ischemia in rats. Stroke. 2007; 38: 2795–2803. https://doi.org/10.1161/STROKEAHA.107.483008 PMID: 17702962

72. Ming li G, Song H. Adult Neurogenesis in the Mammalian Brain: Significant Answers and Significant Questions. Neuron. 2011. pp. 687–702. https://doi.org/10.1016/j.neuron.2011.05.001 PMID: 21609825

73. Lindvall O, Kokaia Z. Neurogenesis following stroke affecting the adult brain. Cold Spring Harb Perspect Biol. 2015; 7: 1–20. https://doi.org/10.1101/cshperspect.a019034 PMID: 26525150

74. Jin K, Wang X, Xie L, Mao XO, Zhu W, Wang Y, et al. Evidence for stroke-induced neurogenesis in the human brain. Proc Natl Acad Sci U S A. National Academy of Sciences; 2006; 103: 13198–202. https://doi.org/10.1073/pnas.0603512103 PMID: 16924107

75. Zhang Z, Chopp M. Neural Stem Cells and Ischemic Bra. J stroke. 2016; 18: 267–272. https://doi.org/10.5853/jos.2016.00206 PMID: 27488979

76. Bossenmeyer-Pourié C, Chihab R, Schroeder H, Daval JL. Transient hypoxia may lead to neuronal proliferation in the developing mammalian brain: From apoptosis to cell cycle completion. Neuroscience. 1999; 91: 221–231. https://doi.org/10.1016/S0306-4522(98)00565-X PMID: 10336073

77. Santilli G, Lamorte G, Carlessi L, Ferrari D, Nodari LR, Binda E, et al. Mild hypoxia enhances proliferation and multipotency of human neural stem cells. Najbauer J, editor. PLoS One. Public Library of Science; 2010; 5: e8575. https://doi.org/10.1371/journal.pone.0008575 PMID: 20052410

78. Hyvärinen J, Hassinen IE, Sormunen R, Mäki JM, Kivirikko KI, Koivunen P, et al. Hearts of hypoxia-inducible factor prolyl 4-hydroxylase-2 hypomorphic mice show protection against acute ischemia-reperfusion injury. J Biol Chem. 2010; 285: 13646–13657. https://doi.org/10.1074/jbc.M109.084855 PMID: 20185832

79. Nakada Y, Canseco DC, Thet S, Abdisalaam S, Asaithamby A, Santos CX, et al. Hypoxia induces heart regeneration in adult mice. Nature. 2016; 541: 222–227. https://doi.org/10.1038/nature20173 PMID: 27798600

80. Helton R. Brain-Specific Knock-Out of Hypoxia-Inducible Factor-1 Reduces Rather Than Increases Hypoxic-Ischemic Damage. J Neurosci. 2005; 25: 4099–4107. https://doi.org/10.1523/JNEUROSCI.4555-04.2005 PMID: 15843612

81. Zhang L, Feliciano DM, Huang T, Zhang S, Bordey A. Hypoxia-inducible factor-1a contributes to dendritic overgrowth in tuberous sclerosis. Neurosci Lett. NIH Public Access; 2016; 612: 43–7. https://doi.org/10.1016/j.neulet.2015.11.038 PMID: 26655465